Force Determination of Bimetal Tube Drawing on a Mandrel or Floating Plug

Siew Kheong Loke

Department of Production Technology and Production Management

Supervisor: Professor D.H. Sansome

Date: April 1979

A thesis submitted to the University of Aston in Birmingham for the Degree of Ph.D.

This is to certify that no part of the work in this thesis has been submitted for any other award.

Contents

Force Determination of Bimetal Tube Drawing on a Mandrel or Floating Plug

Siew Kheong Loke

Ph.D. 1979

SUMMARY

This investigation was prompted by the absence of published work on the drawing of bimetal tube with a mandrel and the drawing of bimetal with a floating plug whilst these tubes are being produced and used in Industry. Initially, an equilibrium approach was used to analyse the bimetal tube mandrel drawing process. The proposed theory assumed that the tube-die interface and the clad-matrix interface converge towards an arbitrary intersection point. With this assumption, the accuracy of the theory is dependent on the accuracy of the final clad and matrix thicknesses used in the calculations. When final clad and matrix thicknesses, which were obtained from experiment were used, the theoretical solutions for draw load were in good agreement with the experimental results. It is also possible to obtain the die pressure, interfacial shear stress and stresses acting on the clad and matrix using the proposed theory.

When the assumption was made that the proportion of clad thickness remains the same after a pass as that before, the theoretical predictions gave reasonably good estimations of the experimental draw loads. The die rotation method was used to obtain the coefficients of friction at the tube-tool interfaces.

Velocity fields were proposed for the two bimetal tube drawing processes in separate theoretical analyses of the processes. Separate computer programmes were written to optimise for minimum stress ratio, σ_x/Y_e. The upper bound solutions for both processes were in reasonably good agreement with the experimental results. The final clad and matrix thicknesses predicted by the separate computer solutions gave good estimations when compared with the clad and matrix thicknesses obtained from the experiments.

Key Words: Bimetal-Drawing
Tube-Drawing
Mandrel-Drawing
Floating-Plug-Drawing

ACKNOWLEDGEMENT

The author wishes to express his sincere gratitude to Professor D.H. Sansome for his interest, encouragement and invaluable advice throughout the course of his research.

The author is also most grateful to the University of Aston for their Studentships without which this research may not have been possible. The author would like to thank Mr. G.M. Jones for his assistance in instrumentation and use of experimental equipment and Mr. S. Twamley and Mr. J. Watters for their cooperation. Thanks are also extended to all members of the technical staff who have assisted in one way or another.

My thanks are due to Mrs. A. Copeland for her assistance and the typing of this thesis and to Mr. P.M. Ingham for his time spent in reading part of this thesis.

Last but not least, the author's appreciation also goes to Miss B.Y.P. Wong for her patience and encouragement during the course of this research.

NOTATIONS

clad	is outer tube material
matrix	is inner tube material
σ, σ_x	total draw stress
σ_c	draw stress on clad
σ_m	draw stress on matrix
σ_p	draw stress on mandrel
α	die semi-angle
β	angle of slope on conical portion of floating plug
D_l	die land
P_l	land on floating plug
τ_s	shear stress at tube-die interface
τ_c	shear stress at clad-matrix interface
τ_m	shear stress at tube-mandrel interface
p	die pressure
q_c	normal pressure at clad-matrix interface
q_m	normal pressure at matrix-mandrel interface
t	thickness of an element of tube wall
h	wall thickness of drawn tube
H	initial tube wall thickness
R_o	initial outside radius of tube
R_1	initial radius of tube bore
R_2	radius of mandrel or radius of parallel land on floating plug
R_3	radius of die
R_4	radius of clad-matrix interface
R_5	initial outer radius of inner tube
R_6	geometry defined in floating plug drawing theory

R_7	initial radius of bore of outer tube
k_1 or k_c	shear yield stress for clad material
k_2 or k_m	shear yield stress for matrix material
Y_c	mean yield stress for clad
Y_m	mean yield stress for matrix
Y_e	modified or equivalent yield stress
R	reduction in cross-sectional area
D	Draw load
D'	Draw load with die rotating
K	$\frac{H_c}{H_c + H_m}$, an assumption used in mandrel drawing theory
W	work done
$\dot{W}$	rate of plastic work done
V	velocity
v	volume
S	axial force on wall of bimetal tube
A	area of velocity discontinuities
A_i	initial cross-section area of bimetal tube
A_f	final cross-section area of bimetal tube
$\dot{\varepsilon}_R$	thickness strain
$\dot{\varepsilon}_\theta$	circumferential strain
$\bar{\dot{\varepsilon}}$	equivalent strain
μ	Coulomb's coefficient of friction
m_1, m_2, m_3	friction factors used in upper bound solutions

Chapter One

INTRODUCTION

1.1 Introduction

The use of articles manufactured from two metals that have been bonded together dates back to the days of the Vikings who made their swords using a combination of two metals. Due to the increasing demand placed on materials by modern Industry, development in the production of clad metal has been rapid in the past few decades. The advantages of combining two metals into a composite are realised in the composite's properties. With the choice of suitable constituents, the benefits attained by a composite could range from low cost in production to corrosion resistance. For example, titanium clad steel is widely used in tube heat exchangers because of the excellent corrosion resistance and anti-fouling properties of the titanium. Nickel has been the base metal for most superalloys developed for gas turbine service - predominantly as a matrix in high temperature applications.

Since the development of stainless steel in the early part of this century, the advantage of cladding mild steel with stainless steel had been recognised and patents[1] were granted shortly after stainless steel was developed. There are a

number of methods used to clad metal to metal. Cladding may be achieved by extruding or rolling two different metals together and metal sheets are cladded on both sides in the sandwich rolling process. Tubes and sheets have been cladded by implosive or explosive bonding techniques. With this method, the materials to be bonded are placed in a confined space and an explosive charge is detonated. The bonding by this technique is good but the thickness of clad may vary quite substantially along the specimen. Another method used is the vacuum brazing technique in which a brazing alloy is placed between the surfaces to be bonded. A combination of induction heating and tube expanding has been patented[2] in the United States. To join metallurgically incompatible bimetallic tubings, Nuclear Metals Division of Whittaker Corporation, West Concord, Massachusetts, devised an extrusion-forging process. It was reported that the process is successful in the joining of steel with titanium and titanium alloys. Other methods of forming bimetallic tubes were reported by Ostrenko et al[3] in the hot pressing and cold rolling of bimetal tubes and by Arkulis[4] in the production of bimetal rod by casting molten copper into a mould.

1.2. Bimetal Tube Drawing

Due to the fact that most of the processes available for the production of bimetal tubes manufacture short lengths of large diameter tubes, such tubes have to be drawn to increase the length and reduce the diameter. Using the explosive and

implosive welding method, 25ft. to 30ft. of bimetal tube with strong interface bonding can be produced but large amounts of energy are required. Consequently, it was found to be more economical to produce shorter lengths of large diameter tube and subsequently draw it to the required size. This is one of the reasons which prompts the study of bimetal tube drawing. Another reason is that although bimetal tubes and related products have been used extensively in Industry, there is still a lack of understanding of the theory behind the relevant production techniques.

In 1974, Townley and Blazynski[5] studied the drawing of bimetal tubes on a fixed plug. In their analysis, Shield's approach was adopted, which incorporated the effect of shear. It should be noted that Shield's method applies to flow in an infinite channel and therefore does not account for end effects. However, it was reported in their study that the numerical error introduced by neglecting these effects was insignificant at large deformations. Further, their analysis assumed a close-pass drawing process and that strain hardening was accounted for by using a value of mean yield stress.

At about the same period, Chia[6] analysed and developed a lower bound theory for the fixed plug drawing of bimetal tubes. Using the equilibrium approach, he formulated equations to determine the draw load, die pressure and plug load. Experiments were performed with a wide range of different metal combinations in the form of bimetal tubes. The

predicted draw loads and plug loads were found to compare well with those obtained in practice. The rotating die method was used to determine the coefficients of friction at the die/tube and tube/plug interfaces. In formulating his theory, plane strain was postulated and it was assumed that the interfacial surfaces converge towards the virtual apex. An assumption Chia made was that the ratio of the clad thickness to the outer radius of the bimetal tube at any stage of deformation is a constant. Thus, the constant term is:

$K = \frac{h_p}{h_c + h_m + h_p}$ where h_c, h_m and h_p are the thicknesses of an element of clad, matrix and radius of fixed plug respectively. In his computations for draw load, the initial clad and matrix thicknesses were used to determine the value of K. This factor alone could account for some of the differences between the experimental and the higher theoretical draw loads obtained when a bimetal tube with a hard clad and relatively soft matrix was drawn.

Chia[6] continued research in bimetal tube drawing and developed a theory for tube sinking using an upper bound approach. In his analysis, he assumed that the bimetal tube experiences no change in wall thickness when sunk and that the tube wall was thin in comparison with the tube's diameter. As with his fixed plug bimetal tube drawing experiments, a wide range of tube combinations in terms of yield stress was used to check the validity of his theory. To obtain a solution using his theory for tube sinking, the aid of a digital computer is required.

In conventional tube sinking, it is known that the tube wall thickness does not usually increase by more than

7% depending on the diameter to thickness ratio of the undrawn tube. Nevertheless, it was reported in Chia's investigation that the general increase in the tube wall thickness after sinking was about 5% and the increase experienced with stainless steel combinations was unusually high and could be as much as 12%. It should be noted that no attempt was made in either of his analyses to predict the final wall thicknesses of the materials in the bimetal tube. Further, this author observed, throughout his experiments, bonding did not occur at the interface although reductions in area in excess of 40% were achieved.

Again no interfacial bonding was reported when Islam[7] investigated the drawing of bimetal tubes using a fixed plug. He proposed a kinematically admissible axisymmetric velocity field using straight lines for velocity discontinuities. The upper bound theory proposed was used successfully in the prediction of both the draw stresses in fixed plug drawing and the final thicknesses of the individual materials of the drawn tube. The theory took into account strength and volume ratio of the component materials, redundant work, friction and strain hardening effects. In his analysis, this author found that for a given friction factor, the shear stress at the interface was higher in the case of soft/hard combinations than in a hard/soft combination. The higher shearing stress at the interface of the soft/hard combination could be explained by the flow of the softer material being impeded by the harder material thus giving rise to a higher difference in velocity

between the two materials. With the harder material on the outside, the flow of the softer material is less restricted and thus the velocity difference of the two materials is lower than in the former case.

In brief, extensive investigations in the fixed plug drawing of bimetal tube have already been undertaken by Townley et al, Chia, and Islam and the tube sinking analysed by Chia. However, to the knowledge of the author, no analysis has been published for bimetal tube drawing with a mandrel or a floating plug. Therefore, in view of the lack of understanding of the mechanics of these two processes, the author has undertaken separate investigations into the two processes.

As the title of this thesis implies, one of the aims of the present investigation was to determine the draw stresses in bimetal tube drawing with a mandrel and a floating plug. An equilibrium approach was used to derive expressions for draw stress and die pressure in the mandrel drawing process. Since the equilibrium approach, i.e. a lower bound analysis, underestimates the draw stress in mandrel drawing, an alternative theory based on an upper bound technique was developed also. Additionally, the upper bound technique was used to analyse the floating plug drawing process. Due to the considerable amount of sink in floating plug drawing, the upper bound technique was chosen for its ability to accommodate redundant work.

In addition to determining draw stresses, attempts were made to incorporate, in all the three theories, means of predicting the final wall thicknesses of the constituent tubes. This would enable passes to be designed in relation to the initial tube geometry to achieve desired final wall thicknesses of the constituent materials.

1.3 Interfacial Bonding

Under severe service conditions in industry, it has been shown that it is detrimental for the interfacial bond of a bimetal tube to fail. Depending on the service conditions failure of the bond leads to high stresses acting on either of the constituent tubes resulting in fracture. Therefore, although it was not the objective of the present investigation to study the element of bonding in bimetal tubes, attempts were made to produce bimetal tubes by processes which would provide high interfacial pressure and a degree of intimate contact.

The parameters which influence bonding at the interface are surface conditions, deformation, surface movements, pressure, and temperature. However, in cold mandrel drawing and floating plug tube drawing, the heat dissipated[8] is not sufficient to raise the temperature to a level which would be expected to significantly affect the promotion of interfacial bonding. Surface movement is a factor which is difficult to control in bimetal tube drawing. Hence, consequently in order to exploit the remaining factors under specified conditions,

a knowledge of the way in which these factors promote interfacial bonding is essential.

Indeed, surface condition[9] markedly affects most if not all bonding situations. Surface contaminants such as oxides, and entrapped water, lubricants and other compounds frequently prevent or reduce full metal contact[10]. In order to attain the maximum bond strength, it was found necessary, for example, to degrease and scratch-brush the surfaces, before applying the pressure. These treatments break up the contaminants and clean the surfaces to reveal oxide-free metal. It has been reported[11] that the bonding efficiency of prepared surfaces declines with subsequent exposure to the atmosphere.

For a strong bond to form at the interface, it is vital that there should be complete contact between the mating surfaces and in order to achieve this condition, the application of a high stress is necessary to cause interpenetration of the surface asperites. For example, a pressure of about four times the shear yield stress of some copper specimens at about 450^{o}F is required to weld the specimens together effectively[12].

When pressure is applied, the metals at the interface normally undergo plastic straining before any strong bond is formed. The greater the strain, the larger is the area of contact between clean, virgin metals and the greater the dispersion of surface contaminants. Thus reports of bond

strength equal to that of the weaker parent metal were published[13]. In order for bonding to occur, a critical threshold deformation has to be exceeded below which no bonding takes place because even with prepared surfaces (that is degreased and scratch-brushed), sufficient interfacial movement must first bring freshly exposed surfaces into intimate contact[14]. The so-called threshold value for deformation varies from metal to metal, for example, with copper and aluminium at room temperature, the values are approximately 45% and 40% respectively, while these reductions had to be raised to 60% and 50% in rolling in order to achieve a bond strength equal to that of the weaker parent metal[15].

The factors discussed give an insight into the conditions which must be met if a strong interfacial bond is required of bimetal tubes drawn on a mandrel or a floating plug. It is possible to degrease the tubes and scratch-brush the surfaces but even with a close pass, the amount of pressure and deformation required to produce a strong interfacial bond can hardly be realised in practice in a single pass. It is, however, possible to achieve the high reductions mentioned earlier by having successive passes. The first pass can be designed to bring the component tubes into intimate mechanical contact breaking-up the surface contaminants and preventing exposure to the surrounding environment. Using successive passes, these surfaces are drawn under as high a pressure as is achieveable with the process. The number of passes required depends on the reactivity of the constituent metals, the strain, and the type of draw process.

1.4. Other Bimetal Forming Processes

1.4.1. Tube on Rod Drawing

Experiments on the drawing of composite rod were made by Atkins and Cartwright[90] in 1931 with the objective of studying the flow of metal in its passage through the die.

The process of drawing tube on rod was studied in depth in 1975 by Chia and Sansome[16] who developed a theory using the equilibrium approach. In their theory, an expression for the draw stress was derived with the assumptions that thin-walled tubes were used and the dies had small die semi-angles. To accommodate redundant work, a redundant work factor was included in the final expression.

1.4.2. Bimetal Strip Drawing

Weinstein and Pawelski[17] conducted experiments in the plane strain drawing of sandwich metals. The analysis was based upon nearly homogeneous straining and a theory was developed for the prediction of draw stress and mean die pressure. The sandwich metals used in their experiments were copper/steel/copper strips and steel/copper/steel strips. Slip line results for plane strain indentation were used to approximate for the effects of redundant straining.

1.4.3. Extrusion - Conventional and Hydrostatic

Conventional extrusion techniques normally incorporate

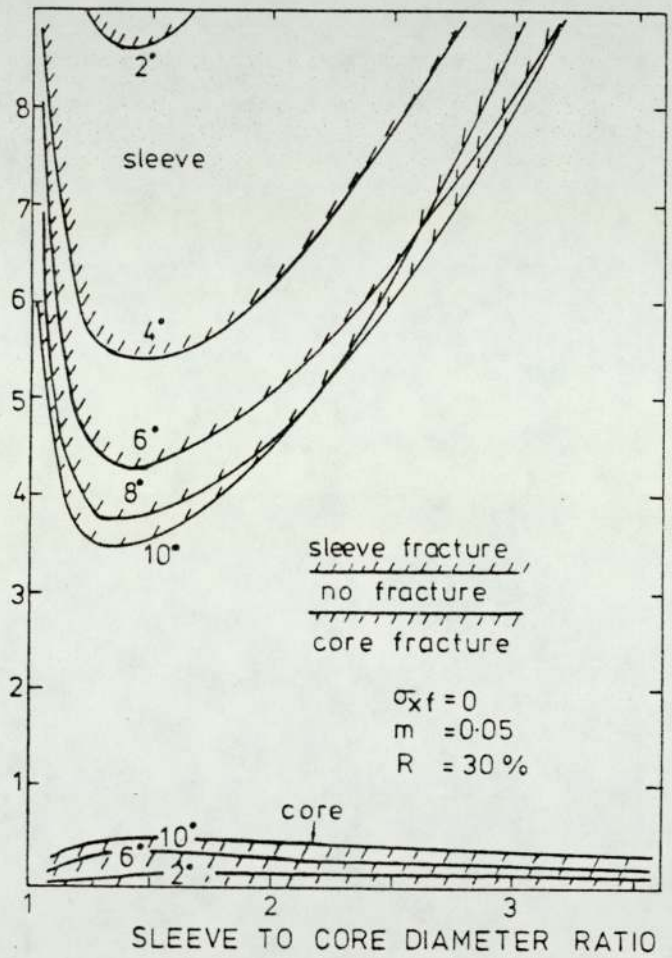

FIGURE 1.1 CRITERION FOR SOUND FLOW IN THE CONVENTIONAL EXTRUSION OF BIMETAL ROD (after Avitzur[89])

high levels of redundant work, and therefore higher risk of material failure. In attempts to overcome this disadvantage, hydrostatic extrusion, which results in greater homogeneity in flow has sometimes been adopted.

The conventional and hydrostatic extrusion of bimetal rod was investigated by Avitzur[18,19] and Osakada, Limb and Mellor[20] respectively. Both processes were analysed with experiments on aluminium and copper combinations. Osakada et al restricted their work to the consideration of a system in which hard core (copper) was always encased in a soft aluminium sleeve whereas Avitzur interchanged the two metals using them, in turn, as either the sleeve or core material.

Both Avitzur and Osakada et al defined zones of possible reduction. In view of the small angles (2° to 10°) employed by Avitzur in his analysis, the effect of the friction factor, m, obviously becomes significant. An illustration of the zones of possible reduction as proposed by Avitzur is given in Figure (1.1).

A general conclusion drawn by Osakada et al is that the hard core will not fail if $fY_c > (1-f) Y_s$ (where f is core volume fraction, Y_c and Y_s are the yield stresses of core and sleeve respectively), provided that the point of intersection of the interfaces does not lie on the central axis of the core. In their analysis large values of interfacial friction

factor, m, were considered, a situation which could very well exist in the case of implosively welded tube. It is interesting to note that in the extrusion of an unwelded tube on rod combination, carried out by Osakada et al, it was in fact the low interfacial shear that contributed to the tensile fracture of the material.

Further research on this topic was undertaken by Niimi and Osakada[21] who used an energy method to obtain an upper bound for the extrusion pressure. A generalized expression for the radial flow field was proposed and the theoretical results were found to be in good agreement with those obtained from the hydrostatic extrusion of aluminium, copper and aluminium-copper composite billets.

Alexander and Hartley[22] employed the finite element method for the analysis of the hydrostatic extrusion of copper covered aluminium rod. A conical interface was chosen as the initial interfacial shape and the final profile differed only slightly from this assumption. Due to the complexity of the finite element technique, the utilisation of computerised iterative procedure was necessary in order to obtain a solution.

In attempts to predict the pressure required to extrude composite billets of two dissimilar metals during cold axi-symmetric extrusion, Holloway et al[23] analysed the process using the following three different techniques:-

(i) the empirical relationship $P = \bar{Y}(a + b \ln R)$ where $\bar{Y}$ is

the mean flow stress

(ii) Avitzur's Upper Bound approach which consisted of a spherical velocity field at entry and exit.

(iii) Semi-empirical method of Johnson and Mellor utilising a system of velocity discontinuities predicted by a plane strain analysis.

In comparing their calculated results with those obtained from experiments, it was found that technique (iii) provided the best prediction of the three techniques applied.

The extrusion of bimetallic strip from separate containers was investigated by Alexander and Whitlock[24]. Attempts were made to predict the deformation and hence to determine the interfacial pressures at the interface. In their analysis, slip-line field solutions were developed and Plasticine was extruded in a Perspex model of the extrusion container to simulate the extrusion process.

1.4.4 Rolling of Sandwiched Materials

The fact that the separating force may be reduced by rolling a hard metal sandwiched between layers of softer metal has been appreciated for many years. One of the early reports of reduction in roll separating force had been that of Pomp and Lueg[91], who hot rolled mild steel sandwiched between layers of copper. Since difficulties have been experienced in the conventional rolling of thin hard metal in an ordinary two high mill and there is a limit of minimum gauge at which the latter process is feasible - most of

the difficulties were overcome by rolling the hard metal or the thin hard strip sandwiched between layers of relatively softer materials. The sandwich rolling process has been examined by a number of investigators[25,27] and in most of the investigations, in order to simplify the analysis, one of the two following hypothesis is usually postulated:

a) The Equal Stress Hypothesis

This hypothesis assumes that the layers of sandwich materials are subjected to equal stresses but different strains. The equivalent strain is given by:

$$\varepsilon_e = B\varepsilon_c + (1 - B)\,\varepsilon_m$$

where ε_e is the equivalent strain

ε_c is the strain in the clad

ε_m is the strain in the matrix

and B is the proportion of clad in the sandwich.

b) The Equal Strain Hypothesis

In this case, it may be assumed that the layers of sandwich materials undergo the same strain, that is, the sandwich layers deform plastically together. The modified or equivalent yield stress of the sandwich material is given by:

$$Y_e = B\,Y_c + (1 - B)\,Y_m \qquad (1.1)$$

where Y_e is the modified or equivalent yield stress

Y_c is the yield stress of the clad

Y_m is the yield stress of the matrix

B is the proportion of clad in the bimetal combination

Similar expressions have been derived by Arkulis[4] for the deformation of composite metals and Gulyaev and Rakov[29] for the rolling of bimetals. Davies[30] tested both hypotheses while he conducted experiments in the plane strain compression of sandwich metals. It was found that the equivalent yield stress obtained by assuming equal strains in the sandwich layers agreed more closely with the measured values.

The equal strain hypothesis was adopted by Holmes[31] in his analysis of the rolling of composite metals and later, by Arnold and Whitton[25] in sandwich rolling. The latter authors derived an expression for the equivalent yield stress in the form:

$$Y_e = \frac{h_c Y_c + h_m Y_m}{h_c + h_m} \qquad (1.2)$$

where h_c is the clad thickness

h_m is half the matrix thickness

In fact, equation (1.1) is the same as equation (1.2) when

$$B = \frac{h_c}{h_c + h_m} \text{ in equation (1.1)}$$

The same authors performed rolling tests with titanium alloy sheet sandwiched between layers of copper, or brass, or mild steel. Reductions in roll separating force of up to 60% were reported, the greatest reduction was achieved

when the softest clad was used.

The work of Arnold and Whitton was extended by Atkins and Weinstein[26] who made allowance for work hardening effects. The application of clad deformation to the rolling of "difficult to work" materials and the extrusion of complex shapes through circular dies were also discussed in their publication. Afonja and Sansome[27,28] further investigated the rolling of sandwich metals by attempting to predict the roll separating force. In their analysis, these authors found that the magnitude of the shear stress at the clad-matrix interface depended on the relative proportion of clad and matrix combination, the reduction achieved, the yield stresses of the component metals and the friction at the roll-clad interface. The effect of the proportion of clad thickness, B, on the shear stress at the clad-matrix interface, τ_m, is shown in Figure 1.2. It can be seen that τ_m attains a maximum value for an optimum value of B. According to Afonja and Sansome, this optimum value of B lies between 0.5 and $0.5(1 + \frac{\tau_c}{(K_m - K_c)\theta_c})$,

where τ_c is the shear stress at the roll-clad interface,

K_m is the mean yield stress of the matrix,

K_c is the mean yield stress of the clad,

θ_c is the angle of bite

In his experiments on plane strain compression tests, Davies[30] reported that the optimum value of B was 0.55 and Arnold and Whitton suggested a value of 0.66 for cold rolling.

As it is possible to obtain a maximum value of shear stress at the strip interface for a particular set of physical and geometrical process parameters, it is equally possible that a maximum reduction in roll separating force could be obtained for an optimum combination of these parameters. This was observed by Arnold and Whitton, and Afonja and Sansome.

Experiments were initiated by Hawkins and Wright[32] in 1972 to examine the tensile, pressforming and plane strain compression properties of roll bonded combinations of copper and mild steel. The equal strain hypothesis was used in their attempt to predict the stress-strain characteristics of symmetrical and asymmetrical sandwiched sheet in tension well into the useful plastic deformation range. These authors reported in their publication that it was not conclusive from their work whether the limiting draw ratios of composites may be predicted by the equal strain hypothesis. Further, three factors were suggested to explain the existence of an optimum clad to core thickness ratio for a given reduction in rolling which were reported by previous workers such as Alexander[24] Atkins and Weinstein[26].

1.4.5. Indentation of Bimetallic Strip

Although the Watts and Ford type of plane strain compression test has proved to be successful in the determination of the stress-strain characteristic of monometals, the same procedure has, however, been inadequate for tests on bimetal combinations. Thus, other methods of determiningthe stress-strain characteristics for bimetal combinations were investigated.

The indentation of bimetal combinations was investigated by several workers and among the notable investigations are those of Boyarshinov[33], Agers[34], Rychewski[35], Arkulis[4] and Arcisz[36]. Generalized solutions for the case of a curvilinear punch used in the indentation of bimetal combinations were proposed by Druyanov[37] and then later by Sokolovski[39]. In 1960, Druyanov[38] analysed the process and presented a solution for a medium with continuous plastic inhomogeneity.

In his investigation of the indentation of bimetal combinations, Arcisz[36] performed the experiments with rigid punches applied on rigid perfectly-plastic material. Good approximations were obtained from an expression proposed for the estimation of the force required for the process and the range of the validity of the solution was also derived. Basically, the Riemann method of integrating equations was used to obtain the solution. To augment his findings, Arcisz found a velocity field and slip lines for the process.

In 1965, Davies[30] investigated the plane strain compression of copper strip, sandwiched between two layers of aluminium. He reported a 30% reduction in load when the aluminium was bonded to the copper strip but the load was reduced by only 20% with unbonded cladding. It was found that for reductions exceeding 11%, there exists an optimum thickness of aluminium cladding (55%) for which the deformation load is a minimum. From these results, he concluded that the choice of cladding thickness is important in sandwich rolling and that the coefficient of friction at the clad-matrix interface should be high to achieve high reductions in load.

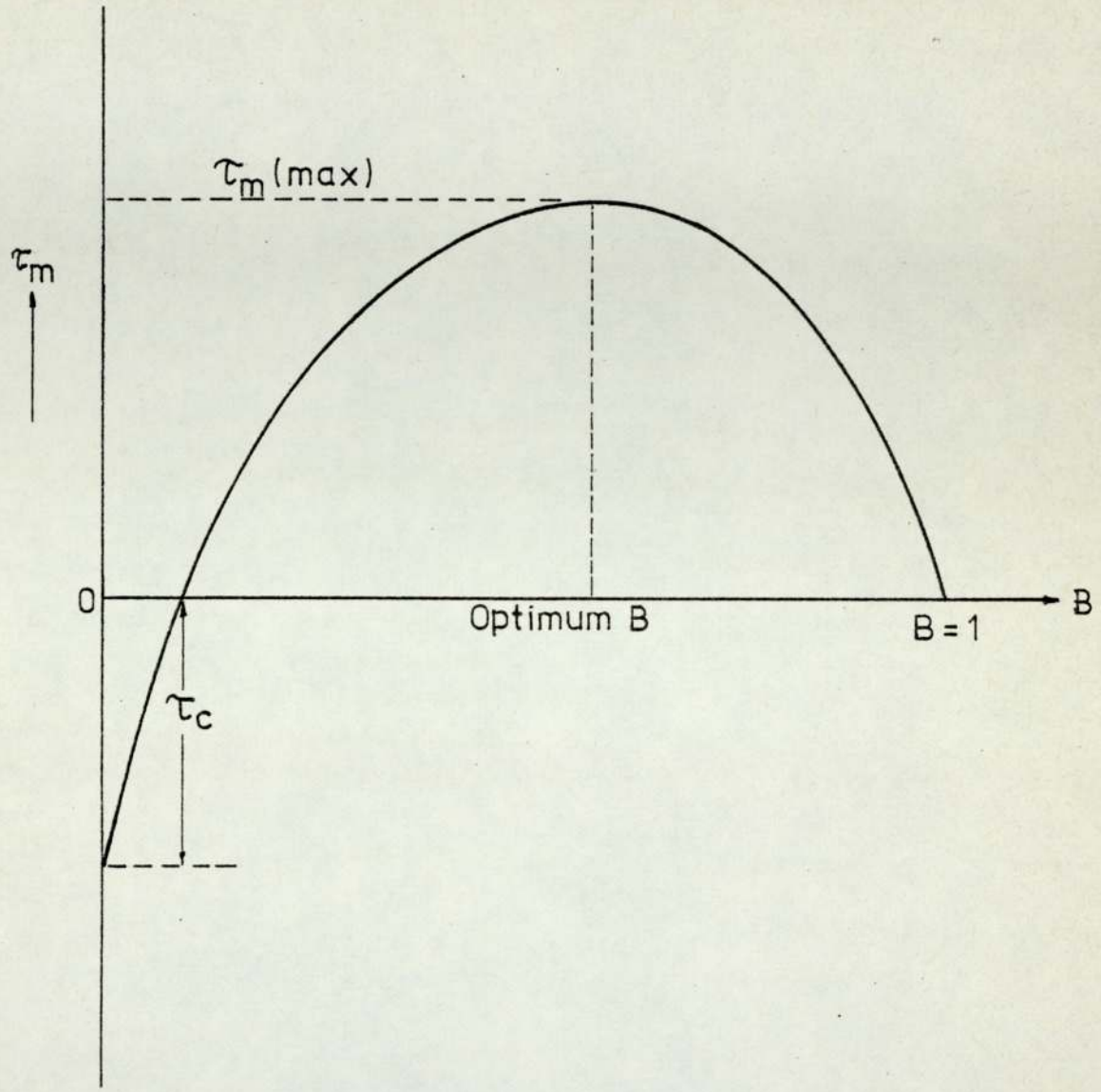

Fig. 1.2 Variation of the interfacial shear stress with the clad-sandwich thickness ratio in sandwich rolling.

(after Afonja & Sansome[28])

1.5 Monometal Drawing

The drawing of metals is an ancient process since non-ferrous wires were first drawn in the days of the Egyptian Pharoahs. Perhaps, the first elementary discussions of wire drawing were provided by Smith[40] and Musiol[41]. Later, authors like Lewis[42], Elder[43], Horsburgh[44], Thompson and Francis[45] began treating the process quantitatively. In 1927, Sachs using the equilibrium approach, proposed a theory which proved to be the most important among the early theories on wire drawing. Later, Korber and Eichinger[46], Davis and Dokos[47], and Lunt and MacLellan[48] refined and improved his theory. Nevertheless, the first really extensive experimental and theoretical investigation of the mechanics of this process was made by Wistreich[49], who considered the effect of back-pull[50]. Comprehensive critiques of the work of other investigators could be found in papers published by Wistreich[51] and MacLellan[52]. Other theories worth noting are one by Shield[53] for flow through a converging channel and another by Avitzur[54], who employed the upper-bound technique in his study of the mechanics of wire drawing.

Analyses of tube drawing in terms of sinking, fixed plug drawing and mandrel drawing have been undertaken by Sachs and his collaborators. Of particular interest in tube sinking is the work done by Sachs and Baldwin[55], complemented by Swift[56] and Chung and Swift[57]. The latter authors produced expressions for the prediction of draw stress and the

final tube wall thickness in tube sinking. The mandrel tube drawing process was investigated by Sachs, Lubahn and Tracy[58], and Espey and Sachs[59] in separate studies. A short account of the expressions for draw stress derived by Sachs, Lubahn and Tracy[58] is given in the Appendix. Problems associated with tube drawing on a fixed plug were also examined by Sachs[60].

Basically, all these theories proposed by Sachs and his collaborators were for stress determination and include frictional but not redundant effects. In all cases, stress distribution across the tube wall was assumed to remain constant which only applies to thin-walled tubing. However, Avitzur[54] proposed an upper bound solution for the sinking process, incorporating an assessment of redundancy. A more general method of accounting for the effect of redundancy was proposed by Cole and Blazynski[61,62] in their investigation of the sinking, mandrel and fixed plug drawing process. The method, a modification of the Hill and Tupper's concept of equivalent total mean strain, relies on a partly theoretical and partly empirical approach. The same method was applied again when Blazynski[63] analysed mandrel drawing in tandem with back-pull. Green[64] proposed a correction for redundant work in tube drawing basing his work on the analogy between strip drawing and close-pass tube drawing assuming conditions of plane strain. However, Green's approach cannot, of course apply to conditions developing in a sinking operation.

A tube-drawing process which involves a considerable amount of sink is the floating plug drawing operation. The floating-plug-drawing process had been studied by, among others, Schneider and Piwowerski[65] who, in addition to their own contribution, based on the equilibrium approach, reviewed the work of a number of Soviet investigators. Recently, a more detailed study of the mechanics of the floating plug process was reported by Smith and Bramley[66] who employed the upper bound approach and incorporated effects of redundancy. The upper bound limit analysis proposed was an adaptation of Johnson's method for representing velocity discontinuities and hodographs. To obtain a value of draw stress for any given reduction using this theory, the use of a digital computer is necessary.

As detailed derivation of the expressions for the various tube drawing processes, using the equilibrium approach, can be found in standard texts such as that by Rowe[67], no attempt will be made to reproduce the same work here.

1.6 Die Pressure and Coefficient of Friction

1.6.1 Split Die Method

In 1952, MacLellan[68] used the split die technique to ascertain the mean die pressure in his experiments in wire drawing. The die was in two halves and the forces, tending to separate the two halves were measured concurrently with the drawing force. The coefficient of friction between the die and the wire was assumed constant and an expression was

proposed to estimate its value using the draw force, die-splitting force and the die semi-angle, all of which could be obtained from experiments.

Later, Wistreich[51] using the same technique and with the aid of sophisticated equipment succeeded in measuring accurate values of coefficient of friction. In his experiments, Wistreich drew lightly drawn electrolytic copper wire and recorded values of coefficient of friction between 0.02 and 0.03. He found that the coefficient of friction did not vary significantly with the die pressure and if all other parameters were kept the same, the greater the friction, the lower was the value of die pressure measured. It is interesting to note that for certain combinations of die angle and reduction, Wistreich obtained die pressures which greatly exceeded the values of yield stress of the material used in the tests.

The split die method was improved by Yang and later modified by Major, who simplified the procedure. However, calibration of the die is still a problem but it should be mentioned that this method of measuring the die pressure gives accurate values of the coefficient of friction.

1.6.2 Oscillating Die Method

In 1965, Moore and Wallace[69] developed a torsionally oscillating die to determine the coefficient of friction in their tube sinking experiments. With this technique, it was found that the calibration of the equipment used in the experi-

ment was considerably simpler than that required by the split die method. In oscillating the die, inertia problems arose and it was deemed necessary to rotate the die continuously to eliminate these problems.

1.6.3 Die Rotation Method

It has been known for quite a long time that by rotating the die, it is possible to draw with a lower value of draw load. In 1931, Greenwood and Thomson, and Linicus and Sachs, all used the rotating die method to determine the coefficient of friction between wire and die in wire drawing experiments. The die rotation method was also used by Nishihara, Kakuzen and Nakamura in 1955 to draw wires. Later, this technique was investigated by Rothman and Sansome[70] with experiments in drawing rods through a rotating die. A theory was proposed by these authors to explain the reduction in draw load when the die was rotated and hence the difference used to calculate the coefficient of friction between the rod and the die. It is noted that this method of calculating the coefficient of friction is not accurate at high rotational speed due to the condition produced at high speed. For example, Hofsten, and Linstrand have reported temperature increases of approximately 25% as compared with a stationary die. The rotating die technique was also used by Chia in his bimetal tube drawing experiments and was shown to produce reasonable and reliable results.

1.7 Upper-Bound Solutions of Axisymmetric Forming Problems

Perhaps, the first successful use of assumed velocity fields for predicting the mean pressure when extruding round bar was that of Johnson and Kudo[71]. A year later, Kudo[72] extended his concept of a "unit deforming region" for plane strain to the solution of axisymmetric problems. He introduced conical surfaces as discontinuity surfaces in the cylindrical deforming region in order to obtain an upper bound solution for average forming pressures. The resulting velocity field proposed by Kudo, however, was found to yield better solutions over only a limited range of conditions when compared with that obtained by the simple uniform velocity field.

Further improvement to Kudo's work was proposed by Kobayashi[73,74] who also considered the plane strain drawing of wires and thin-walled tubes. He proposed that it is possible to assume a series of deformation patterns given in Figure (1.4) for axisymmetric cases. In 1965, Halling and Mitchell[76] showed how to extend the idea of the simple plane strain hodograph proposed by Johnson[75] to axisymmetric extrusion through conical dies. Their physical plane diagram and hodograph are shown in Figure (1.3).

Material AB undergoes a tangential velocity discontinuity parallel to AB, i.e. ab in the hodograph and proceeds thereafter parallel to the die face. Its velocity increases as AC is approached and on encountering AC, a velocity discontinuity ca is imposed and the material emerges parallel to the extrusion axis.

Adie and Alexander[77] extended the applicability

and usefulness of Halling and Mitchell's approach to various complicated forms of extruded products, e.g. rod-can and tube-can. The same approach was applied to axisymmetric forming problems by Smith and Bramley[66] in their investigation of the floating plug tube drawing process. Recently, Islam[7] using the same idea, successfully proposed a velocity field for the drawing of bimetal tube on a fixed plug.

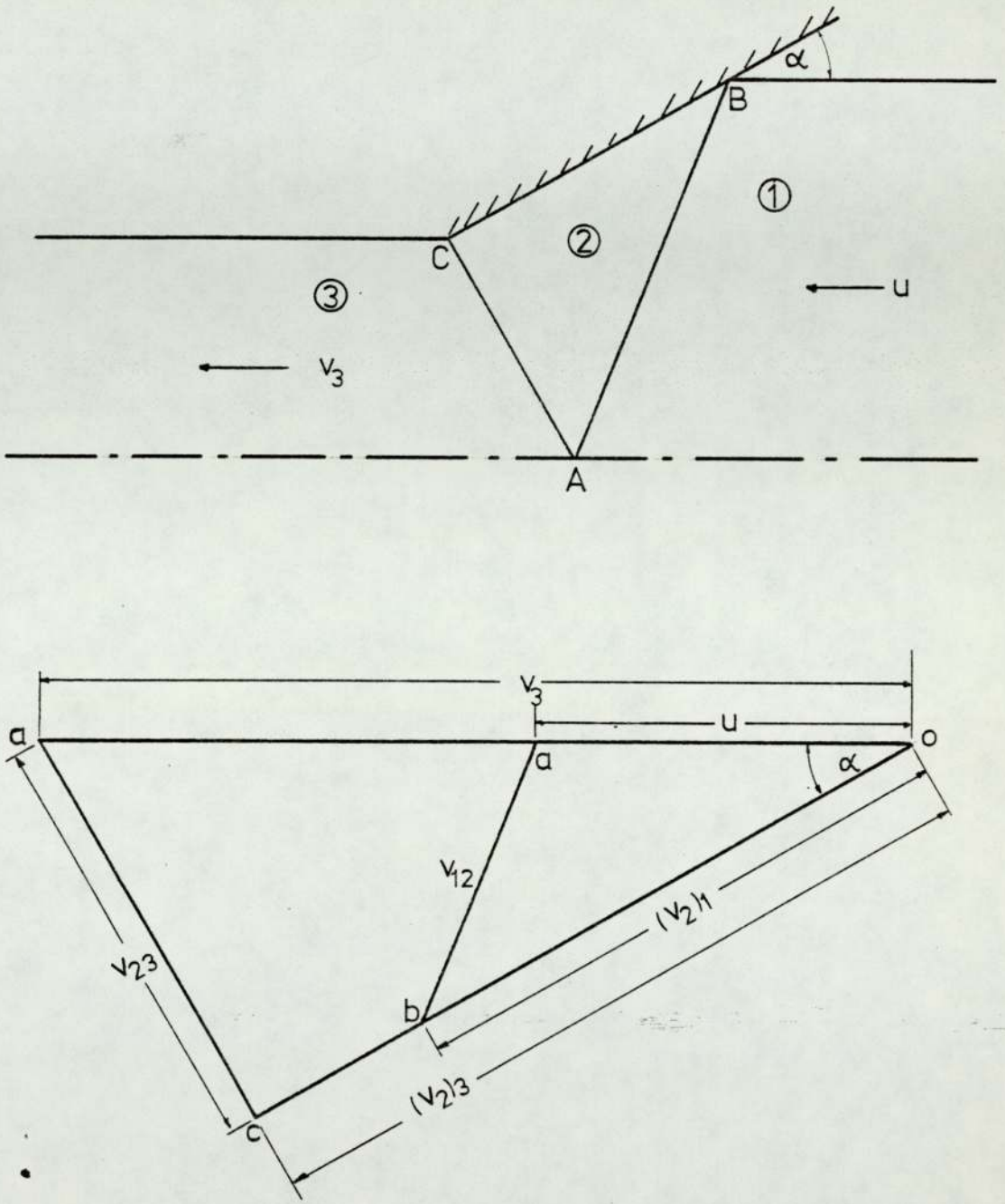

Fig. (1.3) VELOCITY DISCONTINUITY PATTERN
AND HODOGRAPH FOR AXISYMMETRIC EXTRUSION
(after Halling and Mitchell)

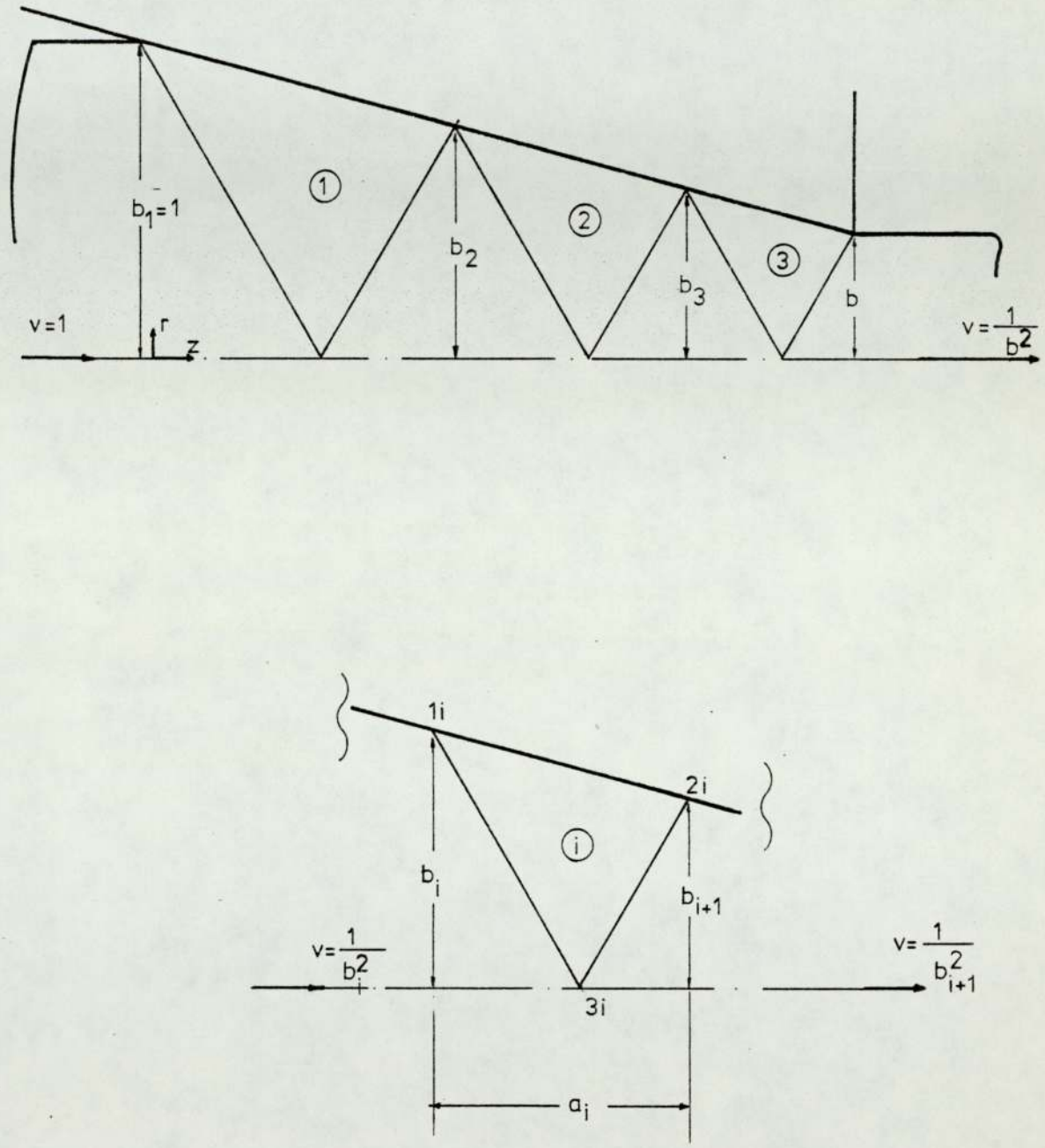

Figure 1.4 ASSUMED VELOCITY FIELD FOR FLOW THROUGH CONICAL DIES (n = 3)
(after KOBAYASHI[74])

Chapter Two

THEORETICAL STUDY OF BIMETAL TUBE DRAWING

with (a) a Mandrel
and (b) a Floating Plug

2.1. Introduction

As suggested by the heading above, this chapter will be devoted to the theoretical analysis of the mechanics of bimetal tube drawing with a mandrel or with a floating plug. Mathematical models are developed to predict the draw load or tag load required to reduce a given combination of bimetal tube by a chosen reduction in cross-sectional area. Two separate mathematical models are built to analyse the bimetal tube mandrel drawing process. One of the models is based on the equilibrium approach while the other is an energy method. For the bimetal tube floating plug drawing process, a mathematical model is developed employing an energy approach. In order to verify these theories, experiments are conducted with specimens of bimetal tubes of different combinations of metal. The equipment and experimental technique used in the tests are described in Chapter 3. In Chapter 4, the experimental results and the theoretical results are compared.

2.2. Theoretical Analysis of the Drawing of Bi-metal Tube on a Mandrel using the Equilibrium Approach

In the following analysis, the following assumptions are made:

a) The materials used are rigid-plastic and hence no work-hardening effect is assumed.

b) The tubes used have thin walls, i.e. the diameter to thickness ratio is greater than 20.

c) The draws are close pass, that is having a negligible amount of sinking.

d) The axial and radial stresses are uniformly distributed and principal stresses.

e) It is assumed that the coefficients of friction involved are less than 0.1, which commonly occurs in cold drawing.

f) The die semi-angle is small and using a conical die it is assumed that the die surface and the clad-matrix interface converge towards an arbitary point of intersection.

g) The die has zero land.

h) The two tubes are in intimate contact, i.e. there is no space at the interface.

The drawing of a bi-metal tube on a mandrel assuming close pass drawing is effectively a plane strain drawing process. A mean yield stress is used to account for the strain hardening effect of the tube materials.

Figure 2.1. shows a cross-sectional view of an element of bimetal tube on a mandrel being drawn through a conical die. In Figure 2.2, a more detailed diagram of the stresses acting is shown.

Summing the horizontal forces acting on the mandrel, for equilibrium:

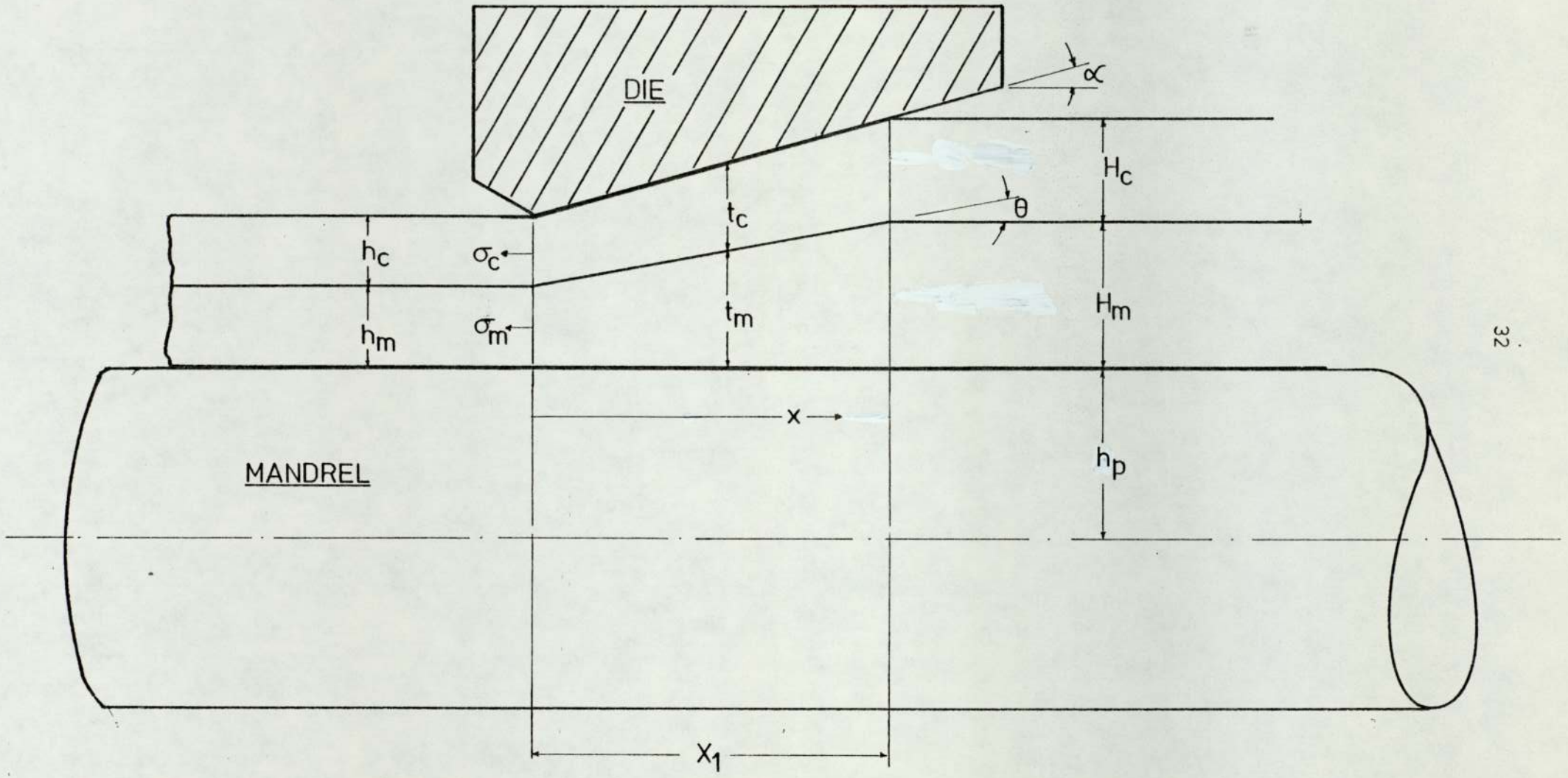

Figure 2.1 CLOSE-PASS BIMETAL TUBE DRAWING ON A MANDREL

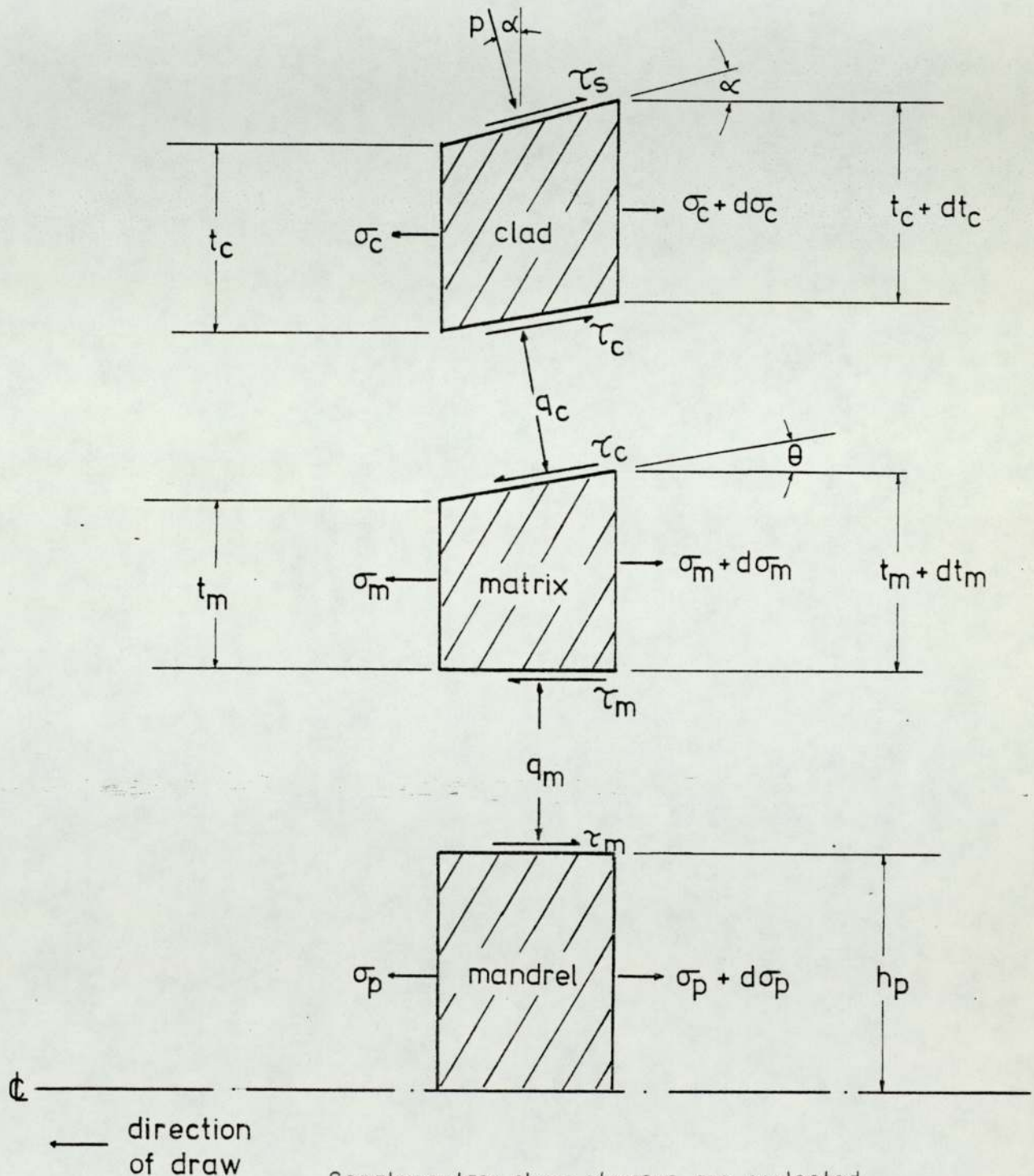

Figure 2.2 An Element of BIMETAL TUBE drawn on a mandrel through a conical die. (hard matrix)

$$(\sigma_p + d\sigma_p)\pi h_p^2 + \tau_m 2\pi h_p . dx - \sigma_p \pi h_p^2 = 0 \qquad (2.1)$$

Similarly, considering the equilibrium of the outer tube and for a large diameter to thickness ratio, this gives:

$$- \sigma_c . 2\pi (t_m + h_p) h_c + (\sigma_c + d\sigma_c) . 2\pi (h_p + t_m + dt_m) (t_c + dt_c)$$

$$- q_c 2\pi (t_m + h_p) \tan\theta \, dx + p . 2\pi (t_c + t_m + h_p) \tan\alpha dx$$

$$+ \tau_s 2\pi (t_c + t_m + h_p) dx + \tau_c 2\pi (h_p + t_m) dx = 0 \qquad (2.2)$$

With the same assumptions, the equilibrium of the inner tube gives:

$$(\sigma_m + d\sigma_m) . 2\pi h_p (t_m + dt_m) - \sigma_m . 2\pi h_p t_m - \tau_m 2\pi h_p dx$$

$$- \tau_c 2\pi (t_m + h_p) dx + q_c 2\pi (t_m + h_p) \tan\theta . dx = 0 \qquad (2.3)$$

Simplifying equations (2.1), (2.2) and (2.3), the equations become:

$$\frac{d\sigma_p}{dx} + \frac{2\tau_m}{h_p} = 0 \qquad (2.4)$$

$$\frac{d(\sigma_c t_m t_c)}{dx} + \frac{h_p \, d(\sigma_c t_c)}{dx} + \tau_c (t_m + h_p)$$

$$- q_c (t_m + h_p) \tan\theta + p(t_c + t_m + h_p) \tan\alpha + \tau_s (t_c + t_m + h_p)$$

$$= 0 \qquad (2.5)$$

$$h_p \frac{d(\sigma_m t_m)}{dx} - \tau_m h_p - \tau_c (t_m + h_p) + q_c (t_m + h_p) \tan\theta = 0 \qquad (2.6)$$

Considering the equilibrium of the outer tube in the radial direction:

$$p = \tau_s \tan\alpha - \tau_c \frac{\sin\theta}{\cos\alpha} + q_c \frac{\cos\theta}{\cos\alpha} \qquad (2.7)$$

Similarly for the inner tube, equilibrium in the radial direction gives:

$$q_c = \frac{q_m}{\cos\theta} + \tau_c \tan\theta \qquad (2.8)$$

If the contribution of friction to the die pressure is assumed to be small and as thin-walled tubes and dies with small semi-angles are used, it is reasonable to write equations (2.7) and (2.8) as:

$$p \simeq q_c \simeq q_m$$

since angle θ is likely to be small when angle α is small.

From figure 2.1, $$X_1 = \frac{H_c + H_m - h_c - h_m}{\tan\alpha} \qquad (2.9)$$

$$\tan\theta = \frac{H_m - h_m}{X_1} \qquad (2.10)$$

$$t_m = h_m + x\tan\theta \qquad (2.11)$$

$$t_c + t_m = h_c + h_m + x\tan\alpha \qquad (2.12)$$

Equation (2.12) minus equation (2.11) gives:

$$t_c = h_c + x(\tan\alpha - \tan\theta) \qquad (2.13)$$

but from equation (2.11): $x = \frac{t_m - h_m}{\tan\theta}$

$$\therefore\ t_c = h_c + \frac{(t_m - h_m)}{\tan\theta}(\tan\alpha - \tan\theta) \qquad (2.14)$$

It can also be written as: $t_m = h_m + \frac{(t_c - h_c)\tan\theta}{\tan\alpha - \tan\theta}$

Differentiation of equation (2.11) with respect to x gives: $\frac{dt_m}{dx} = \tan\theta$ for a given value of h_m.

Similarly, differentiation of equation (2.13) gives:

$\frac{dt_c}{dx} = \tan\alpha - \tan\theta$ for a given value of h_c.

Using Tresca'a Yield Criterion:

$$\sigma_c + q_c = Y_c$$

and:

$$\sigma_m + q_c = Y_m$$

By subtraction: $\sigma_c - \sigma_m = Y_c - Y_m$ (2.18)

If this relationship is to be maintained throughout the deformation, the axial gradients of these stresses may be written as:

$$\frac{d\sigma_c}{dx} = \frac{d\sigma_m}{dx}$$

This assumes either a constant mean value for Y_c or Y_m, or that the work-hardening rates of the two materials are equal, i.e.

$$\frac{dY_c}{dx} = \frac{dY_m}{dx}$$

Substituting these values into equation (2.5) and simplfying gives:

$$\frac{d\sigma_c}{dx} = \frac{1}{t_c}\left(Y_c\tan\theta - \sigma_c\tan\alpha - \frac{\sigma_c t_c \tan\theta}{t_m + h_p} - p\left[\frac{t_c}{t_m + h_p} + 1\right]\tan\alpha - \tau_s\left[\frac{t_c}{t_m + h_p} + 1\right] - \tau_c\right) \quad (2.16)$$

Similarly for equation (2.6):

$$\frac{d\sigma_m}{dx} = \frac{1}{t_m}\left(-\sigma_m\tan\theta + \tau_m + \tau_c\left[\frac{t_m + h_p}{h_p}\right] - q_c\frac{(t_m + h_p)}{h_p}\tan\theta\right) \quad (2.17)$$

Equating equation (2.16) to (2.17) and simplifying:

$$\tau_c = \left(\frac{t_c\, t_m\, h_p}{(t_m\, h_p + t_c\, h_p + t_c\, t_m)}\right)\left(\frac{\sigma_m}{t_m}\tan\theta + \frac{Y_c}{t_c}\tan\theta - \frac{\sigma_c}{t_c}\right.$$

$$- \frac{\sigma_c \tan\theta}{t_m + h_p} - p\left[\frac{1}{t_m + h_p} + \frac{1}{t_c}\right]\tan\alpha - \tau_s\left[\frac{1}{t_m + h_p} + \frac{1}{t_c}\right]$$

$$\left. - \frac{\tau_m}{t_m} + q_c\left[\frac{1}{t_m} + \frac{1}{h_p}\right]\tan\theta\right) \qquad (2.18)$$

Substituting for $dx = \frac{dt_m}{\tan\theta}$ and τ_c (from equation (2.18) in equation (2.16) and letting $\tau_m = \mu_m p$ and $\tau_s = \mu_s p$, on simplification gives:

$$\frac{d\sigma_m}{dt_m} = \frac{1}{\tan\theta}\left(\frac{1}{(t_c\, t_m + (t_c + t_m)\, h_p)}\right) - \sigma_m\, h_p \tan\theta - Y_c\left[(t_m + h_p)\tan\alpha\right.$$

$$+ (t_c - t_m - h_p)\tan\theta\Big] + \Big[Y_m - \sigma_m\Big]\Big[(t_c - t_m - h_p)\tan\theta$$

$$\left. - t_c \tan\alpha + \mu_m h_p - \mu_s(t_c + t_m + h_p)\right]\Big) \qquad (2.19)$$

Substituting for $\tau_m = \mu_m p$ and $dx = \frac{dt_m}{\tan\theta}$ into equation (2.4) and re-arranging, gives: $\frac{d\sigma_p}{dt_m} = -\frac{2\mu_m(Y_m - \sigma_m)}{h_p \tan\theta}$ (2.20)

By letting $\tau_s = \mu_s p$ and substituting for $p = Y_c - \sigma_c$ and putting $dx = \frac{dt_m}{\tan\theta}$ equation (2.16) gives:

$$\frac{d\sigma_c}{dt_m} = \frac{1}{t_c \tan\theta}\left(Y_c \tan\theta - \sigma_c \tan\alpha - \frac{\sigma_c\, t_c \tan\theta}{t_m + h_p} - \left[Y_c - \sigma_c\right]\right.$$

$$\left.\left|\frac{t_c}{t_m + h_p} + 1\right|\left|\tan\alpha + \mu_s\right| - \tau_c\right), \qquad (2.21)$$

where τ_c in equation (2.21) is obtained from equation (2.18) with the σ_m term on the right hand side of equation (2.18),

$\sigma_m = Y_m - Y_c + \sigma_c$

By substituting for t_c, from equation (2.14), in equations

(2.19) and (2.21), these two equations each become an ordinary differential equation. Due to recurring terms, it is not possible to integrate either of these equations (2.19) and (2.21) completely using the integrating factor method. However, the three equations (2.19) to (2.21) can be integrated as a system of ordinary differential equations using a numerical method. σ_m, σ_p and σ_c are integrated between limits of zero and σ_m, σ_p and σ_c respectively while t_m is integrated between H_m and h_m. However, before a bimetal tube is drawn, the value of h_m, the final matrix thickness is not known and thus the value of $\tan\theta$ in equation (2.19) is also an unknown. In attempts to determine the final matrix thickness, h_m, for a given reduction in area and given initial thicknesses of clad and matrix, it was decided to show how the interfacial shear stress, the die pressure and draw load varies with incremental values of h_m for a given reduction in area. A Fortran programme was written for the integration of equations (2.19), (2.20) and (2.21). The numerical integration is done with the aid of a NAG library subroutine D02ABF which is called up in the main programme during the computation process. The results are shown in Figures 4.06 to 4.16 .

Analysis of these results did not yield any evidence that either the interfacial shear stress or the die pressure or draw load can be used to ascertain the final thickness of the clad or the matrix. As this analysis was not based on an energy method, it is not possible to determine the final thickness of the matrix by a criterion of minimum work done.

Nevertheless, if it is assumed that the proportion of clad thickness remains constant before and after a given reduction, then the final clad thickness, h_c = K x final

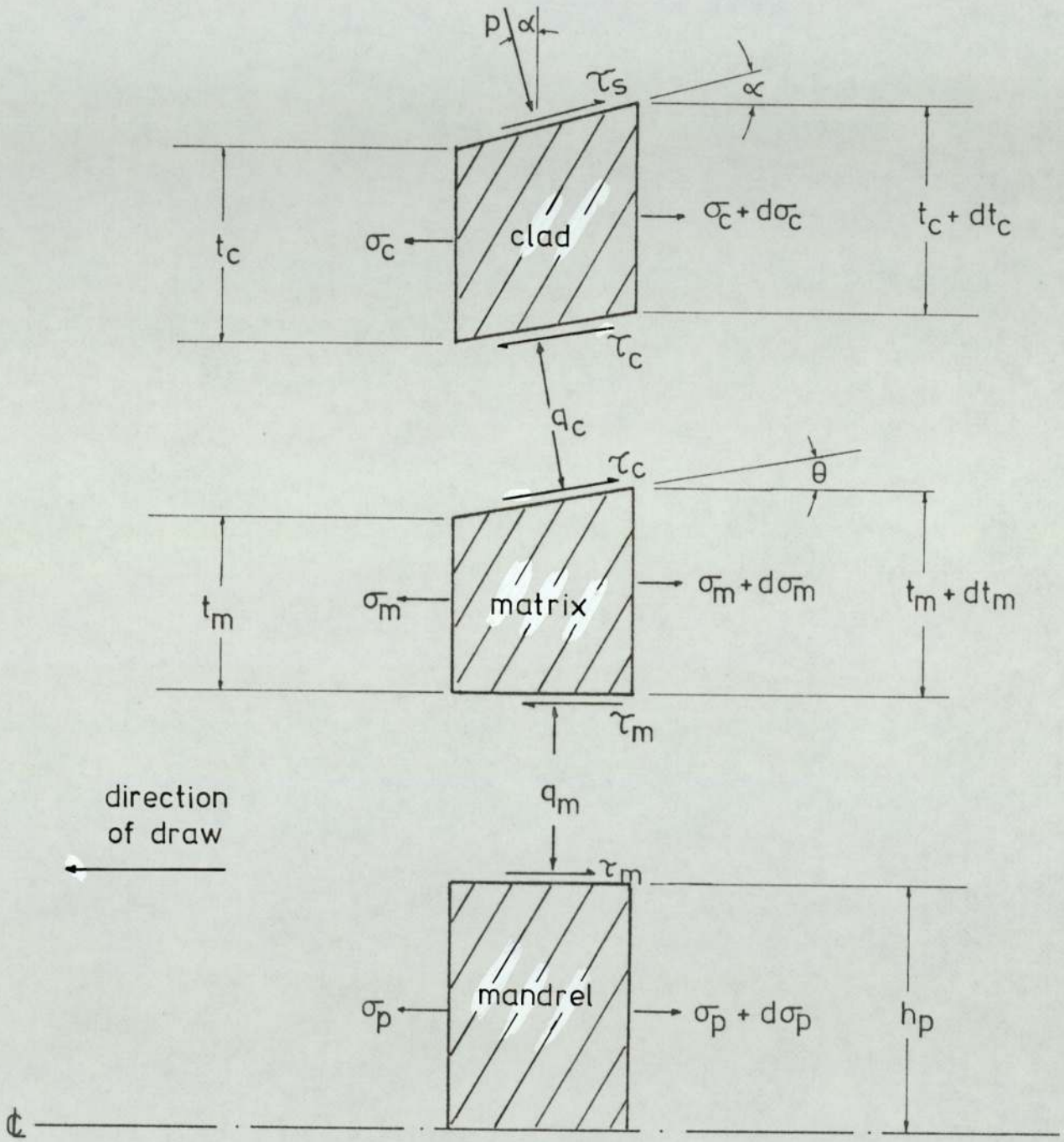

Figure 2.3 An Element of BIMETAL TUBE drawn on a mandrel through a conical die. (soft matrix)

bimetal tube wall thickness where $K = \frac{H_c}{H_c + H_m}$. The final matrix thickness, h_m is given by: (Final bimetal tube thickness - h_c). Using this value of h_m, it would then be possible to compute the draw stress for a given reduction in area.

For a hard clad and soft matrix combination, the interfacial shear stress, τ_c obtained from equation (2.18) would give a negative value, since τ_c on the clad in figure (2.2) is assumed to act upstream. With this configuration, the matrix is assumed to flow relatively slower than the clad. Thus, the clad shears on the matrix in a direction similar to the clad shearing on the die. On the other hand, if it is a hard clad and soft matrix combination, the interfacial shear stress τ_c is as shown in Figure (2.3). In this case, because of the harder clad, the direction of τ_c on the matrix is the same as the direction of τ_s on the clad. Although the interfacial shear stress, τ_c changes in direction, equations (2.19) and (2.21) are not affected. This is due to τ_c being obtained by equating $d\sigma_c$ to $d\sigma_m$ and substituting into the individual equations to obtain (2.19) and (2.21).

Integration of the equations (2.19) to (2.21) gives values of σ_c, σ_m and σ_p.

$$\text{Draw Load} = \sigma_c A_c + \sigma_m A_m + \sigma_p A_p$$

where A_c = final cross sectional area of clad,

A_m = final cross sectional area of matrix, and

A_p = cross sectional area of mandrel.

$$\text{Mean Draw Stress, } \sigma_x = \frac{\text{Draw load}}{A_c + A_m}$$

$$\frac{\sigma_x}{Y_e} = \frac{\text{Draw load}}{Y_e \times (A_c + A_m)}$$

where Y_e is the modified or equivalent yield stress for the bimetal tube.

A computer programme named "MANDREL" was written in the Fortran Language to do all the above-mentioned calculations. The NAG library subroutine D02ABF was called upon in the main programme for the numerical integration of the ordinary differential equations (2.19) to (2.21). The numerical method used is basically a combination of Merson's method and the Runge Kutta method for initial values problems. Except for the value of h_m, μ_s and μ_m, all the values in equations (2.19) and (2.21) can be easily obtained from the geometry of the die and the tubes.

The coefficient of friction in conventional drawing processes can be determined using any one of the four methods listed here:

1) Rotating Die method
2) Torsionally Oscillating Die method
3) Split Die method and
4) Pin Die Load Cell method

Due to the simplicity of instrumentation and availability of equipment and the reliability of the method, the rotating die method was used for the present investigation.

2.3. Determination of coefficients of friction for bi-metal tube drawing on a mandrel

The forces acting on the bi-metal tube and mandrel are shown in Figure (2.4). Considering the bi-metal tube as a free body and equating the forces acting horizontally:

$$S + F_2 - P \sin\alpha - F_1 \cos\alpha = 0 \qquad (2.22)$$

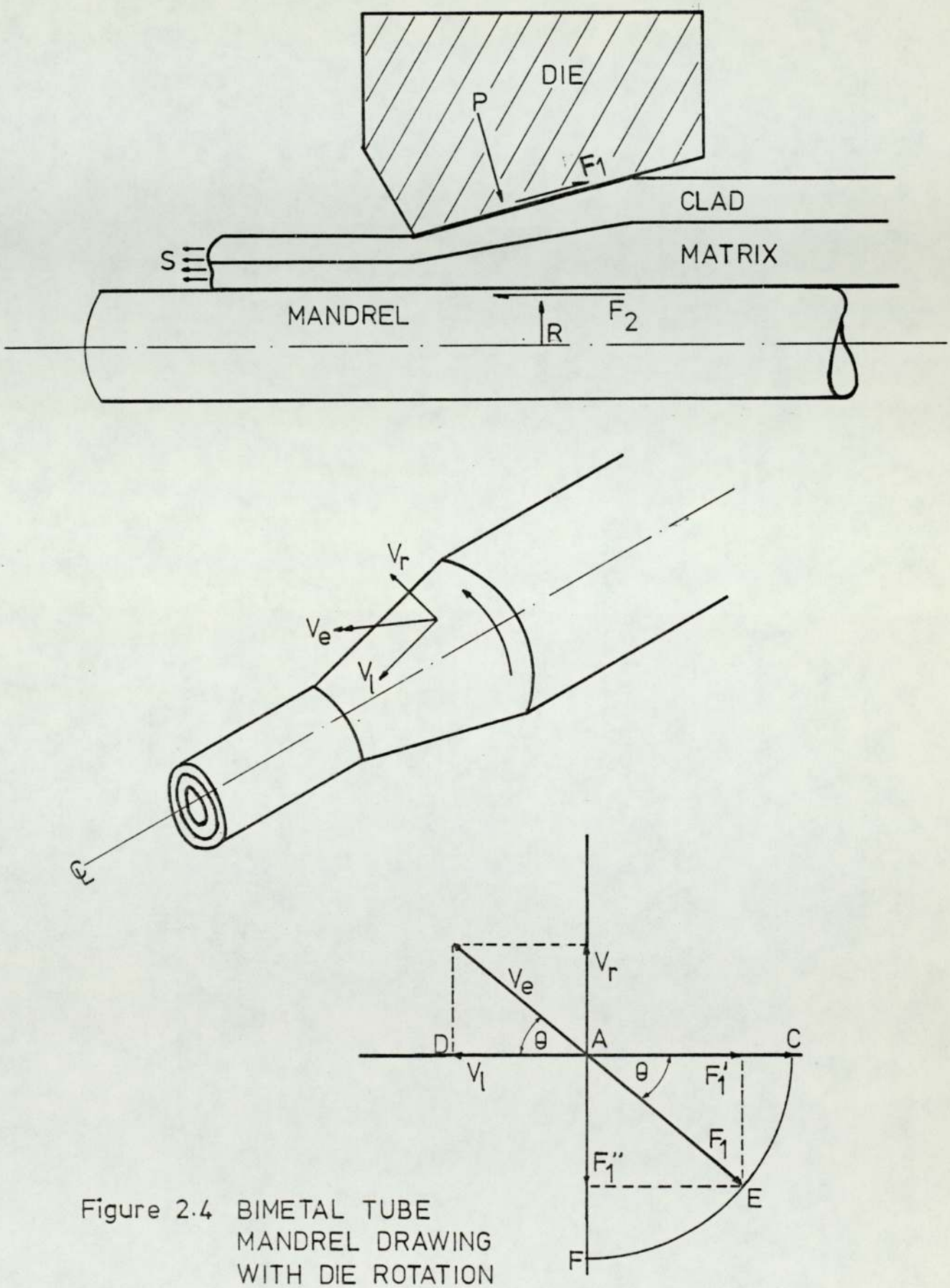

Figure 2.4 BIMETAL TUBE MANDREL DRAWING WITH DIE ROTATION

When the die rotates, assuming that the magnitude of the frictional force remains unchanged and the die pressure remains very nearly the same, the friction vector between the die and the outer tube swings through an angle θ. This is illustrated in figure (2.4) which can be constructed if the draw speed and the speed of rotation of the die are known. In this figure the friction vector without die rotation is shown as AC and on rotation of the die, it swings to position AE. Hence, when the die is rotating, the frictional force in the longitudinal direction changes from F_1 to F_1' giving a reduction of F_1-F_1' in this direction. As a result, the draw load in the axial direction is reduced by $(F_1-F_1')\cos\alpha$.

Rewriting equation (2.22) and equating it to the draw load or tag load: $D = S + F_2 = P\sin\alpha + F_1\cos\alpha$ (2.23)

With the die rotating, this equation becomes:

$$D' = S' + F_2 = P\sin\alpha + F_1' \cos\alpha \qquad (2.24)$$

where $F_1' = F_1 \cos\theta$.

Therefore equation (2.24) is:

$$D' = P\sin\alpha + F_1 \cos\theta\cos\alpha \qquad (2.25)$$

Subtracting equation (2.25) from (2.23) gives:

$$D-D' = (F_1-F_1\cos\theta)\cos\alpha$$

$$\therefore \quad F_1 = \frac{D - D'}{(1-\cos\theta)\cos\alpha}$$

and $$P = \frac{D\cos\theta - D'}{(\cos\theta-1)\sin\alpha}$$

Coefficient of friction between die and bimetal tube:

$$\mu_s = \frac{F_1}{P}$$

$$\mu_s = \frac{(D-D')\tan\alpha}{D'-D\cos\theta} \qquad (2.26)$$

From equation (2.23)

$$F_2 = D-S$$

Equating for radial equilibrium:

$$R = \frac{(D\cos\theta - D')\cot\alpha + (D-D')\tan\alpha}{\cos\alpha - 1}$$

Coefficient of friction between bi-metal tube and mandrel:

$$\mu_m = \frac{F_2}{R}$$

$$\mu_m = \frac{(D-S)(\cos\theta-1)}{(D\cos\theta-D')\cot\alpha + (D-D')\tan\alpha} \qquad (2.27)$$

The values of D, D' were measured by the draw load cell and in order to obtain S, strain gauges were placed on the outer tube of the drawn bi-metal tube. Assuming that the strain on the outer tube, inner tube and mandrel are the same at the position of the strain gauges on the bi-metal tube,

$$\frac{\sigma_c}{E_c} = \frac{\sigma_m}{E_m} = \frac{\sigma_p}{E_p} = e_c$$

$$D = \sigma_m A_m + \sigma_c A_c + \sigma_p A_p \qquad (2.28)$$

where σ_p and A_p are the stress and cross-sectional area of the mandrel respectively.

Since $S = \sigma_m A_m + \sigma_c A_c$

and $F_2 = \sigma_p A_p$

For a given draw, S is obtained by calibrating the strain gauge without the mandrel after each experiment for the same value of strain e_c. Thus, the value of F_2 can be deduced from $F_2 = D-S$.

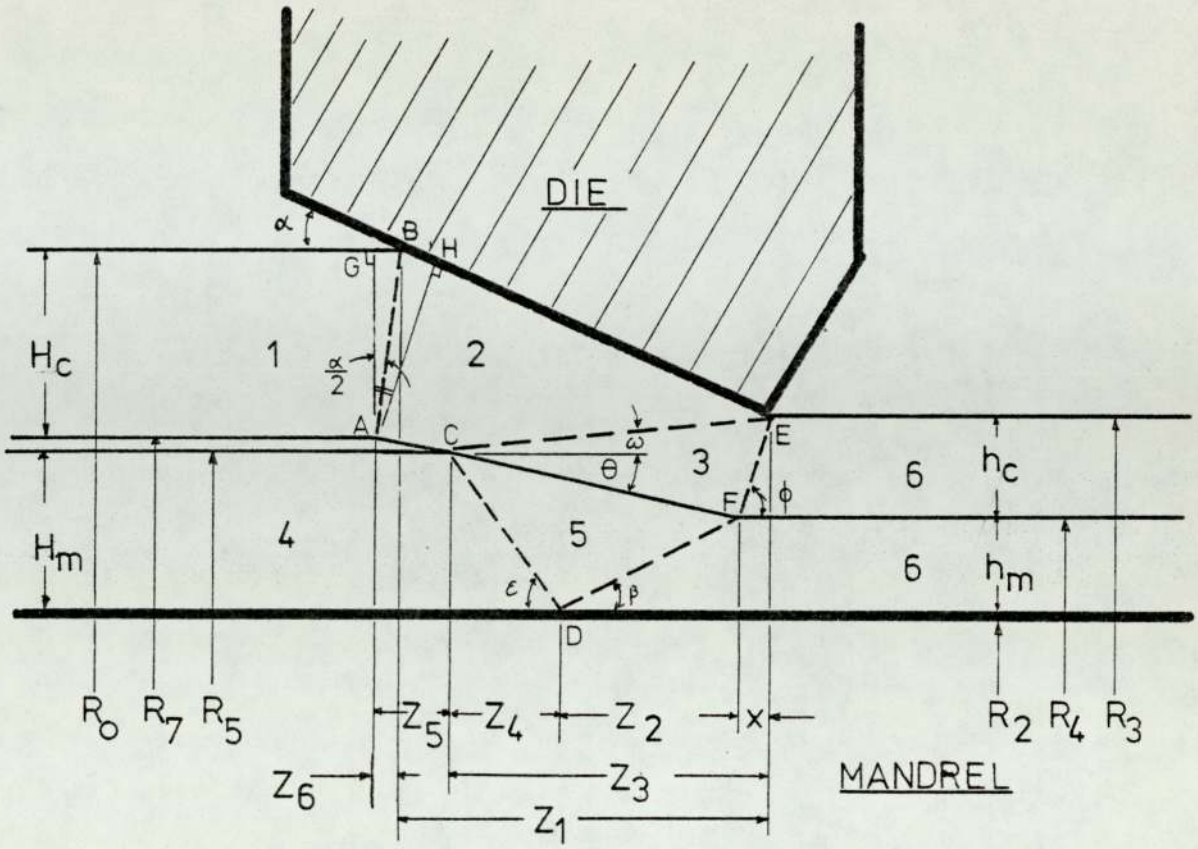

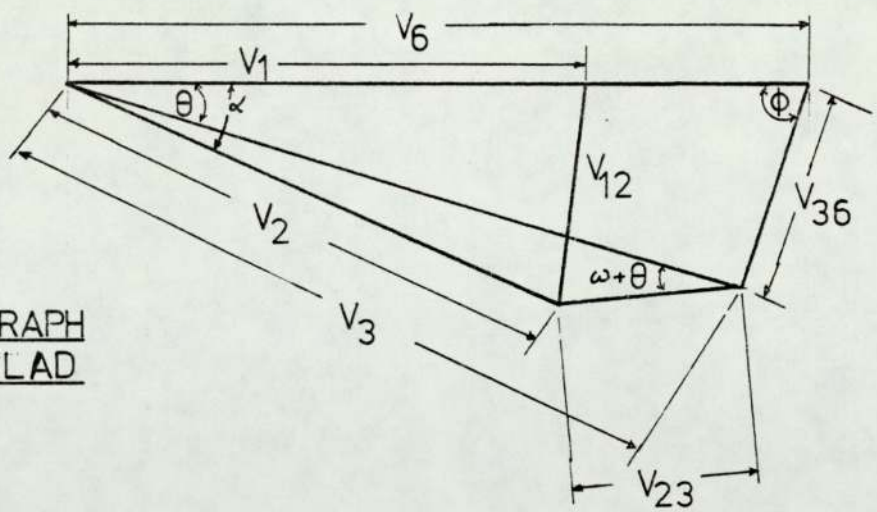

HODOGRAPH FOR CLAD

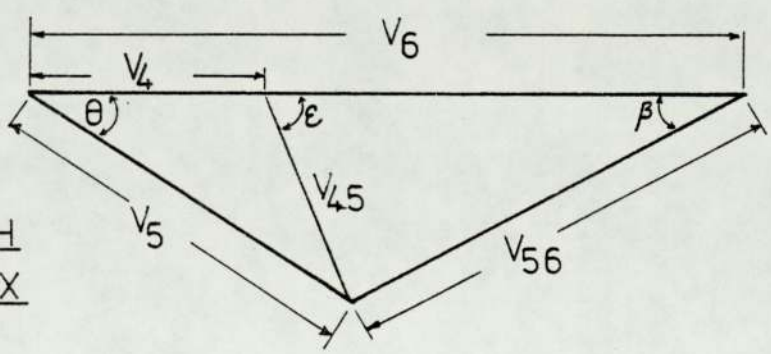

HODOGRAPH FOR MATRIX

Fig. 2.5 VELOCITY FIELD AND HODOGRAPHS BIMETAL TUBE MANDREL DRAWING

2.4 Theoretical Analysis of the Drawing of Bimetal Tube on a Mandrel - An Upper Bound Approach

2.4.1 Introduction

Drucker, Greenberg, and Prager[81] described the technique of calculating upper-bounds and lower-bounds for the load in a given forming operation. One of the theorems that these authors employ states that if a velocity field can be found, for which the rate of work due to the deforming load exceeds the rate of internal energy dissipation, this calculated deformation load would not be sustained above the critical value. According to Prager and Hodge[82], the upper-bound theorem for a Von Mises' perfectly plastic material is given as : " Among all kinematically admissible strain rate fields, the actual one minimizes the expression :-

$$J^* = \frac{2}{\sqrt{3}} \sigma_o \sqrt{\tfrac{1}{2}\dot{\varepsilon}_{ij}\dot{\varepsilon}_{ij}}\, dv + \int_{S_r} \tau |\Delta V| dS - \int_{S_1} T_i . V_i . dS \quad "$$

Hill derived a similar theorem based on his maximum work-rate principle, which can be stated as follows :

$$Lu \leqslant \int_v \bar{\sigma}\dot{\bar{\varepsilon}} dv + \int_S \tau_s . V dS \qquad (2.29)$$

where L is the true forming load

u is the forming velocity

$\dot{\bar{\varepsilon}}$ is the effective strain rate in an element of volume dv

V is the relative slip along the surface S

τ_s is the shearing stress

$\bar{\sigma}$ is the effective or representative stress

Johnson[84] proposed a simplified slip-line field, composed of a series of straight lines along which the velocity discontinuities act. The deforming metal moves between these velocity discontinuities as a rigid body and Johnson sets the first integral of the right-hand side of equation (2.29) to zero giving :-

$$\dot{W}_p = \int_S \tau_s V dS \qquad (2.30)$$

The best solution is that particular configuration of slip lines which gives the minimum load. However, the best solution in an upper bound solution may not necessarily be the actual solution in experiments because all plastic flow energies are nonconservative processes.

2.4.2 The Upper Bound Analysis

In the following analysis, the close-pass drawing of thin-walled bimetal tubes on a mandrel is assumed. Thus, the conditions of deformation would be considered to be those of plane strain. It is assumed that rigid perfectly plastic materials are used and the dies have minimum land.

Adopting Johnson's proposal of using straight lines as velocity discontinuities, a kinematically admissible velocity field and its corresponding hodographs are proposed for the bimetal tube combination. Hodographs for the clad and matrix have been drawn separately to give clearer diagrams. The velocity field and hodographs are illustrated in figure (2.5).

Plastic work is dissipated by friction at the tool-tube interfaces and shearing at the clad-matrix interface. Further work is dissipated by material shearing across the velocity discontinuities. In figure (2.5), the space between the clad and matrix in regions (1) and (4) is exaggerated for analysis purposes only; in reality, this space may not exist at all. Thus, points A and C can be superposed. The material in region (2) flows parallel to the die surface. The material in regions (3) and (5) flow at an arbitrary angle θ to the drawing axis. When the clad or matrix is in region (6), both materials exit at the same speed from the die. At the interface between regions (3) and (5), there exists a velocity difference due to the difference in speed of flow between the materials in the two adjoining region.

When all the velocity discontinuites are straight lines, and in this case, the velocity along any line of velocity discontinuity is constant, it is not necessary to use the integral sign in expression (2.30). The sum of the rate of plastic working is then given by :

$$\dot{W}_p = \Sigma \tau_s V A \qquad (2.31)$$

where A is the surface area of the velocity discontinuity,

τ_s is the shear stress in pure shear.

For work against friction, the shear stress may be represented by $\tau_s = mk$ where m is a constant friction factor. Thus the rate of working across the tool-tube interfaces and the clad-matrix interface is calculated using :-

$$\dot{W} = m.k.V.A$$

The power required for the external pull for unit cross-section area is given by :

$$\sigma_x . V_6 . T$$

where T is wall thickness of the drawn tube.

By working out the terms in equation (2·31) and equating it to this expression, the draw stress can be evaluated as follows :-

$$\frac{\sigma_x}{Y_e} = \frac{1}{T.Y_e}\left\{ \frac{2.k_c.\sin\Phi\sin(\theta+\omega)\tan\frac{\alpha}{2}\,H_c}{\sin(\Phi+\theta)\,\sin(\alpha+\omega)} + \frac{k_c.(R_3-R_5)\sin\Phi\sin(\alpha-\theta)}{\sin\omega\sin(\Phi+\theta)\sin(\alpha+\omega)} \right.$$

$$+ \frac{k_c.h_c.\sin\theta}{\sin\Phi\sin(\theta+\Phi)} + \frac{k_m.H_m.\sin\theta\sin\beta}{\sin\varepsilon\sin\varepsilon\sin(\theta+\beta)}$$

$$+ \frac{k_m.h_m.\sin\theta}{\sin\beta\sin(\theta+\beta)} + \frac{m_1.k_c.(R_0-R_3)\sin\Phi\sin(\theta+\omega)}{\sin\alpha\sin(\Phi+\theta)\sin(\alpha+\omega)}$$

$$+ m_2.k_m.\left| 1 - \frac{\sin\beta\sin(\varepsilon-\theta)}{\sin\varepsilon\sin(\theta+\beta)} \right| .A_7$$

$$\left. + \frac{m_3.k_i.V_i.(R_5-R_4)}{\sin\theta} \right\} \qquad \ldots\ldots\ldots (2.32)$$

where $A_7 = Z_3 - \frac{h_m}{\tan\beta} - \frac{h_c}{\tan\Phi}$

$$\varepsilon = \text{TAN}^{-1}\left[\frac{R_5 - R_2}{Z_4}\right]$$

$$\theta = \text{TAN}^{-1}\left[\frac{R_5 - R_4}{Z_3 - x}\right] \quad \text{and} \quad x = \frac{h_c}{\tan\Phi}$$

$$Z_3 = (R_0-R_7)\tan\frac{\alpha}{2} + \frac{(R_0 - R_3)}{\tan\alpha} - \frac{(R_7-R_5)}{\tan\alpha}$$

$$\omega = \text{TAN}^{-1}\left[\frac{R_3-R_5}{Z_3}\right]$$

$$Z_4 = Z_3 - Z_2 - x \qquad \text{and} \quad Z_2 = \frac{h_m}{\tan\beta}$$

$$V_i = |V_3 - V_5|$$

$$= \left| \frac{\sin\Phi}{\sin(\Phi+\theta)} - \frac{\sin\beta}{\sin(\theta+\beta)} \right|$$

$$k_i = k_c \qquad \text{when} \quad k_c < k_m$$

and $$k_i = k_m \qquad \text{when} \quad k_m < k_c$$

Details of the derivation of equation (2.32) is given in Appendix A3. The equation for the draw stress is completely defined by the geometry of the bimetal tube, the die semi-angle, α, and the arbitrary values of R_4, Φ and β.

To compute the initial value of Φ, it is necessary to calculate the initial value of θ. The initial value of θ is given by :

$$\tan\theta = \frac{R_5 - R_4}{Z_3 - h_c \tan\theta} \qquad \text{when } \angle \text{ EFC} = 90^\circ$$

By solving this equation, we obtain

$$\tan\theta = \frac{Z_3 \pm \sqrt{Z_3^2 - 4h_c(R_5 - R_4)}}{2h_c}$$

therefore, initially,

$$\theta = \text{TAN}^{-1}\left[\frac{Z_3 \pm \sqrt{Z_3^2 - 4h_c(R_5 - R_4)}}{2h_c}\right]$$

The ± sign is chosen to keep the value of angle θ in the first quadrant i.e. less than 90° . The maximum value of angle θ is when θ approaches α, i.e. when the material flows parallel to the die surface.

By optimising for R_4, Φ and β, the minimum draw stress obtained is the upper bound solution for the reduction considered. A computer programme has been written for the above equations and minimization of the draw stress. In addition, the optimum value of R_4 gives the final wall thickness of the clad and matrix materials. The programme can be found in Appendix A6.

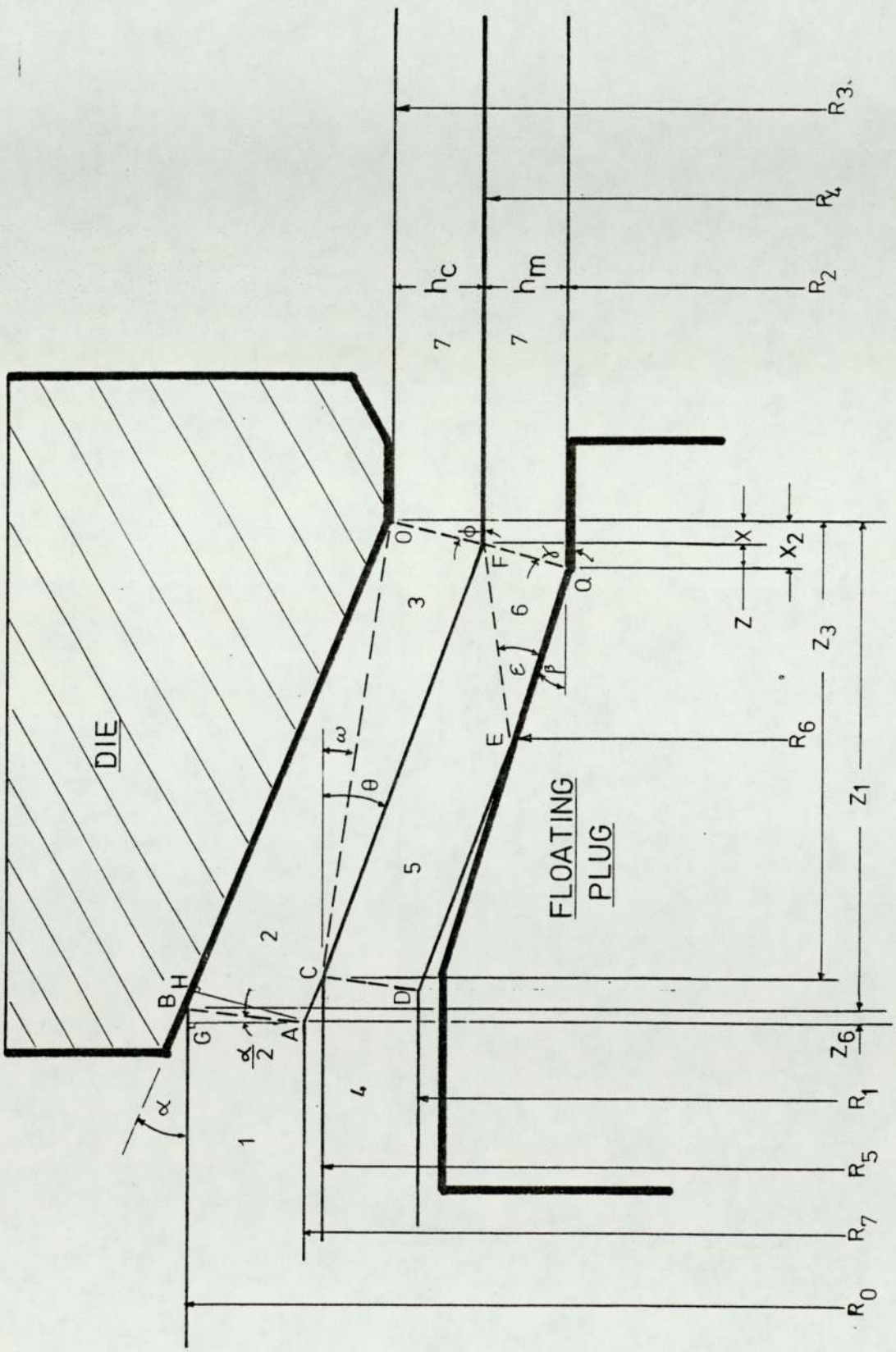

Fig. 2.6 VELOCITY FIELD FOR BIMETAL TUBE DRAWING ON A FLOATING PLUG

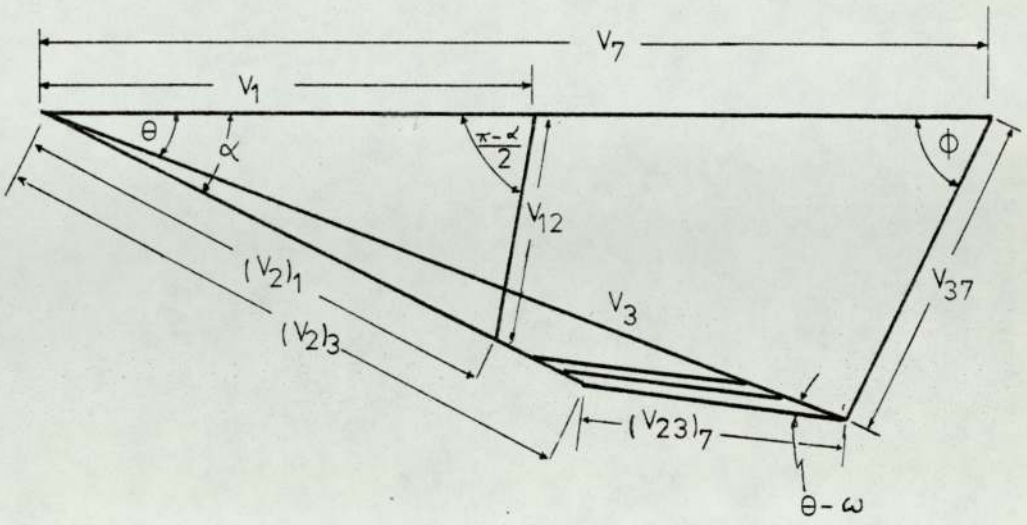

HODOGRAPH FOR CLAD

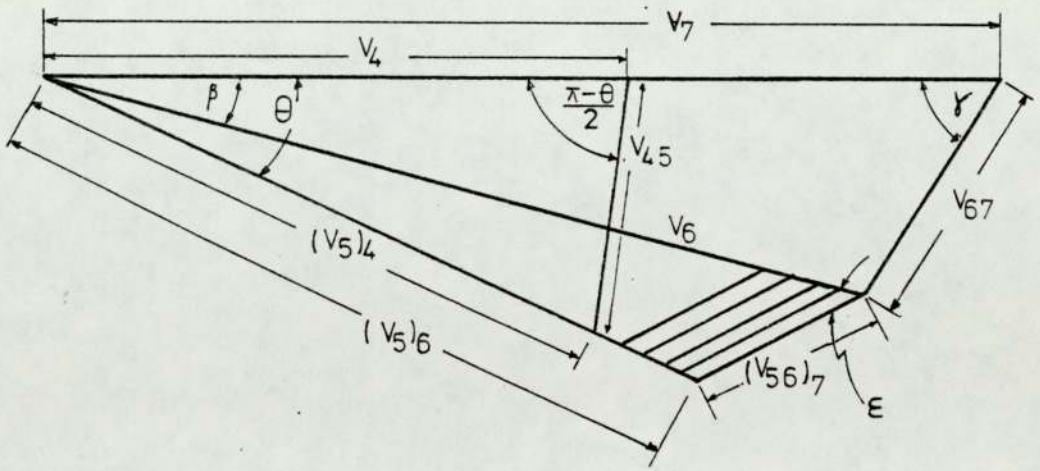

HODOGRAPH FOR MATRIX

Fig. 2.7 HODOGRAPHS FOR VELOCITY FIELD SHOWN IN Fig. 2.6

2.5. Theoretical Analysis of Bi-metal Tube Drawing on a Floating Plug - an Upper Bound Approach

In the following analysis, the materials used are assumed to be rigid perfectly plastic materials. Bearing in mind that the drawing of tube on a floating plug is an axi-symmetry drawing process, a kinematically admissible axisymmetric velocity field and its corresponding hodographs are proposed for the bi-metal combination and is shown in Figures (2.6) and (2.7). Plastic work is dissipated by friction at the tool-workpiece interfaces, by shearing across the velocity discontinuities and at the clad-matrix interface. Due to circumferential straining and thickness straining, further plastic work is dissipated in regions (2), (3), (5) and (6) causing an increase in velocity in these regions. It is assumed that no change in clad and matrix thicknesses is experienced during sinking. Also, it is assumed that the shear yield stress, $k = Y/2$ where Y is the mean yield stress obtained from Watts and Ford plane strain indentation test.

Initially, both tubes in regions (1) and (4) move in a direction parallel to the drawing axis. In region (2), the

clad material flows parallel to the die at an angle α to the drawing axis. It is assumed that the materials in regions (3) and (5) move at an arbitrary angle θ to the drawing axis and the matrix material in region (6) flows parallel to the conical portion of the floating plug. As the bi-metal tube moves into region (7), both the clad and matrix flow at the same speed and exit from the die. It is noted that in regions (2), (3), (5) and (6) the magnitude of the velocity of flow is not constant but increases because of circumferential straining. At the interface between regions (3) and (5), there exists a shearing stress due to the difference in the velocity of flow between the clad and the matrix in the adjoining region.

According to Hill's maximum work-rate principle, equation (2.29) gives:

$$Lu \leqslant \int_V \bar{\sigma}\,\dot{\bar{\varepsilon}}\,dv + \int_S \tau_s V\,dS \qquad (2.29)$$

for the rate of working across a velocity discontinuity, $\tau_s = k$, the shear stress in pure shear, and to allow for friction, the shear stress acting along a surface against friction is assumed constant and is given by: $\tau_s = m.k$.

To account for work done due to circumferential straining, the power dissipated is given by the first term on the right hand side of expression (2.29), i.e.:

$$\dot{W} = \dot{v}\,\bar{\sigma}\,\bar{\varepsilon} \qquad (3.33)$$

where $\bar{\sigma} = \sqrt{3}k$ and $\bar{\varepsilon} = \frac{2}{\sqrt{3}}\left[\varepsilon_R^2 + \varepsilon_R\varepsilon_\theta + \varepsilon_\theta^2\right]^{\frac{1}{2}}$

The hodographs shown in Figure (2.7) are associated with the velocity discontinuities in Figure 2.6. The hodographs for

the clad and matrix have been drawn separately for clarity.

The power required by the draw-dog is given by:

$$\pi(R_3^2 - R_2^2).V_7.\sigma_x \qquad (2.34)$$

By equating this expression to the sum of the powers formulated using equations (2.29), (2.33), and (2.34), the draw stress (see Appendix A4) can be evaluated from the following:

$$\frac{\sigma_x}{Y_e} = \frac{1}{[R_3^2 - R_2^2].Y_e} \left(2k_c(R_3^2 - R_4^2) \tan\frac{\alpha}{2} + \frac{2k_c R_3 |R_5 - R_3| \sin(\alpha-\theta)\sin\phi}{\sin\omega \sin(\alpha \pm \omega)\sin(\theta+\phi)} \right.$$

$$+ \frac{k_c(R_3^2 - R_4^2)\sin\theta}{\sin\phi \sin(\theta+\phi)} + 2k_m(R_4^2 - R_2^2)\tan\frac{\theta}{2}$$

$$+ \frac{2k_m R_4 |R_4 - R_6| \sin\gamma \sin(\theta-\beta)}{\sin(\gamma+\beta)\sin(\theta-\beta+\varepsilon)\sin(\varepsilon-\beta)} + \frac{k_m(R_4^2 - R_2^2)\sin\beta}{\sin\gamma \sin(\beta+\gamma)}$$

$$+ 2m_1 k_c \frac{R_o(R_o - R_3)(R_3^2 - R_4^2)}{(R_o^2 - R_2^2)\sin\alpha} + 2m_2 k_m \frac{\sin\gamma R_2(R_6 - R_2)}{\sin\beta\sin(\gamma+\beta)}$$

$$+ 2m_3.k_i \frac{R_4(R_5 - R_4)}{\sin\theta} \left| \frac{\sin\phi}{\sin(\phi+\theta)} - \frac{\sin\gamma \sin\varepsilon}{\sin(\beta+\gamma)\sin(\theta-\beta+\varepsilon)} \right|$$

$$+ 2m_1 k_c R_3 D_1 + 2m_2 k_m R_2 P_1$$

$$\left. + 2k_c(R_3^2 - R_4^2) \ln\left[\frac{R_o + R_7}{R_3 + R_4}\right] + 2k_m(R_4^2 - R_2^2) \ln\left[\frac{R_5 + R_1}{R_2 + R_4}\right] \right) \qquad (2.35)$$

where, $Z_3 = \dfrac{R_o + R_5 - R_3 - R_7}{\tan\alpha}(R_o - R_7)\tan\dfrac{\alpha}{2}$

$$\omega = \text{TAN}^{-1}\left[\frac{|R_5 - R_3|}{Z_3}\right]$$

$$\theta = \text{TAN}^{-1}\left[\frac{R_5 - R_4}{Z_3 - x}\right] \quad \text{and} \quad x = \frac{h_c}{\tan\phi}$$

$$\gamma = \text{TAN}^{-1}\left[\frac{h_m}{Z}\right] \tag{2.36}$$

$$T_1 = \frac{H_m - (h_m + x\tan\beta)\cos\theta}{\sin(\theta-\beta)} - \frac{x}{\cos\beta} \tag{2.37}$$

$$R_6 = R_2 + T_1\sin\beta$$

$$\varepsilon = \beta + \text{TAN}^{-1}\left[\frac{R_4 - R_6}{T_1\cos\beta + Z}\right]$$

In the above equations, the absolute term $|R_5 - R_3|$ takes into consideration the values of R_3 which can be greater or smaller than R_5. Full details of the derivation of equations (2.35) and (2.37) are given in the Appendix A4. Equation (2.35) is completely defined by the yield stresses of the materials, the geometry of the pass, the variables x_2, R_4 and the angle ϕ.

For the tube to be effectively drawn on the floating plug, i.e. the plug should be 'floating' in the die, the value of x_2 defining the position of the floating plug in the die must lie within a range of values which is determined by the geometry of the zone.

x_2 is given by: $x_2 = x + Z$ (2.38)

According to Bisk et al[85], Orro and Savin[86], and Bisk and Shveikin[87], and Schneider and Piwowarski[65] the minimum value of x_2 is zero. However, if x_2 is zero, the current wall thickness of the bimetal tube in the working zone of the pass, say OQ in Figure (2.6) would be less than the wall thickness of the drawn tube, which is clearly impossible when drawing on a conical plug. Nevertheless, in practice, the minimum value of x_2 is very small and may be taken to be zero.

Referring to equation (2.38), the value of x at any instant is given by: $x = h_c/\tan\phi$

and the value of Z varies between $Z = (H_m - h_m \cos\theta)/\sin\theta$ (i.e. when $T_1 = 0$) and $Z = h_m \tan\frac{\beta}{2}$ (i.e. when the plug is at the most forward position in the die). For a given value of h_c, it should be noted that x varies as a function of ϕ, and that ϕ is related to angle θ. The value of x is a minimum when ϕ is a maximum and θ a minimum. When θ is a minimum:

$$\tan\theta = \frac{R_5 - R_4}{Z_3 - h_c \tan\theta}$$

Rearranging: $h_c \tan^2\theta - Z_2 \tan\theta + (R_5 - R_4) = 0$

$$\therefore \tan\theta = \frac{Z_3 \pm \sqrt{Z_3^2 - 4.h_c.(R_5-R_4)}}{2\,h_c}$$

The $\pm$ sign is chosen accordingly to give a positive value of $\tan\theta$

$$\therefore \theta = \text{TAN}^{-1}\left[\frac{Z_3 \pm \sqrt{Z_3^2 - 4.h_c.(R_5-R_4)}}{2\,h_c}\right]$$

The maximum value of θ is when $\theta = \alpha$ i.e. the material in region (3) flows parallel to the die surface. There the value of α varies as θ changes within these limits. The miminum value of Z is $h_m \tan \beta/2$ and the maximum value of Z for a given value of θ is when $T_1 = 0$, i.e. when the floating plug is in such a backward position that there is no contact between the conical portion of the plug and the tube. It is interesting to note that as T_1 approaches zero, all the reduction in wall thickness of the tube is produced by the cylindrical land of the plug and thus the process becomes similar to mandrel drawing. However, in practice, it would be quite impossible to maintain the plug at a position where $T_1 = 0$ without any physical support. This is due to the fact that without the

tube acting on the conical portion of the plug, the frictional forces acting on the cylindrical portion of the plug would pull the plug into the die until this frictional force is balanced by the horizontal component of the die pressure acting on the conical portion of the plug. When this happens, T_1 is no longer equal to zero and the plug 'floats' in the die.

To accommodate strain hardening of the two metals, the mean yield stress value is used to obtain the value of k for each material. In these equations, the angles ϕ and γ and the radius R_4 are the arbitrary values which determine the pattern of deformation of the bimetal tube. By optimising for ϕ, γ and R_4, these equations will therefore yield a lower upper-bound solution for the drawing stress and will predict the final clad and matrix thicknesses of the bimetal tube from the value of R_4.

As most of the available mini-computer and 'desk-top' computer uses the BASIC programming language, a programme based on the BASIC language was written to minimise σ_x/Y_e and to predict the final clad and matrix thicknesses. This programme is included in the Appendix.

Chapter Three

EXPERIMENTAL TECHNIQUE AND EQUIPMENT

Detailed descriptions of the technique and equipment used in the drawing of bimetal tube with a mandrel are given of the following:-

(a) The draw bench

(b) Drawing dies and mandrel

(c) Materials of the tube-on-tube combination

(d) Load cells

(e) Calibration of Load cells

(f) Experimental procedure and technique

Figure 3.1. Draw Bench and Instrumentation

3.1 The Draw Bench

The draw bench available was originally used for the drawing of tube with ultrasonic vibrations[78]. It was later used for experiments on the drawing of bimetal tube on rod[6] and was subsequently modified for the present investigation.

The draw bench is made up of fabricated structure angled plates and a U-channel section bar which supports a 2½ in diameter hydraulic cylinder. The piston has a stroke of 25 inches and is powered by hydraulic oil supplied by a gear pump which is driven by an electric motor.

The maximum pressure of the oil supply is approximately 1200 $lbf.in^{-2}$ and the maximum draw load is about 2.0 tonf. A valve controls the speed of the piston and hence the draw speed. The maximum speed attainable is about 5.6 $ft.min^{-1}$. However, the valve markings illustrating the approximate position of the valve opening are too coarse to be used in estimating the drawing speed.

The hydraulic piston is in turn connected to a draw dog through two horizontal bars mounted on four small wheels as shown in figure (3.2). Two pairs of jaws were available and are suitable for ¼ in and ½ in diameter tubes. They are made of En33 material and were case hardened to about 0.020 in deep.

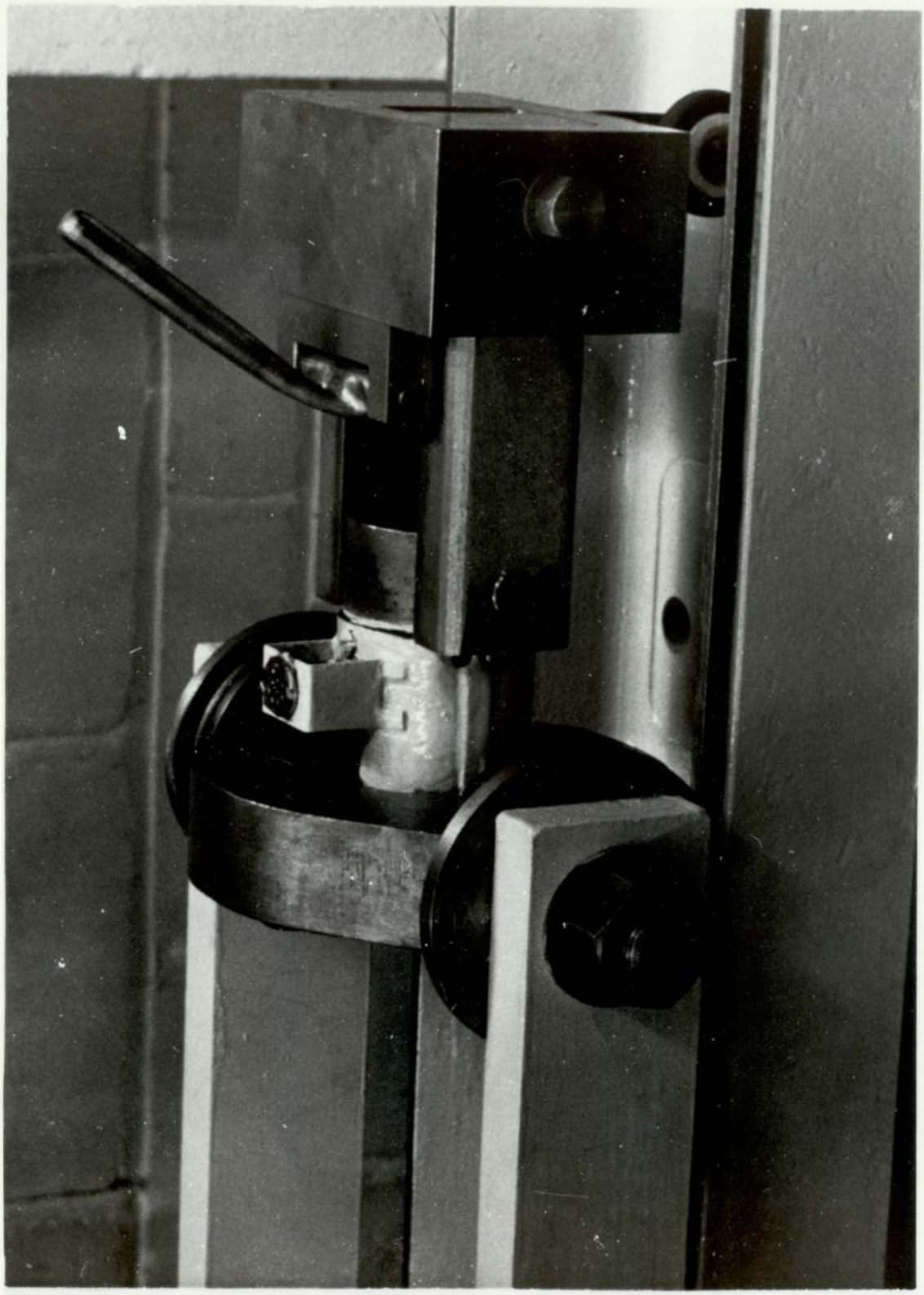

FIG. 3.2 DRAW DOG CONNECTED TO DRAW LOAD CELL

3.2. Drawing Dies and Mandrel

For reasons of economy, the dies used were those used formerly for experiments on the drawing of bimetal tube on tube with a fixed plug and bimetal tube on tube sinking [6] The dies are as shown in figure (3.3). These dies were designed for experimental purposes and thus have almost no land. The material used for the dies were UHB ARNE steel rather than the more conventional tungsten carbide, again for reasons of economy. Further, the number of tubes to be drawn with these dies were very many fewer compared with the dies used in Industry.

The Swedish-made cold work steel ARNE has the following composition:

C	Mn	Cr	W	V
0.9%	1.2%	0.5%	0.5%	0.1%

The steel was a manganese-chromium-tungsten alloy characterised by high surface hardness after tempering, good dimensional stability in hardening and good machinability.

There were 14 dies and each of them had a die semi-angle of 9° and minimum land. None of these dies was chromium-plated, all were held in mild steel holders. In order to rotate the die while the bimetal tubes were being drawn, it was necessary to mill four equal flats at right angles to each other on the die holders.

To check the profile of the dies, replicas were made using Rank-Taylor Hobson plastic replica kit, code number 112/727. Before the replicas were made, the dies were degreased with a degreasing agent and Plasticine was used to partition the die into two halves. The exit end of the die was sealed with a piece of wood and some Plasticine.

According to the instructions enclosed with the kit, the releasing agent should be smeared on to the Plasticine and the die. The viscous liquid plastic was prepared and poured immediately into one half of the die, the other half having been filled earlier with Plasticine. When the replica had set, the Plasticine was stripped from the die and the replica removed. The profile of the replica was examined under a Nikon profile projector. It was observed that there was no land on the dies and that the die semi-angle was accurate to $\pm$ 6 minutes.

The circularity of the throat of the dies was checked using a Taylor-Hobson Talyrond (model 1) machine. The actual size of the die was checked using a Universal measuring machine with a feeler-gauge attachment. Table 3.1 gives the list of dies available for the bimetal tube mandrel drawing experiments.

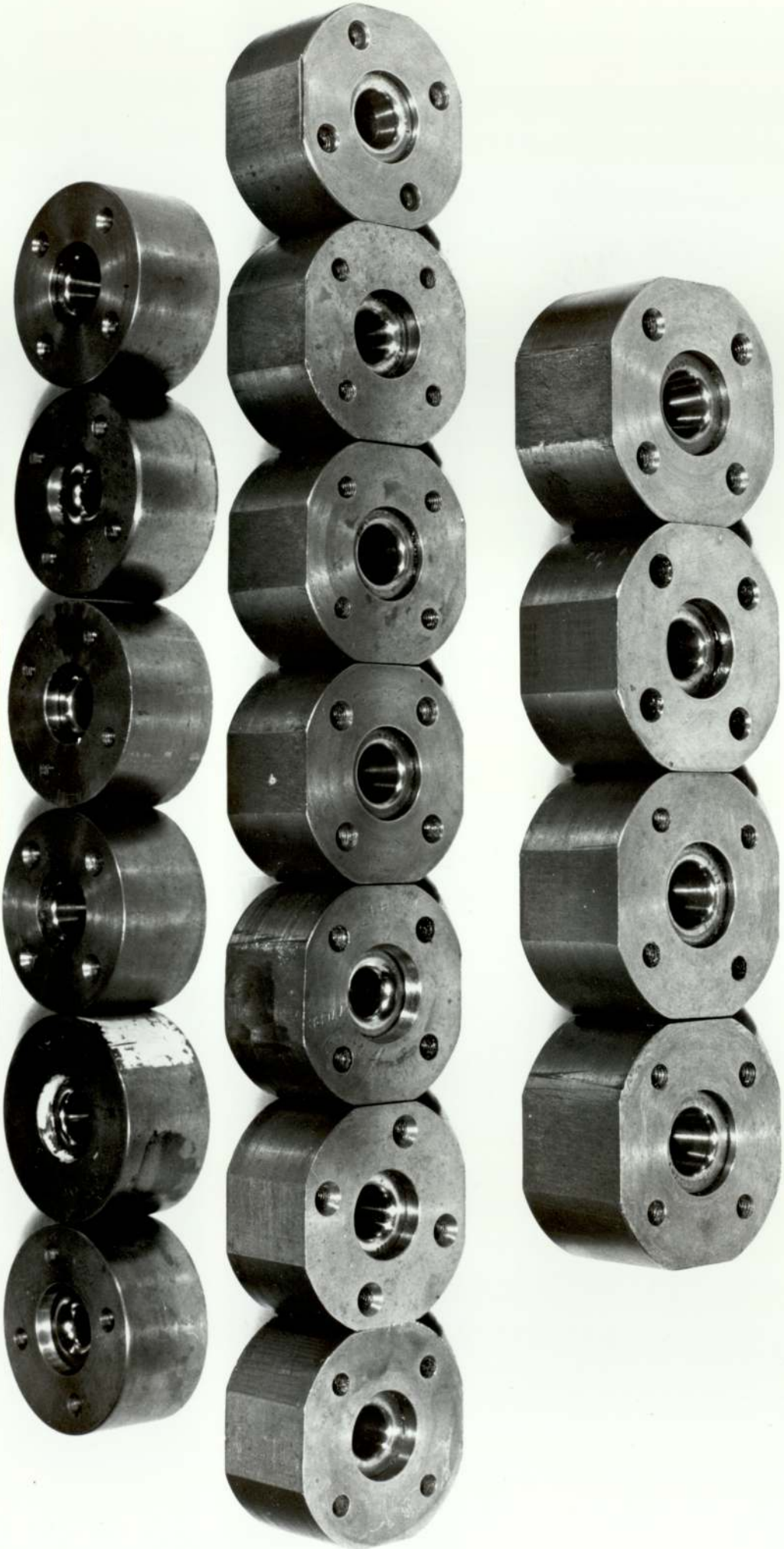

Figure 3.3. Dies used in Bimetal tube mandrel drawing experiments.

Die No.	Die Size (in)
1	0.5
2	0.4975
3	0.4953
4	0.492
5	0.486
6	0.484
7	0.4815
8	0.4778
9	0.475
10	0.4716
11	0.467
12	0.46
13	0.447
14	0.419

Table 3.1 List of dies available for the Bimetal tube Mandrel drawing experiments

Two mandrels were manufactured from En 26 material to B.S. 970; this is a 2½% Ni-Cr-Mo steel. The material supplied has the following composition :-

C	Mn	Cr	Mo
0.4%	0.6%	0.65%	0.55%

The high molybdenum content enables it to be free from temper-brittleness and may be tempered at any temperature up to 660°C. The material supplied in the form of a rod was machined according to the dimensions specified in the drawing (MT001)in the Appendix but with allowance for heat treatment and subsequent grinding. The rod was hardened by quenching in oil at approximately 840°C; it was subsequently tempered. After grinding and finishing to the required dimensions, the mandrels were found to have a hardness of 47 on the Rockwell C scale. The sizes of the two mandrels were 0.412 in. and 0.399 in. in diameter and 22 in. in length.

3.3 Materials

Four different tube materials were used to make up 12 different combinations of bimetal tube on tube. The tubes used were stainless steel, mild steel, copper and brass. All these tubes remained after experiments of tube on tube sinking[6]. The stainless steel and mild steel tubes were ½ in. diameter, 0.013 in. thick and 6 ft. in length as delivered. Both stainless steel and mild steel tubes were annealed before they were delivered.

Material specifications of the stainless steel and mild steel tubes are given in the Appendix. The copper and brass tubes were supplied hard drawn and were 6 ft in length, 0.75 in diameter and about 0.020 in thick. The material specification of these tubes is also given in the Appendix.

As the copper and brass tubes were hard drawn, the tags wrinkled when they were swaged; indeed the brass tubes split in a longitudinal direction. To overcome these difficulties, the tubes were cut up into lengths of 2 ft and annealed in the Metallurgy Department. Due to the lack of facilities a reducing atmosphere could not be provided in the furnace while the tubes were being annealed, thus the tubes were scaled by an oxide film. The tubes were pickled in the Laboratory with materials obtained from the Chemistry Department.

96% concentrated sulphuric acid was diluted to 10% volume and then heated to about 50 ^{o}C. The copper and brass tubes were immersed in the solution for about 3 min with slight agitation of the solution. After all the tubes were pickled they were immersed in a solution of sodium dichromate (0.025 kg/l) dissolved in 10% sulphuric acid for about ½ a minute. The tubes were thoroughly cleaned with water and dried in air.

3.4.1 Draw Load Cell

The draw load cell used was designed to have a maximum strain of 0.1% for a 2 tonf. load. It was made of En 24 and machined with a hollow cylindrical section. One end of this load cell was flanged and this end was connected to the hydraulic piston by two parallel bars supported on four small wheels as shown in figure 3.2. The other end of the load cell was connected to the draw dog with a pin. To protect the wires and strain gauges, the load cell was covered by brass plates divided in two halves.

Two sets of strain gauges were bonded to the load cell. One set was arranged in a pattern to facilitate the measurement of torque while the other set measured the draw load. Eight strain gauges measured the draw load and each had a resistance of 97 ohm . These gauges were from the same batch of manufacture. Four of the strain gauges were mounted longitudinally parallel to the axis of the load cell and the other four were aligned transversely as shown in figure 3.4. To balance the circuit, a 5K ohm resistance was connected in parallel to one of the four arms. This arrangement of strain gauges ensured that temperature and bending were compensated. The circuit was checked and the resistance to earth was in excess of 200 megohms.

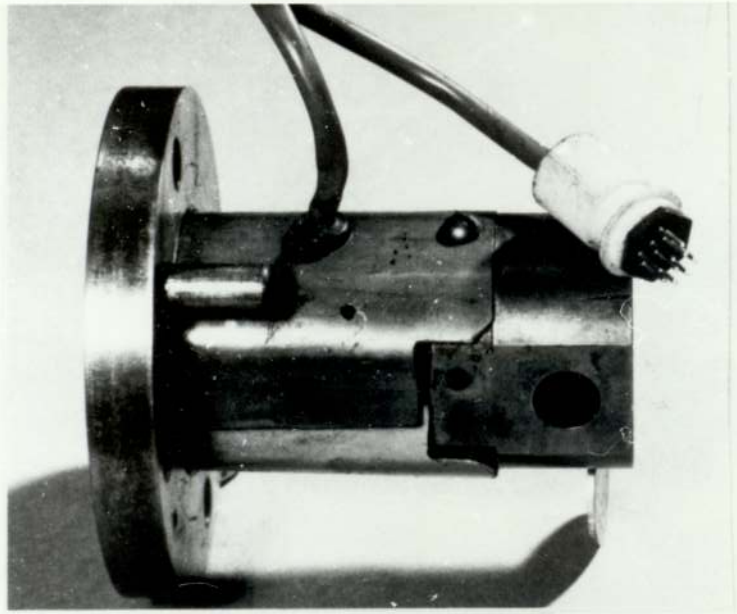

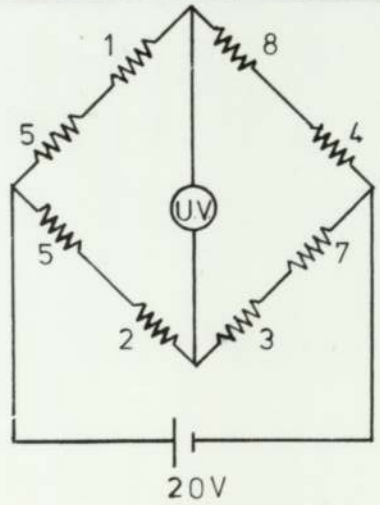

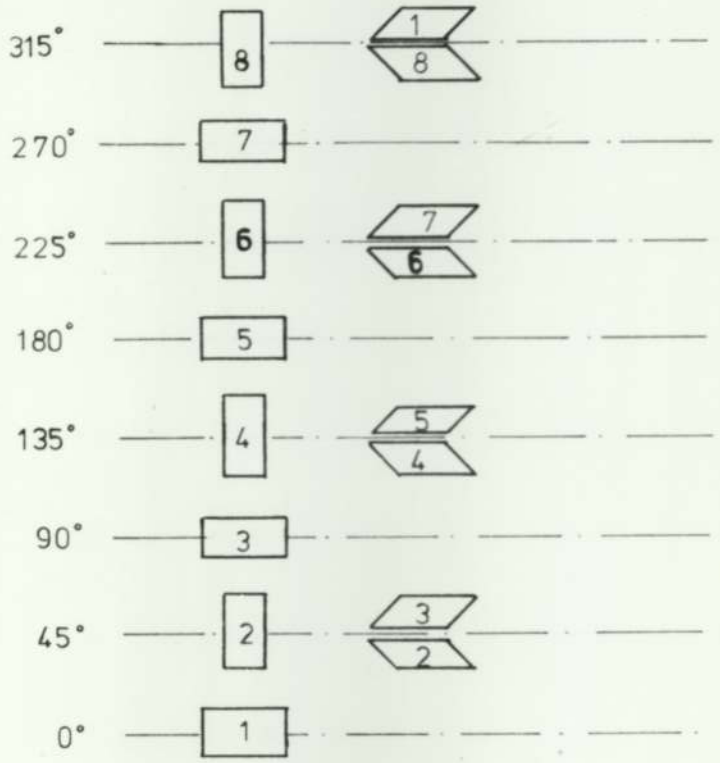

FIGURE 3.4 WHEATSTONE BRIDGE CIRCUIT FOR DRAW LOAD CELL

Though the load cell had strain gauges already mounted for use to measure torque, it was not used as it was not necessary.

3.4.2 Die Load Cell

The die load cell is of a thin hollow cylindrical section, 1¾ in. diameter, with flanges at both ends. Both faces of the flanges were machined and ground flat to ensure good contact with the mounting face. Further, one of the faces had a needle roller bearing thrust on it while the die was rotating. The die load cell was made of En24. The set-up of the die and die load cell is illustrated in figure 3.5. There were eight strain gauges used for measuring the die load. These strain gauges were arranged in the same pattern as those in the draw load cell and hence both temperature and bending were compensated. The bridge was sealed by tape except for wires running from the four corners of the bridge to a socket. A variable resistor of 5K ohm was connected in parallel across one of the four arms of the bridge to balance the circuit. Earth leakage was checked and found to be in excess of 200 megohms.

3.5 Calibration of Load Cells

The two load cells used in the experiments were

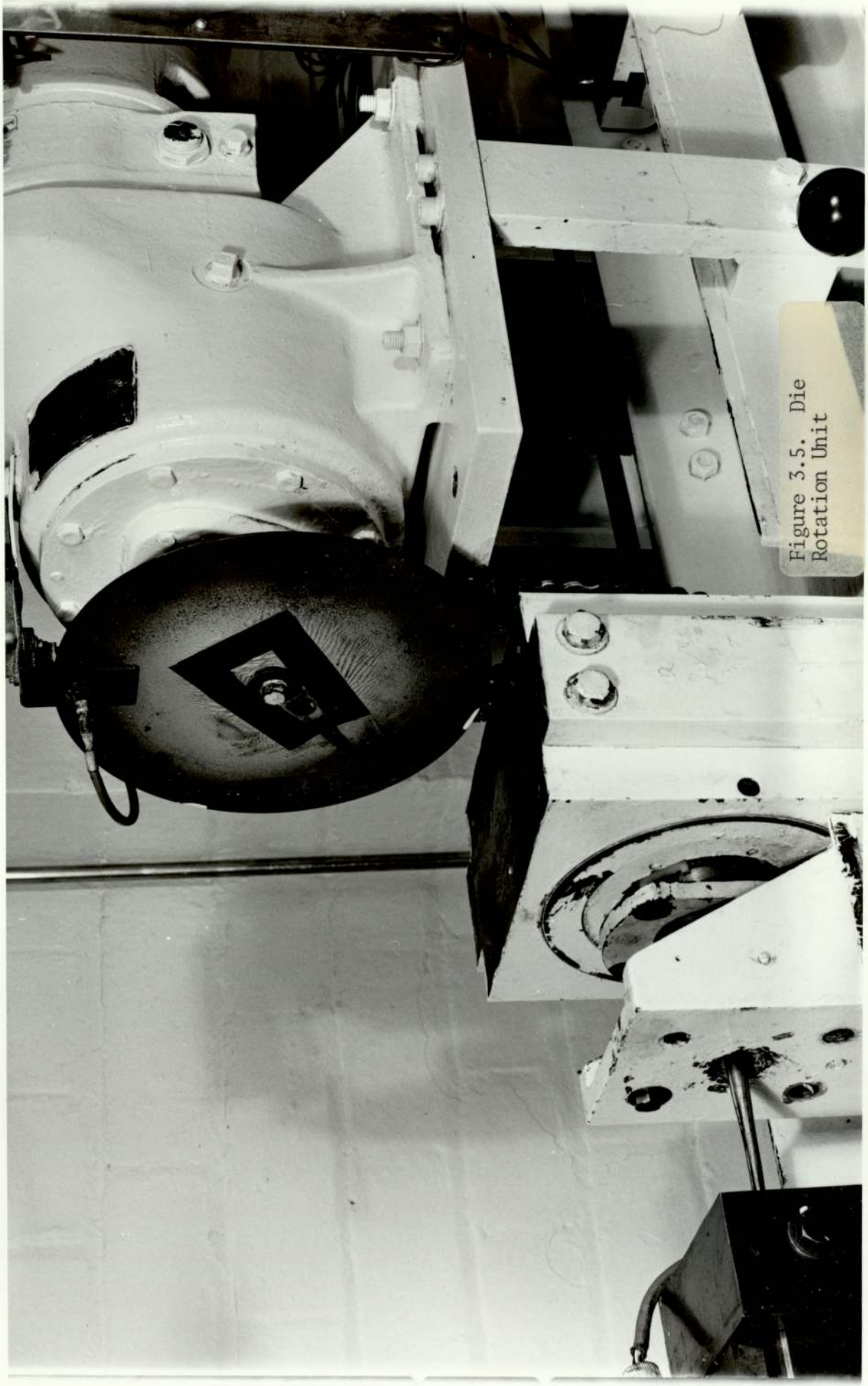

Figure 3.5. Die Rotation Unit

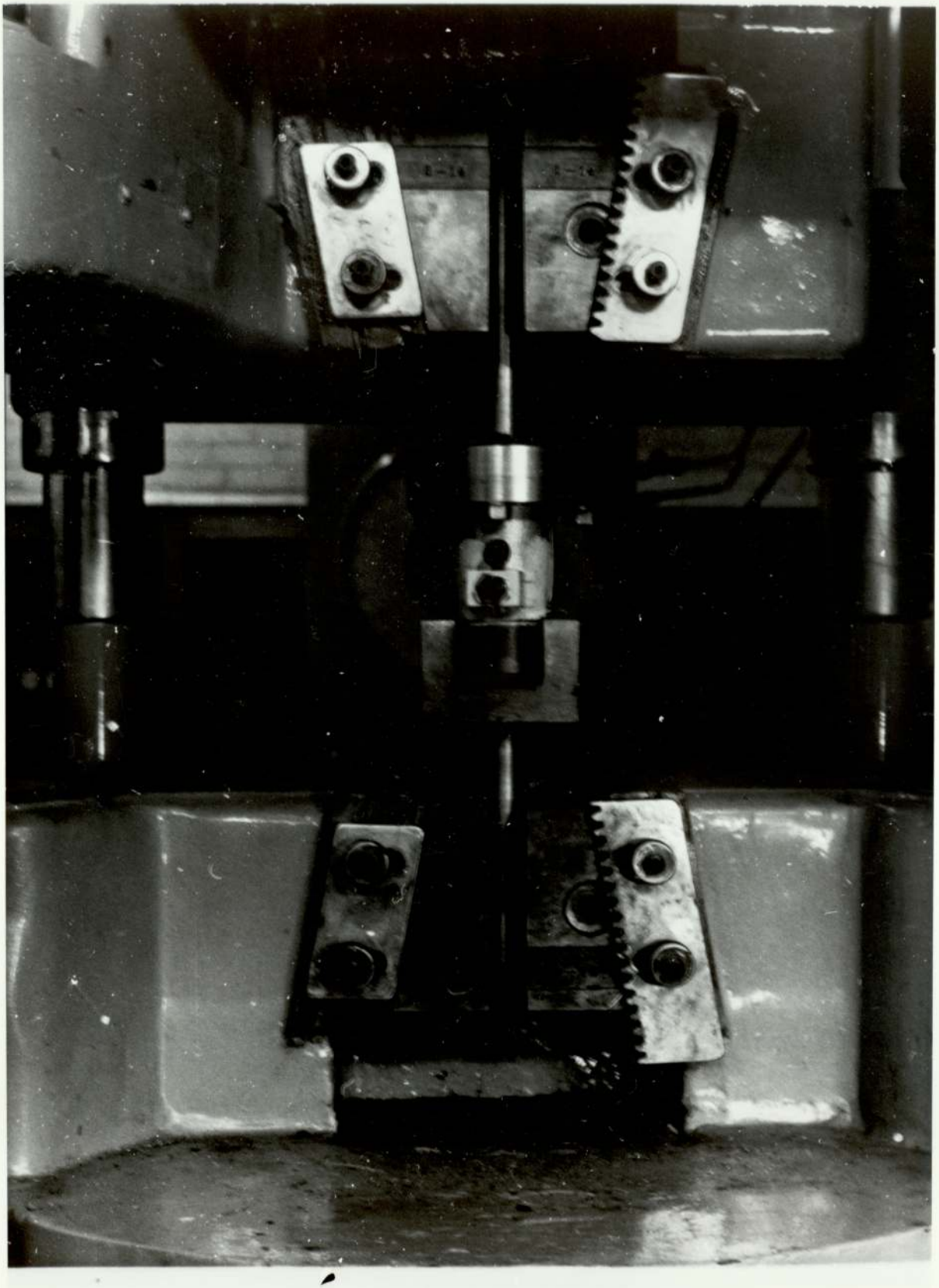

FIG. 3.6 CALIBRATION OF DRAW LOAD CELL USING A DENISON MACHINE

connected to a common power pack, supplying stabilised direct current, and a U.V. recorder. Since the draw load cell and the die load cell were connected to the same power pack during the experiments, these load cells were calibrated individually but remained connected as when used in the experiment. The two load cells were consistently maintained at a fixed voltage of 20 volts and continuously checked by a digital voltmeter.

A 50 tonf. Denison machine was used for the calibration of the load cells. The draw load was held in the jaws of the Denison machine with the aid of two adaptors as shown in Figure 3.6. The draw load cell was calibrated in tension. The die load cell was placed between the two platens of the machine and loaded in compression. The Denison had been calibrated.

Before the calibration was started, it was necessary to stabilise the equipment by having the instruments switched on for about half an hour. Both load cells were loaded between 0 to 20 tonf. at incremental loads of 0.1 tonf. At each increment, the load cell was held at that particular load for a short time while the paper of the U.V. recorder was switched on and off. The galvanometers were chosen to give a deflection of about 13 cm. for a load of 2 tonf. The experiment was repeated twice to ensure reproducible results.

The calibration graphs for the draw and die load cells are shown in figures 3.7 and 3.8.

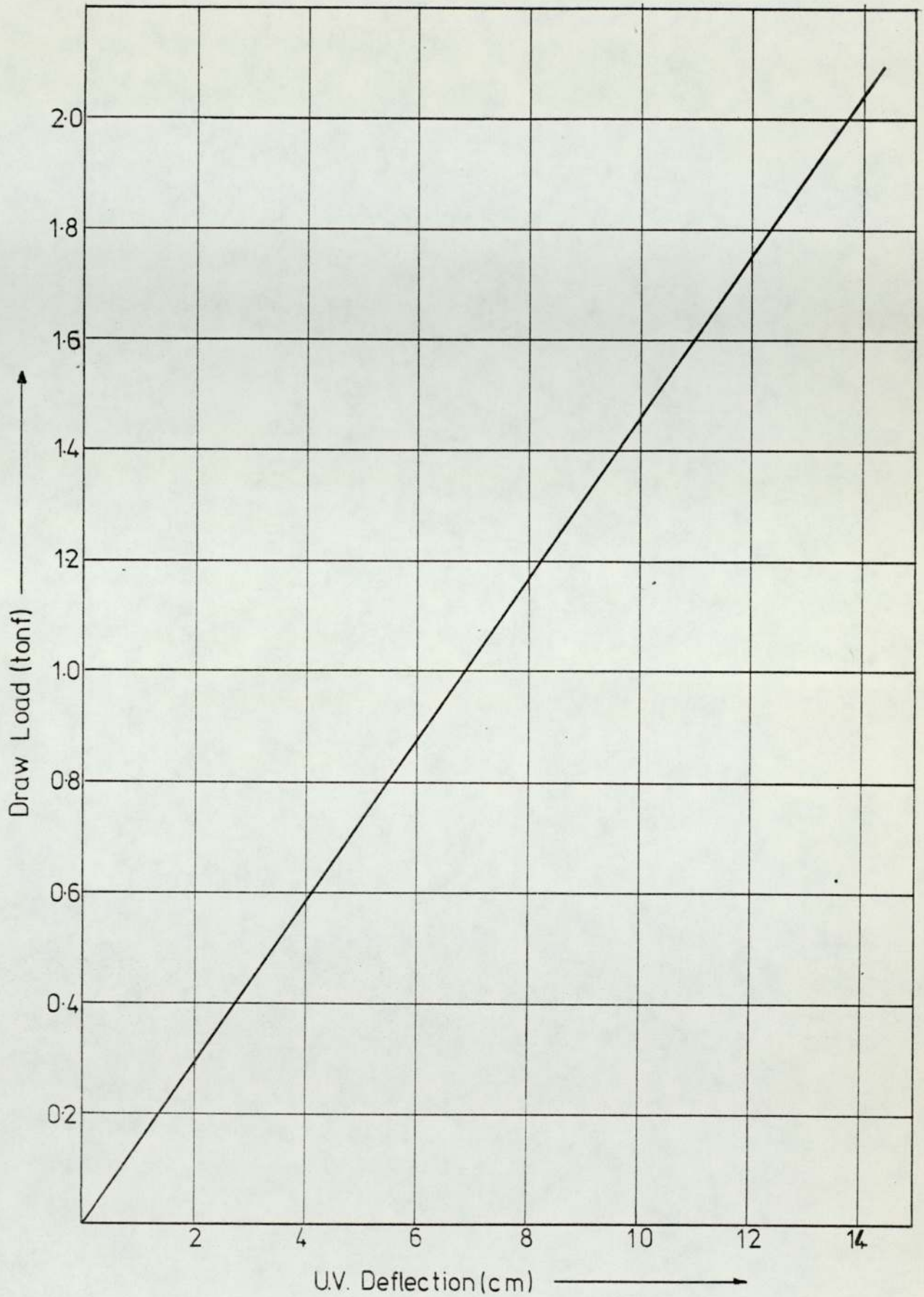

Figure 3·7 Calibration graph for draw load cell.
Galvanometer no. S511

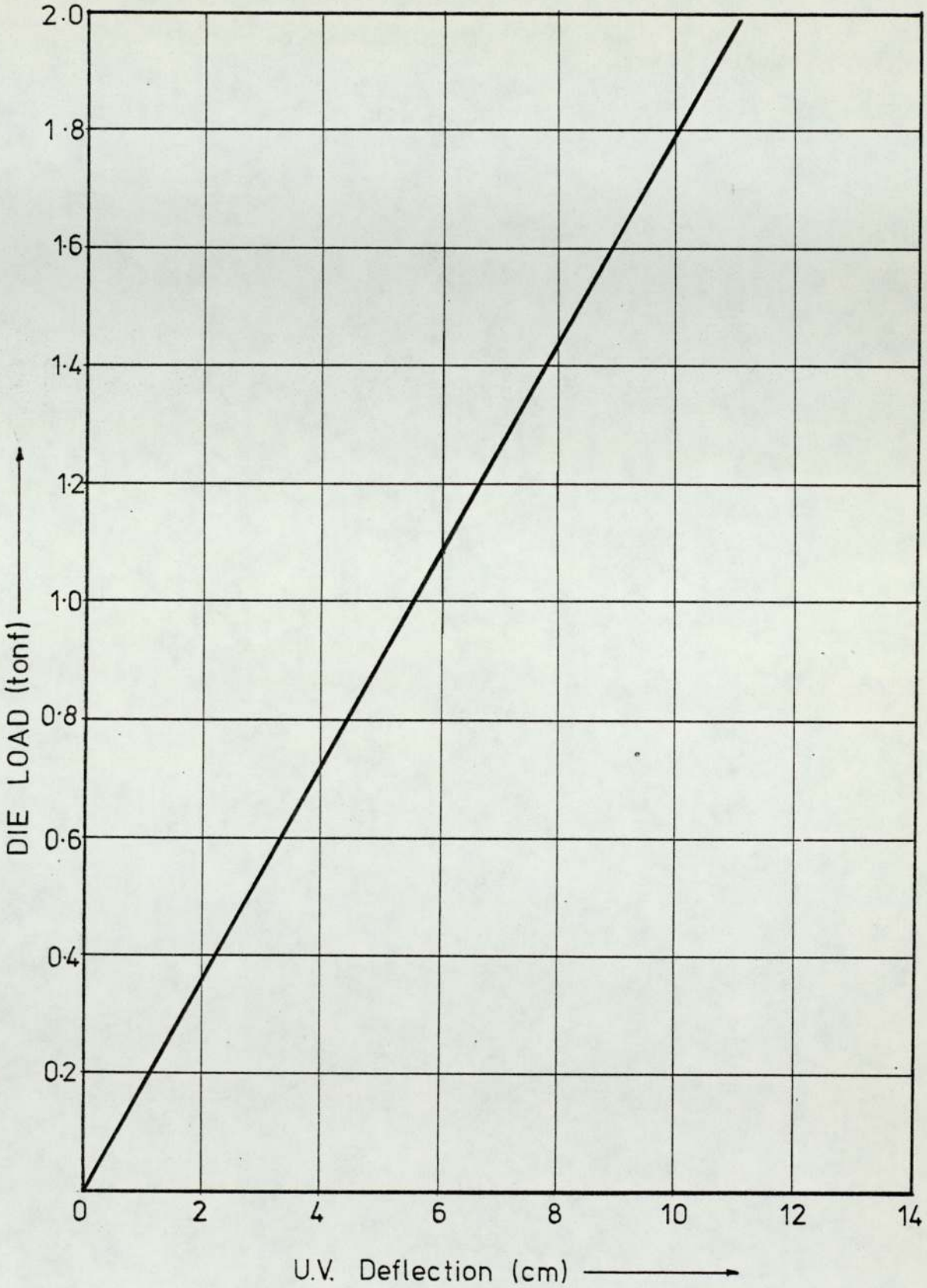

Figure 3·8 Calibration graph for die load cell
Galvanometer no: S515

3.6 Experimental procedure and technique

3.6.1 Preparation of Tube

Before the experiments, it was necessary to prepare the bimetal tubes required and 12 different combinations of bimetal tubes were produced; these are illustrated in the table below :-

Clad \ Matrix	Stainless Steel	Mild Steel	Copper	Brass
Stainless Steel	---	✓	✓	✓
Mild Steel	✓	---	✓	✓
Copper	✓	✓	---	✓
Brass	✓	✓	✓	---

The bimetal tubes with stainless steel and mild steel as clad or outer material had to have the inner tube (matrix) sunk to a diameter which allowed the matrix to be a push fit into the outer tube. Thus the copper and brass tubes were sunk from 0.75 in. diameter to an appropriate diameter to allow them to be push-fitted together. The appropriate diameter was about 0.4715 in. and 0.4696 in. diameter (the dimensions corresponded to the next nearest die size available). Due to these excessive sinking stages which represented a total reduction in area of about 60%, the brass and copper tubes were quite hard drawn again and

thus they had to be annealed a second time.

To produce bimetal tubes with copper and brass as the outer tube, the copper and brass tubes were sunk from 0.75 in. outside diameter to 0.575 in. outside diameter. For the copper/brass and brass/copper combinations, the brass or copper inside was sunk to 0.5 in. diameter for fitting into a 0.575 in. outside diameter copper or brass tube. The individual tubes were degreased and fitted together immediately. These tubes with copper or brass as clad were drawn down to produce 0.5 in. outside diameter bimetal tubes i.e. the clad metal was sunk on to the matrix material excluding any space between the two tubes. Due to the hardening of the non-ferrous metals and in order to have reproducible results that would be comparable to the other bimetal combinations with stainless steel or mild steel as clad, these tubes with copper or brass as clad were also annealed again at 600^{o}C. At this temperature, only the copper and brass in the bimetal tubes were annealed while the stainless steel and mild steel were not affected.

After the second annealing, the brass and copper tubes were pickled, neutralised, washed and dried. The bimetal tubes with stainless steel or mild steel as clad were fitted together as soon as possible to ensure there was no rust or grease between the tubes. To simulate close pass drawing, all the bimetal tubes were given a

small reduction and sunk to dimensions which enabled either the 0.412 in. or the 0.399 in. diameter mandrel to be push-fitted into the bimetal tubes. It should be noted that all the bimetal tubes, once fitted together were also swaged so as to have a common tag. This prevented the outer tube from being stripped off the inner tube during drawing.

Before the experiments began, the equipment was switched on for at least half an hour for the instruments and circuits to stabilise. The draw load cell and the die load cell were connected to the same power pack and the same U.V. recorder. The voltage output from the power pack was constantly checked by a digital voltmeter connected to it. It was found necessary to re-adjust the voltage control of the power pack after the equipment had been operating for the initial half hour. The bridges of both the draw load cell and die load cell were balanced and the zero was adjusted on the output of the U.V. recorder by adjusting the respective variable potentiometer connected to the load cells.

3.6.2 Test Procedure

Before each bimetal tube was drawn, a short length of the tube was cut off and a number given to both the tube and cut-off piece for identification purposes. The dimensions of the outside diameter and bore of the bi-

metal tube were taken with a calliper which had a hemispherical anvil for bore measurements and a flat anvil for outside diameter measurements. This calliper had an accuracy of ± 0.0001 in.

The outer surface and the bore of the bimetal tube were lubricated. All the stainless steel and mild steel surfaces were lubricated with lubricant TD45 and all brass and copper surfaces were lubricated with lubricant 5585C. The mandrel was pushed in until the end of the tag was reached. For each metal combination, the experiment was repeated with different bimetal tubes for increasing reductions in area until the tube fractured. If a bimetal tube fractured when drawn at a reduction in area which was below 40%, the experiment was repeated.

3.6.3. Retention and Testing of Samples

After each tube was drawn, a short length of the drawn bimetal tube was retained and labelled with the appropriate identification number. The drawn tube was stripped from the mandrel by drawing on the draw bench again. To enable this to be done, a circular piece of mild steel ½ in thick with a hole in the centre (as illustrated in drawing MT 002) was used. The hole of this gate was slightly bigger than the mandrel used but smaller than the bimetal tube. Thus the protruding end of the mandrel was gripped by the draw dog and separated from the tube by pulling as in ordinary tube drawing. When separation was

complete it was unusual for more than 1 in. of bimetal tube to be corrugated. The corrugated portion of the drawn tube was discarded and measurements made on the sound tube.

As explained the samples of bimetal tubes were removed before the tubes were drawn and again after drawing. Strips were cut from these samples and the thicknesses of the individual materials in each bimetal tube were measured with a pointed anvil micrometer. The micrometer has an accuracy of $\pm$ 0.0001 in.

These samples were used also in the plane strain compression test to determine the stress-strain characteristic of the material following the procedures used by Watts and Ford[79]. A detailed description of the method used is given in a later section of this chapter. The stress -strain curves obtained for the different materials are shown in figures 3.9 and 3.10.

3.6.4 Determination of Friction

During the experiments it was necessary to determine the friction factor between the bimetal tube and the die. This was done with the aid of a rotating die unit which is discussed in the next chapter. When the bimetal tubes were being drawn with a mandrel the die was rotated after approximately 1 ft. of the tube had been drawn and thus the remaining length of bimetal tube was drawn in a rotating die. The reduction in draw load was duly recorded

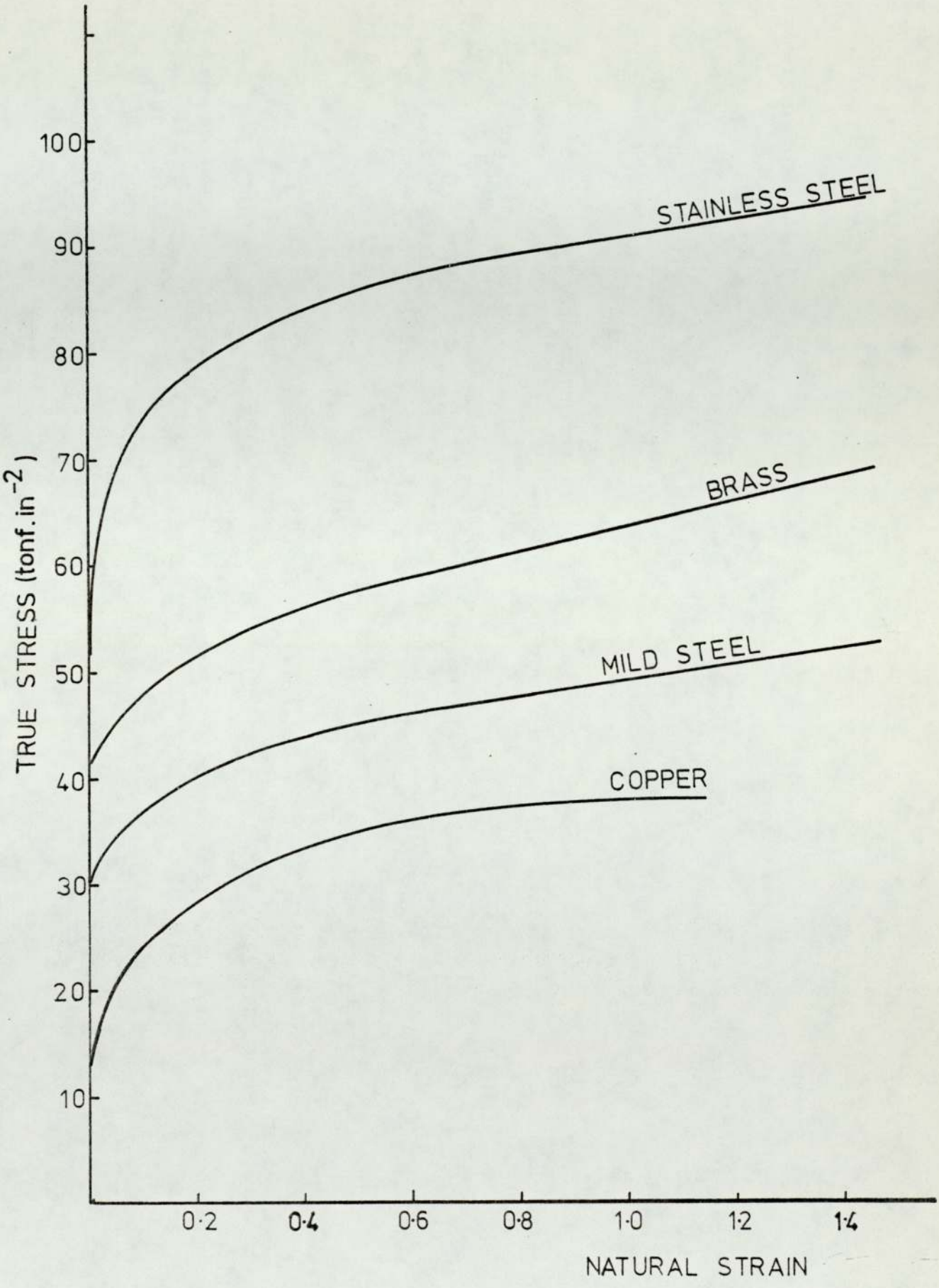

Figure 3.9 Stress-Strain curves of the materials used in the bimetal tube on mandrel experiments

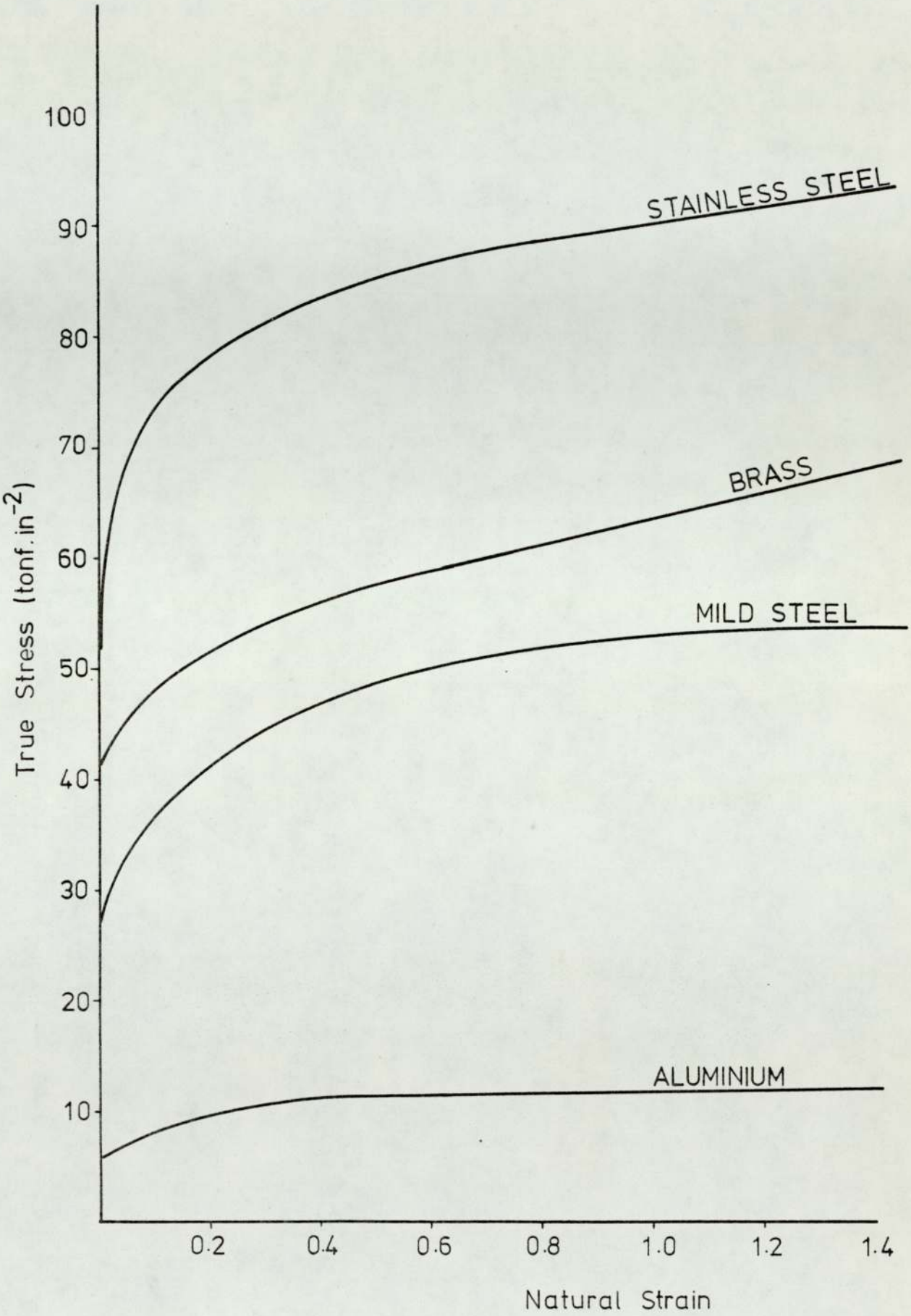

Figure 3·10 Stress Strain curves of the materials used in the bimetal tube on floating plug experiments

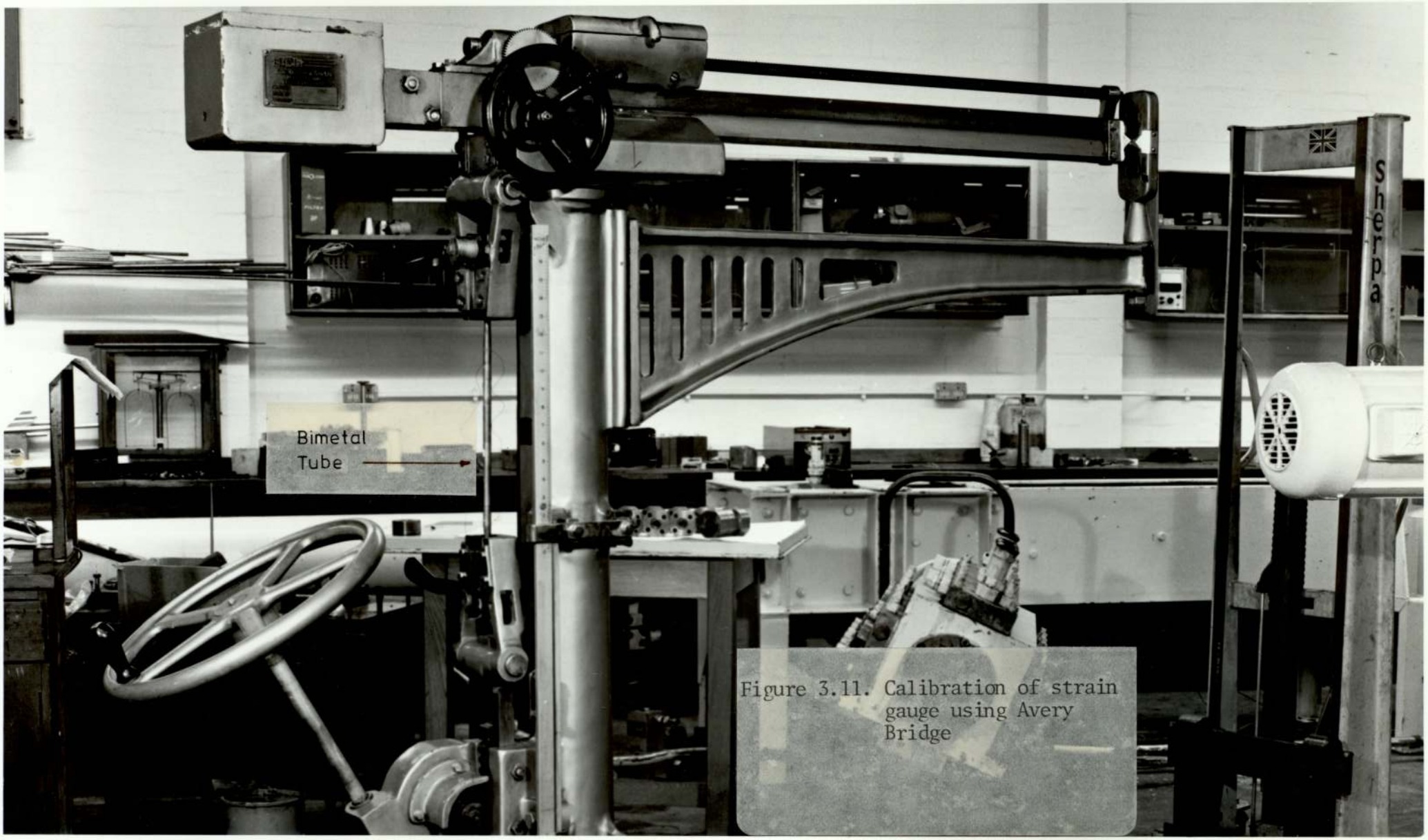

Figure 3.11. Calibration of strain gauge using Avery Bridge

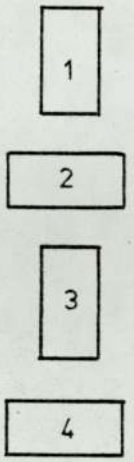

Strain gauge orientation

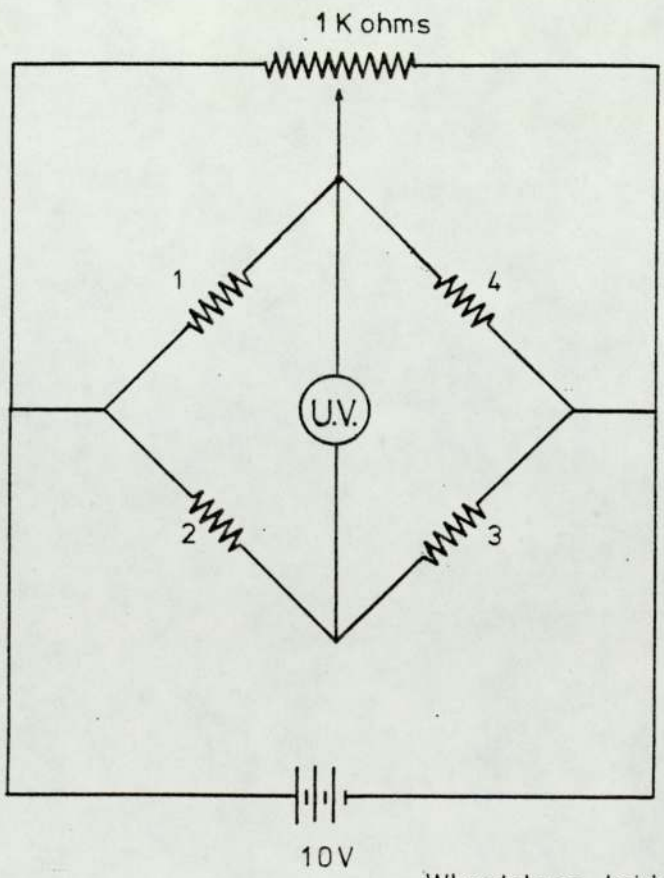

Wheatstone bridge

Figure 3·12 Wheatstone bridge circuit for determination of axial load during bimetal tube mandrel drawing.

in each case.

To determine the coefficient of friction between the bore of the bimetal tube and the mandrel, it was necessary to bond strain gauges on to the bimetal tube. When half the bimetal tube was drawn, the draw was stopped and a site for the gauges was selected at approximately one quarter of the length of the bimetal tube from the tag end. The site was degreased and a strain gauge was bonded longitudinally on the bimetal tube with a "super glue". Care was taken to exclude air bubbles under the strain gauge. Meanwhile a "dummy" bimetal tube of the same materials with three strain gauges carefully mounted was used to complete the bridge. For reasons of economy this dummy bridge was re-used in the next experiment of the same nature. The strain gauges were connected, balanced and checked for leakage before the draw was continued.

After the draw, the mandrel was removed but care was taken not to damage the attached strain gauges. The strain gauge was calibrated using an Avery Yard Stick to provide the tension as shown in Fig. (3.11). The load that provided the same strain on the tube as when the bimetal was being drawn with a mandrel was noted. The arrangement of strain gauges used is shown in fig. (3.12). It was necessary to have both ends of the drawn bimetal tube tagged before they could be held in the jaws of the Avery Yard Stick.

3.6.5. Plane Strain Compression Test

The procedures used in the plane strain compression test were those used by Watts and Ford[79,80].

The equipment used was a sub-press built at the University of Aston and a Denison testing machine. A mild steel tube of about 1½ in in length before bimetal drawing was sawn longitudinally into four parts. To avoid damaging the specimen and to enable the tube to be prepared quickly the test strips of the tube were sawn into half and then sheared into half again with hand held shearing cutters. The indentation test was performed with accurately ground platens in the longitudinal direction of the tube. The platen was selected carefully so that its breadth was 2 to 4 times the thickness of the tube specimen. The length of the tube specimen was much greater than 5 times the platen breadth.

A lubricant consisting of graphite with machine oil was smeared on the specimen which was then aligned so that the platens were in the longitudinal direction of the tube. A load was applied to the specimen until there was about 5% reduction in thickness of the strip. The load was read from the Denison machine. The specimen was removed from the platen, cleaned of graphite and the indented area of the strip measured for thickness. The thickness measurement was done with a pointed anvil micrometer. The indented area of the specimen was relubricated and replaced into the platens at exactly the same position as before. At every 5% reduction in thick-

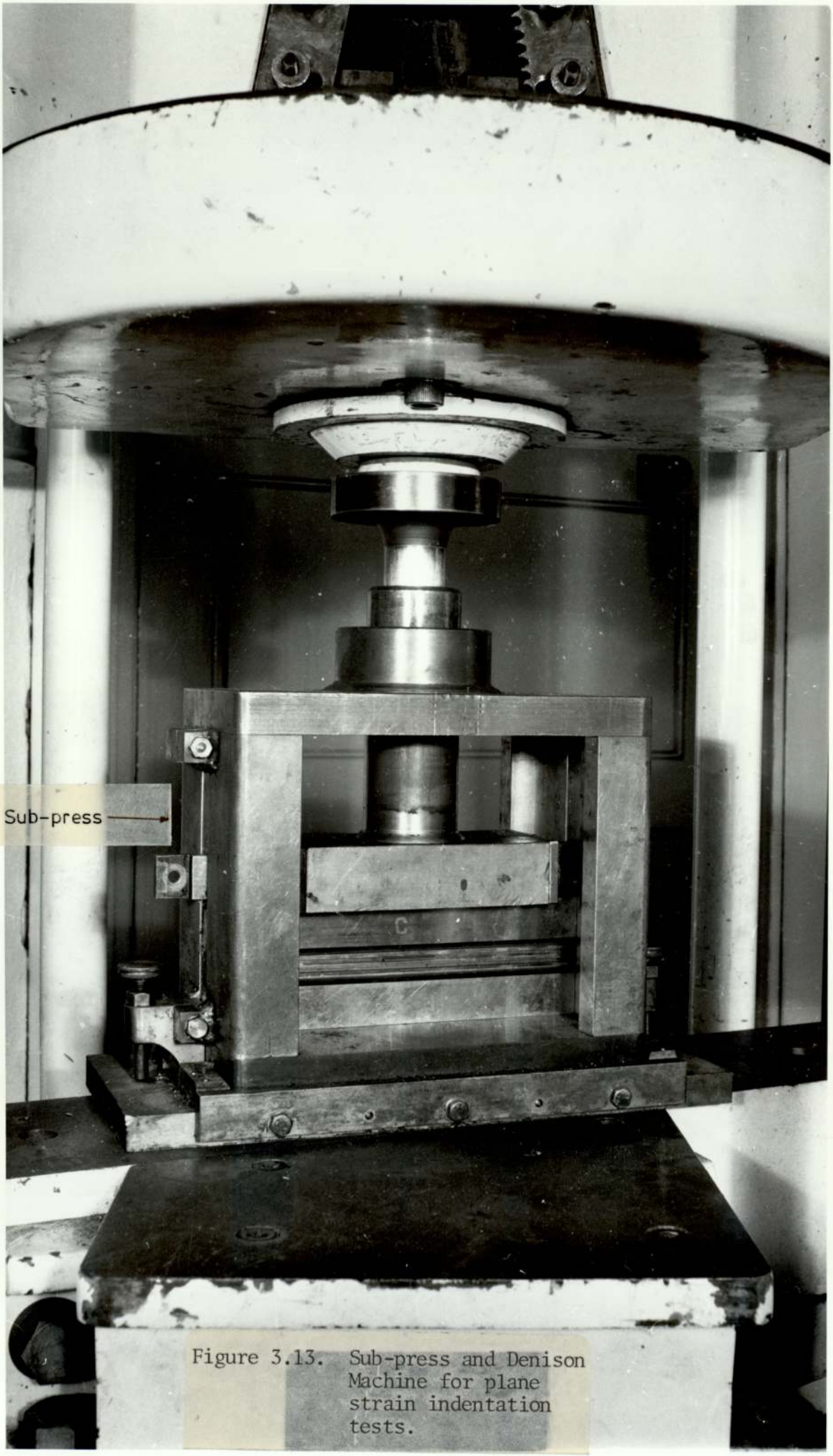

Figure 3.13. Sub-press and Denison Machine for plane strain indentation tests.

ness, the strip was removed, cleaned and measured. As the thickness of the strip decreased, the ratio of the platen breadth to strip thickness was checked and the platen changed accordingly so that the mentioned ratio remained within 2 to 4 throughout the test. The experiment was repeated for all four materials and each material was tested three times to ensure reliable results.

The sub-press and the Denison testing machine is shown in figure 3.13.

3.7 Lubricants

The lubricants chosen and used in the bimetal tube drawing with a mandrel experiment were TD45 and 5585C. In the experiments with a floating plug, the tubes were lubricated with a lubricant named TD50. These lubricants were selected because they performed satisfactorily in the previous project[6] on bimetal tube plug drawing and bimetal tube sinking experiments. Further, a considerable quantity of each lubricant were readily available in the Laboratory.

The lubricant 5585C is reactive and is polar to copper. The fatty acid in this lubricating oil can react with copper to form a film of lubricant capable of producing an excellent surface finish on drawn copper tubes.

The lubricant TD45 is a non-sulphurised lubricating oil recommended by the manufacturers for heavy duty

forming. It is a moderately thick lubricant containing a high proportion of additives based on chlorinated extreme pressure agents and special lubricity compounds. The specific gravity is approximately 1.24 at 15.5°C. Use in industry and the laboratory has shown it to be a very good tube-draw lubricant.

TD50 is a lubricant which is similar to TD45 but is a lighter lubricating oil with its specific gravity at 1.13 @ 15.5 °C . According to the products data sheet, both lubricants are suitable for use on carbon, stainless steel and also non-ferrous materials.

3.8 Experiments on Bimetal Tube on Tube drawing with a Floating Plug

Descriptions of the materials and equipment used in the experiments in bimetal tube drawing with a floating plug are given in the following sections:-

3.8.1 Materials

3.8.2 Drawing Dies and Floating Plug

3.8.3 Experimental procedure and technique

3.8.1. Materials

As the quantity of material left over from the bimetal tube mandrel drawing experiments was inadequate for experiments on bimetal tube drawing with a floating plug, new materials were brought in. A new batch of stainless steel, mild steel and aluminium tubes was donated by Industry. A small quantity of brass tubes was left over from the earlier experiments. Considering likely commercial uses, it was decided to use these brass tubes for bimetal tube combinations of stainless steel on brass and brass on stainless steel.

The stainless steel, mild steel and aluminium tubes were annealed before delivery. Both stainless steel and mild steel tubes supplied were 6 ft in length, 0.508 in outside diameter and 0.015 in thick. The aluminium tubes were 99% pure, 6 ft in length, 0.75 in outside diameter and 0.025 in thick.

3.8.2. Drawing Dies and Floating Plug

The dies and plugs used in the floating plug experiments were designed in accordance with parameters normally practised in Industry. Drawings No. FT-001 and FT-002 in the Appendix illustrate the profile of the dies and plugs used. The dies had a die semi-angle of 15° and the taper on the conical

section of the floating plug is 10° .

Both the dies and plugs were made by die manufacturers in Industry. The material used was tungsten carbide. Altogether, six different diameter dies and two same size plugs were ordered. When they were delivered, the profiles of the dies were checked by casting replicas and examining them under the Nikon Profile Projector as with the dies used in the mandrel drawing experiments. The circularity of the dies also was checked with the Hobson Taylor Talyrond machine and the diameters were checked using the Universal Measuring machine with a feeler gauge attached.

The dimensions of the floating plug were checked with a micrometer and the profile checked using the Profile Projector.

The actual dimensions of the dies are tabulated in Table 3.2. The actual size of the floating plug bearing when delivered was 0.341 in diameter. The measured back diameter of the plug was 0.4194 in diameter and the taper was correct to the nearest 10 minutes.

Die Size (in)		Out of
Designed Dimensions	Actual Dimensions	Roundness
0.406	0.40605	0.00003
0.404	0.40415	0.00004
0.400	0.39955	0.00001
0.396	0.39625	0.000015
0.392	0.39275	0.000016
0.388	0.38765	0.00004

Table 3.2 :- Dies used in experiments in the Drawing of bimetal tubes with a Floating plug

3.8.3 Experimental Procedures and Technique

The draw bench and recording equipment used in the bimetal tube drawing with a floating plug experiments were the same as those used in the bimetal tube mandrel drawing experiments. As in the previous tests, the bimetal tubes were prepared with much care to ensure reproducible results. It should be noted, during the preparation of the bimetal tubes for the floating plug experiments, after the tubes were cleaned and put together, the bimetal tubes were tagged and drawn together with a fixed plug. The fixed plug was used to ensure that the floating plug could enter the prepared bimetal tube and also to control the amount of sinking when the bimetal tube was being drawn with a floating plug. When the bimetal tube was drawn with the fixed plug, the amount of draft was kept to the minimum by estimating the final bore size of the bimetal tube from the initial tube wall thickness.

After the bimetal tubes were prepared, a short sample was taken and subsequently each tube was given an indentification number. The dimensions of the bimetal tubes and wall thicknesses were taken before and after each draw. The plane strain compression test was repeated with the samples taken from these bimetal tubes. The combinations of bimetal tubes used in the floating plug experiments are shown in the following table :

Matrix / Clad	Stainless Steel	Mild Steel	Aluminium	Brass
Stainless Steel	---	✓	---	✓
Mild Steel	✓	---	---	---
Aluminium	✓	✓	---	---
Brass	✓	---	---	---

✓ :- denotes bimetal tubes used in experiments with a floating plug.

The lubricant used in bimetal tube drawing experiments with a floating plug was TD50. This lubricating oil was used on all materials regardless of the tube combination.

It was noted that the floating plug was pushed hard into the tag end of the bimetal tube before it was drawn. This encouraged the plug bearing to float in the die throat instead of being pushed back while the tube was being drawn through the die. The bimetal tubes were drawn at a speed of 1 $ft.min^{-1}$ and because of this slow speed it was found unnecessary to taper the tail-end of the bimetal tube to break the "shooting" of the floating plug at the end of each draw.

As before, in the experiments with a mandrel, the brass tubes were annealed and pickled before they were drawn together to make a bimetal tube.

3.9 Experimental technique used to determine the coefficients of friction

The following section describes the equipment used for the determination of the coefficients of friction for the bimetal tube on mandrel drawing experiments. A rotating die unit was used for the estimation of the coefficients of friction between the clad/die and matrix/mandrel interfaces. The rotating die method was chosen because of its simplicity, accuracy and repeatability. The theory behind this experimental method is given in the former Chapter.

The rotating die unit was originally used for the same purpose in experiments of drawing bimetal tube with a fixed plug and also pure sinking. Since then the rotating die unit had been modified so that the horizontal force on the die could also be measured while the bimetal tube was being drawn. A drawing of the modified rotating die unit can be found in the Appendix. Slots were cut accurately and orthogonally to each other in the unit to accommodate ladder roller bearings. Flats were also accurately milled on the die holders as shown in Drawing No. MD-5 in the Appendix. These flats enabled the die to be rotated without slipping and the ladder roller bearings allowed the die to slide forward to press against the die load cell with a minimum friction. With the aid of a bearing holder mounted on the die, a ring bearing of type NTA 828 was placed between the die and the die load cell. This arrangement is shown in figure 3.5. During the experiments, when

the bimetal tube was being drawn, the die moved forward very slightly pressing against the ring bearing which in turn pressed against the die load cell. When the die was rotated, the die holder rotated pressing against the ring needle bearings.

The drive to the rotating die unit was provided by a Kopp Variator and a Duplex chain from a ½ h.p. motor. The Duplex chain was used because it gave a positive drive. When the drive was first designed[6] the system was meant to be used to draw tubes of maximum diameter ½ in and the maximum draw load was to be 2 tonf. The size of chain was subsequently calculated using the design procedures outlined in a Fenner mechanical power transmission catalogue.

The Duplex chain used was of Fenner number 42 with ½ in pitch. The sprockets to drive the chain were type 1, 19 teeth, reference No. 42-19 and a bush, size 1210 with a maximum bore size of 1¼ in. Another bush with diameter ⅞ in was used for attaching the drive sprocket to the output shaft of the Kopp Variator Unit.

To estimate the coefficients of friction, as described in Chapter two, it was necessary to determine the linear speed of draw and the rotational speed of the rotating die. Thus an arrangement as illustrated in Figure 3.14 was set up to enable the drawing speed to be measured. For the measurement of drawing speed, an aluminium angle (¾ in x ¾ in x ⅛ in) was mounted on to the bed of the draw bench directly under the travel area of the hydraulic

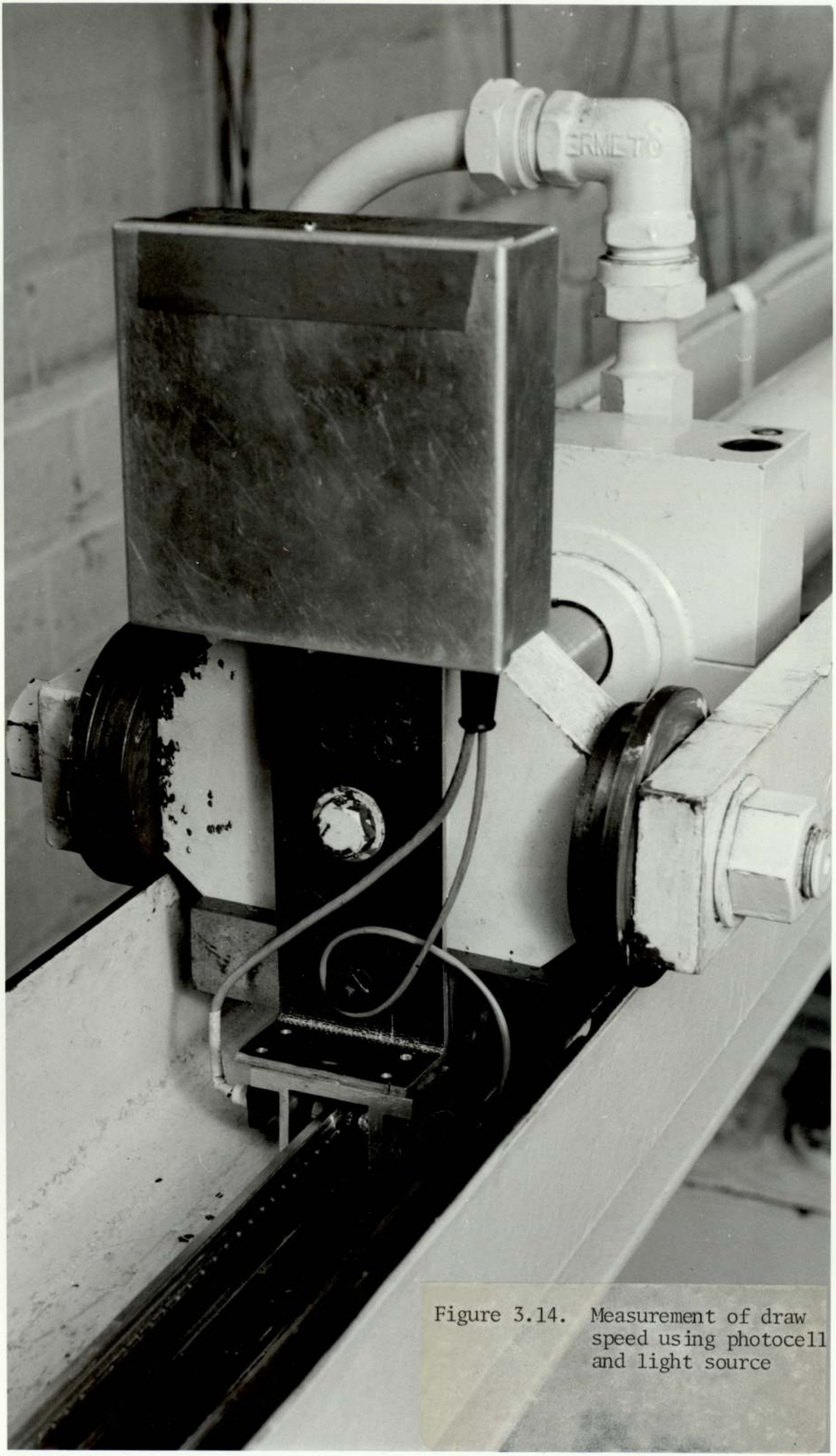

Figure 3.14. Measurement of draw speed using photocell and light source

piston. The aluminium angle had a straight row of 1 mm. diameter holes spaced at ¼ in. intervals. A photocell unit and a compact power pack capable of providing 20 volts d.c. were attached to the hydraulic ram. A light source was fixed together at the same level with the photocell using a bracket but were separated by the aluminium angle. As the ram moved, the photocell picked up light whenever it reached a hole on the aluminium angle. Hence an intermittent signal was sent out from the photocell when the ram moved and the signal was fed to the same U.V. recorder used to measure the draw load. Hence a signal was noted on the U.V. recorder every ¼ in. movement of the hydraulic ram and this was timed using the timer in the U.V. recorder. The timer was capable of giving a mark every 0.1 sec. or 1 sec. as required and this was set depending on the speed of the draw and paper speed used.

The rotational speed of the die was measured using the same principle as for the measurement of the linear speed. The light source and photocell were mounted as shown in figure 3.5. The die-cast box at the top of the light source contained the photocell circuit. The disc attached to the output shaft of the Kopp Variator had 36 holes drilled at equal intervals at a pitch circle diameter of 7 in. The size of the holes, which were very near the circumference of the disc, was 1 mm. in diameter. The power supplied to the photocell was from the same power source as the draw load cell. Again the output from this photocell was connected to the U.V. recorder giving another mark on the tracing paper whenever there was a signal.

When the experiments were performed it was necessary to reduce the output of the photocells using resistors before the signals were fed into the U.V. recorder. The distance between the photocells and the light sources was approximately 5 mm. Torch light bulbs powered from a power pack at 3 volts d.c. were used as the light source. The photocell light-activated circuit is illustrated in figure 3.15.

To measure the coefficient of friction between the bimetal tube and the mandrel, as described previously, a "dummy" set of gauges was arranged so as to complete the bridge with the active gauge on the bimetal tube being drawn. It should be noted that all the strain gauges used come from the same batch. The gauges had a gauge factor of 2.12 and of resistance 120 ohm. $\pm$0.1% . About 6 in. of bimetal tube was degreased and three strain gauges were bonded appropriately - two were bonded transversely while one was bonded longitudinally. The arrangement is shown in figure 3.12. As usual care was taken to exclude air bubbles between the strain gauges and the tube. A direct current power pack was used to provide a voltage of 10 volts and a variable potentiometer of 5K ohms was used to balance the circuit. Balancing of the circuit was necessary every time a new active gauge was connected to the circuit. To compensate for temperature variation, the material of the tube bearing the "dummy" gauges was of the same material as the tube being drawn. After each test the strain gauge on the drawn bimetal tube was always calibrated before it was disconnected.

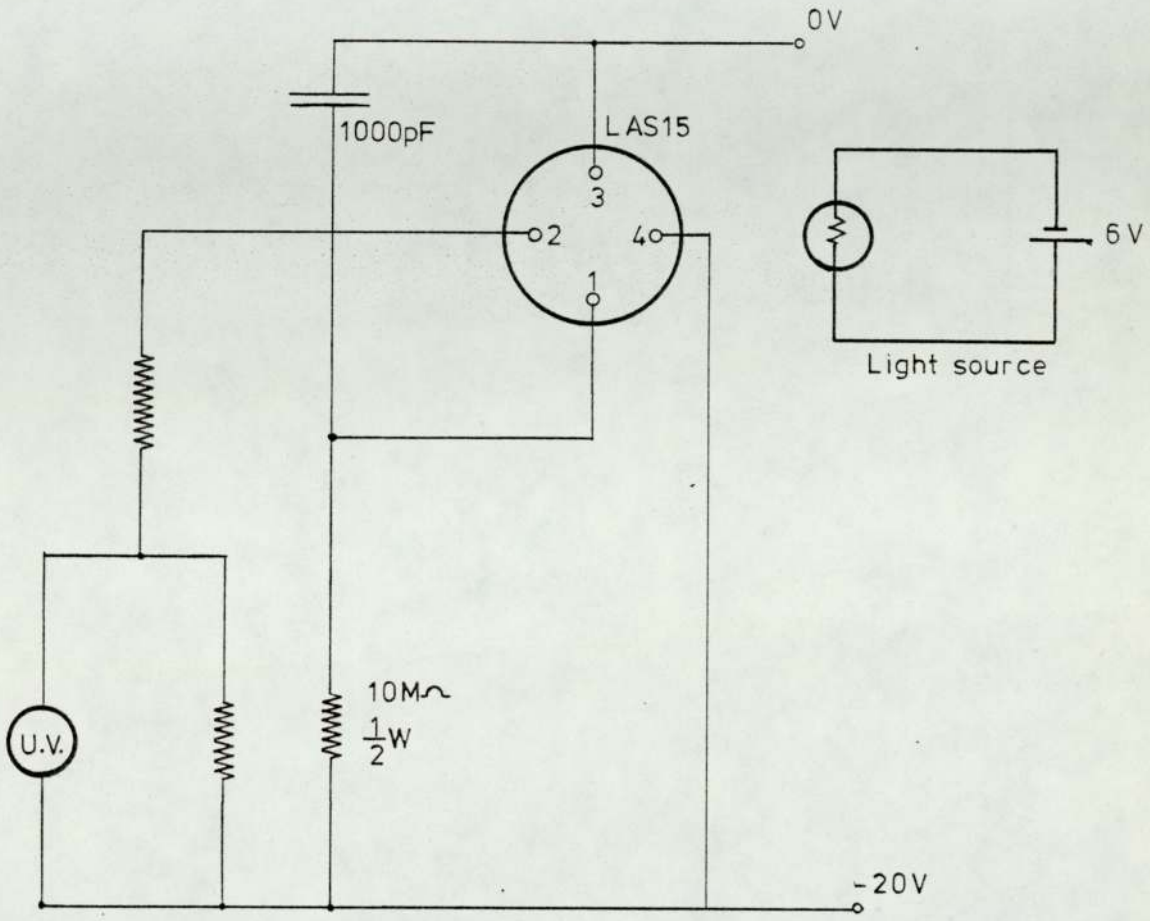

Figure 3·15 Circuit diagram for the light activated switch

Chapter Four

RESULTS

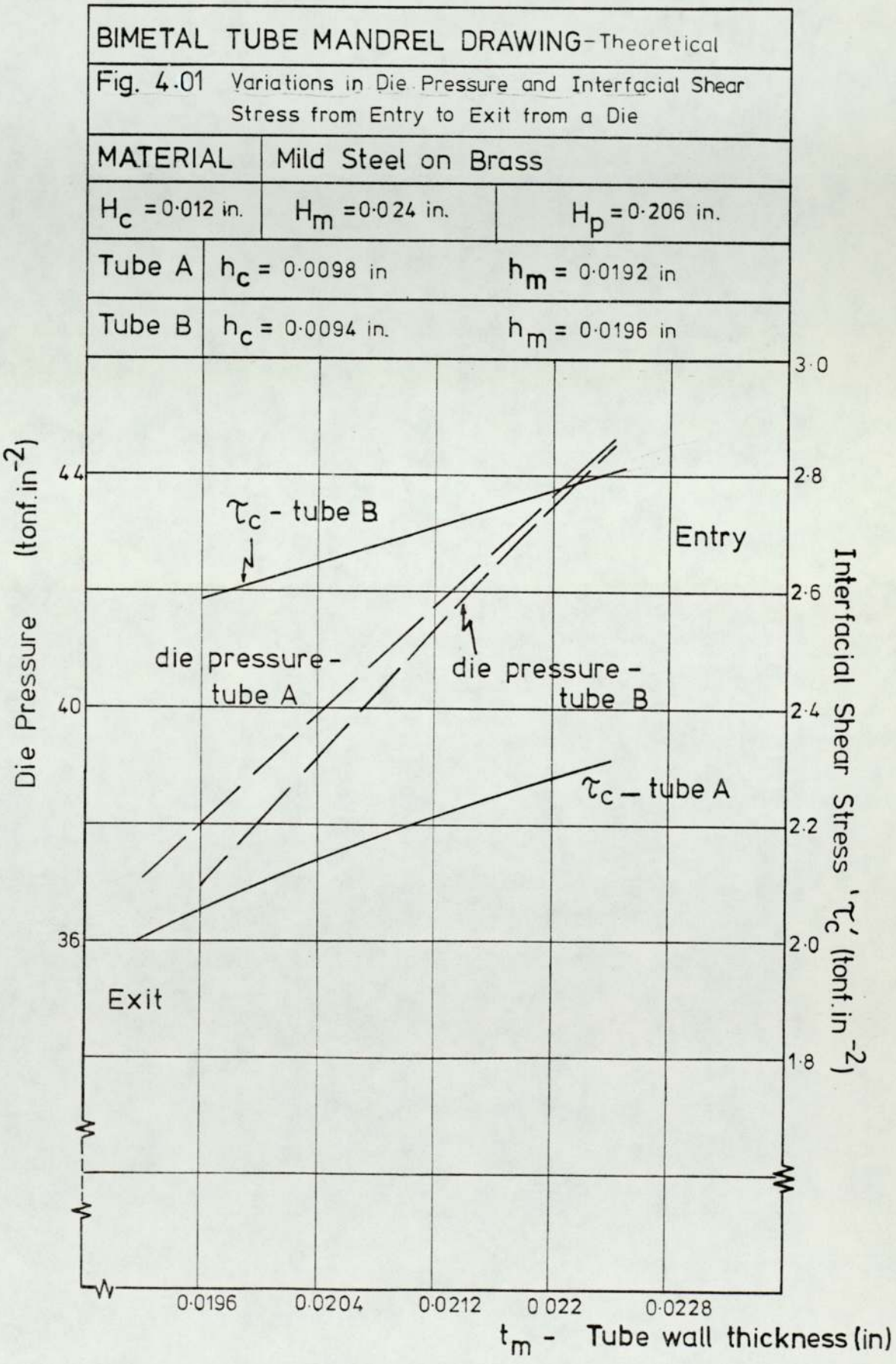
BIMETAL TUBE MANDREL DRAWING - Theoretical
Fig. 4.01 Variations in Die Pressure and Interfacial Shear Stress from Entry to Exit from a Die
MATERIAL
Mild Steel on Brass
H_c = 0·012 in.
H_m = 0·024 in.
H_p = 0·206 in.
Tube A
h_c = 0·0098 in
h_m = 0·0192 in
Tube B
h_c = 0·0094 in.
h_m = 0·0196 in
Die Pressure (tonf.in^{-2})
44
40
36
τ_c - tube B
Entry
die pressure - tube A
die pressure - tube B
τ_c – tube A
Exit
3·0
2·8
2·6
2·4
2·2
2·0
1·8
Interfacial Shear Stress 'τ_c' (tonf.in^{-2})
0·0196
0·0204
0·0212
0 022
0·0228
t_m - Tube wall thickness (in)

BIMETAL TUBE MANDREL DRAWING – Theoretical

Fig. 4.02 The Effect of final Matrix thickness on Draw Load

Material		Mean Yield Stress
Clad	Mild Steel	42.5 tonf.in^{-2}
Matrix	Brass	44.8 tonf.in^{-2}

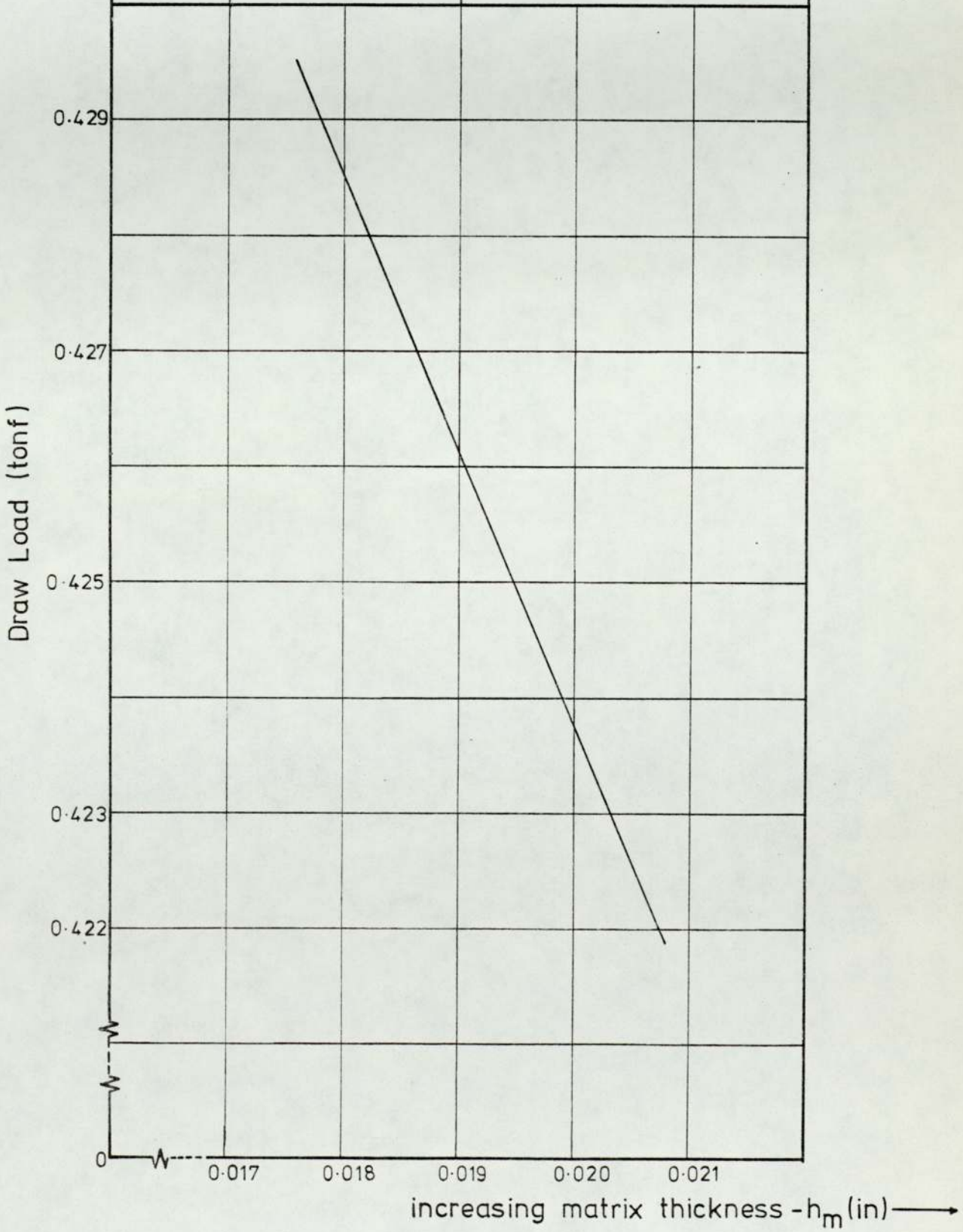

BIMETAL TUBE MANDREL DRAWING – Theoretical

Fig. 4.03 The effect of final Matrix thickness on Draw Load

Material		Mean Yield Stress
Clad	Stainless Steel	79.0 tonf.in^{-2}
Matrix	Brass	44.8 tonf.in^{-2}

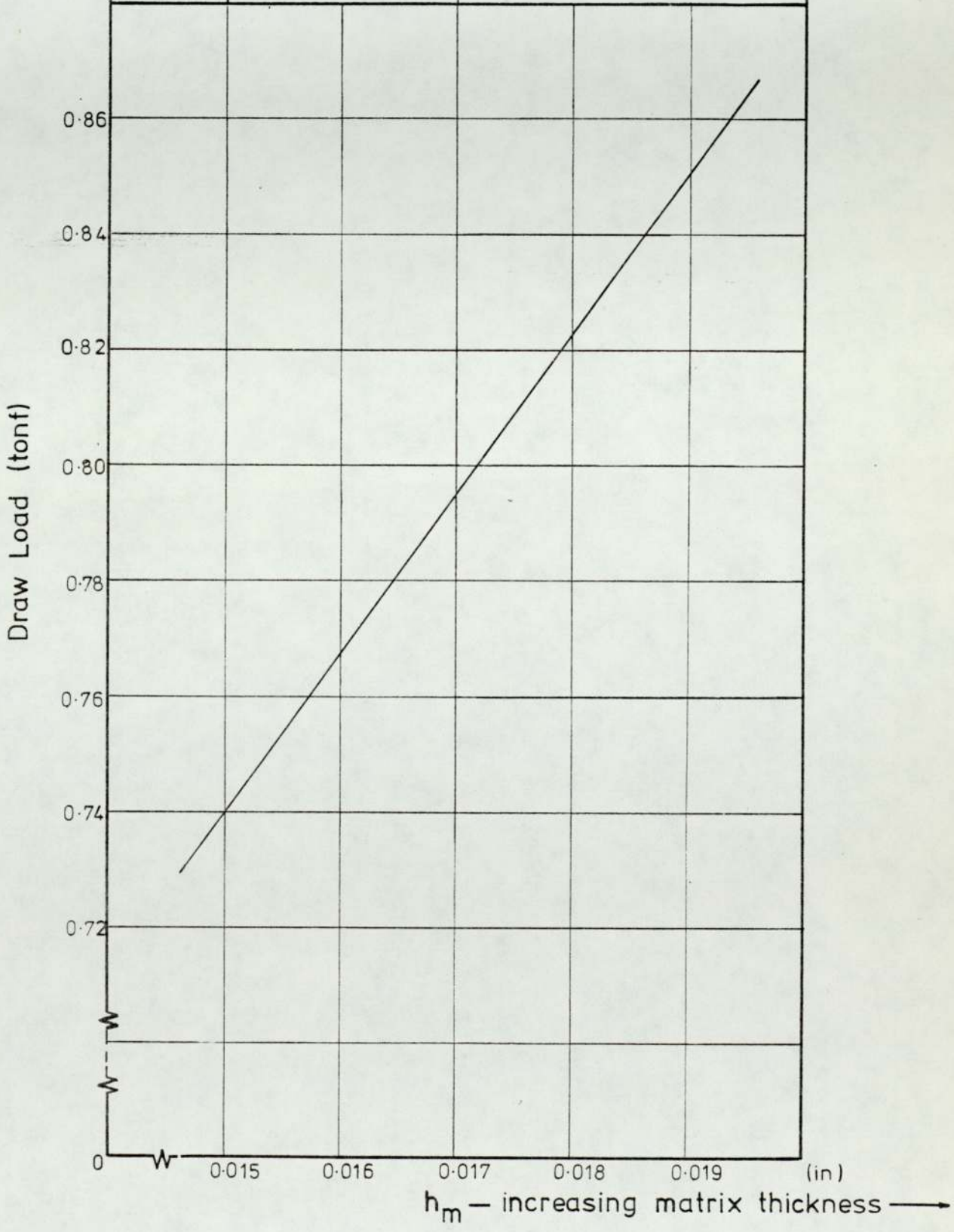

BIMETAL TUBE MANDREL DRAWING – Theoretical

Figure 4·04 — Reduction in area: 19·7%

Tube combination	H_c	H_m
Brass on Stainless Steel	0·024	0·0125
Stainless Steel on Brass	0·0117	0·0215

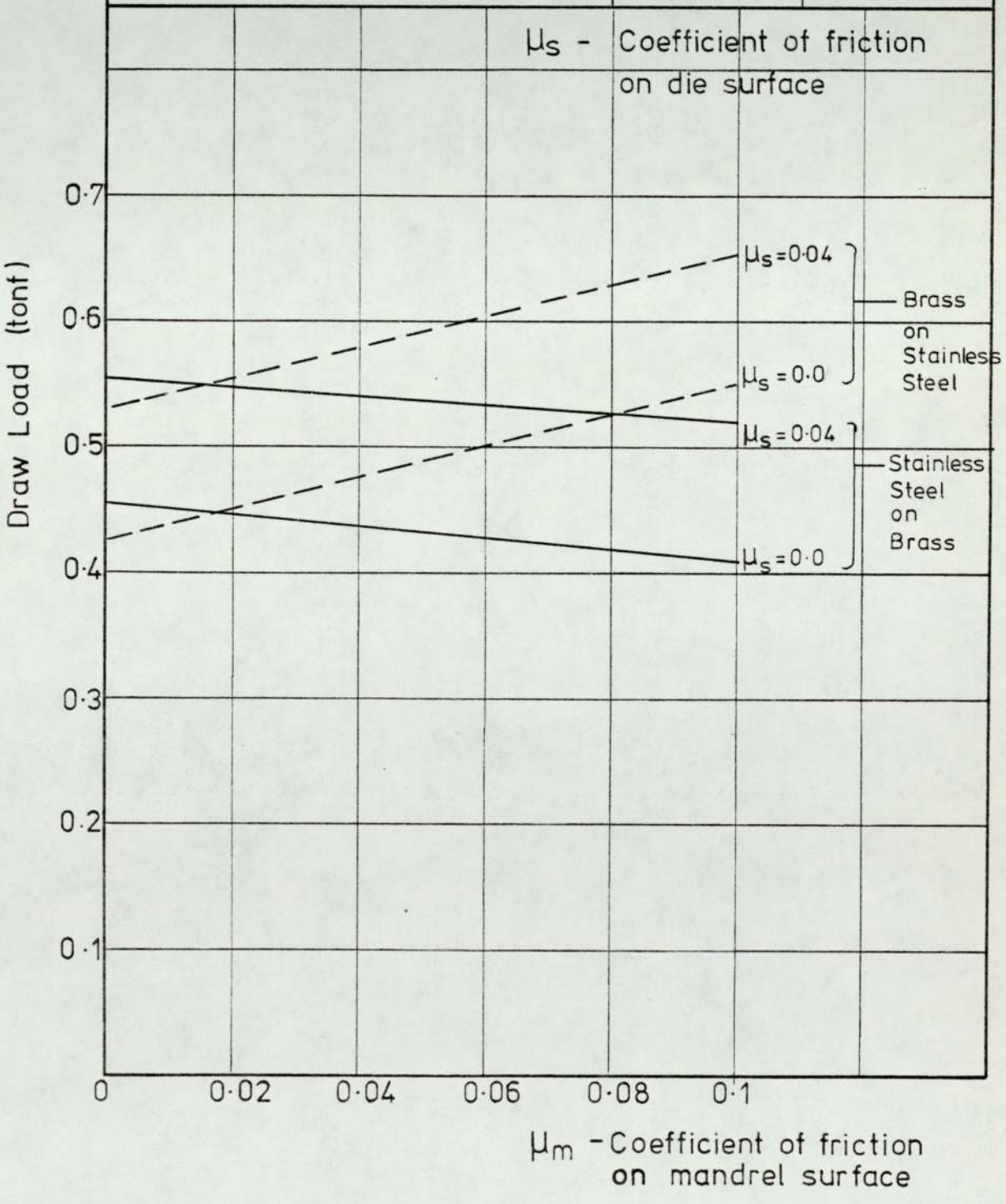

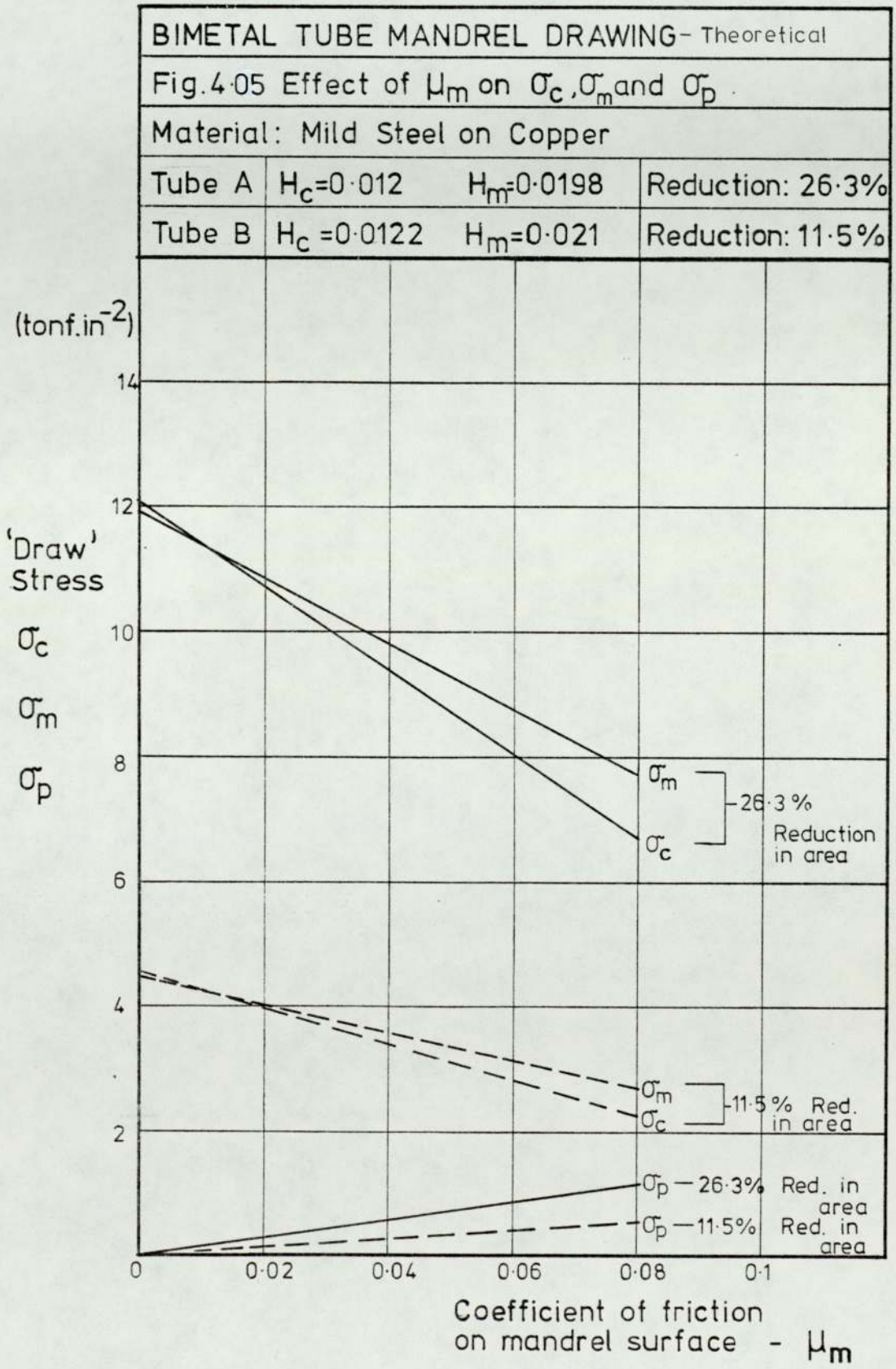
BIMETAL TUBE MANDREL DRAWING - Theoretical
Fig.4·05 Effect of μ_m on σ_c, σ_m and σ_p
Material: Mild Steel on Copper
Tube A H_c=0·012 H_m=0·0198 Reduction: 26·3%
Tube B H_c =0·0122 H_m=0·021 Reduction: 11·5%
(tonf.in^{-2})
'Draw' Stress
σ_c
σ_m
σ_p
14
12
10
8
6
4
2
0
0·02
0·04
0·06
0·08
0·1
σ_m
σ_c
26·3 % Reduction in area
σ_m
σ_c
11·5 % Red. in area
σ_p — 26·3% Red. in area
σ_p — 11·5% Red. in area
Coefficient of friction on mandrel surface - μ_m

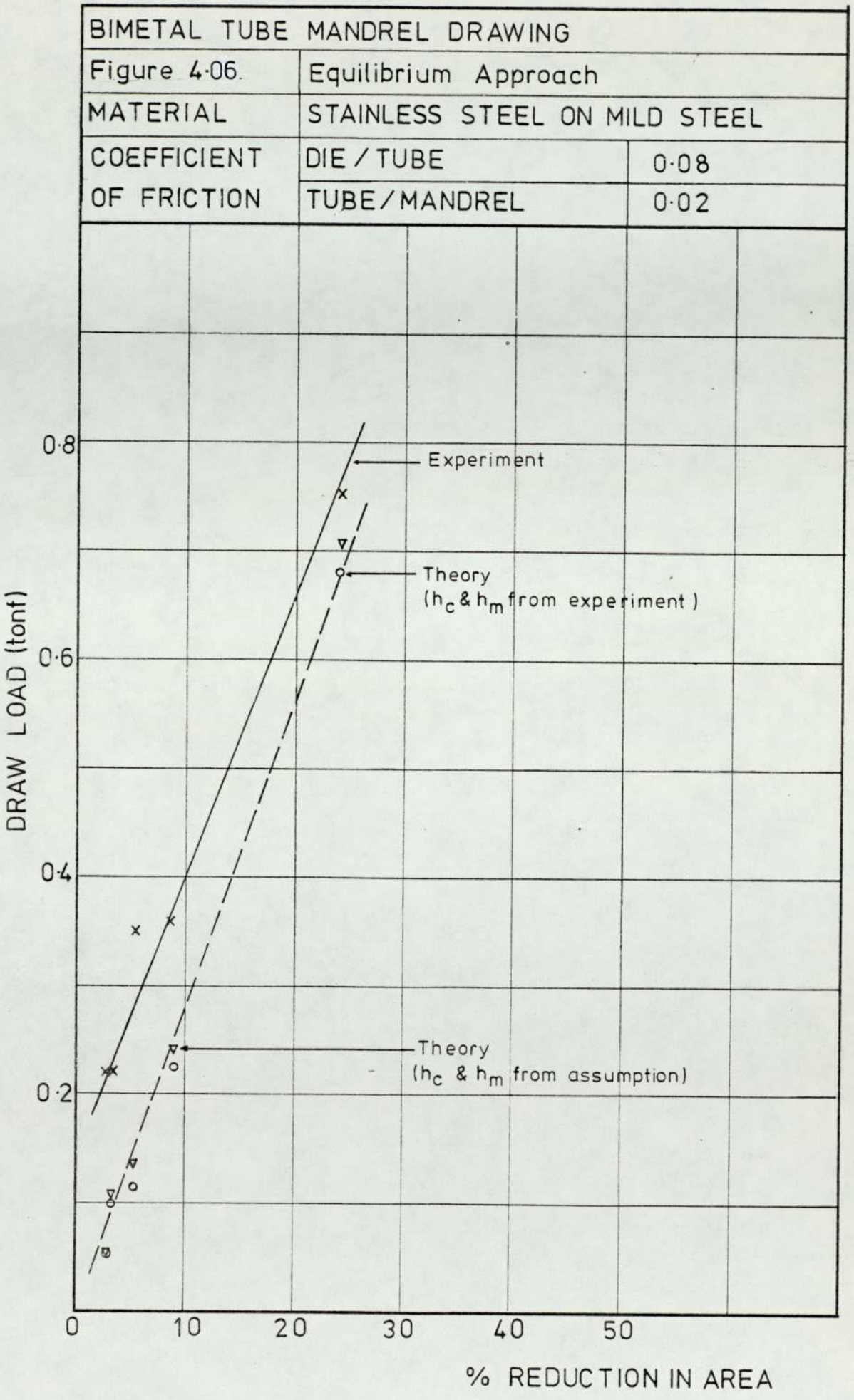
BIMETAL TUBE MANDREL DRAWING
Figure 4·06.
Equilibrium Approach
MATERIAL
STAINLESS STEEL ON MILD STEEL
COEFFICIENT OF FRICTION
DIE / TUBE
0·08
TUBE / MANDREL
0·02
Experiment
Theory
(hc & hm from experiment)
Theory
(hc & hm from assumption)
DRAW LOAD (tonf)
0·8
0·6
0·4
0·2
0
10
20
30
40
50
% REDUCTION IN AREA

BIMETAL TUBE MANDREL DRAWING		
Figure 4·07	Equilibrium Approach	
MATERIAL	STAINLESS STEEL ON COPPER	
COEFFICIENT OF FRICTION	DIE / TUBE	0·08
	TUBE/MANDREL	0·04

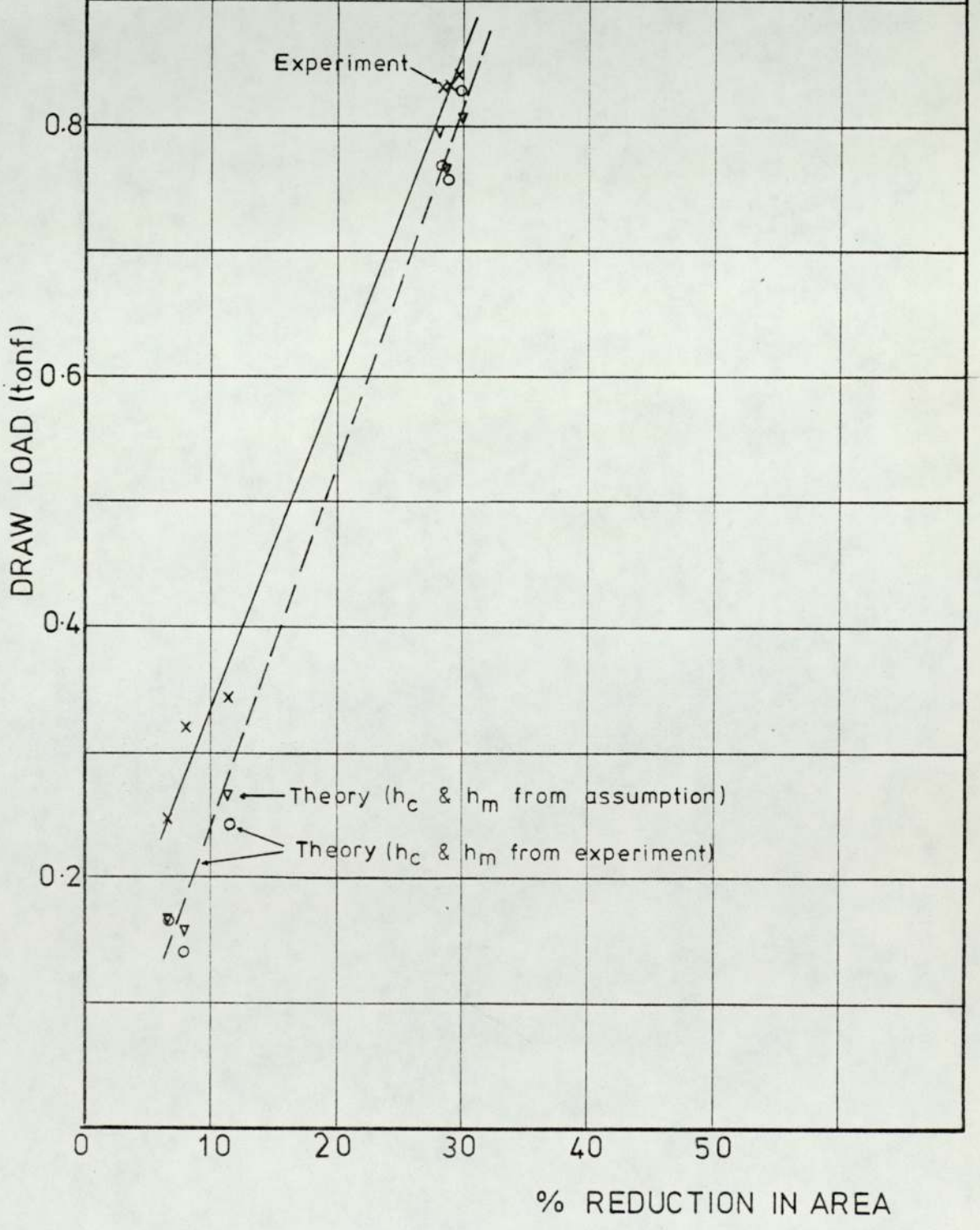

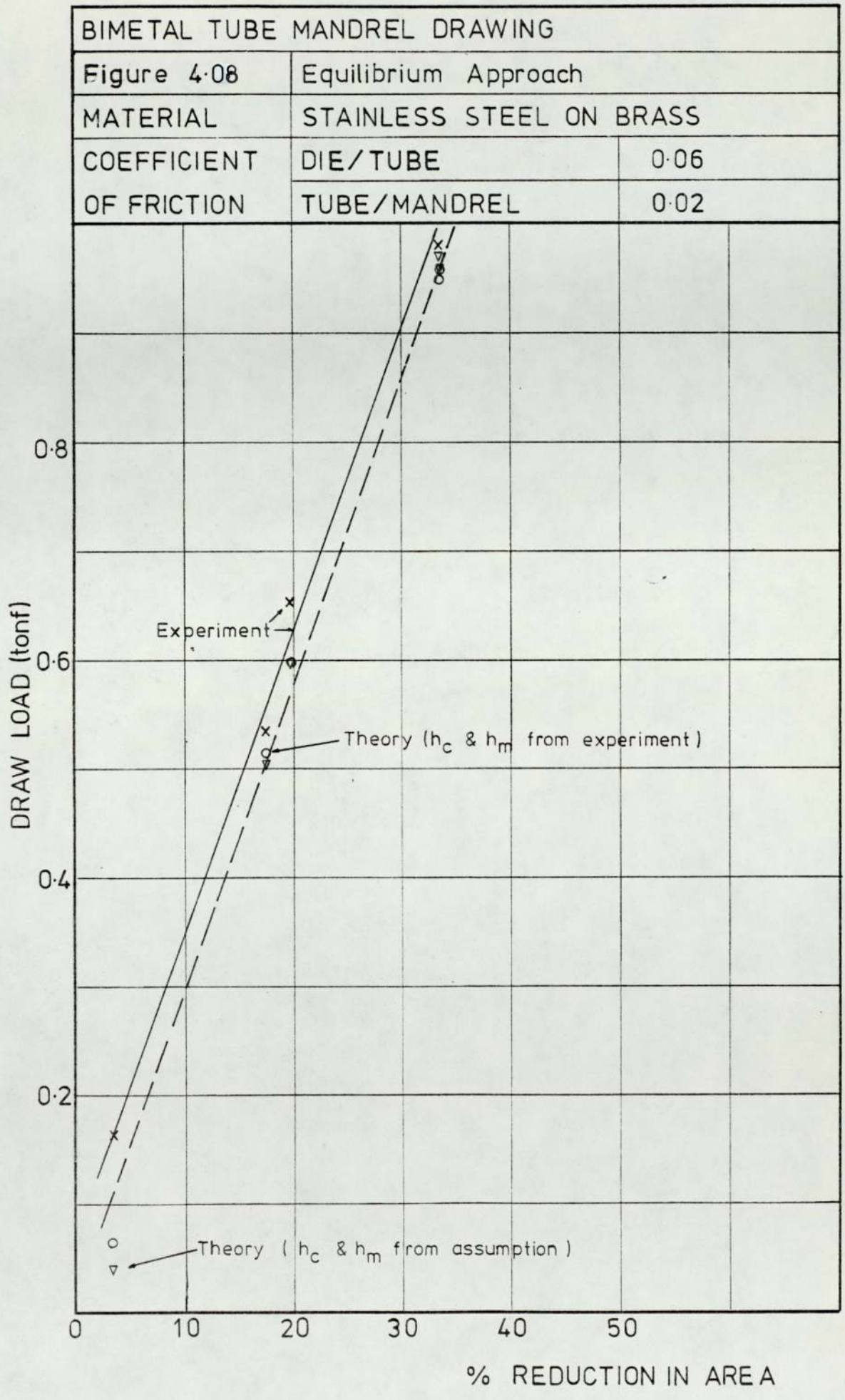
BIMETAL TUBE MANDREL DRAWING
Figure 4·08
Equilibrium Approach
MATERIAL
STAINLESS STEEL ON BRASS
COEFFICIENT OF FRICTION
DIE/TUBE
0·06
TUBE/MANDREL
0·02
DRAW LOAD (tonf)
0·8
0·6
0·4
0·2
Experiment
Theory (h_c & h_m from experiment)
Theory (h_c & h_m from assumption)
0
10
20
30
40
50
% REDUCTION IN AREA

BIMETAL TUBE MANDREL DRAWING		
Figure 4.09	Equilibrium Approach	
MATERIAL	MILD STEEL ON COPPER	
COEFFICIENT OF FRICTION	DIE/TUBE	0·04
	TUBE/MANDREL	0·02

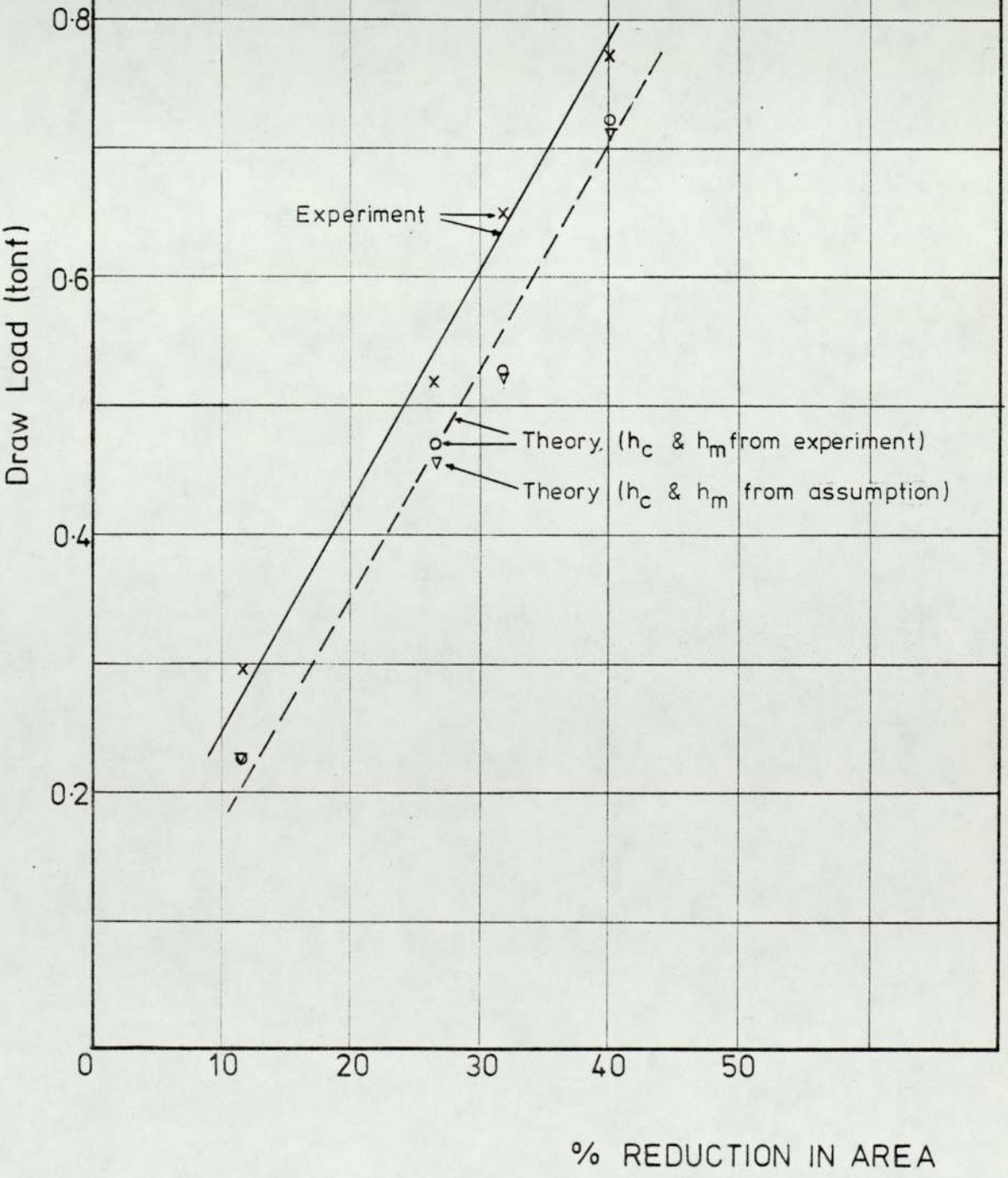

BIMETAL TUBE MANDREL DRAWING		
Figure 4·10	Equilibrium Approach	
MATERIAL	MILD STEEL ON BRASS	
COEFFICIENT OF FRICTION	DIE / TUBE	0·02
	TUBE / MANDREL	0·02

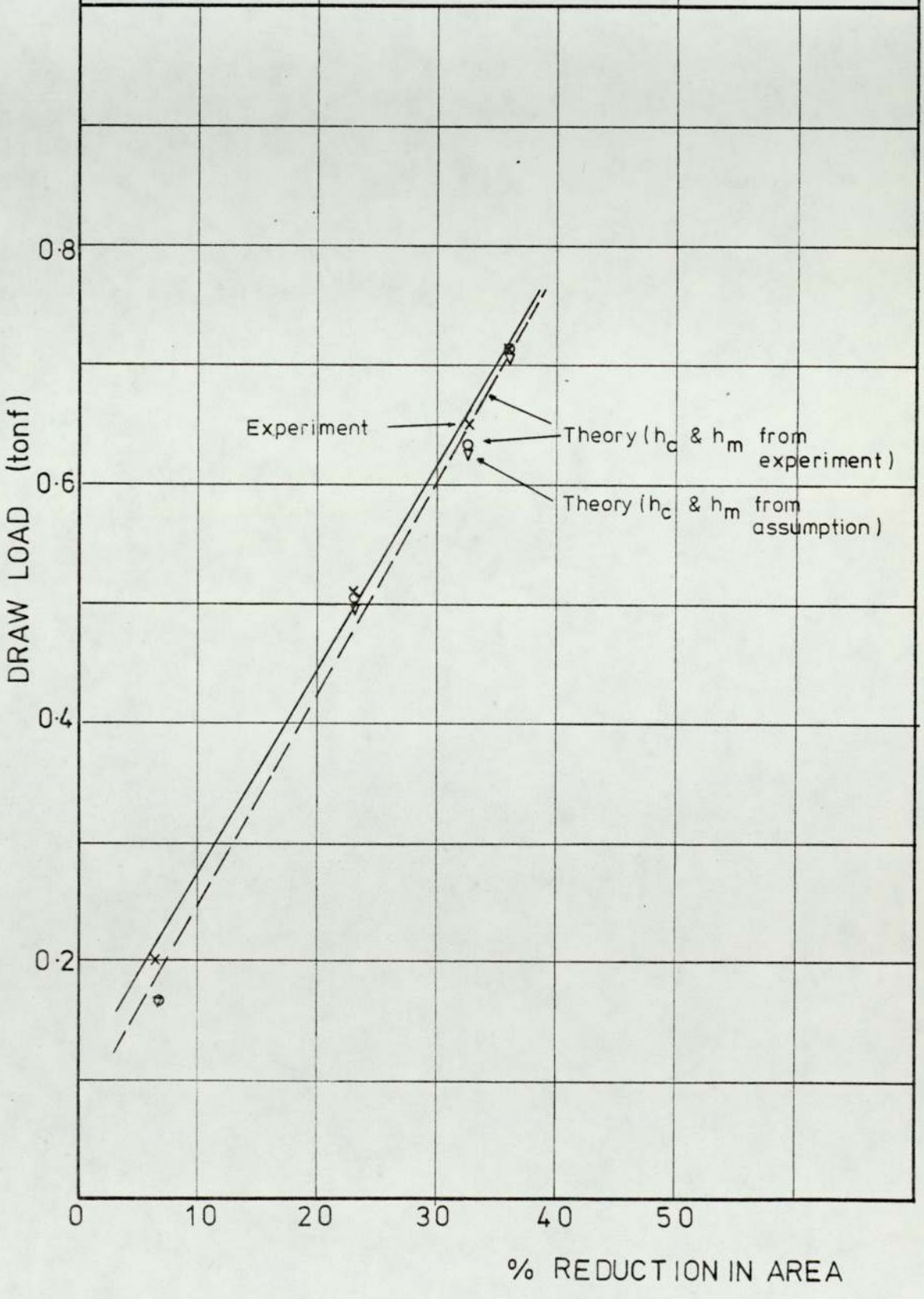

BIMETAL TUBE MANDREL DRAWING		
Figure 4·11	Equilibrium Approach	
MATERIAL	COPPER ON STAINLESS STEEL	
COEFFICIENT OF FRICTION	DIE/TUBE	0·02
	TUBE/MANDREL	0·03

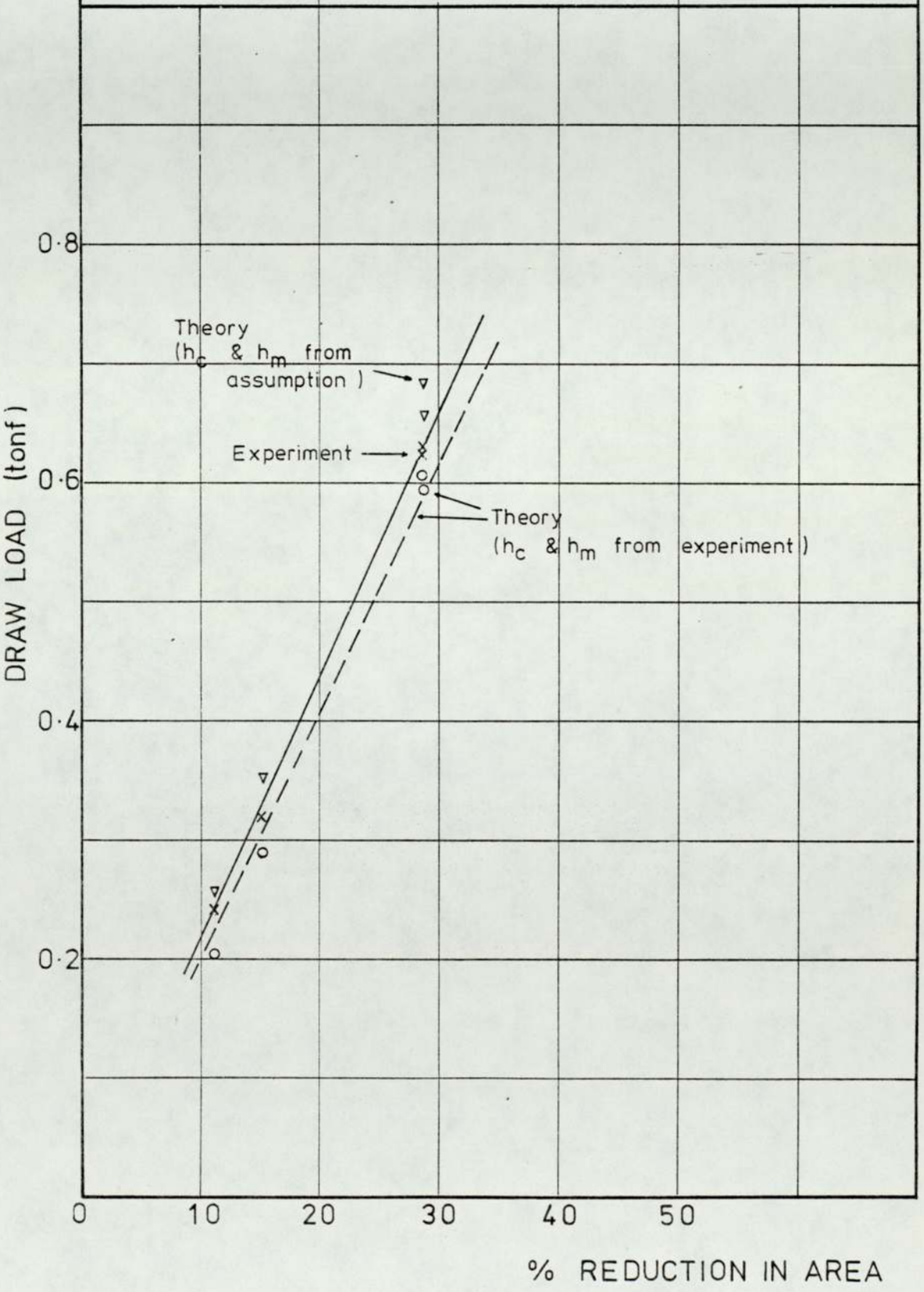

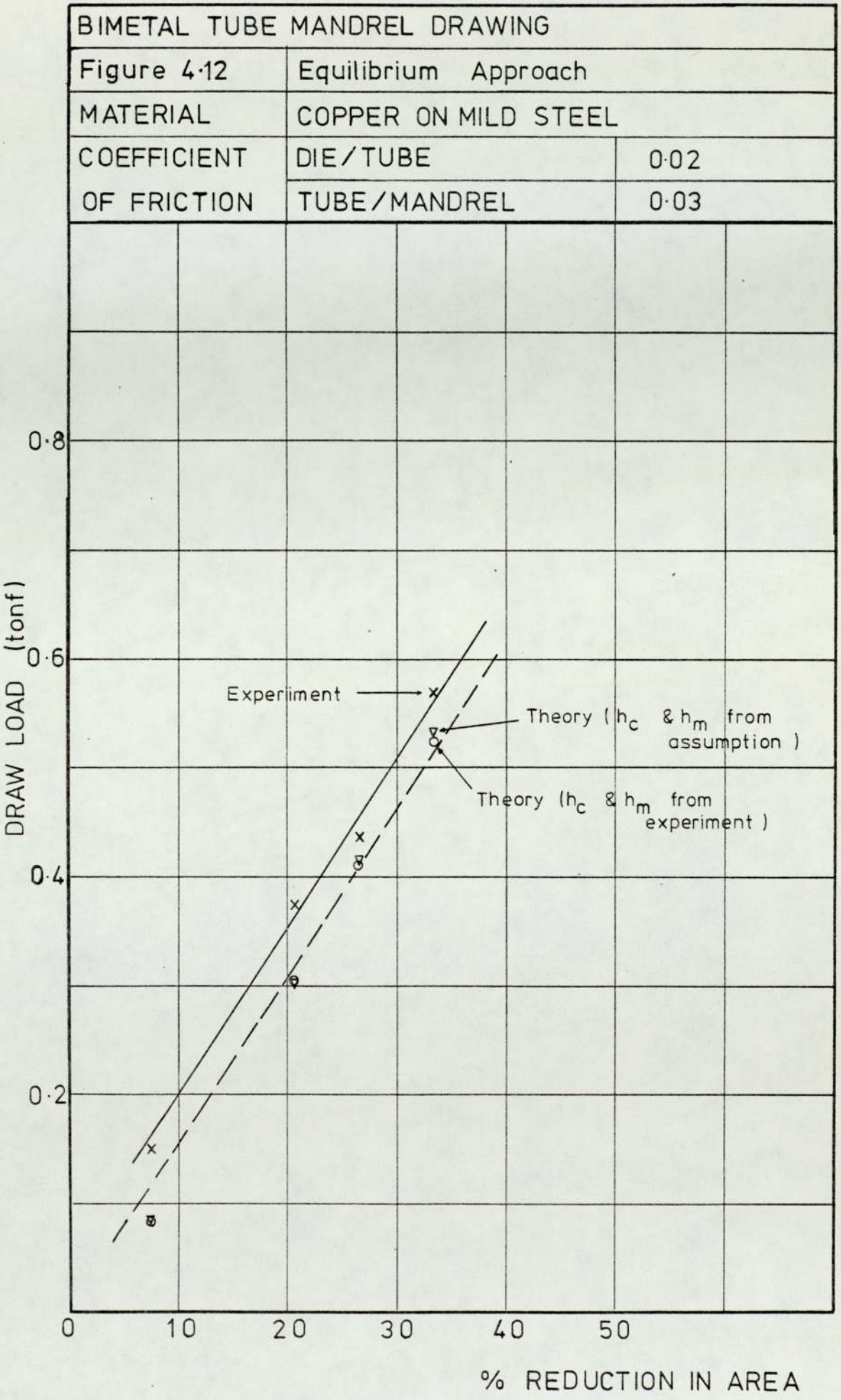
BIMETAL TUBE MANDREL DRAWING
Figure 4·12
Equilibrium Approach
MATERIAL
COPPER ON MILD STEEL
COEFFICIENT OF FRICTION
DIE/TUBE
0·02
TUBE/MANDREL
0·03
DRAW LOAD (tonf)
0·8
0·6
0·4
0·2
0
10
20
30
40
50
% REDUCTION IN AREA
Experiment
Theory (h_c & h_m from assumption)
Theory (h_c & h_m from experiment)

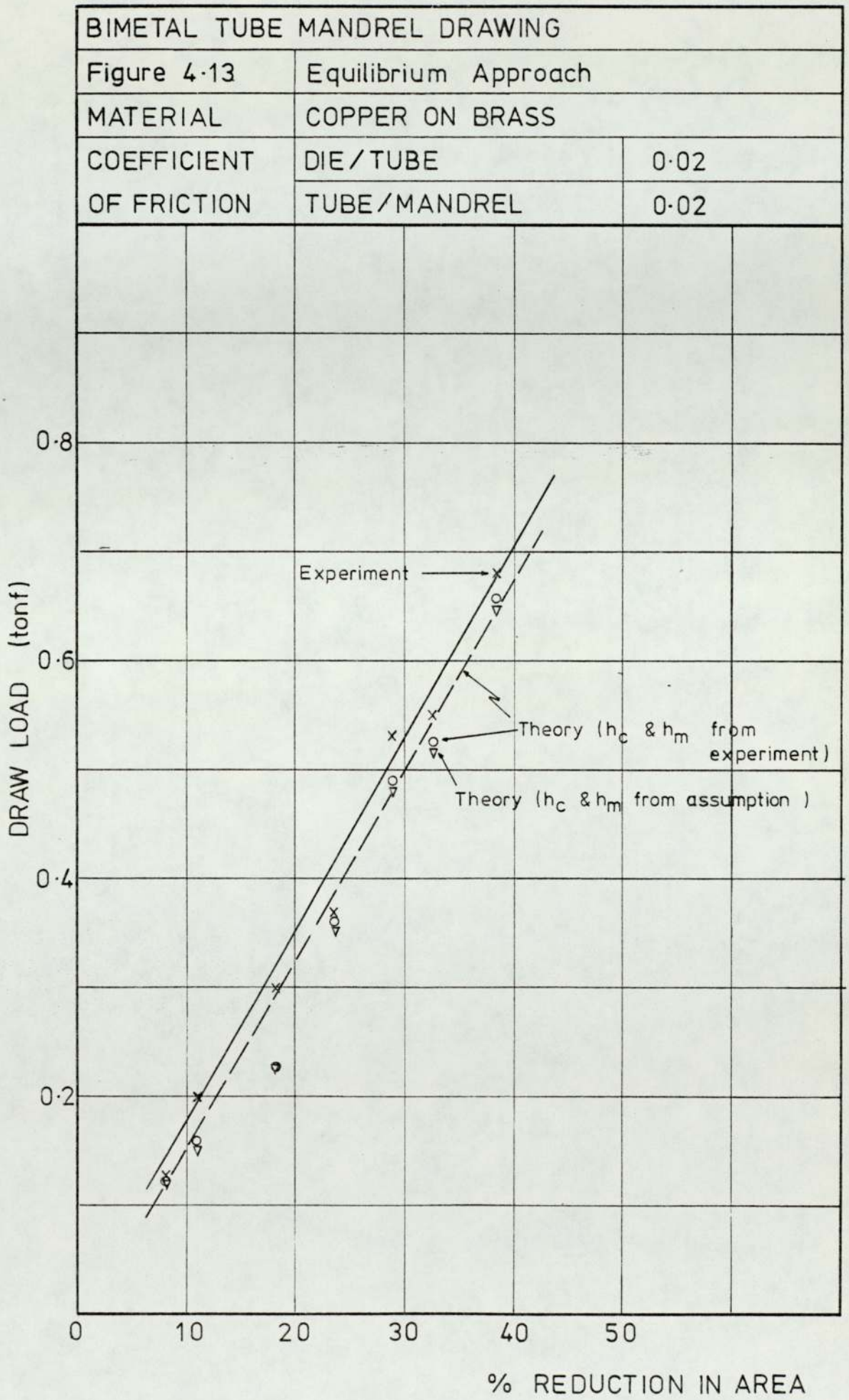
BIMETAL TUBE MANDREL DRAWING
Figure 4·13
Equilibrium Approach
MATERIAL
COPPER ON BRASS
COEFFICIENT OF FRICTION
DIE / TUBE
0·02
TUBE / MANDREL
0·02
Experiment
Theory (h_c & h_m from experiment)
Theory (h_c & h_m from assumption)
DRAW LOAD (tonf)
0·8
0·6
0·4
0·2
0
10
20
30
40
50
% REDUCTION IN AREA

BIMETAL TUBE MANDREL DRAWING		
Figure 4·14	Equilibrium Approach	
MATERIAL	BRASS ON STAINLESS STEEL	
COEFFICIENT OF FRICTION	DIE/TUBE	0·02
	TUBE/MANDREL	0·03

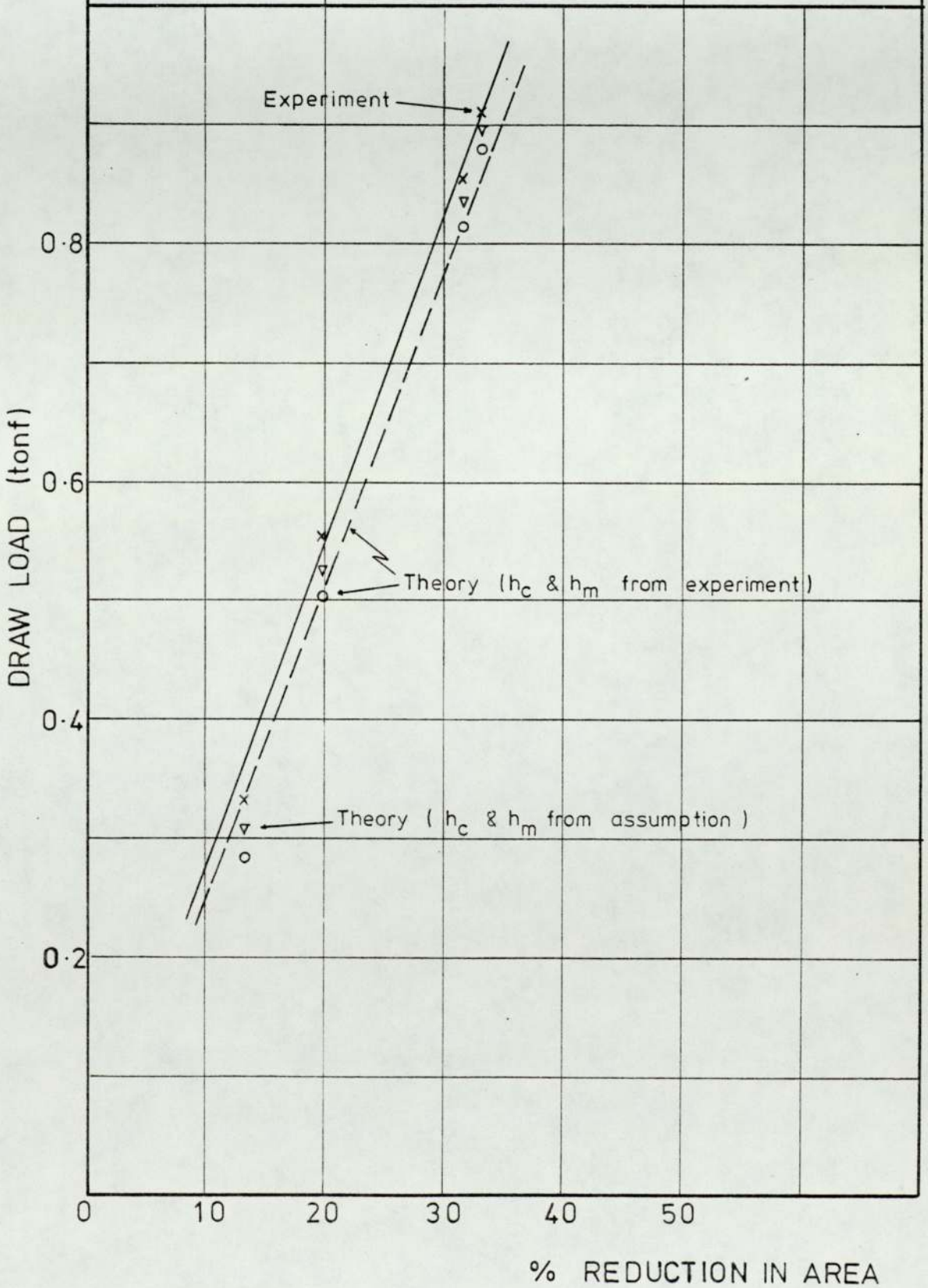

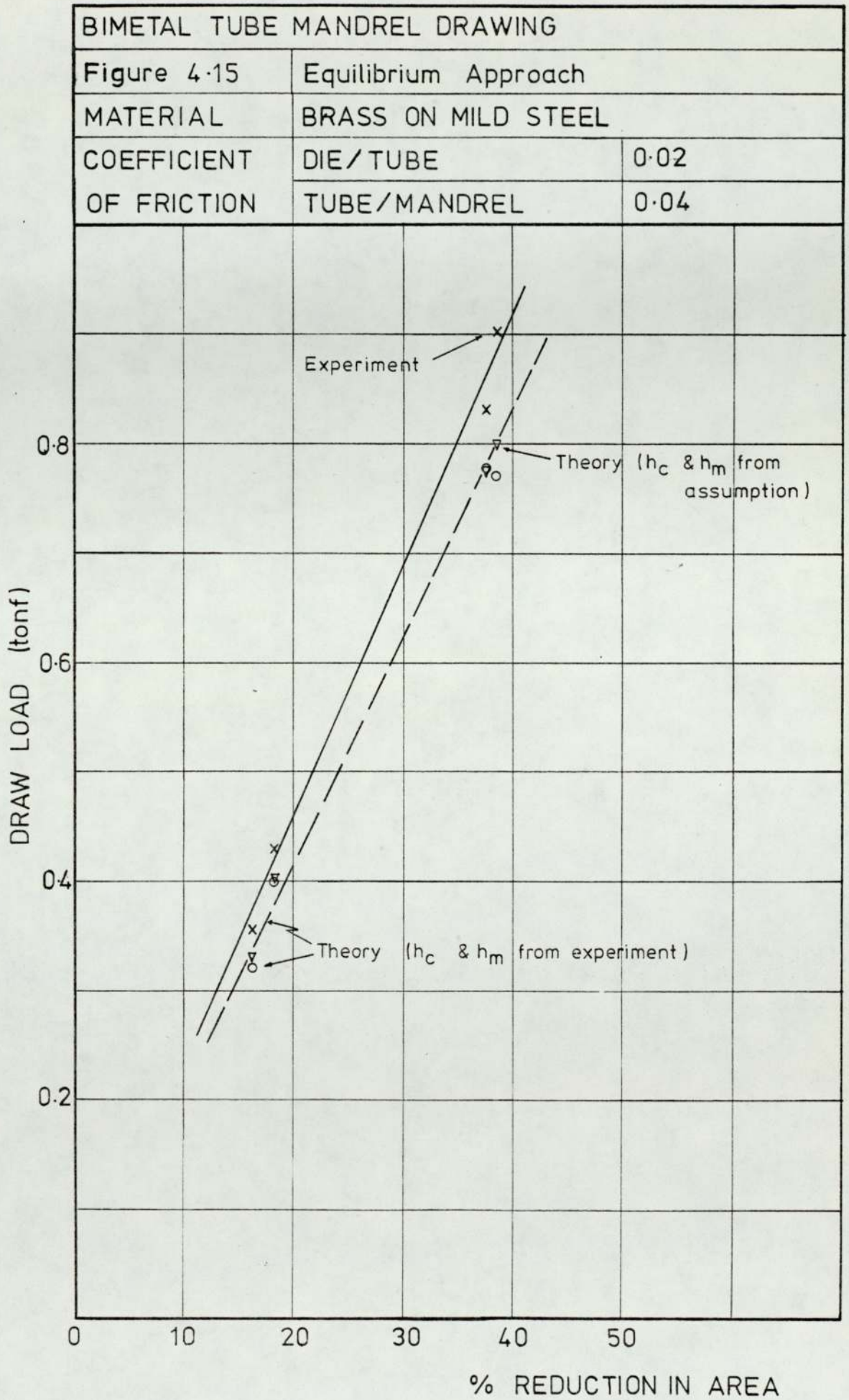
BIMETAL TUBE MANDREL DRAWING
Figure 4·15
Equilibrium Approach
MATERIAL
BRASS ON MILD STEEL
COEFFICIENT OF FRICTION
DIE / TUBE
0·02
TUBE / MANDREL
0·04
Experiment
Theory (hc & hm from assumption)
Theory (hc & hm from experiment)
DRAW LOAD (tonf)
0·8
0·6
0·4
0·2
0
10
20
30
40
50
% REDUCTION IN AREA

BIMETAL TUBE MANDREL DRAWING		
Figure 4·16	Equilibrium Approach	
MATERIAL	BRASS ON COPPER	
COEFFICIENT OF FRICTION	DIE/TUBE	0·02
	TUBE/MANDREL	0·01

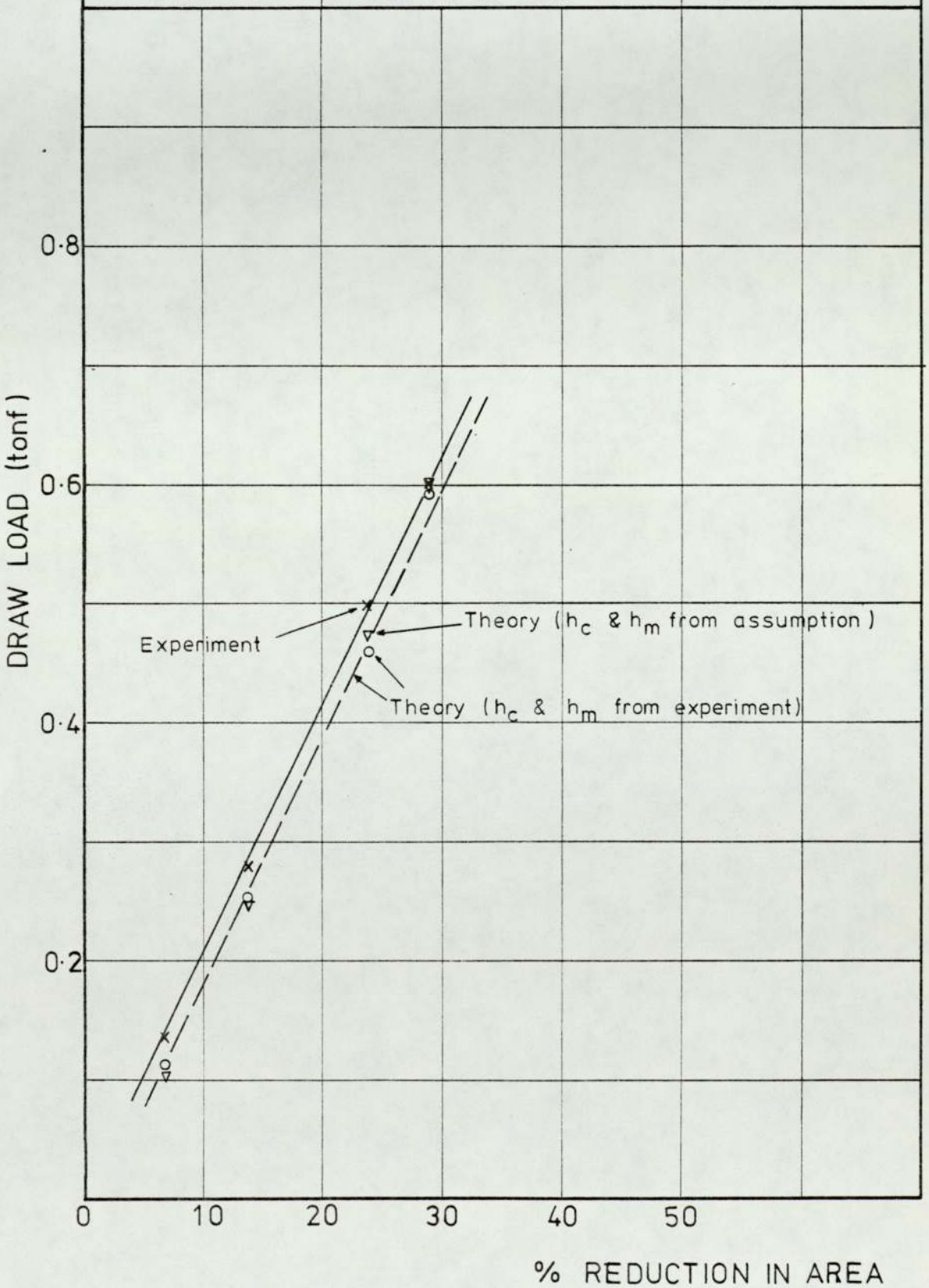

BIMETAL TUBE MANDREL DRAWING	
Figure 4·17	Equilibrium Approach
Material	Mild Steel on Brass

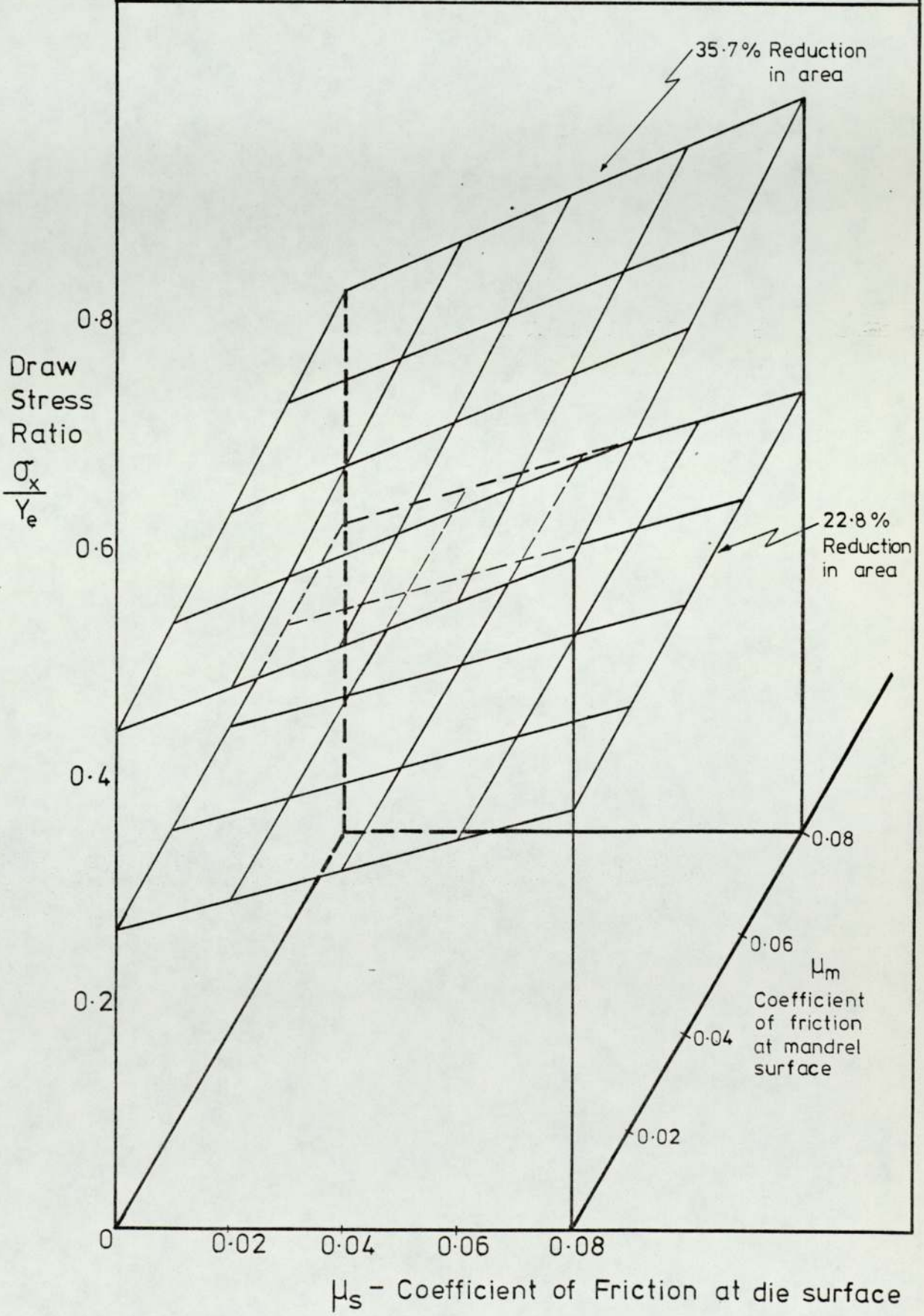

BIMETAL TUBE MANDREL DRAWING	
Figure 4·18	Equilibrium Approach
Material	Stainless Steel on Brass

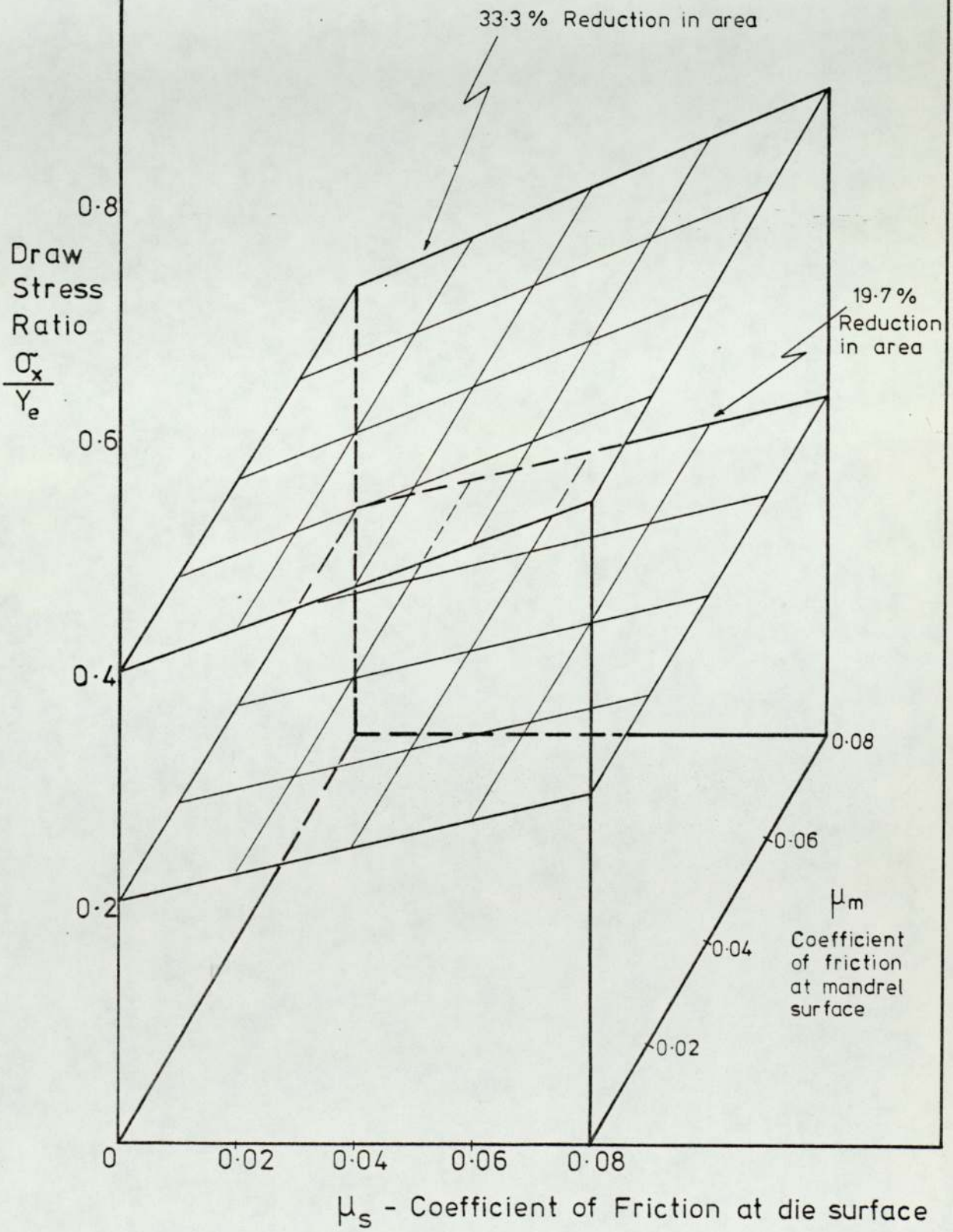

BIMETAL TUBE MANDREL DRAWING		
Figure 4·19	Equilibrium Approach	
MATERIAL	Stainless Steel on Mild Steel	
COEFFICIENT OF FRICTION	DIE / TUBE	0·08
	TUBE / MANDREL	0·02

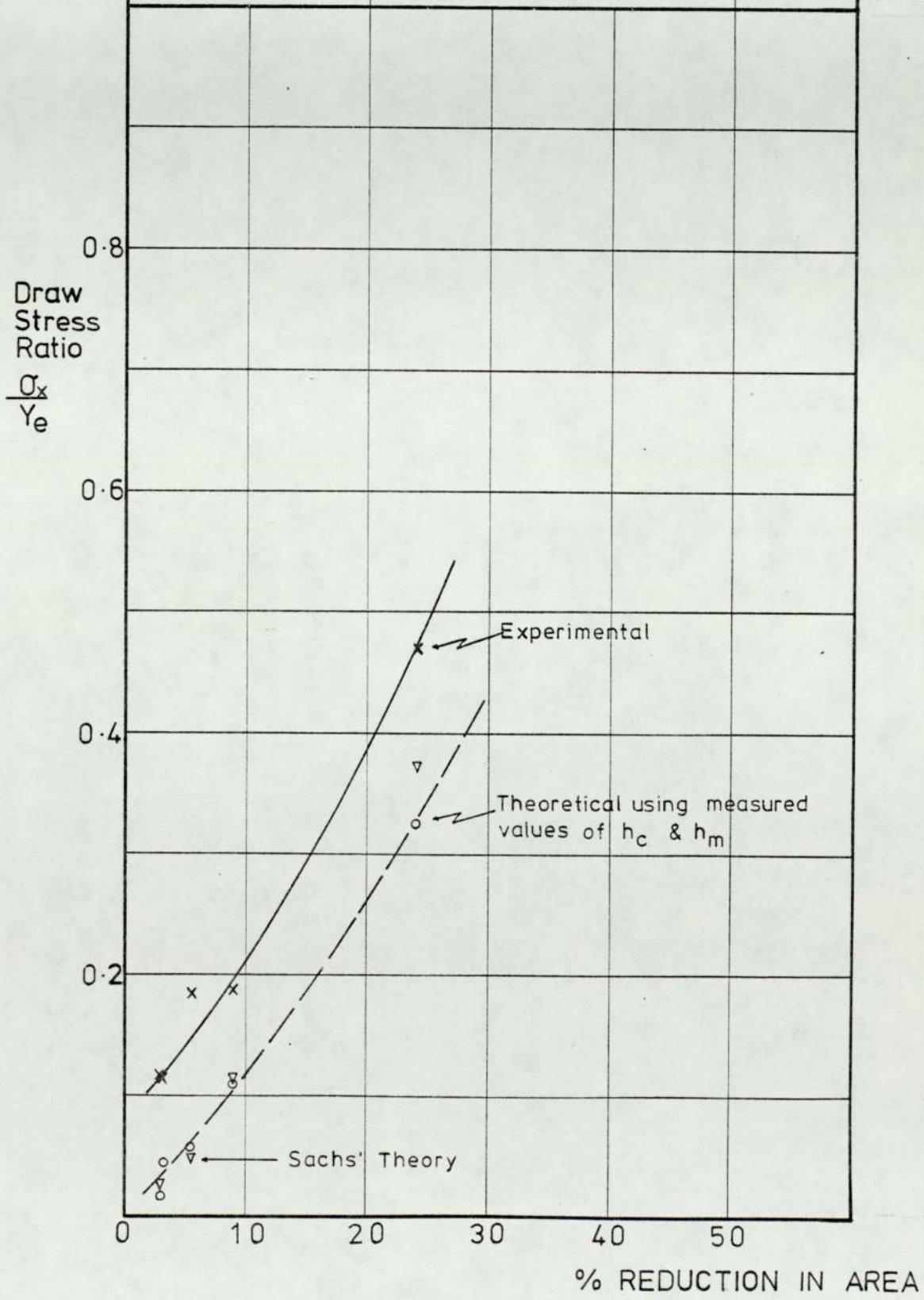

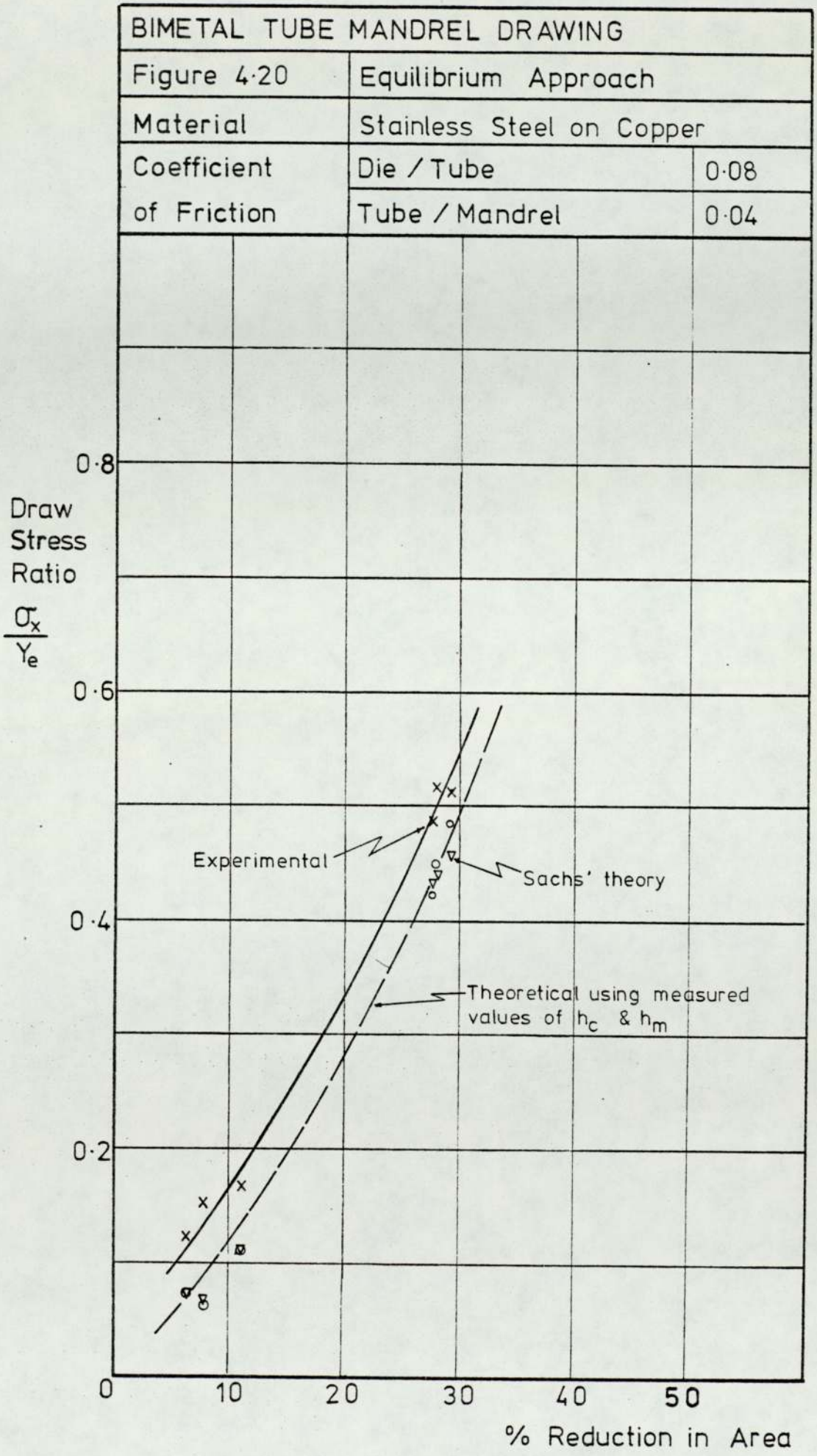
BIMETAL TUBE MANDREL DRAWING
Figure 4·20
Equilibrium Approach
Material
Stainless Steel on Copper
Coefficient of Friction
Die / Tube
0·08
Tube / Mandrel
0·04
Draw Stress Ratio
$\frac{\sigma_x}{Y_e}$
0·8
0·6
0·4
0·2
0
10
20
30
40
50
% Reduction in Area
Experimental
Sachs' theory
Theoretical using measured values of h_c & h_m

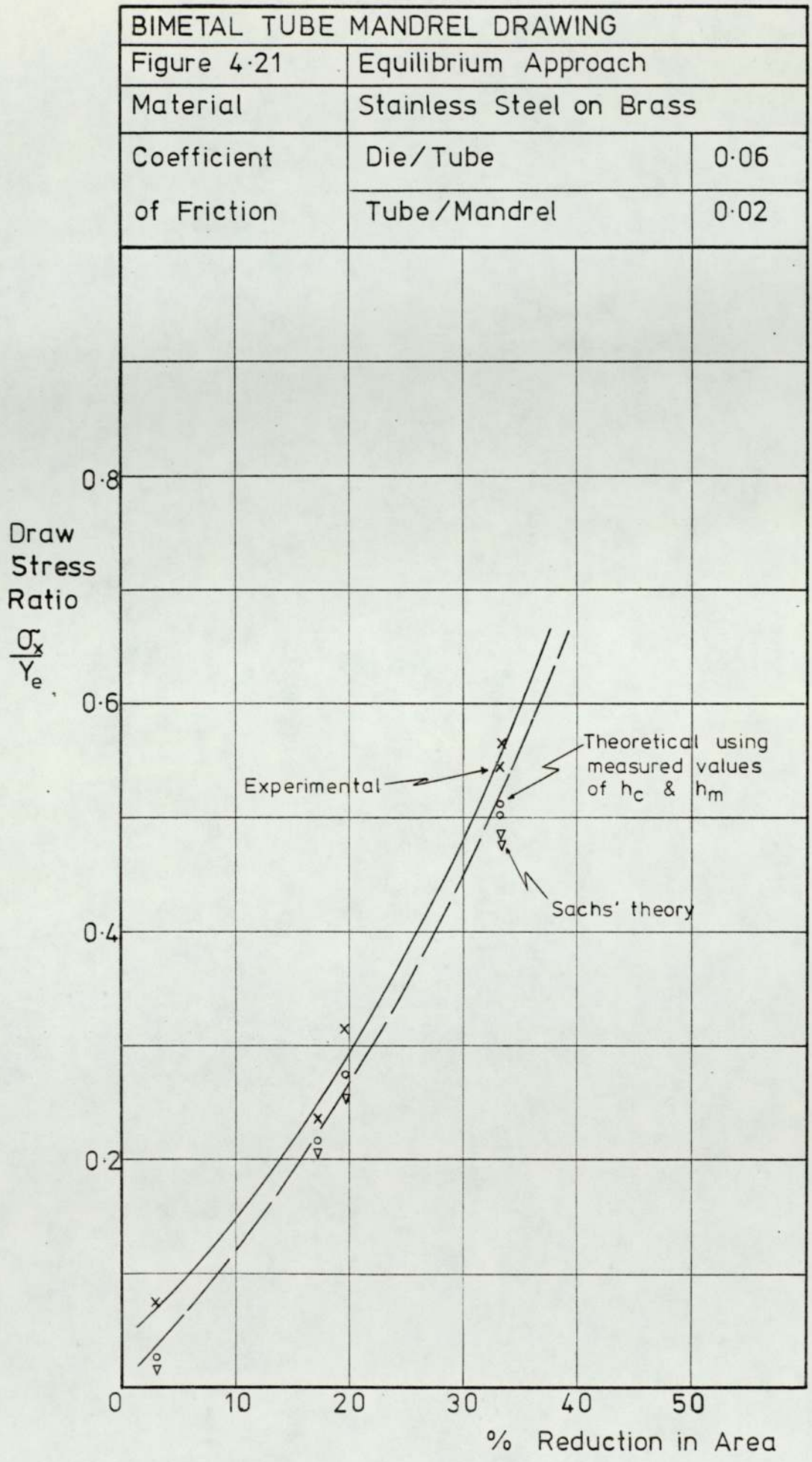
BIMETAL TUBE MANDREL DRAWING
Figure 4·21
Equilibrium Approach
Material
Stainless Steel on Brass
Coefficient of Friction
Die/Tube
0·06
Tube/Mandrel
0·02
Draw Stress Ratio
$\frac{\sigma_x}{Y_e}$
0·8
0·6
0·4
0·2
0
10
20
30
40
50
% Reduction in Area
Experimental
Theoretical using measured values of h_c & h_m
Sachs' theory

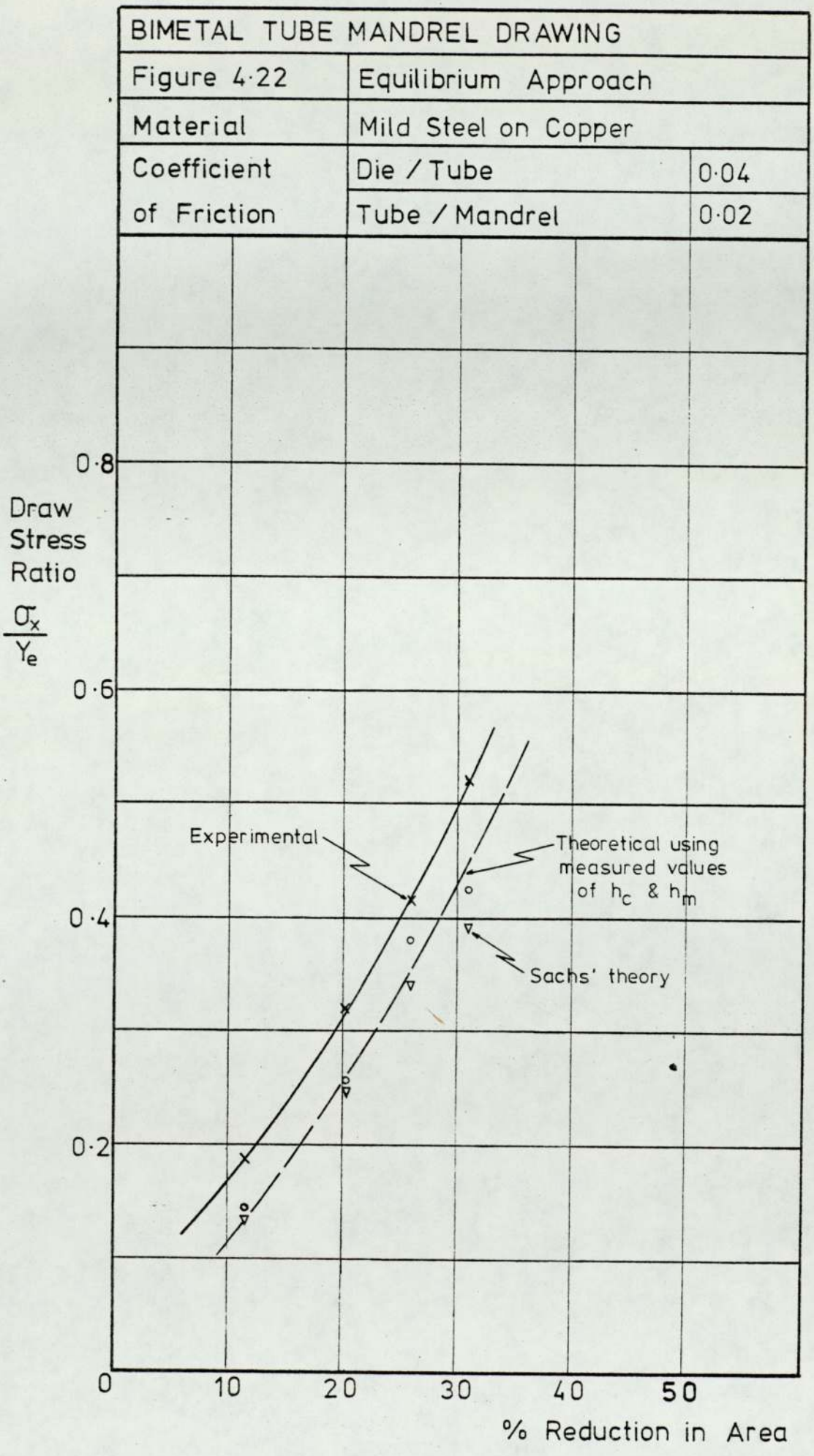
BIMETAL TUBE MANDREL DRAWING
Figure 4·22
Equilibrium Approach
Material
Mild Steel on Copper
Coefficient of Friction
Die / Tube
0·04
Tube / Mandrel
0·02
Draw Stress Ratio
$\frac{\sigma_x}{Y_e}$
0·8
0·6
0·4
0·2
0
10
20
30
40
50
% Reduction in Area
Experimental
Theoretical using measured values of h_c & h_m
Sachs' theory

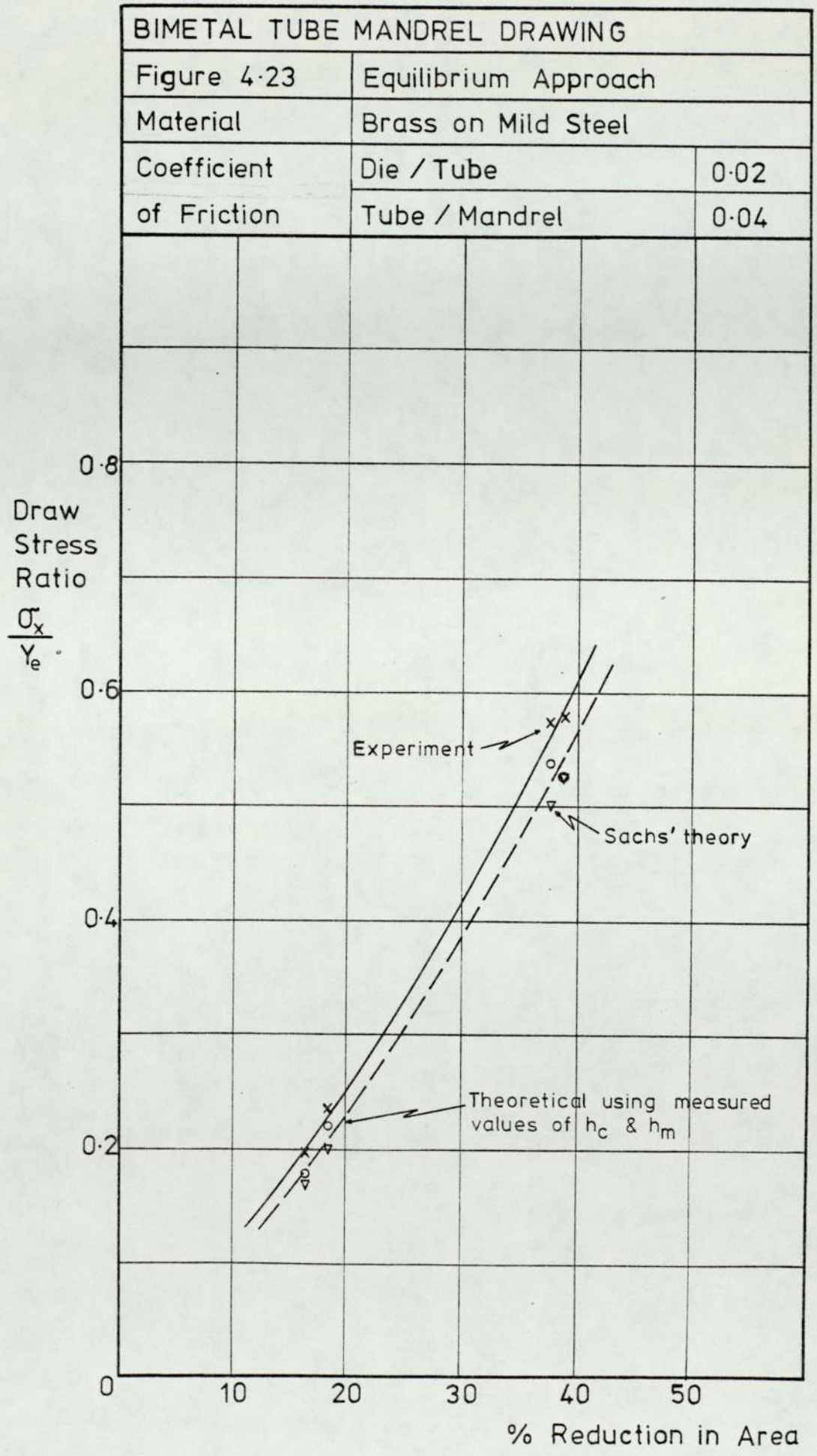
BIMETAL TUBE MANDREL DRAWING
Figure 4·23
Equilibrium Approach
Material
Brass on Mild Steel
Coefficient of Friction
Die / Tube
0·02
Tube / Mandrel
0·04
Draw Stress Ratio
$\frac{\sigma_x}{Y_e}$
0·8
0·6
0·4
0·2
0
Experiment
Sachs' theory
Theoretical using measured values of h_c & h_m
10
20
30
40
50
% Reduction in Area

Figure 4·24	BIMETAL TUBE MANDREL DRAWING AN UPPER BOUND SOLUTION				
Material	Stainless Steel on Mild Steel				
Mean Yield Stress	Clad	79·0 tonf.in^{-2}	Matrix	42·5 tonf.in^{-2}	
Assumed Friction Factor at tube-tube interface = 0·02					

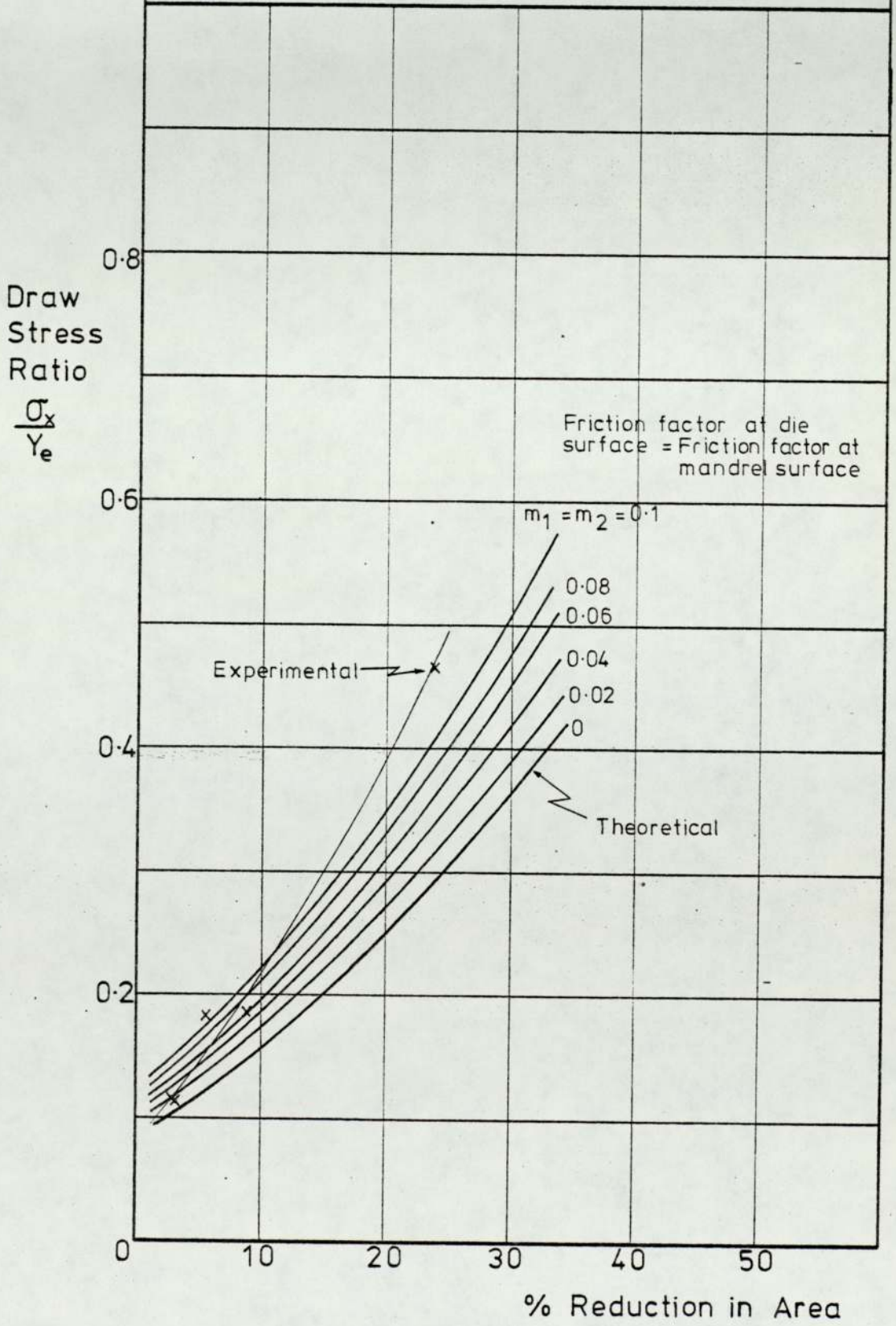

Figure 4·25	BIMETAL TUBE MANDREL DRAWING AN UPPER BOUND SOLUTION				
Material	Stainless Steel on Copper				
Mean Yield Stress	Clad	79·0 tonf.in^{-2}	Matrix	34·0 tonf.in^{-2}	
Assumed Friction Factor at tube-tube interface = 0·02					

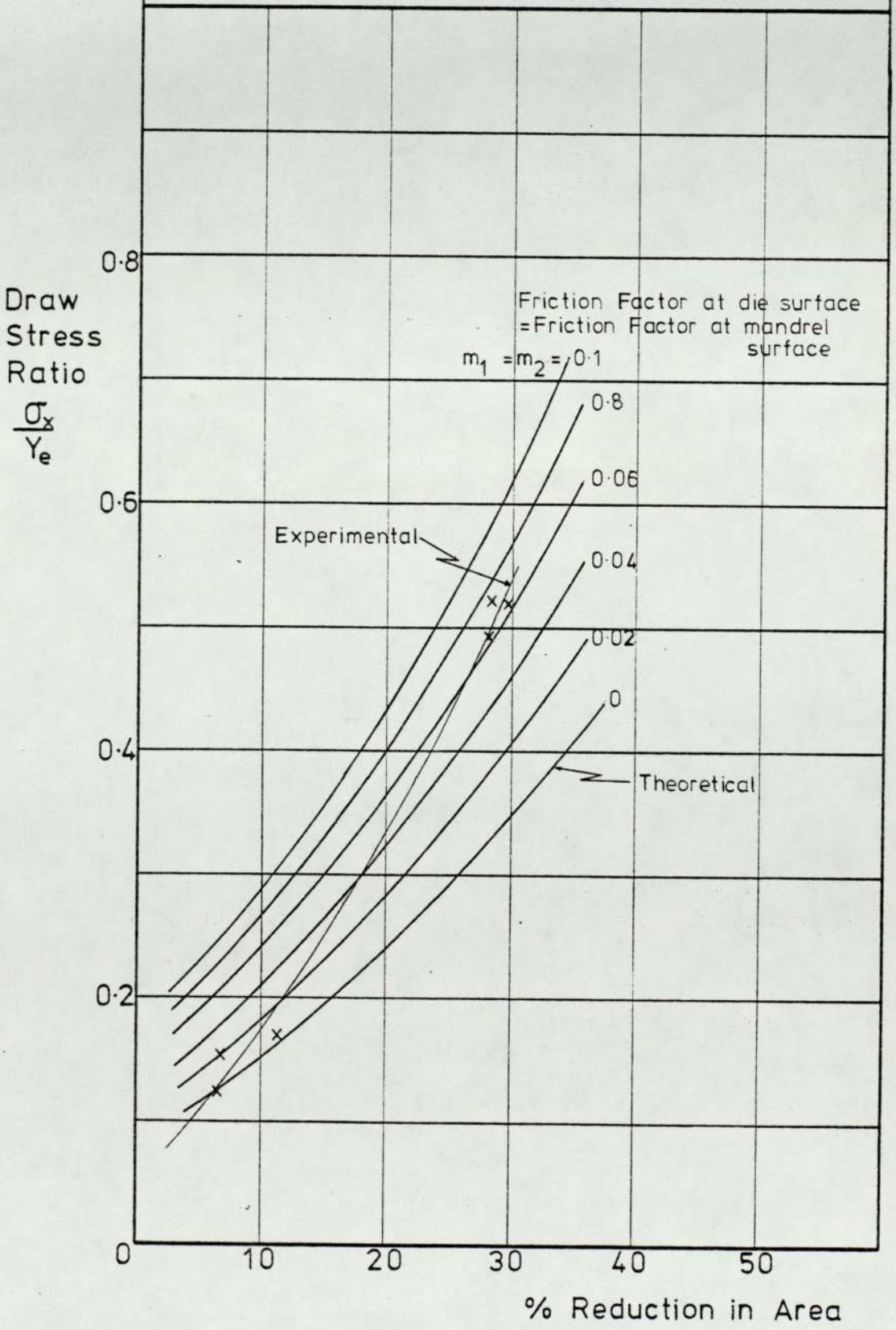

Figure 4·26	BIMETAL TUBE MANDREL DRAWING AN UPPER BOUND SOLUTION				
Material	Stainless Steel on Brass				
Mean Yield Stress	Clad	79·0 tonf.in^{-2}	Matrix	44·8 tonf.in^{-2}	
Assumed Friction Factor at tube-tube interface = 0·02					

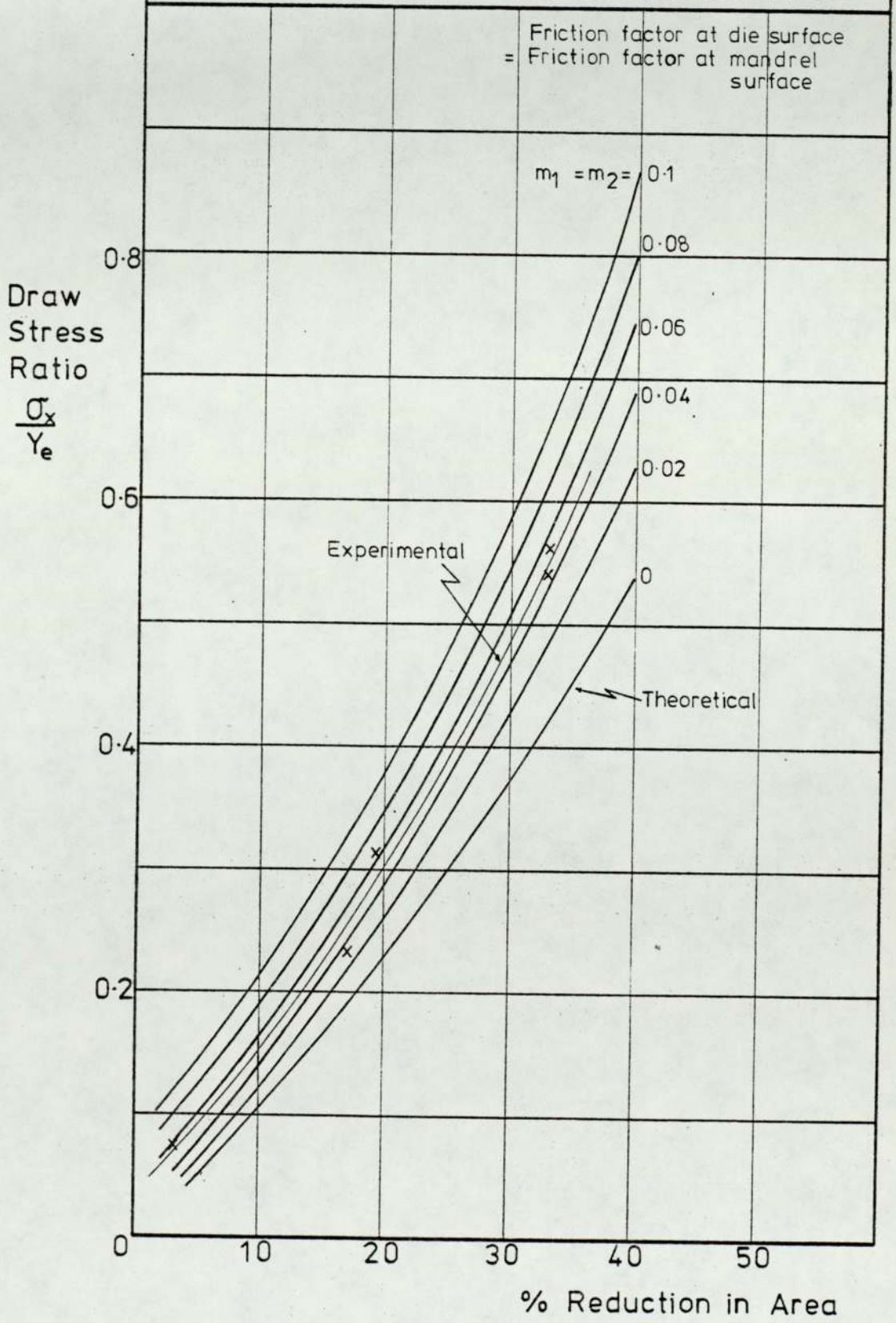

Figure 4·27	BIMETAL TUBE MANDREL DRAWING AN UPPER BOUND SOLUTION				
Material	Mild Steel on Copper				
Mean Yield Stress	Clad	42·5 tonf.in^{-2}	Matrix	34·0 tonf.in^{-2}	
Assumed Friction Factor at tube-tube interface = 0·02					

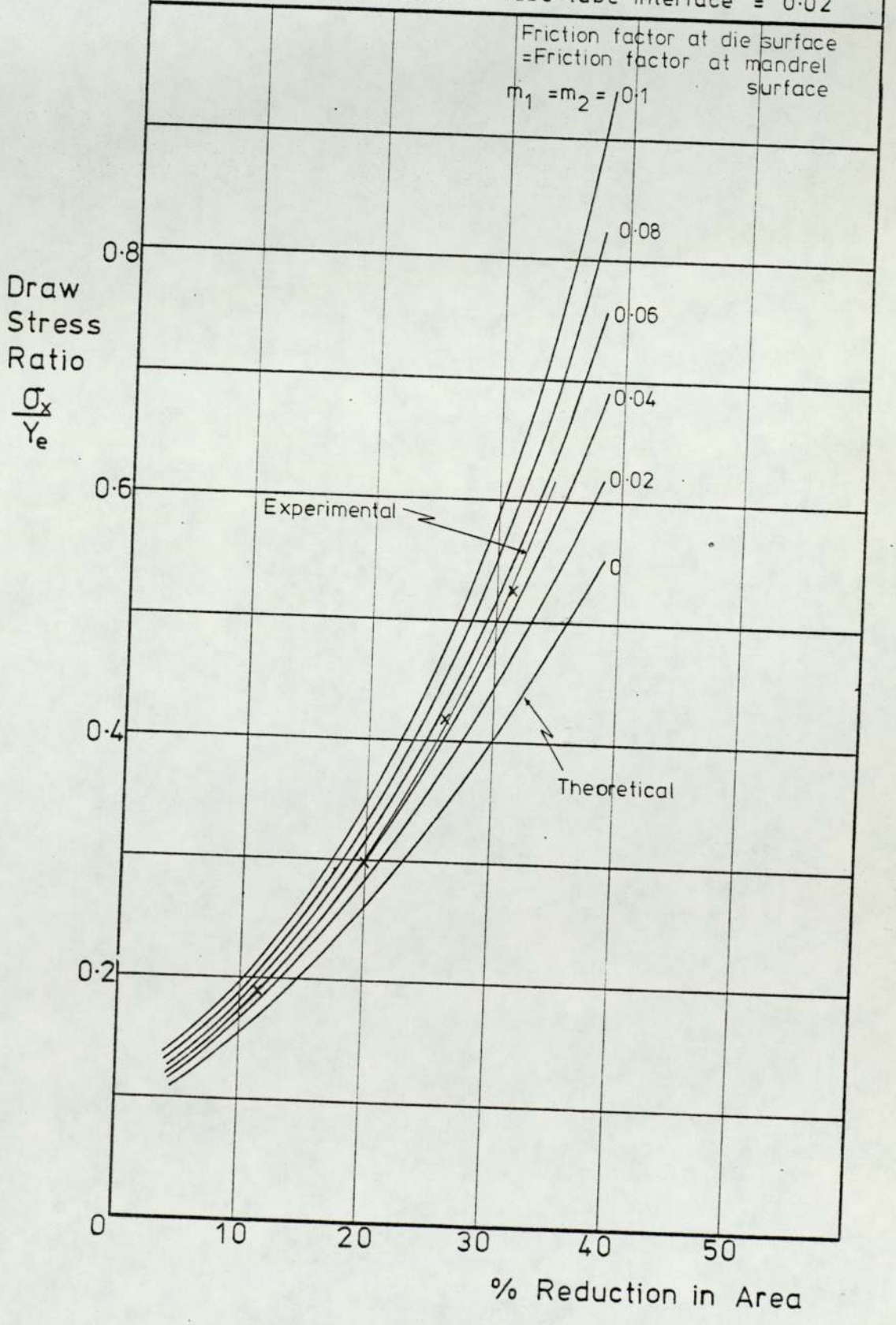

Figure 4·28	BIMETAL TUBE MANDREL DRAWING AN UPPER BOUND SOLUTION				
Material	Mild Steel on Brass				
Mean Yield Stress	Clad	42·5 tonf.in^{-2}	Matrix	44·8 tonf.in^{-2}	
Assumed Friction Factor at tube-tube interface = 0·02					

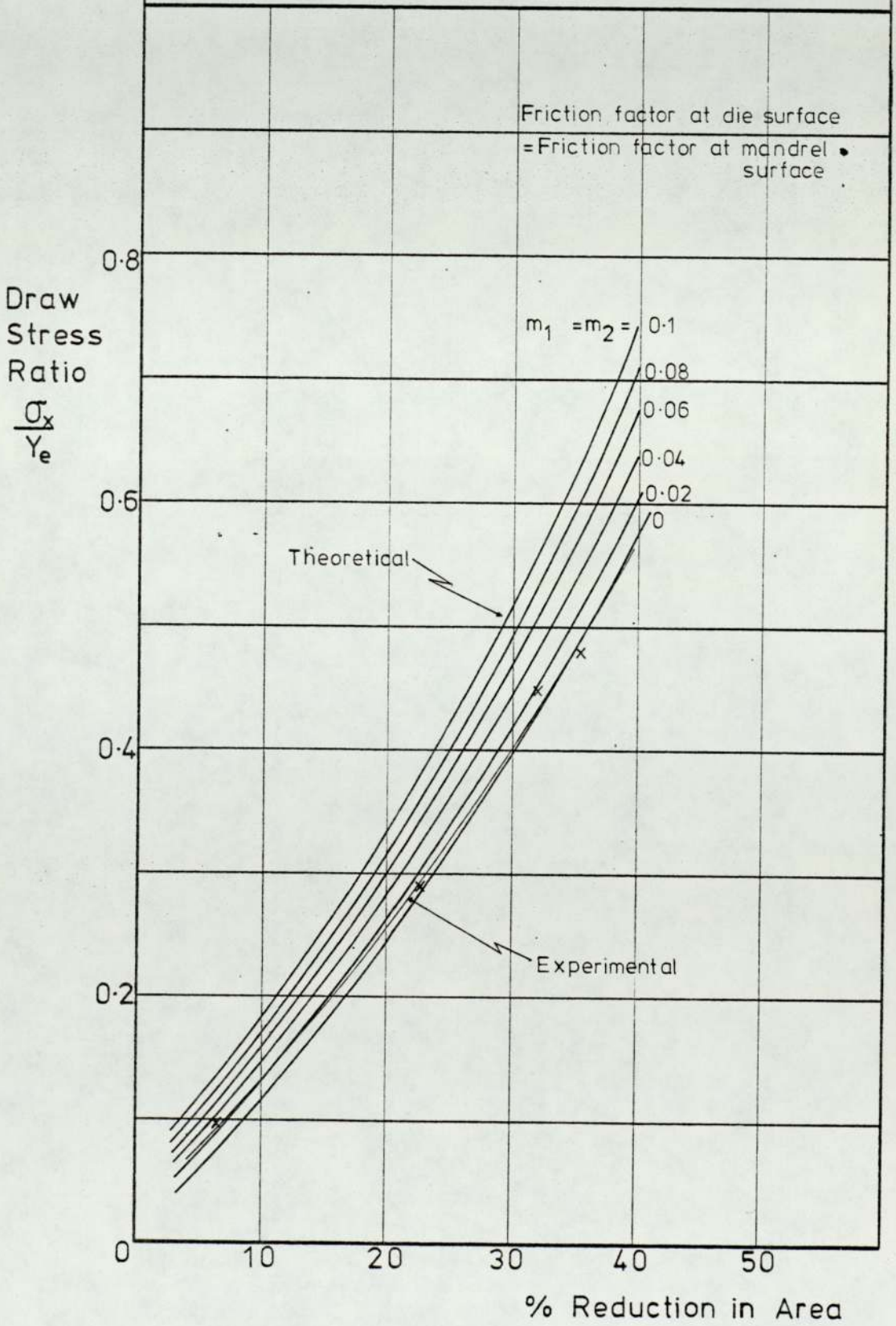

Figure 4·29	BIMETAL TUBE MANDREL DRAWING AN UPPER BOUND SOLUTION				
Material	Copper on Stainless Steel				
Mean Yield Stress	Clad	34·0 tonf.in^{-2}	Matrix	79·0 tonf.in^{-2}	
Assumed Friction Factor at tube-tube interface = 0·02					

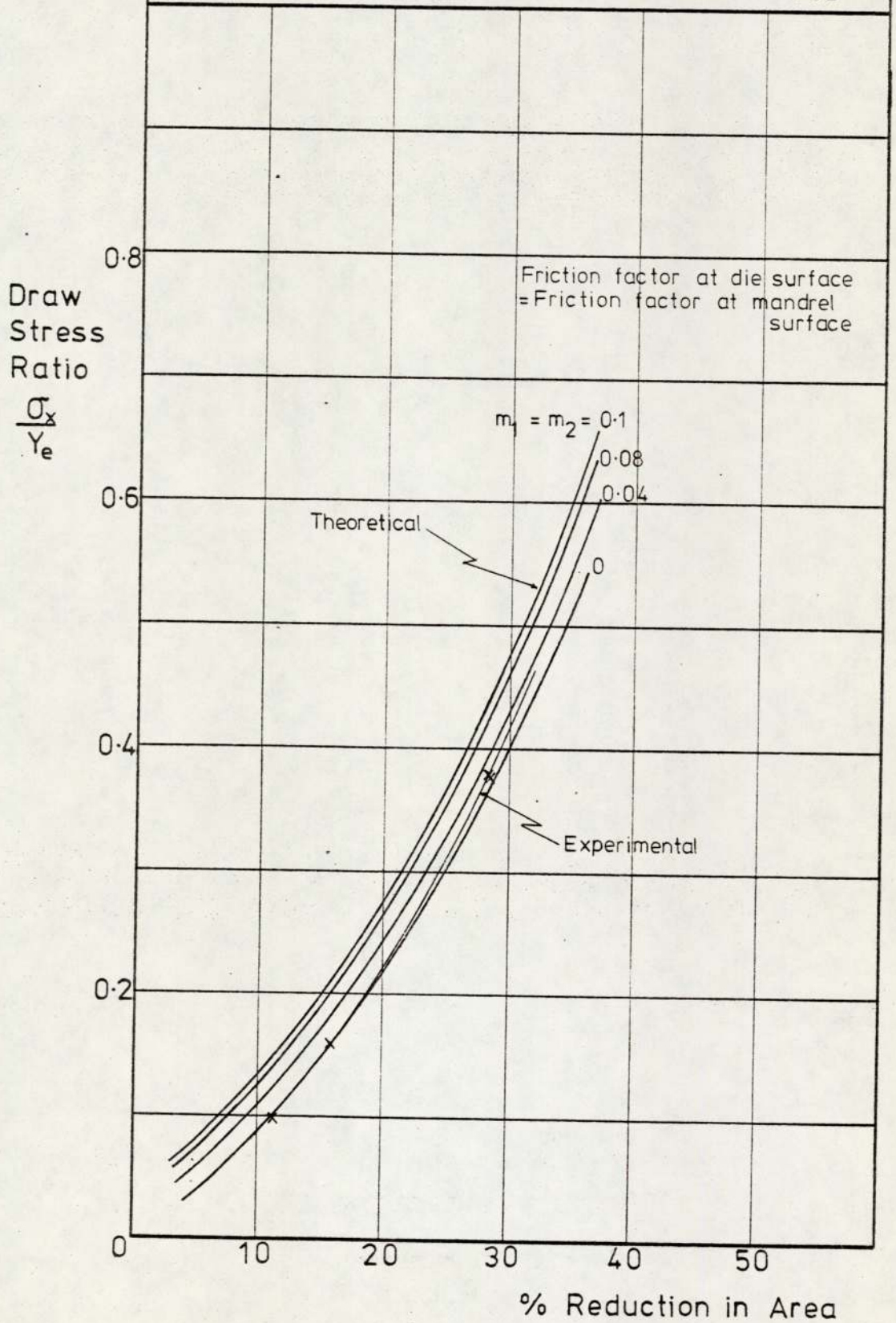

Figure 4·30	BIMETAL TUBE MANDREL DRAWING AN UPPER BOUND SOLUTION				
Material	Copper on Mild Steel				
Mean Yield Stress	Clad	34·0 tonf.in^{-2}	Matrix	42·5 tonf.in^{-2}	
Assumed Friction Factor at tube-tube interface = 0·02					

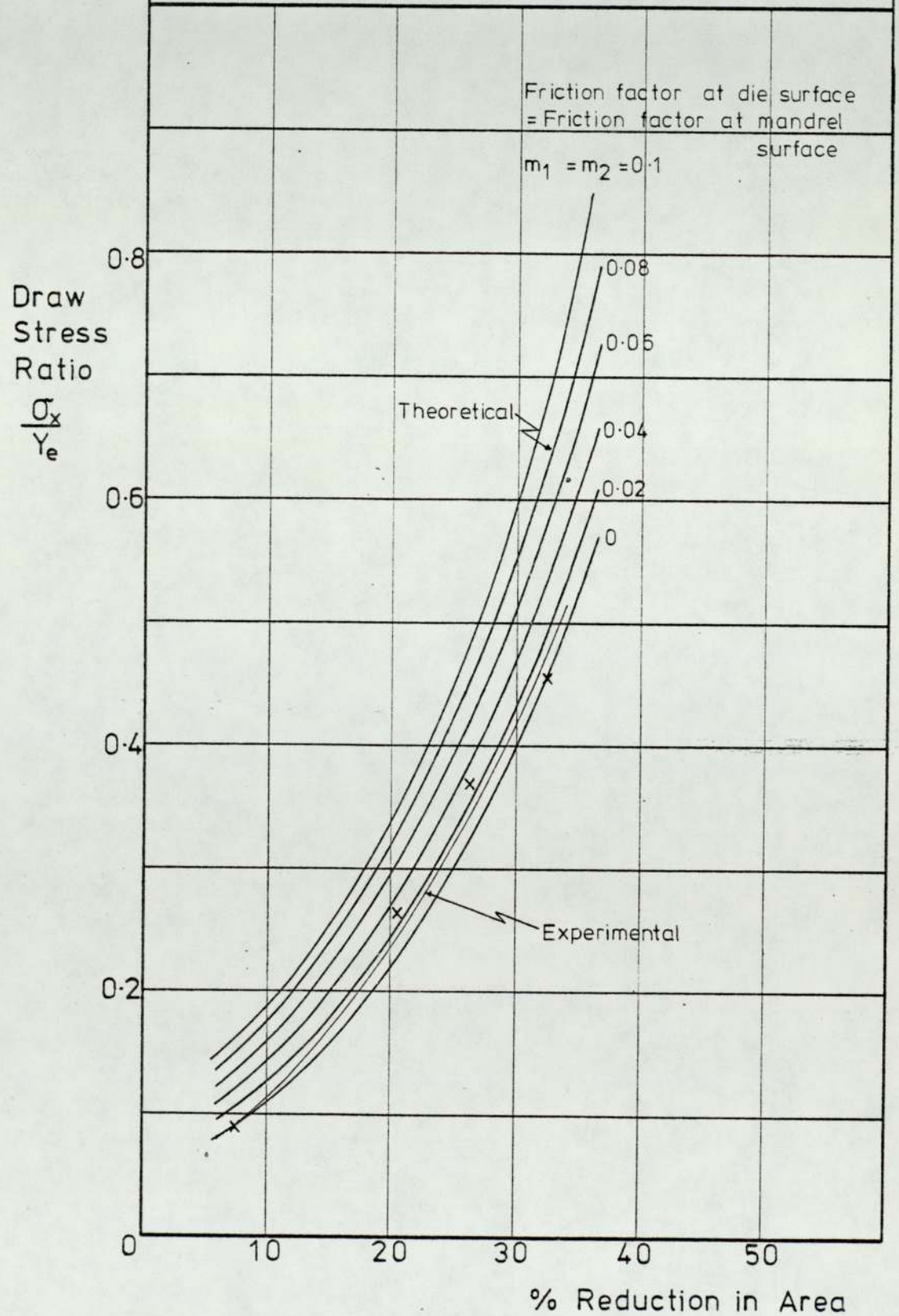

Figure 4·31	BIMETAL TUBE MANDREL DRAWING AN UPPER BOUND SOLUTION				
Material	Copper on Brass				
Mean Yield Stress	Clad	34·0 tonf.in^{-2}	Matrix	44·8 tonf.in^{-2}	
Assumed Friction Factor at tube-tube interface = 0·02					

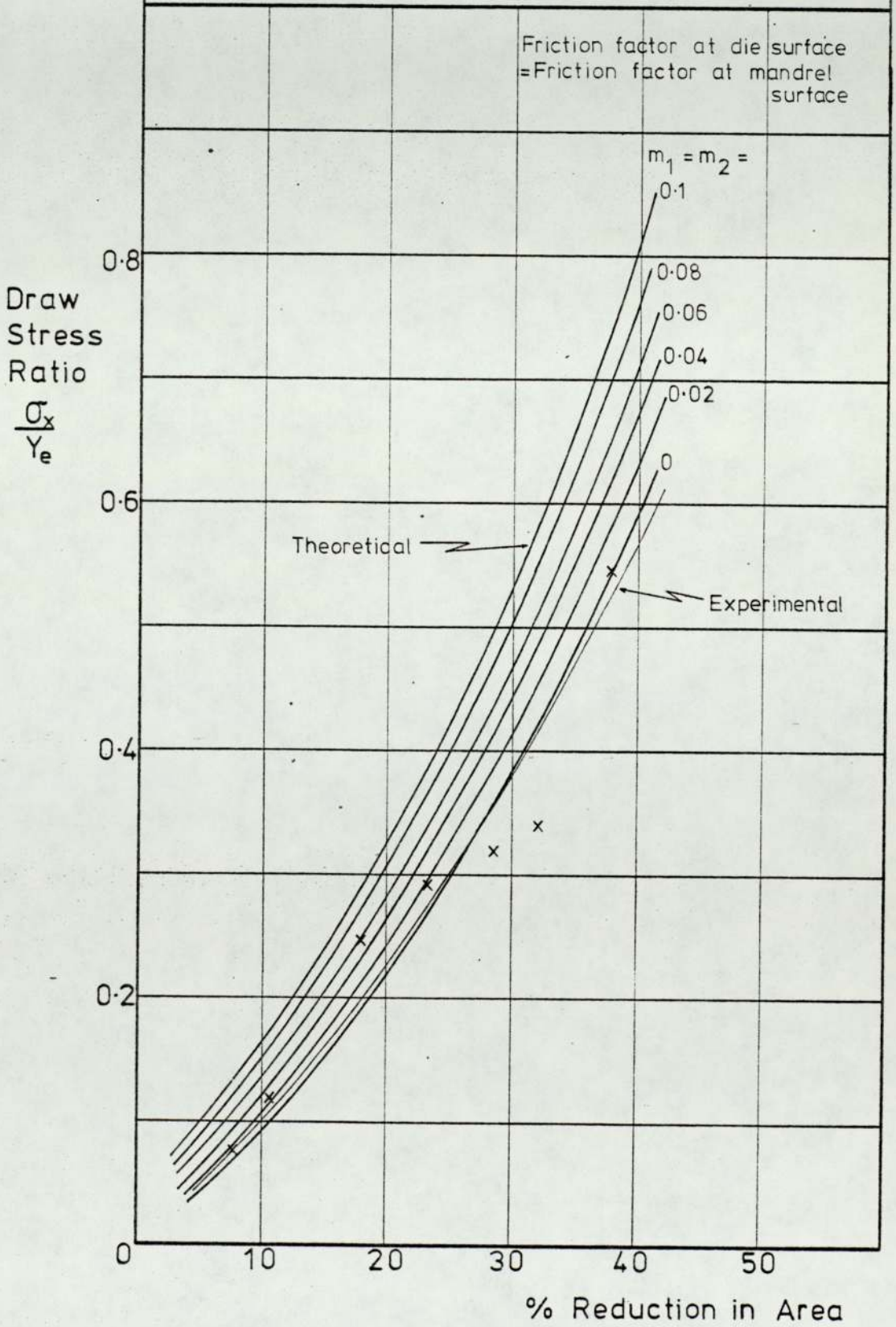

Figure 4·32	BIMETAL TUBE MANDREL DRAWING AN UPPER BOUND SOLUTION				
Material	Brass on Stainless Steel				
Mean Yield Stress	Clad	44·8 tonf.in^{-2}	Matrix	79·0 tonf.in^{-2}	
Assumed Friction Factor at tube-tube interface = 0·02					

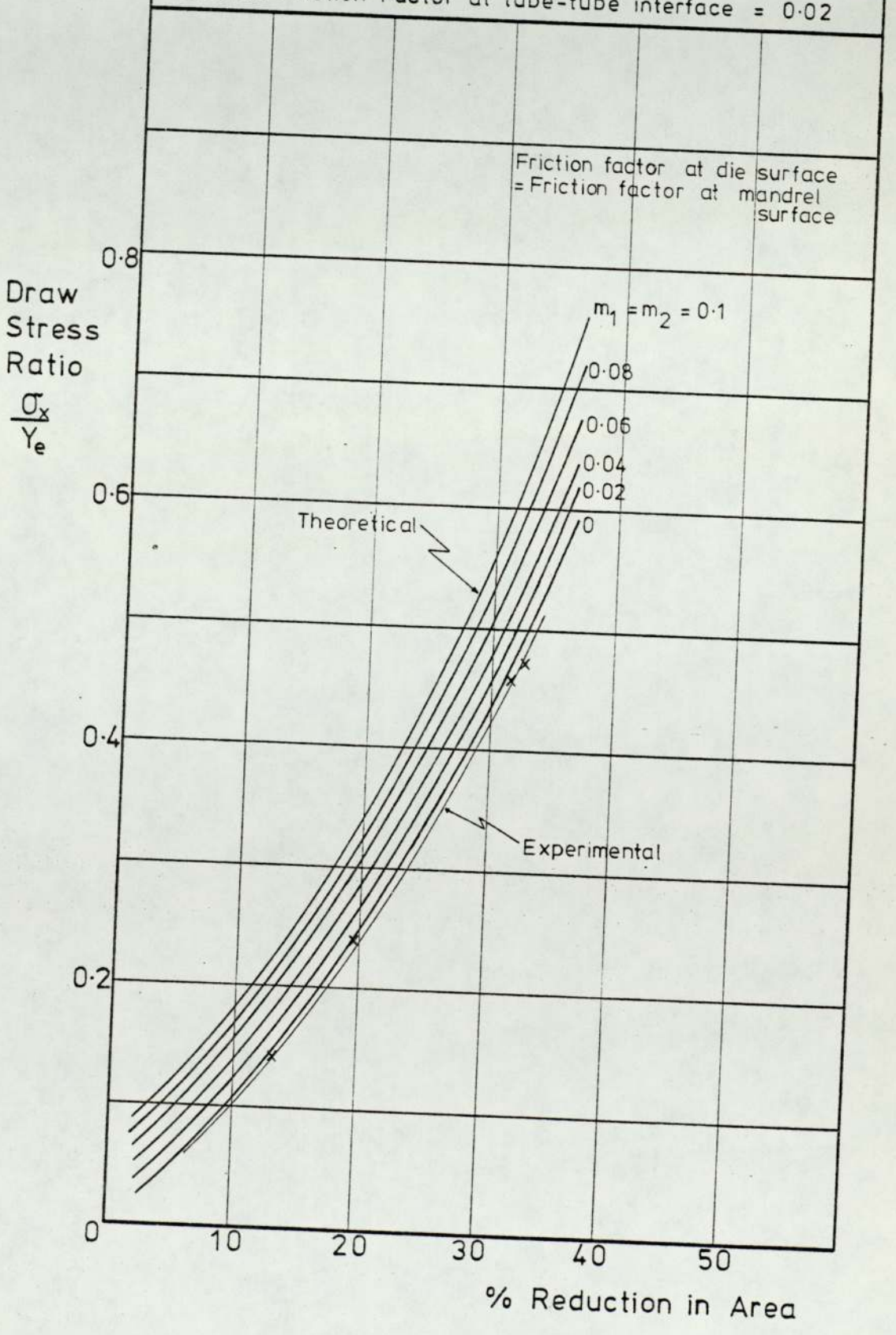

Figure 4·33	BIMETAL TUBE MANDREL DRAWING AN UPPER BOUND SOLUTION				
Material	Brass on Mild Steel				
Mean Yield Stress	Clad	44·8 tonf.in^{-2}	Matrix	42·5 tonf.in^{-2}	
Assumed Friction Factor at tube-tube interface = 0·02					

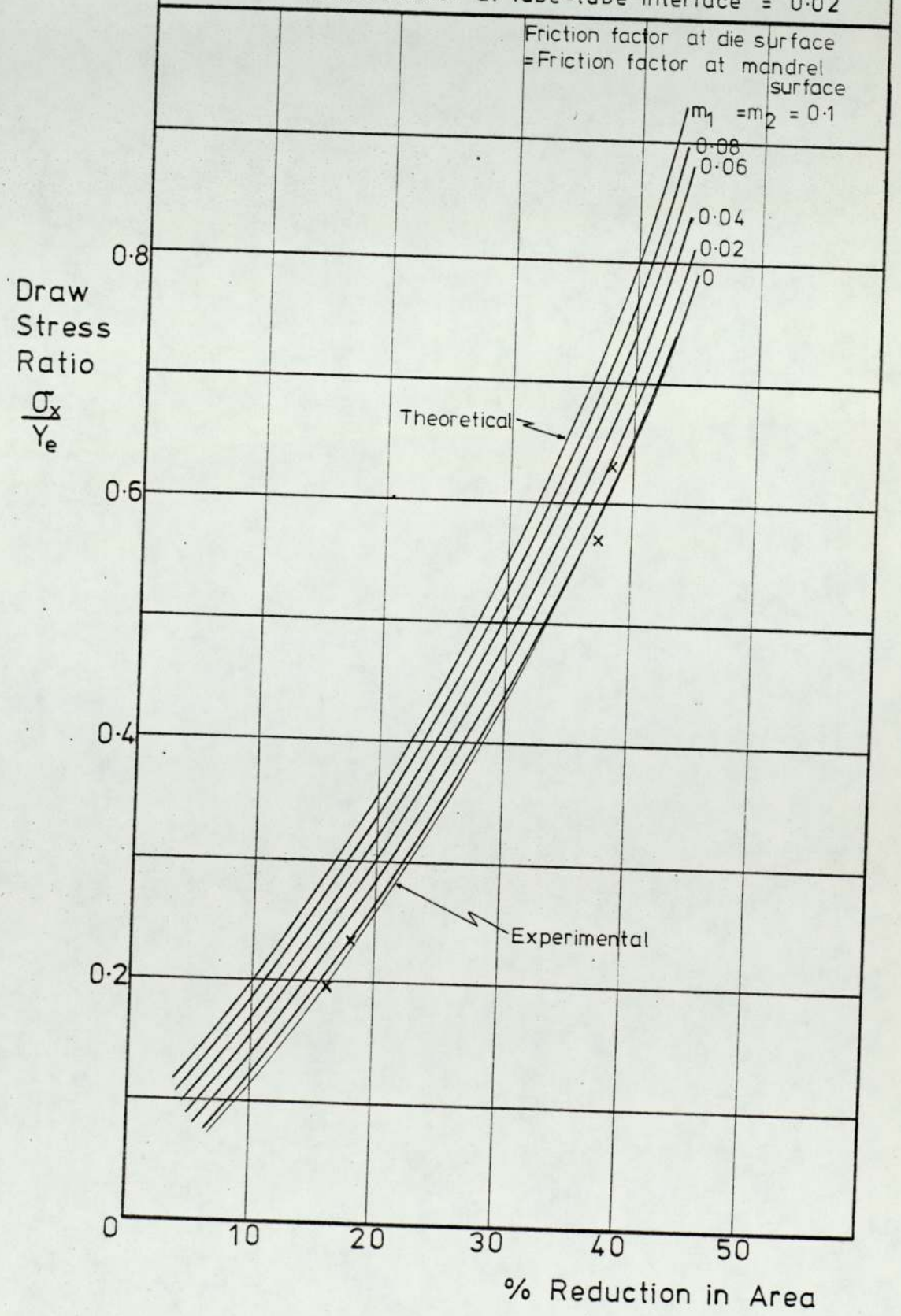

Figure 4·34	BIMETAL TUBE MANDREL DRAWING AN UPPER BOUND SOLUTION				
Material	Brass on Copper				
Mean Yield Stress	Clad	44·8 tonf.in^{-2}	Matrix	34·0 tonf.in^{-2}	
Assumed Friction Factor at tube-tube interface = 0·02					

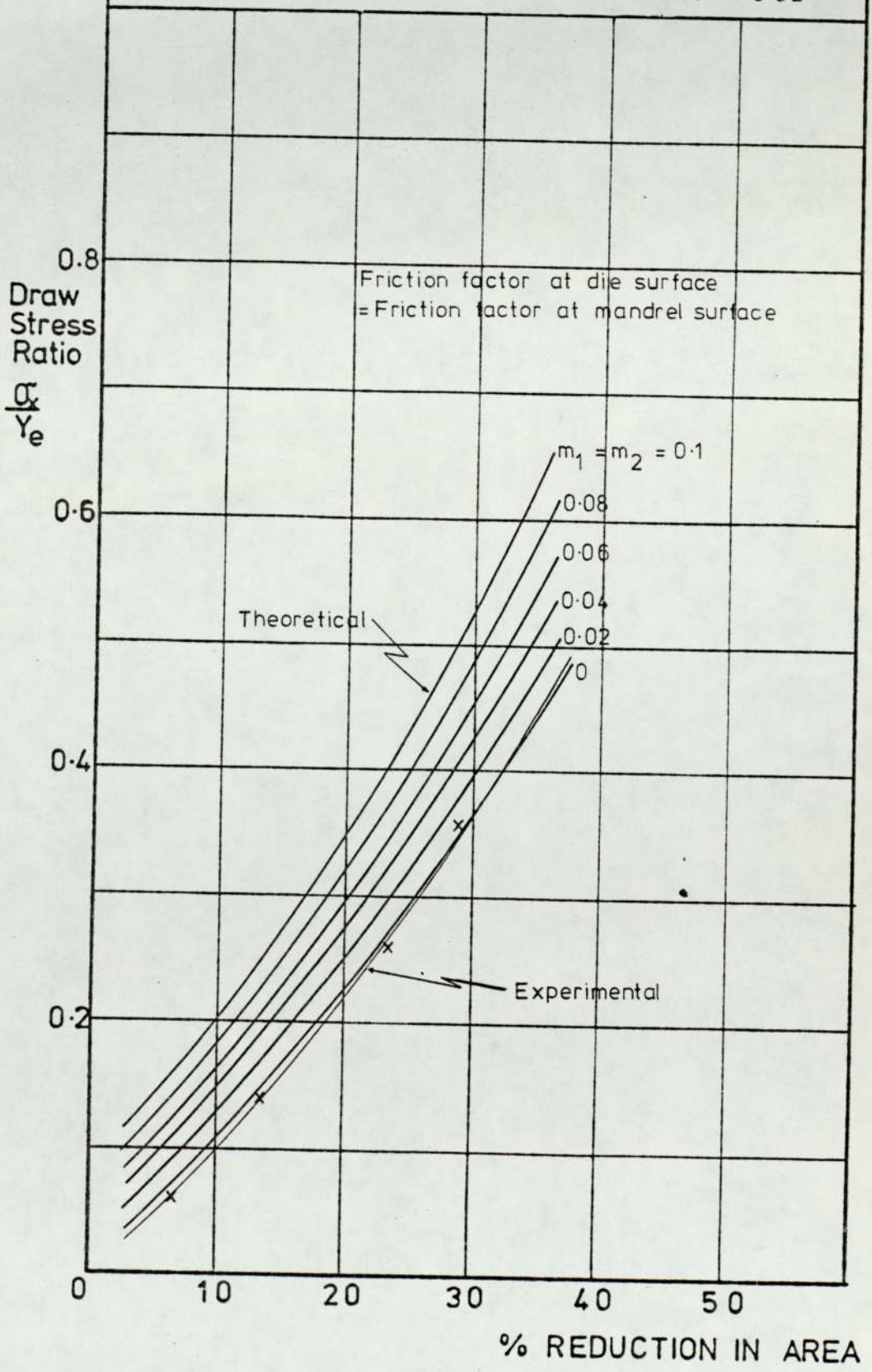

Figure 4·35	BIMETAL TUBE MANDREL DRAWING AN UPPER BOUND SOLUTION
Material	Stainless Steel on Brass

Assumed friction factor at tube-tube interface = 0·02

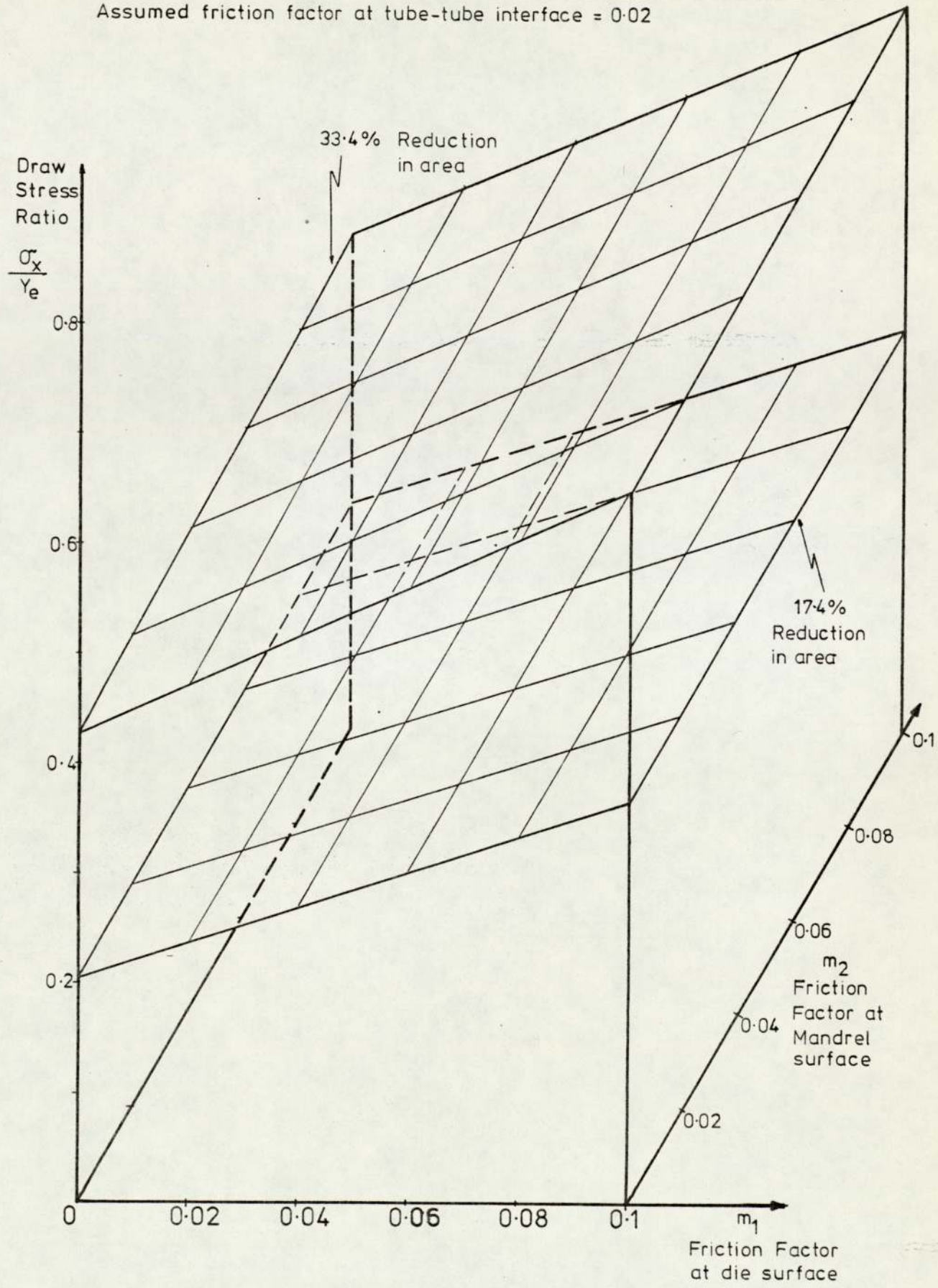

Figure 4.36	BIMETAL TUBE MANDREL DRAWING AN UPPER BOUND SOLUTION
Material	Mild Steel on Brass
Graph for the case when friction factor at mandrel surface = 0·0 Assumed friction factor at tube-tube interface = 0·02	

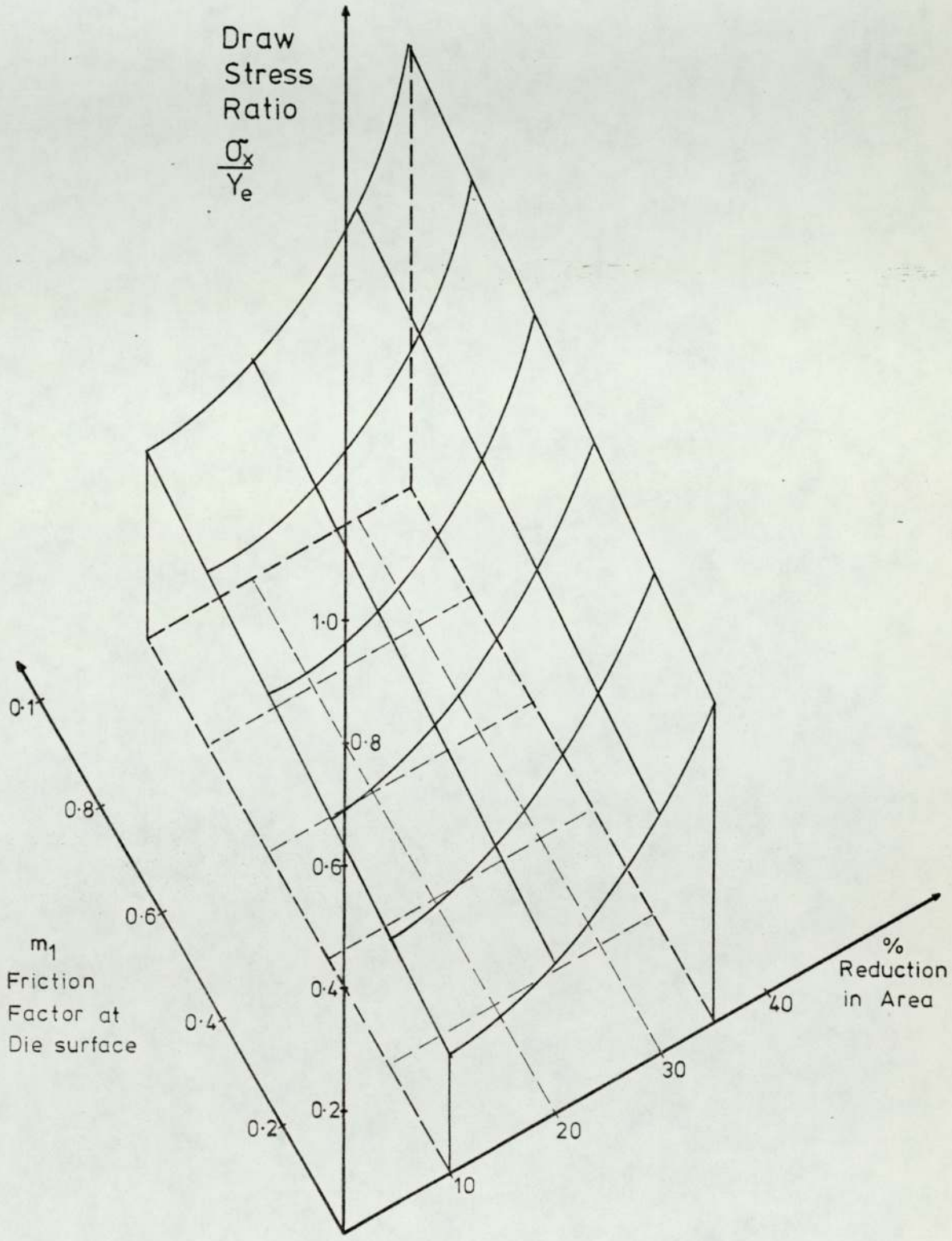

Figure 4·37	BIMETAL TUBE DRAWING ON A FLOATING PLUG AN UPPER BOUND SOLUTION			
Material	Stainless Steel on Mild Steel			
Mean Yield Stress ($tonf.in^{-2}$)	Clad	76·2	Initial Clad Thickness (in)	0·015 & 0·016
	Matrix	46·0	Initial Matrix Thickness (in)	0·016 & 0·015

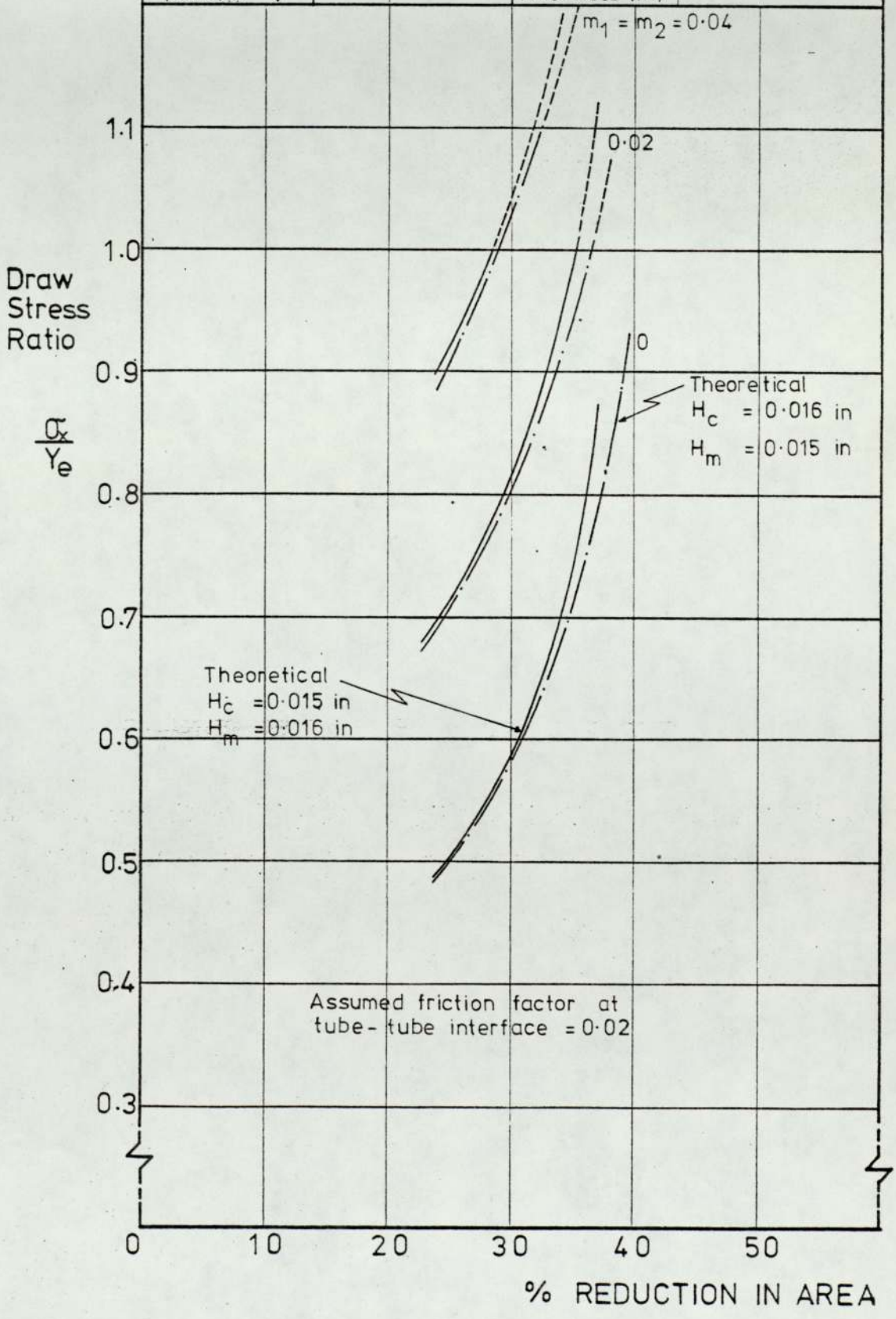

Figure 4·38	BIMETAL TUBE DRAWING ON A FLOATING PLUG AN UPPER BOUND SOLUTION			
Material	Stainless Steel on Mild Steel			
Mean Yield Stress ($tonf.in^{-2}$)	Clad	76·2	Initial Clad Thickness (in)	0·016
	Matrix	42·5	Initial Matrix Thickness (in)	0·015

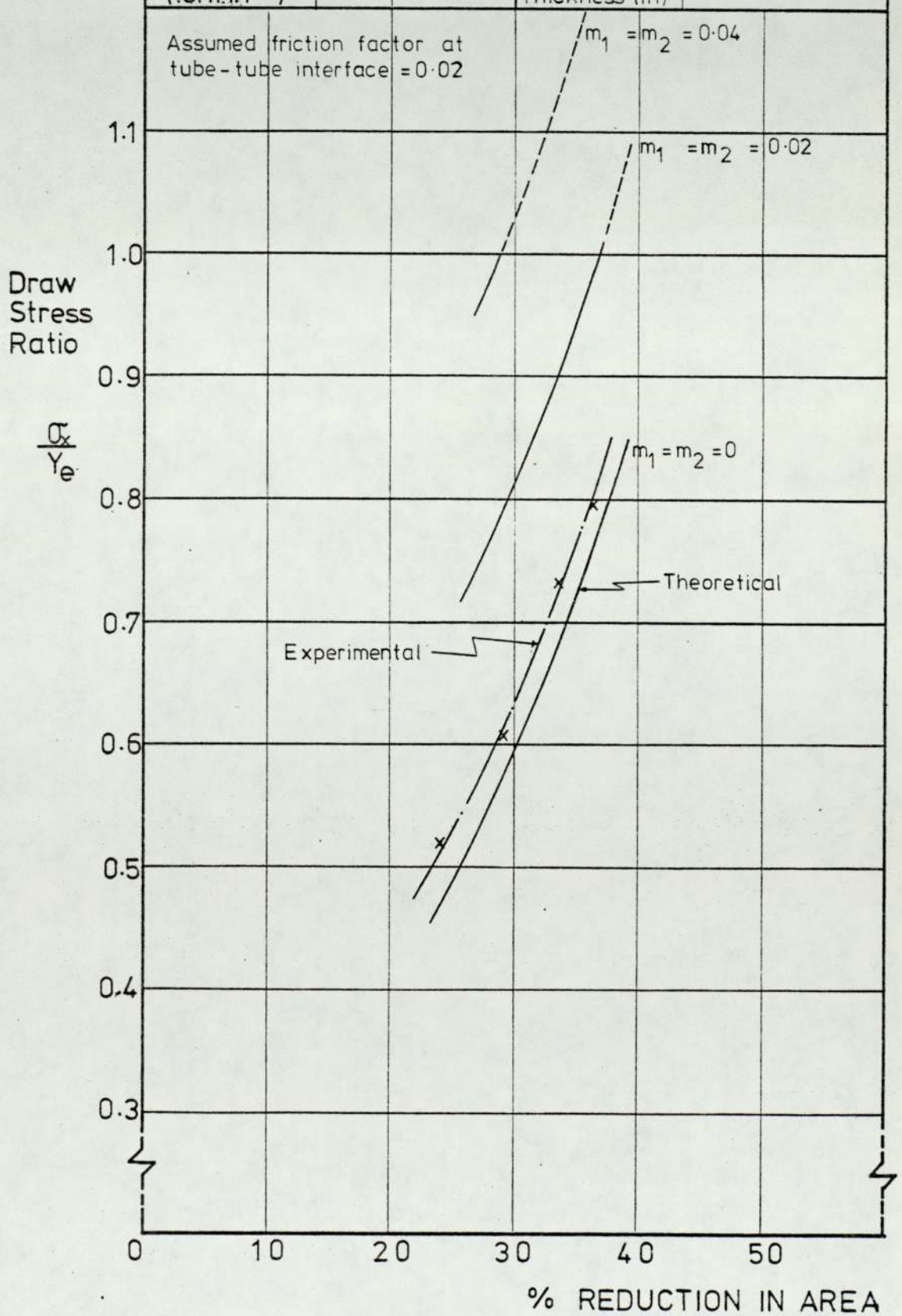

Figure 4·39	BIMETAL TUBE DRAWING ON A FLOATING PLUG AN UPPER BOUND SOLUTION			
Material	Stainless Steel on Brass			
Mean Yield Stress (tonf.in^{-2})	Clad	76·0	Initial Clad Thickness (in)	0·0155
	Matrix	42·4	Initial Matrix Thickness (in)	0·020

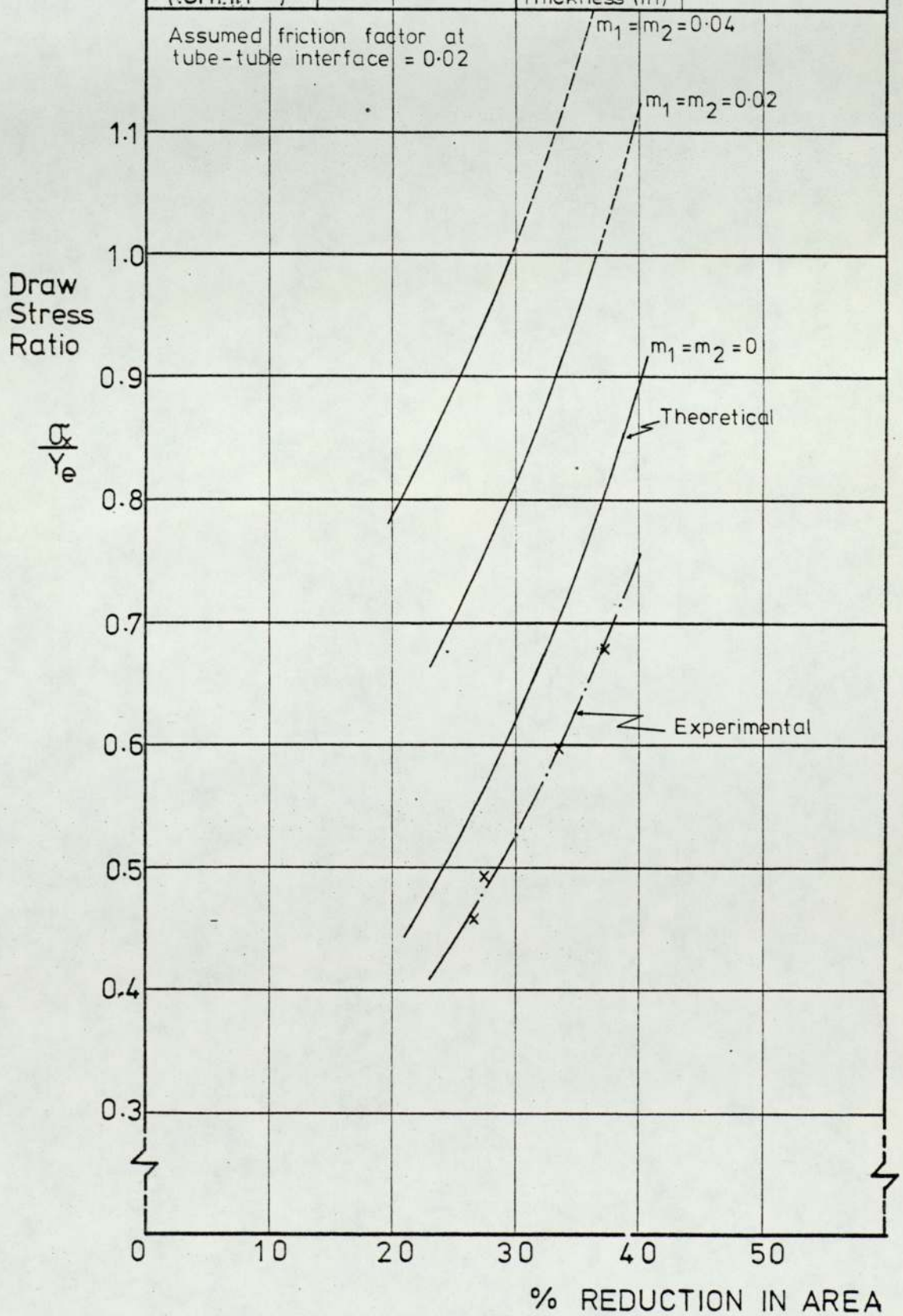

Figure 4·40	BIMETAL TUBE DRAWING ON A FLOATING PLUG AN UPPER BOUND SOLUTION			
Material	Aluminium on Stainless Steel			
Mean Yield Stress (tonf.in^{-2})	Clad	11·0	Initial Clad Thickness (in)	0·0225
	Matrix	76·2	Initial Matrix Thickness (in)	0·0132

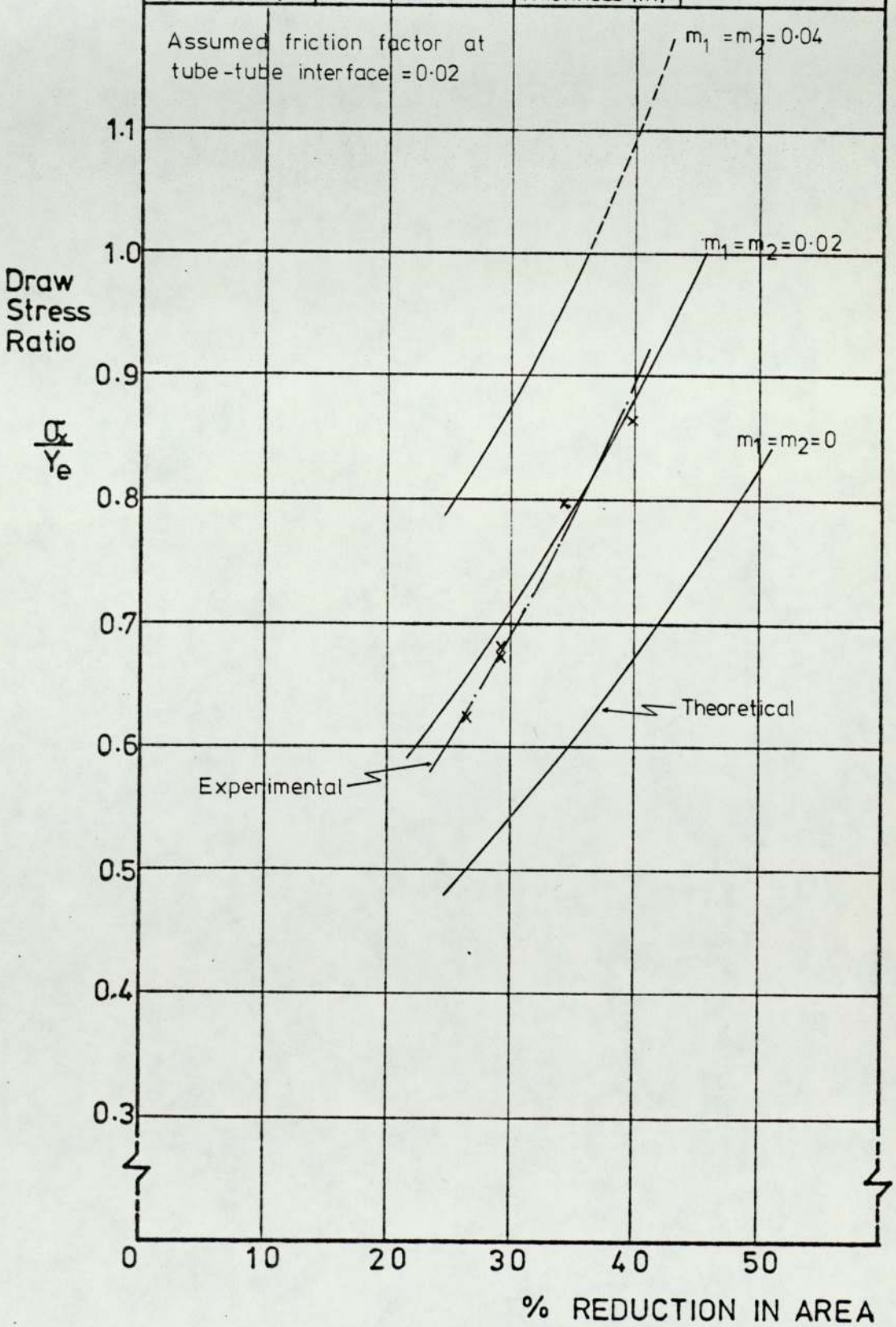

Figure 4·41	BIMETAL TUBE DRAWING ON A FLOATING PLUG AN UPPER BOUND SOLUTION			
Material	Aluminium on Mild Steel			
Mean Yield Stress ($tonf.in^{-2}$)	Clad	11·0	Initial Clad Thickness (in)	0·022
	Matrix	46·0	Initial Matrix Thickness (in)	0·0148

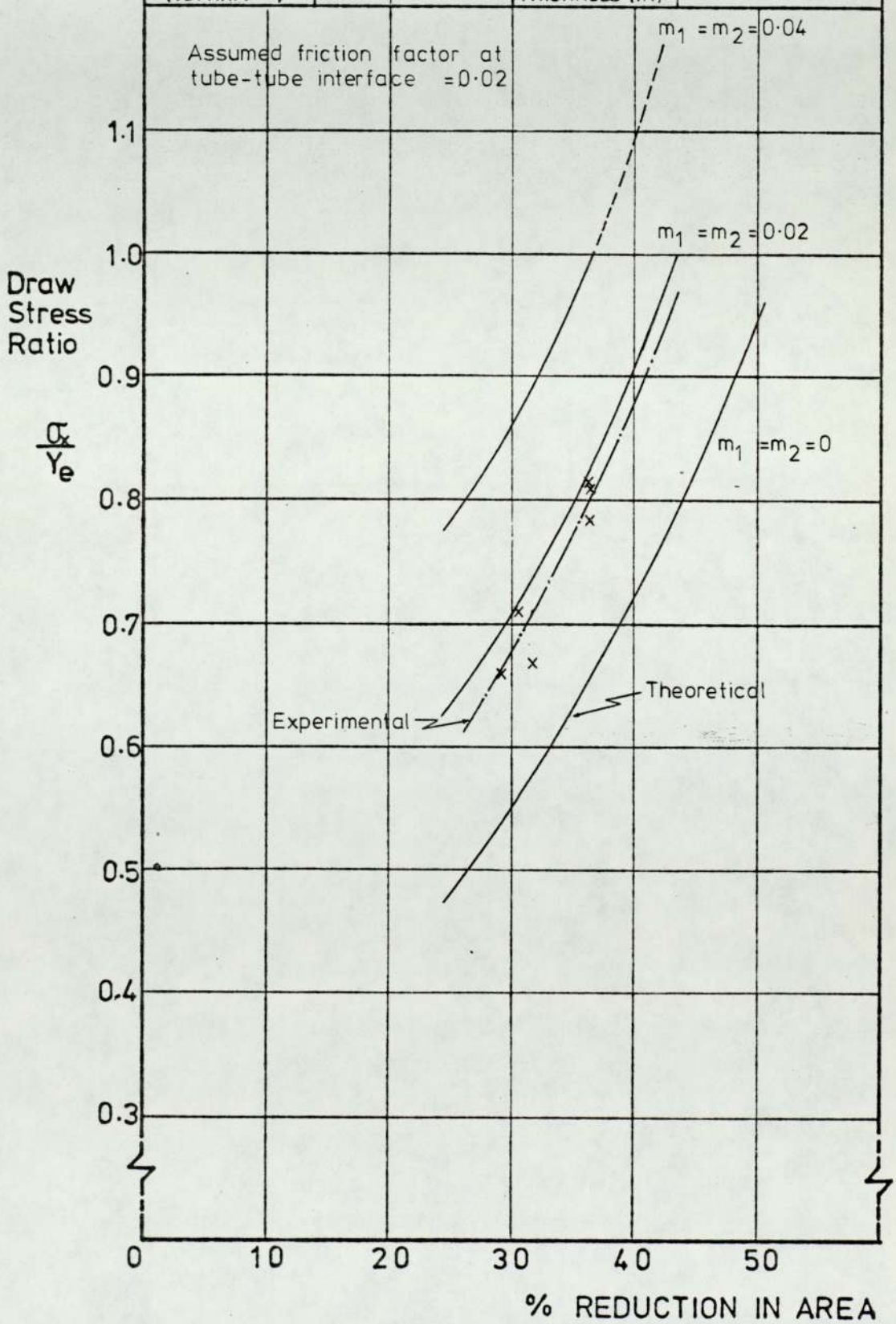

Figure 4·42	BIMETAL TUBE DRAWING ON A FLOATING PLUG AN UPPER BOUND SOLUTION			
Material	Brass on Stainless Steel			
Mean Yield Stress (tonf.in^{-2})	Clad	42·4	Initial Clad Thickness (in)	0·0215
	Matrix	76·2	Initial Matrix Thickness (in)	0·0155

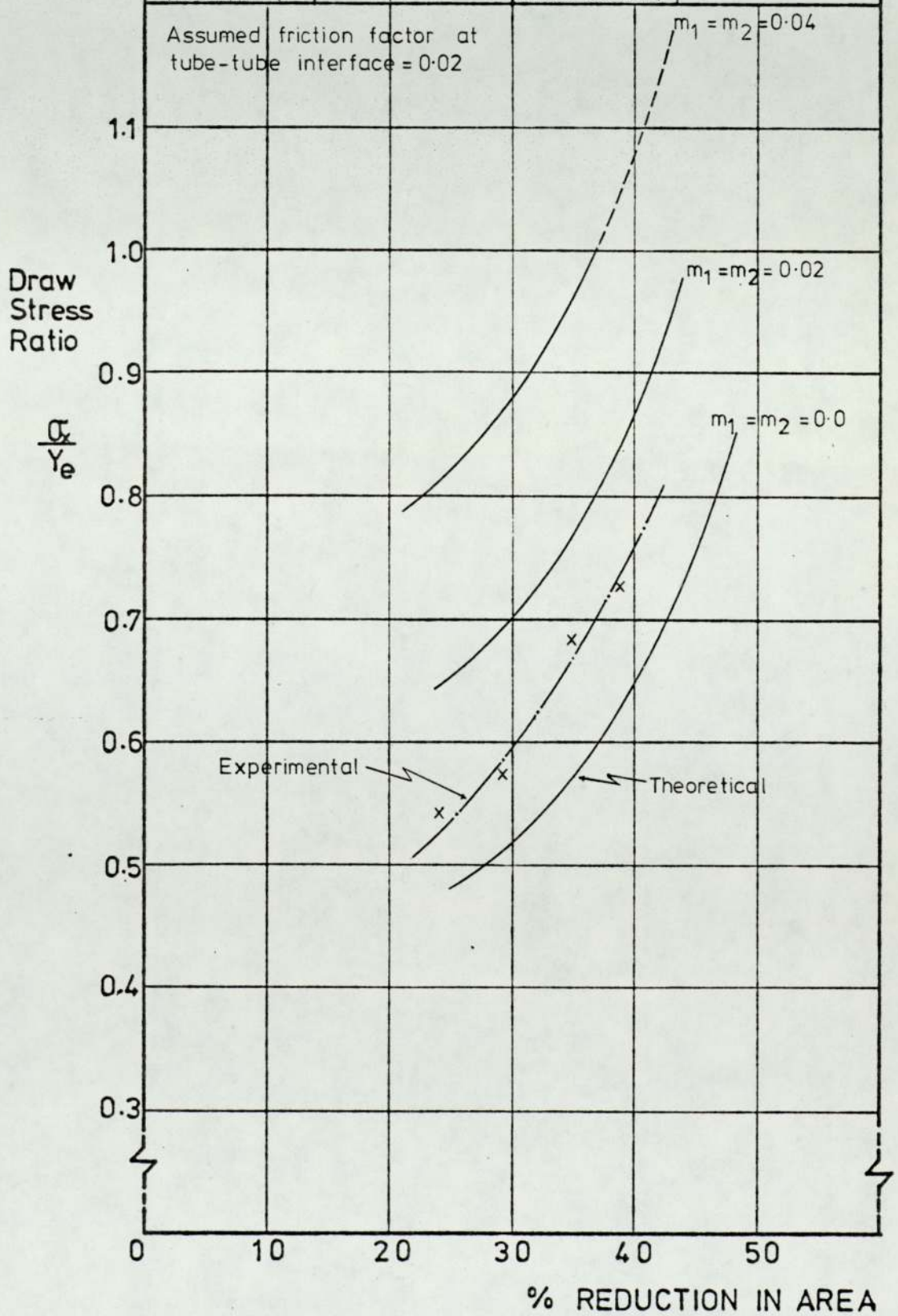

Figure 4·43	BIMETAL TUBE DRAWING ON A FLOATING PLUG - AN UPPER BOUND SOLUTION					
Material	Stainless Steel on Brass					
Mean Yield Stress	Clad	78·5	tonf.in^{-2}	Matrix	44·8	tonf.in^{-2}
Assumed friction factor at tube-tube interface = 0·02	Initial Clad thickness	0·0152	in			
	Initial Matrix thickness	0·0218	in			

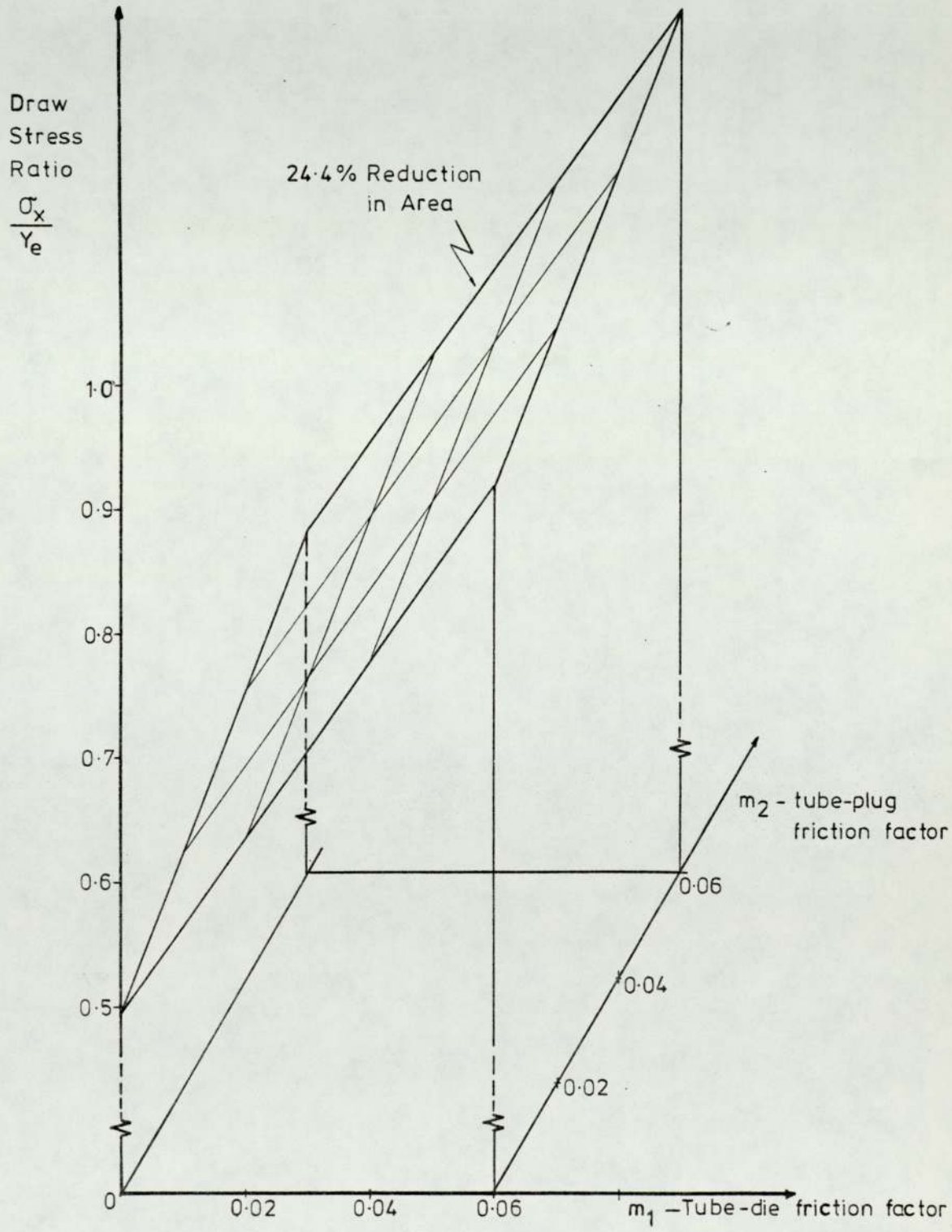

Figure 4·44	BIMETAL TUBE DRAWING ON A FLOATING PLUG An Upper Bound Solution

Material: Stainless Steel on Brass

Mean Yield Stress ($tonf.in^{-2}$)	Clad	78·5
	Matrix	44·8
Initial Clad Thickness		0·0152 in
Initial Matrix Thickness		0·0218 in
Assumed friction factor at tube-tube interface = 0·02		

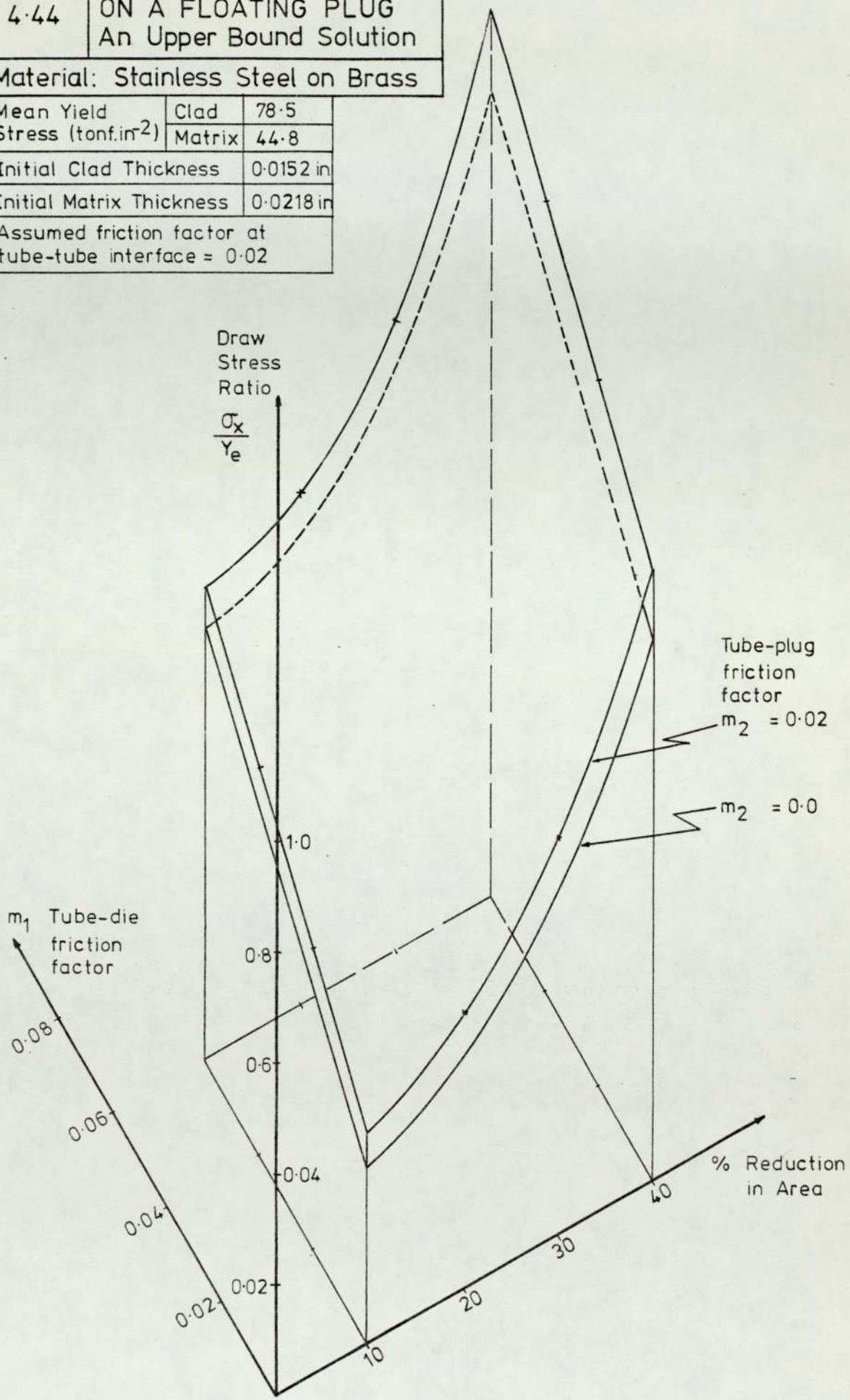

Chapter Five

DISCUSSIONS and OBSERVATIONS

5.1. Theoretical Analysis of Bimetal Tube Mandrel drawing using an Equilibrium Approach

This analysis is based on the assumption that this is a plane strain drawing process. It was also assumed that the coefficients of friction involved are less than 0.1. The coefficient of friction at the tube-die and tube-mandrel interfaces were obtained using the die rotation method. The two tubes, which were drawn together to make the bimetal tube, were assumed to be in intimate contact and that during drawing shearing occurred at the interface due to relative movement of the two tubes. Since the conical die surface and the clad-matrix interface were assumed to converge towards an arbitrary point of intersection, it is necessary to know the final thickness of the clad or the matrix before any calculation of the draw stress is possible. The determination of thickness straining for a given metal in a bimetal tube combination with this method of analysis is complex. The final clad and matrix thicknesses are a function of the die pressure, the friction at the tool-tube interfaces, the interfacial shear stress, the yield stresses of the constituent metals and the initial thicknesses of the clad and the matrix.

Since this is not an energy method, and the theory of

minimum work could not be used to determine the final clad and matrix thicknesses, the experimental findings of h_c and h_m were used to calculate the die pressure, interfacial shear stress and draw load for a given reduction in area. A sample of these results are given in Figures 4.01 to 4.05. Analysis of these results did not, however, provide any evidence that could be used to determine the final clad and matrix thicknesses.

For a given reduction in area, when a strain is imposed on the hard matrix of a bimetal tube with a soft clad, the softer clad has to be strained more in order that the given reduction be satisfied. If a hard metal and soft metal are to be equally strained, a lower stress value is required to maintain the strain on the soft metal than that required to do the same for the harder metal. Hence, figure 4.02 shows that if conditions demand that a bimetal tube of soft clad and hard matrix is drawn so that the matrix is thicker, the resulting draw load decreases, i.e. the draw load decreases with increase in h_m. On the other hand, if a bimetal tube has a soft matrix and hard clad, the draw load increases with increasing values of h_m. In practice, it is quite impossible to control all the parameters mentioned, to achieve any required condition which affects the final clad and matrix thickness. However, these results suggest a means of reducing the draw load as the roll separating force in the rolling of sand-wiched laminates may be reduced by determining the optimum clad thickness ratio. In order to establish the existence of a clad to matrix thickness ratio which gives a minimum draw load, extensive tests would have to be made with bimetal tubes of different initial clad and matrix thicknesses.

Since this was not within the scope of the present investigation, the tests were not made.

In Figure 4. , where the die pressure and the interfacial shear stress are plotted against t_m for a given reduction, both the die pressure and the interfacial shear stress decreases approximately linearly from entry to exit from the die. This showed the effect of the die pressure on the interfacial shear stress; decreasing the die pressure thus reduces the magnitude of the interfacial shear stress. It is interesting to note that with a coefficient of friction, say 0.04, the product $\mu \times p$, where p is a mean value of die pressure, gives a value which is an approximation to the mean interfacial shear stress. With the coefficients of friction at the tool-tube interfaces, generally having a value in the region of 0.02, this shows that the magnitude of the interfacial shear stress at the clad-matrix interface is higher than that at the tool-tube interfaces.

Again, it is interesting to find that Sachs, Lubahn and Tracy[58] in their analysis of the monometal tube mandrel drawing process recorded that the die pressure gradually decreases with increasing reduction as the metal passes through the die. Sachs et al plotted the effect of friction and reduction on die pressure and this is illustrated in Figure 5.1.

The theoretical results which were obtained using the experimental values of h_c and h_m are given in Figures 4.06 to 4.16. In these figures, the results obtained by using the assumption that the proportion of clad thickness remains the same after the reduction as before are also plotted for comparison. Using this assumption the final clad thickness

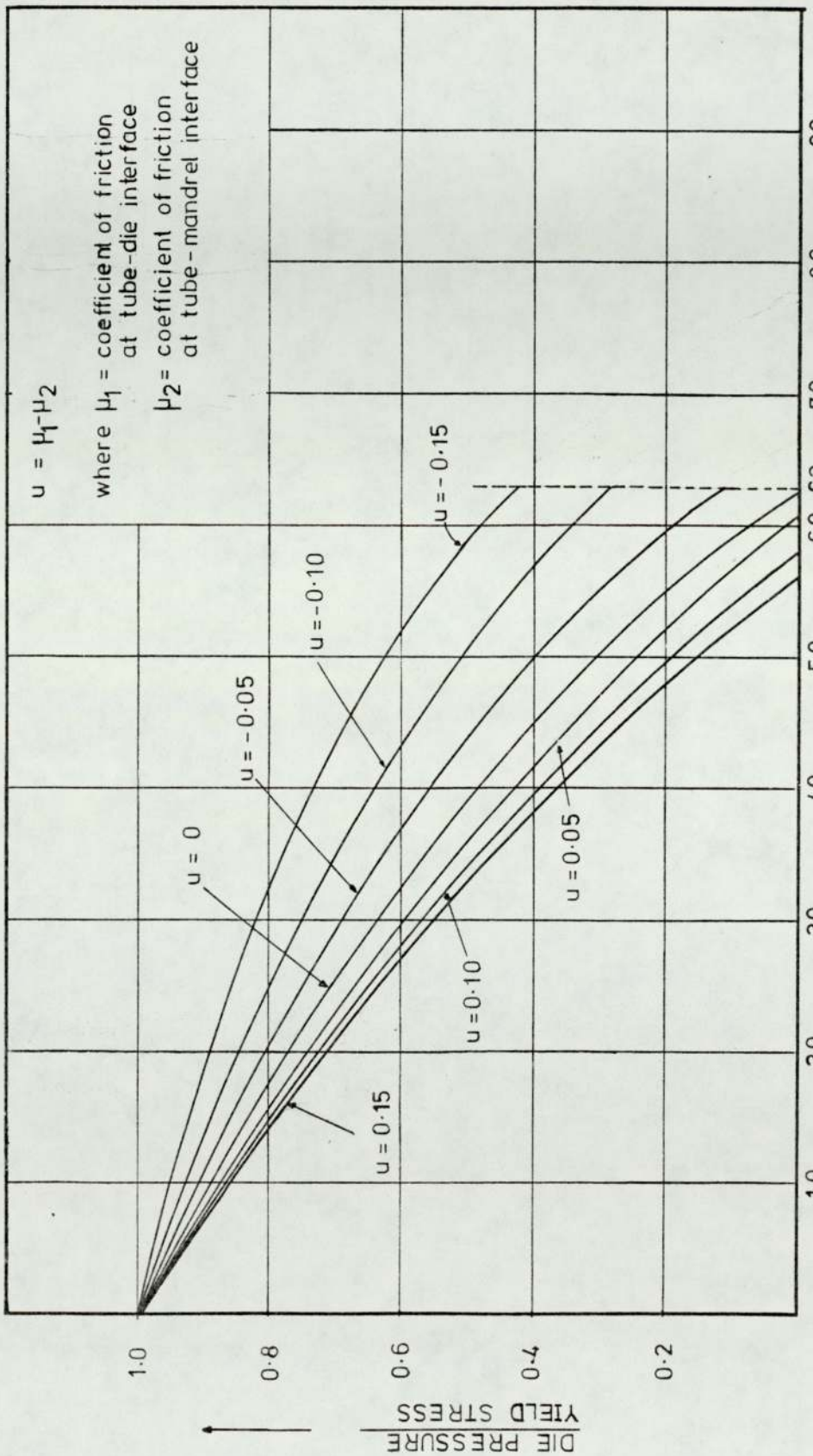

FIG. 5·1 EFFECT OF FRICTION AND REDUCTION ON DIE PRESSURE FOR $\alpha = 15^{\circ}$
(after Sachs, Lubahn & Tracy[58])

is calculated from h_c = K x final bimetal tube thickness

where $K = \frac{H_c}{H_c + H_m}$.

The theoretical draw loads obtained using the experimental values of h_c and h_m and K all underestimate the load. This is to be expected since the theory assumes a close-pass draw whilst in practice a small amount of sink is unavoidable in the early stages of each draw. For a given reduction in area, the proportion of sink would be higher for a lower reduction than for a higher reduction. Also, the author has observed that for low strain passes a short length of the tube bulges at entry to the die. This radial strain increases the actual stress required to deform the bimetal tube but it is not accounted for in the proposed theory. Therefore, by using values of h_c and h_m obtained from experiment, the theoretical solution gave better estimations of draw load for higher reductions than for lower reductions.

As the wall thicknesses in the tubes supplied were not very consistent and as there were wall thickness changes during the preparatory stages of the bimetal tube, the bimetal tubes used for the tests had slightly different clad and matrix thicknesses. This is one factor which accounts for the scatter in the experimental data and also explains the scatter in the theoretical solution. Since the theoretical solution is sensitive to both initial and final tube wall thicknesses, accuracy in the determination of these parameters is essential. Thus with variations in tube wall thickness for a given tube, a more accurate estimation of the average tube wall thickness would give a more accurate theoretical solution.

The theoretical predictions obtained with the assumption that the proportion of clad remains constant are in reasonably good agreement with the experimental results for all bimetal combinations. When these predictions are compared with those obtained using values of h_c and h_m obtained experimentally, there is no distinct evidence as to which prediction is more accurate. For certain combinations, the experimental values of h_c and h_m gave better estimations whilst for others using the assumption could provide closer estimations.

From Figure 4.19 to 4.22, theoretical solutions of Sachs' theory for mandrel-tube drawing are superposed on the theoretical and experimental results of the present investigation. Analyses of these results showed that in general, the solutions from Sachs' theory gave reasonable estimations of the stress ratio although these solutions underestimate more than the solutions obtained using the actual experimental values of h_c and h_m in the proposed theory. It should be noted that Sachs' theory cannot take into account the interfacial shear stress; i.e. using Sachs' theory, the tubes have to be treated as though they are composed of a single metal having a mean yield stress, Y_e. Since Sachs' theory gives a solution for stress ratio, σ_x/Y_e, it is necessary to obtain accurate values of Y_e when reliable values of draw load are required.

Figure 4.05 is an example of how the stresses, σ_c, σ_m and σ_p in Figure 2.1. are affected by increases in the coefficient of friction at the tube-mandrel interface. For all metal combinations, increases in the value of the coefficient of friction, μ_m, increases the longitudinal

stress on the mandrel, σ_p but the drawing stresses in the clad (σ_c) and the matrix (σ_m) decrease.

Usually, it was found that for hard clad and soft matrix combinations, increasing the friction at the tube-mandrel interface decreases the draw load; this is because the sum of the effect, on the draw load, of the decrease in σ_c and σ_m is greater than the effect of the increase in σ_p. A decrease in the draw load with an increase in the value of μ_m, the coefficient of friction at the tube-mandrel interface, is shown in Figure 4.04. In this figure it can be seen that for a soft clad and hard matrix combination, the draw load increases with increasing values of μ_m. Although in both cases, the values of σ_c and σ_m decrease and σ_p increases with increasing μ_m, with a soft clad hard matrix combination, the effect of the increase in σ_p is greater than the decrease in σ_c and σ_m thus giving a net increase in draw load.

It was found that for all combinations of bimetal tubes, increasing the coefficient of friction at the tube-die interface increases the values of σ_c and σ_m but decreases σ_p very slightly. Thus, in all cases, increasing the value of μ_s increases the draw load regardless of the bimetal arrangement.

The effect of coefficients of friction on the draw stress ratio is illustrated in Figures 4.17 and 4.18. It can be concluded from these graphs that the coefficient of friction at the tube-die interface has more effect on the draw load than the value of the coefficient of friction at the tube-mandrel interface. This can be explained from the difference in the magnitude of the die pressure and the normal

pressure at the tube-mandrel interface. From equations (2.7) and (2.8), it can be deduced that the die pressure is greater than the pressure between the tube and the mandrel. Therefore, for the same increase in the coefficients of friction, the friction at the die increases more than the friction at the mandrel surface. Thus, the draw load is more affected by the coefficient of friction at the die surface than that at the tube-mandrel interface. For the reductions in area illustrated in Figures 4.17 and 4.18, it is possible to obtain values of the draw stress ratio for the range of coefficient of friction shown. However, it should be noted that the values of draw stress ratio obtained from these graphs apply only to those initial tube dimensions for which the draw stress ratios were calculated. Examples of parameters which will affect the draw stress ratio are the die semi-angle and the initial clad and matrix thicknesses. As shown earlier, the initial clad and matrix thicknesses increase the draw load for a given reduction in area.

5.2. Theoretical Analysis of Bimetal Tube Mandrel drawing using an Upper-Bound Approach

The upper-bound theory for bimetal tube mandrel drawing was built on the following assumptions:

a) thin-walled bimetal tubes are drawn,

b) the draw is close-pass,

c) the metals used are rigid perfectly plastic, and

d) the dies have zero land.

By making assumptions (a) and (b), the process may be considered to be one of plane strain. A mean value of yield

stress is used to calculate the shear yield stress, $k = Y/2$ where Y is the yield stress of the individual metals in plane strain. By varying R_4, ϕ and β, the dimensionless ratio of σ_x/Y_e was calculated (using equation 2.32) for a range of draw parameters and a field giving the lowest value of σ_x/Y_e was found. The theoretical calculations were made with the aid of a digital computer for the various metal combinations used for the bimetal tube mandrel drawing experiments.

The results are shown in figures 4.24 to 4.36 with σ_x/Y_e plotted against reduction in area for different bimetal combinations. The theoretical results are presented for various values of friction factor, m, with the experimental data being superimposed. In all cases, the friction factor at the interface was assumed to be equal to 0.02. Due to uncertainty about the value of the friction factors used in the calculations, correlation between experimental and theoretical data is difficult. However, the trend in which the theoretical value of σ_x/Y_e varies with reduction in area compares well with that of the experimental results for all metal combinations considered.

In figures 4.24 and 4.25, the theory underestimates the values of σ_x/Y_e more (for a given friction factor) at higher reductions in area than at the lower reductions in area. This may be explained by the difference in yield stress between the materials used for the clad and the matrix. In both cases, stainless steel occupied the position of the clad, and the yield stress of stainless steel is approximately twice that of the material used for matrix. When such a soft

metal is effectively being drawn between two hard metals which is the clad and the mandrel. As can be seen in Figure 2.5, the proposed velocity field for the matrix, the velocity discontinuities form only one 'triangle'. In cases of high reductions with a hard clad and soft matrix, this configuration may be an inadequate representation of the actual pattern of velocity discontinuities. An improved velocity field may require that the number of 'triangles' be increase to two for the matrix. The 'two triangles' configuration has been shown to be more accurate when used to predict upper bound loads for plane strain forming conditions[75]. However, it should be noted that more computer time would be required to obtain a solution from a more complex 'network' of velocity discontinuities.

Again, it is interesting to note that the increase in the value of the stress ratio with increase in the friction factor is greater with the harder material as clad. This is quite easily discernible from a comparison of the results of stainless steel on copper and copper on stainless steel combinations. This is due to the fact that there is a larger area of contact (where there is relative slip) between the clad and the die surface than between the matrix and the mandrel.

As the tubes are supplied, inescapably with variations in dimensions, and as after initial preparatory drawing, the clad and the matrix of the bimetal tubes do not have the same thicknesses. It should be noted that the theoretical calculations made by the computer do predict the final clad and matrix thicknesses for each reduction in area, for

different combinations of metals and different combinations of initial clad and matrix thicknesses. Due to the variation in the initial clad and matrix thicknesses, it is not possible to compare graphically, the theoretical final clad and matrix thicknesses with those obtained from experiments. These results appear in tables M1 to M11 together with the experimental data. For each reduction in area considered, the percentage errors in the theoretical thicknesses of the clad and the matrix are also given in these tables. The theoretical or predicted results compare reasonably with the experimental results. Thus, this further supports the validity of the proposed velocity field.

Referring to Figure 4.36, it can be seen that the value of the friction factor at the die-tube interface, m_1, has a marked effect on the value of σ_x/Y_e. For a high value of m_1, say 0.08, the value of σ_x/Y_e increases sharply for increasing reductions in area. This effect is more noticeable with bimetal tubes in which the clad is the higher yield stress metal. The contour shown in this figure is only for one value of m_2 and it is possible to plot a series of these contours for incremental values of m_2.

Figure 4.35 shows the combined effect of the friction factors m_1 and m_2 on the dimensionless ratio σ_x/Y_e in a 3-dimensional graph for two specific reductions in area. Using this figure, it is possible to obtain the value of σ_x/Y_e for any combination of m_1 and m_2 between 0 and 0.1.
Similarly, in figure 4.36, for a fixed value of m_2, it is again possible to obtain the value of σ_x/Y_e for any combinations of reduction in area between 10% and 35% and m_1 between 0 and 0.1. Although these graphs can be used to

extract values of stress ratio for the range of reductions and friction factors illustrated, it should be noted that the stress ratio obtained, strictly, is true only for the die angles and initial tube thicknesses used to produce these graphs. There is no doubt that, for example, an increase or decrease in the die semi-angle will affect the value of the resulting draw load. Therefore, a different set of graphs has to be plotted to satisfy the drawing parameters required. For use in the drawing industry, it may be more useful to design nomographs to cover all these parameters as there is a limitation to the number of variables that can be illustrated in the graphs.

5.3. Theoretical Analysis of Bimetal Tube drawing on a Floating Plug using an Upper-bound Approach

The upper-bound solution to the drawing of bimetal tube on a floating plug was obtained with the aid of a digital computer programme named "UBFP". It was assumed in the computation that the metals used were rigid perfectly plastic. This assumption was made to simplify the analysis and to reduce computer time and incur negligible error in the draw stress. To allow for strain-hardening, a mean value of yield stress was used and this was obtained using the concept proposed by Hill and Tupper.

It was assumed that there was no change in tube wall thickness while the tube was sinking. Again, negligible error would be incurred as Chia[6], in his work on the sinking of bimetal tubes, reported an increase in tube wall thickness generally of about 5%. Chia reported that the biggest increase in tube wall thickness was 12% when stainless steel

was used as the clad or the matrix; however, these increases were measured on tubes that were entirely sunk. The proportion of sink to draw in the floating-plug tube-drawing process is generally between 30% and 50%.

The theoretical value of σ_m/Y_e was calculated for a series of deformation modes by varying ϕ, γ and R_4 and a field giving the lowest value of σ_x/Y_e was found. Figure 4.38 to Figure 4.42 show the effect of reduction on σ_x/Y_e for various values of friction factor, m, between 0 and 0.1 with the experimental results being superimposed. Due to uncertainty about the value of the friction factor, correlation between the theoretical results and the experimental data is difficult but the trend of increase of σ_x/Y_e is reasonably consistent with the data obtained from experiment. On inspection, within the given set of results, i.e. figures 4.38 to 4.42, there is reasonably consistent correlation between the experimental and the theoretical results at about $m_1 = m_2 = 0.01$ or $m_1 = m_2 = 0.02$ except for the case of stainless steel on brass. In this case, the theoretical draw stress is in excess of the experimental results. There is reason to believe that this could be due to the stainless steel and brass not being in complete contact along the entire length of the interface of the two metals. Similar observations were reported by Smith and Bramley[66] and Islam[7] in tube drawing experiments. Calculations for the theoretical solutions were based on the brass tube and stainless steel being in intimate contact, thus giving a higher value of work done against friction than in an actual case where there is less surface contact at the interface.

Figure 4.43 illustrates how the draw stress ratio σ_x/Y_e is affected by the friction factors for the tube-die interface and the tube-plug interface, m_1 and m_2 respectively for a given reduction in area. An increase in either of these friction factors increases the draw stress considerably. The draw stress is more affected by an increase in the value of m_1 than an increase in m_2. This difference is due to the larger area of contact between the die and the bimetal tube than that between the floating plug and the tube. Further, the clad is stainless steel which has a higher yield shear stress than that of the matrix (brass in this case). It is noted that, as in the mandrel drawing of bimetal tube that the draw stress is more affected by the coefficient of friction at the die surface than at the plug surface. In the equilibrium analysis in Chapter 2, from equations (2.7) and (2.8) it can be deduced that the die pressure is greater than the pressure between the mandrel and the inner tube. Therefore, for the same increase in the coefficients of friction at the tool-tube interfaces the increase in friction at the die-tube interface would be more than that at the tube-mandrel interface. Thus the draw stress is more affected by the coefficient of friction at the die-tube interface than at the floating plug-tube interface.

A typical trend in which the stress ratio varies with reduction in area and the friction factor m_1 is illustrated in figure 4.44. Increasing the value of m_2 obviously increases the draw stress and forms a similar contour one on top of the next in order of magnitude. It is possible to deduce values of σ_x/Y_e from figures 4.43 and 4.44 for the range of

reductions and friction factors plotted. However, when numerous solutions are required in practice, the task of producing all the graphs would be tedious. A more practical method may be to construct a nomograph to serve the same purpose.

Another parameter which can affect the draw load is the relative portion of the floating plug "floating" in the die. The further the floating plug moves into the die, the higher is the draw load. During the present experiments, the author has noted that the draw stress can fluctuate by as much as 10% about a mean depending on the position of the floating plug. This conclusion was drawn from results of tests where there was notable 'chatter' during part of the draw. To check that the plug was actually floating in the die when these readings were taken, the tube was cut into several portions and the final bore size measured. Therefore, depending on the finish of the floating plug surface, the surface of the bore of the bimetal tube and the effectiveness of the lubricant used, the draw load can be affected notably.

The predicted final clad and matrix thickness using this upper-bound theory is tabulated with the actual experimental results in tables F1 to F4. It can be seen that within the limits of error, the theoretical results give reasonably accurate predictions of the actual values of h_c and h_m. Therefore, this confirms that the proposed velocity field is reasonably close to the actual velocity field. The theoretical solution is sensitive to the initial values of clad and matrix thicknesses. An example of this is illustrated in figure 4.37 for stainless steel on mild steel. Depending on the yield stresses of the constituent metals, the friction factors,

the interfacial shear stress and the geometry of deformation (due to the position of the plug), the final clad and matrix thicknesses could increase or decrease for given initial thicknesses of clad and matrix.

For a given set of initial clad and matrix thicknesses, the draw stress ratio for a range of reductions and a range of friction factors could be plotted as shown in figures 4.43 and 4.44. Conversely, using these graphs, it is possible to deduce the value of draw stress ratio for any reduction and any friction factors within the range of values illustrated. This method of deducing the draw stress is very useful where the initial clad and matrix thicknesses are the same for the reductions required. If, in practice, a wide range of clad and matrix thicknesses are used, it may be more useful to construct a nomograph to cater for all the parameters required.

5.4. Safe Drawing Régime

Although the theoretical draw stress of the upper-bound theory has been used by Islam[7] to predict a safe drawing regime for the drawing of bimetal tube on a fixed plug, the author is of the opinion that it would be inaccurate to use the theoretical draw stresses of the upper-bound theories discussed in the earlier sections for the same purpose. The elements which constitute the draw load for mandrel drawing are as follows:

$$\text{Draw Load} = \sigma_c A_c + \sigma_m A_m + \sigma_p A_p \qquad (5.1)$$

hence:

$$\text{Draw stress} = \frac{\text{Draw load}}{A_c + A_m} \qquad (5.2)$$

where σ_c, σ_m and σ_p are the stress on the clad, matrix and mandrel respectively.

A_c, A_m and A_p are the cross-sectional area of the clad, matrix and mandrel respectively.

For the cases of drawing on a floating plug and drawing on a fixed plug, the $\sigma_p A_p$ term doesnot exist in equation (5.1).

Tensile tests performed on drawn bimetal tubes composed of constituent metals of widely differing yield stresses shew that the softer metal yielded plastically to failure whilst the harder metal remained intact. It was found that irrespective of whether the harder metal was the outer tube or the inner tube, the softer tube started to 'neck' before the harder tube. When the same tests were applied to drawn bimetal tube of constituent metals having approximately equal yield stresses, the two metals failed at the same moment. Thus, the limit of drawing can be taken as when either of the constituent stresses, σ_c or σ_m is equal to the yield stress of the respective metal. From equation (5.1) and (5.2), it can be seen that the mean draw stress is not equal to the constituent stresses, σ_c or σ_m. Therefore, using the mean draw stress to determine the boundaries for safe draw zones would produce unreliable results.

Although the tensile test is a different deformation process when compared with the drawing process, nevertheless, this test gives a good indication of the criterion of failure of the bimetal tube after and at exit from the die. It can

be shown using Sachs' drawing theories[55,58,59], Chia's bimetal tube fixed plug drawing theory[6] and the equilibrium theory in Chapter 2 that the maximum drawing stresses are located at the plane of the die exit. Therefore, tensile failure in tube drawing is most likely to occur at the point of exit from the die. However, to ascertain the exact criterion of failure in the drawing of bimetal tubes would require further tests. As this is not within the scope of the present investigation, this is discussed in the chapter for further work.

It is possible to deduce safe drawing zones for bimetal tube mandrel drawing using both the upper-bound theory and the equilibrium theory. Initially, the upper-bound theory would be used to predict the final clad and matrix thicknesses which are then used in the equilibrium theory to obtain the 'drawing' stresses, σ_c and σ_m. By adopting the criterion of failure mentioned earlier, i.e. the limit of draw is when either σ_c or σ_m attains a value equal to the yield stress of the respective metal, the zones of possible reduction can be established.

5.5. Observations

Although reductions in area of as high as 40% were performed on the bimetal tubes, no bonding was evident in the tubes produced by either the mandrel-drawing or the floating-plug tube-drawing processes. After the tubes were drawn, portions of the tubes were cut longitudinally to measure the final clad and matrix thicknesses. When the tubes were cut, it was observed that the individual tubes could be taken apart though it was more difficult to

separate the tubes for the stainless steel/copper combinations. It was also observed that higher residual stresses were present in bimetal tubes containing stainless steel and/or brass as constituent metal. This observation was based on the amount of splitting when the tubes were cut along its longitudinal axis.

Initially stainless steel on aluminium tubes were prepared for the floating plug drawing experiments. Due to the vast difference in the yield stresses of the two metals, only small reductions were drawn successfully and thus there were not enough data to justify plotting a graph. When this batch of bimetal tubes was drawn, as the aluminium was a much softer metal it thinned down rapidly as it flowed over the conical surface of the floating plug. This resulted in fracture as it changed direction from the conical section of the plug to the parallel position. Therefore, for bigger reductions to be possible, the thickness of the aluminium matrix would have to be increased so that the resulting draw stress on the matrix would be below its yield stress value. It was not possible to increase the matrix thickness and repeat these experiments due to the geometrical constraints of the die and floating plug; also thicker aluminium tubes were not readily available.

It has been observed from the theoretical calculations that the interfacial shear stress is relatively low when compared with the die pressure and drawing stress. An example of the interface shear stress that can be compared with the corresponding die pressure for a given reduction can be found in Figure 4.1.

Chapter Six

CONCLUSIONS

1) Substituting values of final clad and matrix thicknesses, obtained from experiments, in the calculations, the proposed equilibrium theory was shown to give reasonably accurate predictions of the draw load in the drawing of bimetal tube on a mandrel.

2) The proposed equilibrium theory for bimetal tube mandrel drawing necessitates a knowledge of the final clad and matrix thicknesses for accurate solutions. When an assumption that the proportion of clad in a bimetal tube is the same after a pass as it is before was used to predict the final clad and matrix thicknesses, the theoretical predictions of the draw load were also reasonably close to that of the experimental values. Thus, this assumption can be used in the computation of the draw load with sufficiently good estimations but the assumed values of final clad and matrix thicknesses can be misleading except for combinations having metals of nearly equal yield stresses.

3) Sachs' theory on mandrel tube drawing can be used also to obtain a reasonable estimation of the stress ratio in close-pass bimetal tube mandrel drawing. However, a reliable value of the modified mean yield stress, Y_e has to be used in order to obtain a good estimation of the draw stress.

4) It was found that by increasing the coefficient of friction at the tube-mandrel interface, the draw stresses σ_c and σ_m on the clad and matrix respectively are reduced but the stress on the mandrel is increased. However, decreases in σ_c and σ_m did not mean a reduction in draw load for all combinations. It was noted that, in general, increasing the value of μ_m decreases the draw load for bimetal combinations having a hard clad and a soft matrix and increases the draw load for a soft clad and hard matrix combination.

5) A valid velocity field was proposed for the analysis of the bimetal tube mandrel drawing process. An upper bound approach was used in the theoretical analysis giving reasonably good estimations of the draw stress and the final clad and matrix thicknesses. The proposed velocity field was more accurate in the prediction of the stress ratio for soft clad and hard matrix combinations than for hard clad and soft matrix combinations.

6) The theoretical analysis of the drawing of bimetal tube on a floating plug given in Chapter 2 gives an upper bound for the stress ratio, σ_x/Y_e. The stress ratio was calculated for various friction factors, m, between 0 and 0.1 and different reductions in area. The theoretical stress ratio obtained from the computer programme compared favourably with the results obtained from experiment. The same computer programme also gave good estimations of the final clad and matrix thicknesses for a given pass.

7) Friction at the die-tube interface was shown to have a marked effect on the draw load for both processes considered. Increases in friction at the die-tube interface causes the draw load to increase much more significantly than a corresponding increase of friction on the internal tool.

8) Although the tubes were carefully cleaned before assembly and reductions in area in excess of 40% were achieved, no metallurgical bonding was observed when the bimetal tubes were cut after each draw. However, there is evidence of strong mechanical bonding due to residual stress disposition in the drawn tubes.

9) The rotating die method provided reasonable estimations of the coefficients of friction at the die/tube and tube/ mandrel interfaces in bimetal tube mandrel drawing.

Chapter Seven

Suggestions for Further Work

During the past few years, there has been a number of investigations in the extrusion and drawing of bimetal tubes and rods but further investigations of some of these processes are necessary in order to gain a better understanding of these processes.

1) Although a theoretical study of the drawing of bimetal tube on rod has been done by Chia[6], there is still no theory available to predict the final thickness of the tube and the diameter of the rod. It would be most useful to manufacturers if they could predict the final size of the rod and the clad thickness. This could be extended to clad wires which currently are manufactured in quite large quantities. The limits of producing bimetallic rods by extrusion have been analysed by different authors but this information is still lacking in the drawing of bimetallic rods. With the ability to predict the final clad and rod sizes and an understanding of the limits of the safety zones, it would then be possible to organise economical and practical reductions in the drawing of bimetallic rods. The search for the safety limits of draw is an extensive exercise due to the number of variables which can affect the limits of the safety region. Examples of such variables are the die semi-angle, the initial thicknesses of the constituent metals, the yield stress

ratio and maximum reduction possible.

In order to determine the limits of the safety region, it is necessary to decide upon a criterion of failure for the drawing of bimetal tubes. Although the tensile test gives a good indication of what could be the criterion of failure, this should be confirmed by drawing tests performed on bimetal tubes. Further, with tensile tests on thin-walled tubes, it is difficult to obtain reliable results of load against strain which could be used for further analysis. Needless to say the drawing tests should be performed with bimetal tubes of the same metal combination and initial clad and matrix thicknesses. The tests should be repeated with bimetal tubes having the original clad metal as matrix and the original matrix metal as clad. The prepared bimetal tubes would be drawn with different dies to provide incremental increase in the reduction of area to failure. During drawing, however slow the draw speed, it would be very difficult to determine visually the moment of yielding of the clad or matrix at the die exit as it is possible during the tensile tests. Hence a method would have to be developed to determine the 'draw' stresses σ_c and σ_m acting on the clad and matrix respectively. One solution would be to place strain gauges on the tag of the bimetal tube to measure the strain and hence deduce the stresses on the bimetal tube. Due to time constraint, it has not been possible to include these tests into the present investigation and to predict zones of safety for mandrel-tube drawing and floating plug tube drawing.

2) Another area of research which would be interesting is a

study of the optimum conditions that would encourage the metallurgical bonding of bimetal tubes. Chia, Islam and the author have reported in their investigations that no metallurgical bonding was achieved although high reductions were performed. However, it should be noted that none of these experiments were performed with scratch-brushed tubes. Therefore, it may be necessary to scratch-brush or controlled sand blast the contacting surfaces before assembly. Problems of preparation of tubes may be encountered with either of these methods where the repeatability of the experiments are concerned.

An alternative method to encourage metallurgical bonding at the bimetal tube interface would be to apply ultrasonic vibration to the die and the fixed plug or mandrel as the bimetal tube is being drawn. The vibration at the tube-tool interfaces would be transmitted to the clad-matrix interface producing a 'burnishing' action which should enhance the conditions required for metallurgical bonding. As no lubricant is applied to the tube-tube interface whilst the bimetal tube is drawn, the metals in contact would be shearing at high oscillatory velocities in the high stress field at the two contacting surfaces and this would promote metallurgical bonding.

3) Conventional and hydrostatic extrusion of bimetal rods have been quite extensively investigated by various authors[20,22] but the extrusion of bimetal tubes has yet to be investigated. Perhaps the reason why the extrusion of bimetal tubes has not drawn much interest is due to the limited number of metals

that could be successfully extended at room temperature. Nevertheless, there are many alloys of aluminium and copper that could be cold extruded. The extrusion of some bimetal combinations like stainless steel and copper could face some problems because stainless steel cannot be extruded cold whilst copper is usually extruded cold. The hydrostatic extrusion of non-ferrous alloys has produced tubes with accurate dimensions which do not need further drawing or a finishing process. Therefore, it would be reasonable to expect bimetal tubes produced by the same method to attain the same dimensional accuracy.

4) Very often bimetal tubes are not used in straight lengths and bending is necessary to produce the profile required, for example, cooling tubes in heat exchangers. To the knowledge of the author, there is no published work in the bending of bimetal tubes although a large amount of tube bending is practiced in Industry. In an investigation of bimetal tube bending, there would be obvious differences in load in the bending of bimetal tubes which are metallurgically bonded at the interface and those that are only mechanically bonded. There would be questions like: would the bending weaken or break the metallurgical bond at the bend? What is the difference in strain between the two metals? Would one tube become too thin at the bend?

5) It is becoming increasingly expensive to change large quantities of worn or corroded tubes, for example in chemical industries. Perhaps it would be more economical to expand

the worn tube onto a new tube thus producing a thicker tube which should last longer. The U.S. Atomic Energy Commission has been assembling tubes using a combination of drawing and expanding. Initially, the tubes (assembled with 0.03 in radial clearance) are first drawn at room temperature to reduce their diameter and to bring the tubes into closer contact at the interface. The assembly is then expanded at room temperature by drawing an oversize plug through the inner tube with no constraint on the outer tube. Both tubes are strained beyond their elastic limit and the residual stress thus produced causes the outer tube to clamp inward on the inner tube. It is claimed that the bond retains its strength at elevated temperature and when subjected to constant or cyclic temperature gradients.

The structural integrity of non-bonded bimetal tube is dependent on the magnitude of the residual stresses and this is a function of the elastic constant and wall thickness of the tube material. Hence, if a thick tube is to be assembled with a thin tube, the suitability of this technique calls for an investigation. Therefore, it would be interesting to examine this method of producing bimetal tubes in detail. There is no doubt that the thickness of the tubes and their respective yield stresses would be the factor which limits the extent to which one tube could be expanded onto the other. The bigger the increase in diameter of the tubes, the thinner would be the tube wall produced. Thus, an understanding of how these factors would affect the deformation of the two tubes is essential.

6) One process that is worth investigating with the possibility of achieving a metallurgical bond at the clad-matrix interface is the rolling of bimetal tube with or without a mandrel. However, it is more likely for metallurgical bonding to be achieved when the bimetal tube is cold reduced, i.e. cold pilger rolled with a tapered mandrel. The advantages this process has over the drawing process are that the reduction in area is not limited by pickup or tensile failure, and the normal reduction per pass may well be between 60% and 80%; this would enhance the conditions for interfacial bonding. Due to differences in strain on the individual metals which does occur when sandwiched hard and soft metal combinations are rolled[27,28], the limit in reduction for rolling bimetal tubes would most likely be restricted by the final tube wall thickness of the weaker metal.

Again, if a mandrel was used, as in tube drawing, it would be necessary to remove the mandrel after a pass by reeling the tube and mandrel between convex rolls or stripping the tube from mandrel using a 'blank die' as has been done in the present investigation. The disadvantage of the latter method is that material is wasted as part of the drawn tube becomes corrugated as it is drawn against the 'die', but if the reeling process is used, there is the possibility of breaking or weakening the bond at the interface and leaving the inner tube on the mandrel whilst the outer tube is being expanded.

REFERENCES

1. Dietz, Albert G.H. — Composite Engineering Laminates. The MIT Press, Massachusetts Institute of Technology (1965).
2. McQuaid, H.W. & Ulmer, W.L. — U.S. Pat. 3598156 Patented 10 Aug. 71. Bimetal Tubing & Method of Making same.
3. Ostrenko, A.A. et al — Production of High Quality Bimetal Tubes. Steel in the USSR, 1972, Jan, 59-61.
4. Arkulis, G.E. — Compound Plastic Deformation of Layers of Different Metals. Israel Program for Scientific Translations Ltd. (Trans. from Russian by P.Lerman)
5. Townley, S. & Blazynski, T.Z. — The Cold Drawing of Implosively Welded Bimetallic Tubes. Proc. 15th MTDR Conf. (1975)
6. Chia, H.T. — Ph.D. Thesis, 1976. "Mechanics of Bimetal Tube Drawing". Univ. of Aston.
7. Islam, M.N. — Ph.D. Thesis, 1977. Univ. of Leeds.
8. Cunningham, G.W. & Spretnak, J.W. — A study of the effect of Applied Pressure on surface contact area. Int. J. Mech. Sci. 1962, 4, p 231.
9. Tylecote, R.F. — Investigation on Pressure Welding. Brit. Weld. J. 1954 (March), 1, p 117.
10. Tylecote, R.F., Howd, D. & Furnridge, J.E. — The Influence of Surface Films on the Pressure Welding of Metals. Brit. Weld. J. 1955, Jan. 5, p 21.

11. Vaidyanath, L.R. & Milner, D.R. — Significance of surface preparation in cold pressure welding. Brit. Welding J. 1960, 7, p.1.

12. Holms, E. — Influence of relative interfacial movement and frictional resistance in cold pressure welding. Brit. Welding J. 1959, Jan, 6, p.29.

13. Cantalejos, N.A. & Cusminsky, G. — Morphology of the interface of roll bonded aluminium. J. Inst. Metals. 1972, 100, p 20.

14. Vaidyanath, L.R., Nicholas, M.G. & Milner, D.R. — Pressure Welding by Rolling. Brit. Weld. J. 1959, Jan, 6, p.13.

15. Nicholas, M.G. & Milner, D.R. — Roll Bonding of Aluminium. Brit. Weld. J. 1962, 9, p 469.

16. Chia, H.T. & Sansome, D.H. — Theoretical Study of Bimetal Drawing of Rod and Tube. 15th MTDR Conf. (1974).

17. Weinstein, A.S. & Pawelski, D. — Plain Strain Drawing of Sandwich Metals. Proc. 8th Int. MTDR Conf. Sept. 1967, p 961.

18. Avitzur, B. — Analysis of Wire Drawing and Extrusion Through Conical Dies of Small Cone Angles. J. Eng. Ind. Trans. ASME, Series B, 1963, 85, 89.

19. Avitzur, B. — Analysis of Wire Drawing and Extrusion Through Dies of Large Cone Angle. J.Eng. Ind., Trans. ASME, Series B, (1964), Nov. 86, No. 4, 305-316.

20. Osakada, K., Limb, M. and Mellor, P.B. — Hydrostatic extrusion of composite rods with hard core. Int. J. Mech. Sci. 1973, Vol. 15, p 291-307.

21. Osakada, K., & Niimi, Y. — A study on radial flow field for extrusion through conical dies. Int. J. Mech. Sci. (1975), 17, 241-254.

22. Alexander, J.M. & Hartley, C.S. — On the Hydrostatic Extrusion of Copper-covered Aluminium Rods. NEL/AIRAPT Conf. Stirling Univ. 1973, p 141.

23. Holloway, C., Bassett, M.B. & Sheppard, T. — On Load Pressure Requirements during the cold extrusion of composite materials. 17th MTDR Conf. 1976.

24. Alexander, J.M. & Whitlock. — Extrusion of a Bi-metallic strip from separate containers. Proc. Instn. Mech. Engrs. 1965-66. Vol. 150. Pt. 31. pp 250-259.

25. Arnold, R.R. & Whitton, P.W. — Stress and Deformation Studies for Sandwich Rolling Hard Metals. Proc. Inst. Mech. Engrs. (1959), 173, No. 8. p. 241.

26. Atkins, A.G. & Weinstein, A.S. — The Deformation of Sandwich Materials. Int. J. Mech. Sci. 1970, 12 p 641.

27. Afonja, A.A. & Sansome, D.H. — An Experimental Investigation of the Sandwich Rolling of thin hard Sheets. Proc. 13th Int. MTDR Conf. 12-18 Sept. 1972.

28. Afonja, A.A. & Sansome, D.H. — A Theoretical Analysis of the Sandwich Rolling Process. Int. J. of Mech. Sciences. 1973, 15, No. 1. pp 1-14.

29. Gulyaev, A.S. & Rakov, K.M. Calculation of pressure of metals on the Rolls during the Rolling of Bimetal. Izv. Vuz. Tsvetnaya Meta-lurgiya 1965, 2, 140-146.

30. Davies, D.H. A Study of the Compression of Aluminium-Copper Laminates. M.Sc. University of Wales, 1965.

31. Holmes, E. Ph.D. Thesis, University of Birmingham 1955.

32. Hawkins & Wright, J.C. Observation on the deformation prop. of Sandwich Materials. Inst. J. Mech. Sci. 1972, 14, p875.

33. Boyanshinov, M.I. & Zamorueva, I.N. The Effect of Various Factors on Bonding of Copper to Steel in the Solid State. Nanchne Trudy Magnito-gorskogo. Gorno-Metallurgicheskojo Instituta, 1957, 11, Metallurgizdat.

34. Agers, B.M. Ph.D. Thesis. University of Swansea Sept. 1962.

35. Rychlewski, J. Plain Plastic Strain for Jump non-homogeneity. Int. J. non-linear Mech. (1966). 1, 57.

36. Arcisz, M. Cutting of a bimetallic strip by smooth rigid punches. J. Mech. Phys. Solids. 1969, 17. pp 437-458.

37. Drayanov, B.A. Drawing through curvilinear die. Zh. prikl. Mekh. tekh. fiz 1962, 1, 165.

38. Drayanov, B.A. Stress distribution under a punch of curvilinear profile during cutting of an ideally plastic strip. Zh prikl. Mekh. tekh. Fiz. 1961, 6, 155.

39. Sokolovski, V.V. Complete plane problems of plastic flow. J. Mech. Phys. Solids. 1962, 10, 353.

40. Smith, O. Flow of metals in the draw process. J. Franklin Inst. (1886) 122, No. 5, 321-346. (1887), 123, 232.

41. Musiol, K. The Drawing in Extrusion Presses in Theory and Practice. Kingler's Polytech. J. (1900), 315, 428-432, 442-447.

42. Lewis, K.B. Notes on die stresses. Wire and Wire Products. 1938, (Sept.) 13, No. 9, 441-443, 476-477.

43. Elder, F.C. The Wire Drawing Die. Wire and Wire Products (1944), 19, 23.

44. Horsbugh, E.M. Trans. of the Institution of Engineers and Shipbuilders in Scotland. (1930), 74, 318.

45. Francis, E.L. & Thompson, F.C. The drawing of non-ferrous wires. J. Inst. Metals (1931), 46, 213-351.

46. Korber, F. & Eichinger, A. Die grundlagen der bildamen verformung. Mitt. K.W. Inst. Eisenforachung. 1940, 22, 57.

47. Davis, E.A. & Dokos, S.J. Theory of wire drawing. J. of Applied Mechanics, 1944. Dec. A193-A198.

48. Lunt, R.W. & MacLellan, G.D.S. An extension of wire-drawing theory with special reference to the contributions of K.B. Lewis. J.

49. Wistreich, J.G. Die pressures in plain strain drawing: Comparison between theory and experiment. Solid Mechanics Phys. Solids. 1953, 1, 164.

50. Wistreich, J.G. Investigation of the mechanics of wire drawing. Proc. Inst. Mech. Engrs. (1955) 169, 654-5.

51. Wistreich, J.G. The fundamentals of wire drawing. Met. Rev. (1958), 2, (10), 97-142.

52. MacLellan, G.D.S. A Critical Survey of Wire Drawing Theory. J. Iron & Steel Inst. London (1948), 158, 347.

53. Shield, R.H. Plastic flow in a converging conical channel. J. of Mechanics and Physics of Solids. 1955. Vol. 3 pp 246-258.

54. Avitzur, B. Metal-forming processes and analysis. Publisher: McGraw-Hill, New York. (1968).

55. Sachs, G. & Baldwin, W.M. Stress Analysis of tube sinking. Trans. A.S.M.E. 1946, 68, p 655.

56. Swift, H.W. Stresses and Strains in Tube Drawing. Philosophical Magazine. 1949, 308, pp 883-902.

57. Chung, S.Y. & Swift, H.W. A theory of tube sinking. J. Iron steel Inst. (1952) 170, 29.

58. Sachs, G., Lubahn, J.D. & Tracy, D.P. — Drawing thin-walled tubing with a moving mandrel through a single stationary die. J. of Applied Mechanics. 1944, Dec. A-199 to A-210.

59. Espey, G. & Sachs, G. — Experimentation on tube drawing with a moving mandrel. J. Appl. Mechanics (A.S.M.E.) 1947, 14, pp 81-87.

60. Sachs, G. — Spanlose forming der metalle, Springer, Berlin, 1934.

61. Blazynski, T.Z. & Cole, I.M. — An investigation of the plug drawing process. Proc. Inst. Mech. Engrs. London, 1960, 174, pp 797-812.

62. Blazynski, T.Z. & Cole, I.M. — An investigation of the sinking and mandrel drawing process. Proc. Inst. Mech. Engrs. 1963-64. Vol. 198, Pt. 1. No. 33, 894-906.

63. Blazynski, T.Z. — Tandem Mandrel Tube Drawing with Back-pull. J. Iron Steel Inst., (1964, 203, p 693.

64. Green, A.P. — Plain strain theory of drawing. Proc. Inst. of Mech. Eng. 1960, Vol. 174, No. 31. p 847.

65. Schneider, M. and Piwowarski, J. — Parameters of the floating plug tube drawing process. Archeinum Hutnictwa (1966) 11(i), p 40.

66. Smith, D.J. & Bramley, A.N. — A theoretical sutdy of tube drawing with a floating plug. Proc. 14th Int. MTDR Conf (1974).

67. Rowe, G.W. An introduction to the principles of metalworking. Edward Arnold Ltd., 1971.

68. MacLellan, G.D.S. Some Friction Effects in Wire Drawing. J. of the Institute of Metals. 1952-53. Vol. 81. pp 1-13.

69. Moore, G.G., & Wallace, J.F. A method for investigating the co-efficient of friction in tube sinking through conical dies. (Die oscillation method). J. Mech. Eng. Sciences, 1965, 7(3), p 279-282.

70. Rothman, D. & Sansome, D.H. An Investigation of rod drawing with die rotation. International Journal MTDR 1970, Vol. 10, p 179-192.

71. Johnson, W. & Kudo, H. Use of upper bound solutions .... for axisymmetric extrusion processes. Int. J. Mech. Sci. 1960, 1, 175.

72. Kudo, H. Some Analytical and experimental studies of axisymmetric cold forging and extrusion. I and II. Int. J. Mech. Sci. 1960, 2, p 102-127. 1961, 3, p 91-117.

73. Kobayashi, S. Upper-bound solution of axisymmetric forming problems - I. Trans. ASME, (1964) (May) 122, (J. of Eng. for Ind.)

74. Kobayashi, S. Upper Bound solution of axisymmetric forming problems - II. Trans. ASME (1964, (Nov.) 326.

75. Johnson, W. & Kudo, H. — The mechanics of metal extrusion. Manchester University Press.

76. Halling, J. & Mitchell, L.A. — An upper-bound solution for axi-symmetric extrusion. Int. J. Mech. Sci. (1965) Vol. 7, p 277-295.

77. Adie, J.F. & Alexander, J.M. — A graphical method of obtaining hodographs for upper-bound solutions to axiysymmetric problems. Int. J. Mech. Sci. (1967) Vol. 9, p 349.

78. Winsper, C.E. & Sansome, D.H. — Application of ultrasonic vibration to the plug drawing of tubes. Metal Forming (March, 1971) p 71.

79. Watts, A.B. & Ford, H. — An experimental investigation of the yielding of strip between smooth dies. Proceed. Inst. Mech. Eng. 1952 (31), pp 448-453.

80. Watts, A.B. & Ford, H. — On the basic yield stress curve for a metal. Proc. Inst. Mech. Eng. London 1955, 169, 1141-1156.

81. Drucker, D.C., Greenberg, H.J. & Prager, W. — The safety factor of an elastic-plastic body in plane strain. Trans. ASME, J. Appl. Mech. (1951) 18, 371.

82. Prager, W. & Hodge, P.G. Jnr. — Theory of perfectly plastic solids. Chapman and Hall, London (1951).

83. Hill, R. — Mathematical solution of Plasticity Clarendon Press.

84. Johnson, W. — Estimation of upper bound loads for extrusion and coining operations. Proc. Inst. Mech. Engrs. 1959, 173, 61.

85. Bisk, M.B. & Shveikin, V.V. Relation between the shape and position of the self-stopping mandrel in the zone of deformation and the parameters of the tube drawing operation. Stal (1964) 7, p 894.

86. Orro, P.I. & Savin, G.A. Drawing medium-grade carbon steel tubes on a floating mandrel. Stal (1963). 6, p 466.

87. Bisk, M.B., Sominski, Z.A. & Shveikin, V.V. Drawing tubes on a self adjusting mandrel on straight drawing mills. Stal (1963) 6, p 463.

88. Perlin, I.L. Consideration of stability in the floating plug drawing process for tubes. Tsvetyne Metally 31, p 463. 1958.

89. Avitzur, B. "The Production of Bimetal rod and wire" University of Lehigh (1969)

90. Atkins, W.E. & Cartwright, W. Experiments in Wire Drawing Part I - Behaviour of a Composite Rod. J. Inst. Metals (1931), 16, 293-312.

91. Pomp, A. & Lueg, W. Mitt, K.W. Inst. Eisenf (1942), 24, 123.

APPENDIX - A1

Specification of Tube Materials

(a) Mild Steel Tube supplied by Accles and Pollock Spec. J.I.C.
Nearest equivalent EN26
Chemical composition :-

Carbon	0.18% max
Manganese	0.30% to 0.60%
Phosphorus	0.04% max
Sulphur	0.05% max

(b) Stainless steel T.347

Carbon	0.10% max
Chromium	17.0% to 19.0%
Nickel	9.0% to 12.0%

(c) Brass Tubes supplied by Serck Heat Transfer
Composition:- 70/30 brass to B.S.2871
Alloy CZ.126 and contain 70.1% Copper
Arsenic content 0.026%
Hardness : 101 HV/5.

(d) Copper Tubes supplied by Serck Heat Transfer
Composition:- Phosphorus deoxidised 0.022%
Non-arsenical material to B.S.2871
alloy C.106 .
Hardness: 42HV/2½

APPENDIX A2

Sachs Theory on mandrel tube drawing

Initially, the drawing of thin-walled tubes on a mandrel was analysed by Sachs, Lubahn and Tracy[58] in 1944. Using an element (illustrated in Figure (A2.1) and equating for equilibrium, they arrived at an expression for die pressure:

$$p = \sigma_o - \frac{1}{h}\int_o^x pC\,dx$$

where $C = \tan\alpha - \tan\beta + \mu_1 - \mu_2$

σ_o = flow stress or yield stress

However, this equation had to be solved by a method of successive improvement in order to obtain values of p.

Subsequently, by assuming constant yield stress, σ_o, and constant tool angles, the authors simplified and integrated the above expression using boundary conditions. Hence the equation for pressure p becomes:

$$\frac{p}{\sigma_o} = \frac{1}{B}\left[(1+B)\left(\frac{h}{h_o}\right)^B - 1\right] \qquad \text{where } B = \frac{\mu_1 - \mu_2}{\tan\alpha - \tan\beta}$$

The axial draw force on the tube is:

$$F_1 = \frac{\sigma_o h_e}{B}(B+1)\left[1 - \left(\frac{h_e}{h_o}\right)^B\right]$$

where h_o and h_e are the initial and final tube wall thicknesses respectively,

and the force caused by the mandrel is:

$$F_2 = \frac{\sigma_o h_e[\tan\beta + \mu_2]}{B(\tan\alpha - \tan\beta)}\left[1 - \left(\frac{h_e}{h_o}\right)^B\right]$$

Summation of the above two expressions gives:

$$\frac{F}{\sigma_o h_e} = \frac{\tan\alpha + \mu_1}{\mu_1 - \mu_2}\left[1 - \left(\frac{h_e}{h_o}\right)^B\right] \qquad \text{(A2.1)}$$

For the case of $\mu_1 = \mu_2$, the analysis had to be revised and the expression for draw stress to yield stress ratio becomes:

$$\frac{F}{\sigma_o h_e} = \left[\frac{\tan\alpha + \mu_1}{\tan\alpha - \tan\beta}\right] \ln\left(\frac{h_o}{h_e}\right) \qquad \text{(A2.2)}$$

Espey and Sachs[59] extended the work of Sachs, Lubahn and Tracy, and by assuming that $\mu_1 = \mu_2 = \mu$, they proposed an equation for draw stress:

$$S_1 = k_o(1+C) \ln\frac{A_o}{A_e} + S_o\left[1 - C\left(\frac{A_o}{A_e} - 1\right)\right]$$

where $C = \frac{\mu}{\tan\alpha}$ for a straight mandrel and

S_o is the longitudinal stress at entry or back pull stress. Basically, this equation is the same as equation A2.2 except for the additional term on the right hand side of the expression. Nevertheless, for a close pass, $S_o = 0$ and the said term disappears altogher. In their analysis, Sachs and Espey obtained the value of S_o by extrapolating from a graph of draw stress against reduction in area for the case of zero reduction in area.

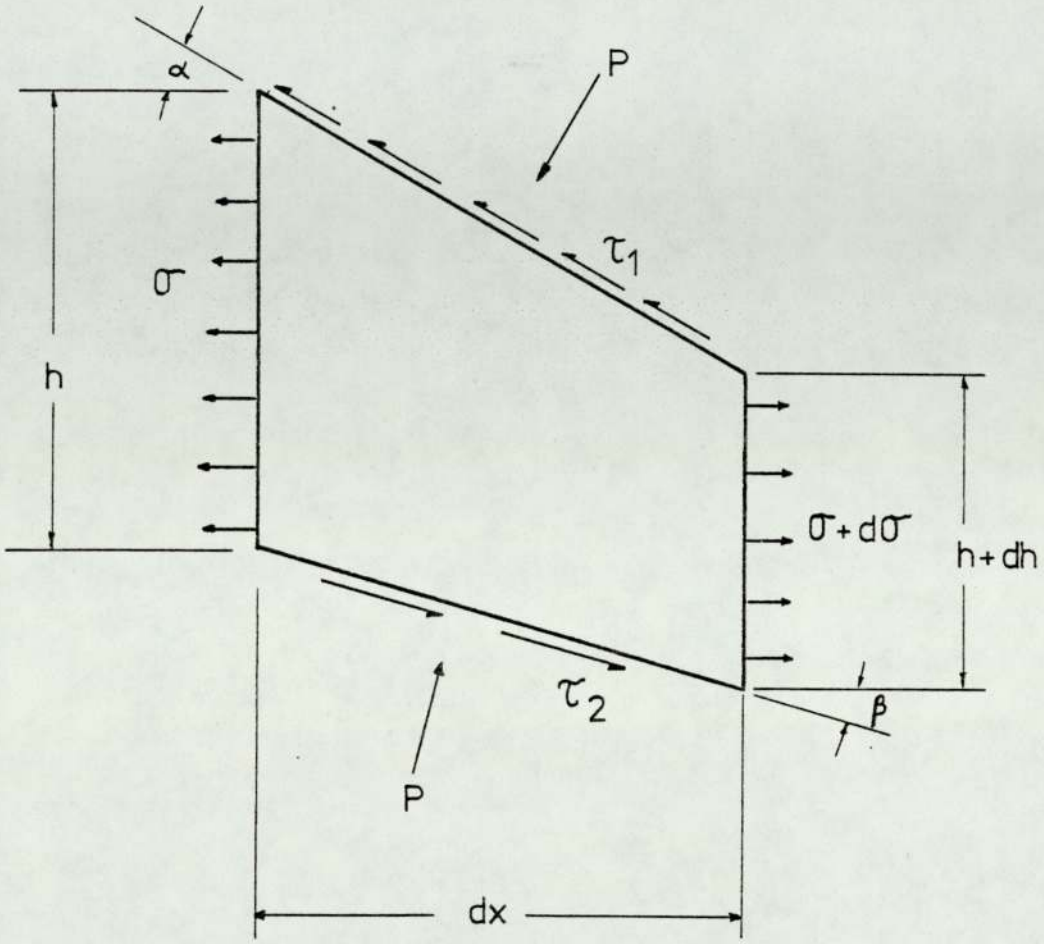

Figure A2.1 Element of Tube in Mandrel Tube Drawing

(after Sachs et al[58])

Appendix A3

Detail Analysis of the Drawing of Bimetal Tube on a Mandrel - An Upper Approach

The deformation field and hodographs used in the following analysis are given in Figure (2.5). Using straight lines to represent lines of velocity discontinuities, the total internal work of deformation is given by equation (2.31) as:

$$\dot{W}_p = \Sigma\, \tau_s . V . A$$

Plastic work across unit cross-sectional area of the velocity dicontinuities.

Considering the velocity discontinuity AB, the rate of working is given as:

$$\dot{W}_{12} = k_c . V_{12} . A_{AB}$$

Assuming that there is no change in tube wall thickness while the tube is sinking, i.e. AH = AG in Figure (2.5), then

$$A_{AB} = H_c / \cos\frac{\alpha}{2}$$

From the hodograph:

$$V_{12} = V_2 \frac{\sin\alpha}{\sin(\frac{\pi}{2} - \frac{\alpha}{2})}$$

$$\text{and } V_2 = V_3 \frac{\sin(\theta+\omega)}{\sin(\pi-(\theta+\omega) - (\alpha-\theta))}$$

$$\text{and } V_3 = V_6 \frac{\sin\phi}{\sin(\phi+\theta)}$$

$$\dot{W}_{12} = 2.k_c . V_6 \frac{\sin\phi \sin(\theta+\omega) \tan\frac{\alpha}{2} . H_c}{\sin(\phi+\theta) \sin(\alpha+\omega)}$$

Referring to the discontinuity CE, its area is given by:

$$A_{CE} = \frac{(R_3 - R_5)}{\sin\omega}$$

From the hodograph for clad:

$$V_{23} = V_3 \frac{\sin(\alpha-\theta)}{\sin(\alpha+\omega)}$$

and $$V_3 = V_6 \frac{\sin\phi}{\sin(\phi+\theta)}$$

The rate of working across velocity discontinuity CE is then:

$$\dot{W}_{23} = k_c V_6 \frac{(R_3-R_5)\sin\phi \sin(\alpha-\theta)}{\sin\omega \sin(\phi+\theta) \sin(\alpha+\omega)}$$

Similarly the rate of working across discontinuity EF is given by:

$$\dot{W}_{36} = k_c . V_{36} . A_{EF}$$

where $$V_{36} = V_6 \frac{\sin\theta}{\sin(\theta+\phi)}$$

$$A_{EF} = \frac{h_c}{\sin\phi}$$

$$\dot{W}_{36} = k_c . \frac{h_c . V_6 . \sin\theta}{\sin\phi \sin(\theta+\phi)}$$

Considering the discontinuity CD, the rate of working across this discontinuity is given by: $\dot{W}_{45} = k_m . V_{45} . A_{CD}$

$$A_{CD} = \frac{H_m}{\sin\varepsilon}$$

Using the hodograph for the matrix:

$$V_{45} = V_{56} \frac{\sin\beta}{\sin\varepsilon} \quad \text{and} \quad V_{56} = V_6 \frac{\sin\theta}{\sin(\theta+\beta)}$$

$$\dot{W}_{45} = k_m . V_6 \frac{H_m \sin\theta \sin\beta}{\sin^2\varepsilon \sin(\theta+\beta)}$$

Similarly for discontinuity FD,

$$A_{FD} = \frac{h_m}{\sin\beta} \qquad \text{and } V_{56} = V_6 \frac{\sin\theta}{\sin(\theta+\beta)}$$

The rate of working across discontinuity FD is then:

$$\dot{W}_{56} = k_m \cdot \frac{V_6 \cdot h_m \cdot \sin\theta}{\sin\beta \sin(\theta+\beta)}$$

Allowance for friction

The shear stress acting at the tube-die interface BE is given by $\tau = m_1 k_c$ and is assumed to be constant. The rate of working across BE is given by:

$$\dot{W}_6 = m_1 k_c \cdot V_2 \cdot A_{BE}$$

$$A_{BE} = \frac{R_o - R_3}{\sin\alpha}$$

From the hodograph for the clad, $V_2 = V_3 \dfrac{\sin(\theta+\omega)}{\sin|\pi-(\theta+\omega)-(\alpha-\theta)|}$

$$V_2 = V_3 \frac{\sin(\theta+\omega)}{\sin(\alpha+\omega)}$$

and $V_3 = V_6 \dfrac{\sin\phi}{\sin(\phi+\theta)}$

$$\dot{W}_6 = m_1 k_c \cdot \frac{V_6 (R_o - R_3) \sin\phi \sin(\theta+\omega)}{\sin\alpha \sin(\phi+\theta) \sin(\alpha+\omega)}$$

The rate of working across the interface between the tube and mandrel where there is relative movement between the tube and mandrel is given by: $\dot{W}_7 = m_2 k_m \cdot V_{4m} A_7 \cdot$

where $A_7 = Z_4 = Z_3 - Z_2 - x$ in figure (2.5)

and $Z_3 = Z_6 + Z_1 - Z_5$

$$Z_3 = (R_o - R_7) \tan\frac{\alpha}{2} + \frac{(R_o - R_3)}{\tan\alpha} - \frac{(R_7 - R_5)}{\tan\alpha}$$

$$Z_2 = \frac{h_m}{\tan\beta} \quad \text{and } x = \frac{h_c}{\tan\phi}$$

From the hodograph for matrix, $V_4 = V_5 \frac{\sin(\varepsilon-\theta)}{\sin\varepsilon}$

$$\text{and } V_5 = V_6 \frac{\sin\beta \sin(\varepsilon-\theta)}{\sin\varepsilon \sin(\theta+\beta)}$$

The absolute difference in velocity between the mandrel and the tube across the area A_7 is given by:

$$V_{4m} = |V_6 - V_4|$$

$$\therefore \quad \dot{W}_7 = V_6 \left| 1 - \frac{\sin\beta \sin(\varepsilon-\theta)}{\sin\varepsilon \sin(\theta+\beta)} \right| \cdot A_7 \cdot m_2 \cdot k_m$$

Due to the difference in velocity between the clad and matrix, the rate of working against friction at the interface CF of the clad and matrix is given by: $W_8 = m_3 \cdot k_i \cdot V_i \cdot A_{CF}$

$$A_{CF} = \frac{(R_5 - R_4)}{\sin\theta}$$

$k_i = k_c$ when $k_c < k_m$

and $k_i = k_m$ when $k_m < k_c$

$$V_i = |V_3 - V_5|$$

$$= \left| \frac{\sin\phi}{\sin(\phi+\theta)} - \frac{\sin\beta}{\sin(\phi+\beta)} \right| \cdot V_6$$

$$\dot{W}_8 = m_3 \cdot k_i \cdot \frac{(R_5 - R_4)}{\sin\theta} \left| \frac{\sin\phi}{\sin(\phi+\theta)} - \frac{\sin\beta}{\sin(\theta+\beta)} \right| \cdot V_6$$

The rate of working of the external pull is given by:

$\sigma_x \cdot T \cdot V_6$ for unit cross-sectional area

where T is the wall thickness of the drawn tube.

By equating the expression for rate of working due to external pull to that of power dissipated in internal deformation:

$$\sigma_x . T . V_6 = \Sigma \tau_s . V . A_s$$

$$\frac{\sigma_x}{Y_e} = \frac{\dot{W}_1 + \dot{W}_2 + \dot{W}_3 + \dot{W}_4 + \dot{W}_5 + \dot{W}_6 + \dot{W}_7 + \dot{W}_8}{T . V_6 . Y_e}$$

The right hand side of this equation is totally determined by the geometries of the tube and the deformation zones and the friction coefficients, all of which could be either obtained or assumed as in the case of the friction coefficients.

APPENDIX A4

Detail Analysis of Bimetal Tube Drawing on a Floating Plug - an Upper Bound Approach

Plastic work across discontinuities.

The rate of plastic working across a discontinuity is given by:

$$\dot{W} = k.A.V.$$

Considering deformation in the clad and referring to Figure (2.6), the rate of working across discontinuity AB is given by: $\dot{W}_{12} = k_c \cdot A_{AB} \cdot V_{12}$

Assuming that there is no thickness change on crossing discontinuity AB, i.e. AG = AH in Figure (2.6)

$$A_{AB} = \frac{(R_o^2 - R_7^2)}{\cos \frac{\alpha}{2}}$$

$$V_1 = V_7 \frac{(R_3^2 - R_4^2)}{R_o^2 - R_7^2} \quad \text{for constancy of volume.}$$

$$\therefore \quad V_{12} = V_1 \frac{\sin\alpha}{\sin(\frac{\pi}{2} - \frac{\alpha}{2})} = V_7 \frac{(R_3^2 - R_4^2)}{R_o^2 - R_7^2} \cdot 2 \sin \frac{\alpha}{2}$$

giving: $W_{12} = 2\pi k_c . V_7 (R_3^2 - R_4^2) \tan \frac{\alpha}{2}$

Similarly, the rate of working across discontinuity CD is given by:

$$W_{45} = 2\pi k_m (R_4^2 - R_2^2) \tan \frac{\theta}{2}$$

The rate of working across discontinuity CO is expressed as

$$\dot{W}_{23} = k_c \cdot \int V_{23} \cdot d A_{co} \qquad \text{(A4.1)}$$

Considering volume constancy: $V_{23} = \frac{R_3}{R} \quad (V_{23})_7$

and from the hodograph for clad, $(V_{23})_7 = \frac{\sin(\alpha - \theta)}{\sin(\alpha \pm \omega)} (V_3)_7$

and $(V_3)_7 = \frac{\sin\phi}{\sin(\theta+\phi)} \cdot V_7$

$$\therefore \quad (V_{23})_7 = \frac{\sin(\alpha-\theta)\ \sin\phi}{\sin(\alpha\pm\omega)\ \sin\ (\theta+\phi)}\ V_7$$

$$\int dA = \int_{R_3}^{R_5} 2\pi \frac{R\ dR}{\sin\ \omega}$$

Substituting into equation (A4.1) and integrating gives:

$$\dot{W}_{23} = 2\pi k_c . V_7 \frac{\sin\phi\ \sin\ (\alpha-\theta)\ .\ R_3 |R_5 - R_3|}{\sin(\alpha\pm\omega)\ \sin\ (\theta+\phi)\ \sin\omega}$$

$|R_5 - R_3|$ is the absolute difference between R_5 and R_3. This is to cater for situations when R_3 can be greater or smaller than R_5. The term sin $(\alpha \pm \omega)$ becomes $\sin(\alpha+\omega)$ when $R_5 < R_3$ and sin $(\alpha-\omega)$ when $R_5 > R_3$.

Considering the discontinuity OF,

$$\dot{W}_{37} = k_c . A_{OF} . V_{37}$$

From the hodograph, $V_{37} = V_7 \frac{\sin\theta}{\sin(180-(\theta+\phi))}$

$$A_{OF} = \pi \frac{(R_3^2 - R_4^2)}{\sin\phi}$$

$$\dot{W}_{37} = \pi k_c . V_7 \frac{(R_3^2 - R_4^2)\ \sin\theta}{\sin\phi\ \sin\ (\theta+\phi)}$$

The rate of working across discontinuity EF is given by:

$$\dot{W}_{56} = k_m \int V_{56} . d\, A_{EF} \qquad (A4.2)$$

$V_{56} = \frac{R_4}{R} (V_{56})_7$ where R is any value between R_6 and R_4

From the hodograph for matrix, $(V_{56})_7 = (V_6)_7 \frac{\sin(\theta-\beta)}{\sin|\pi-(\theta-\beta+\varepsilon)|}$

and $(V_6)_7 = V_7 \frac{\sin\gamma}{\sin(\gamma+\beta)}$

$$\therefore V_{56} = \frac{R_4}{R} \cdot V_7 \frac{\sin\gamma \sin(\theta-\beta)}{\sin(\gamma+\beta) \sin(\theta-\beta+\varepsilon)}$$

$$\int d\, A_{EF} = \int_{R_6}^{R_4} 2.\pi . \frac{R\, dR}{\sin(\varepsilon-\beta)}$$

By substituting the terms for V_{56} and A_{EF} into equation (A4.2) and integrating, the following is obtained:

$$\dot{W}_{56} = 2\pi k_m . V_7 \frac{\sin\gamma \sin(\theta-\beta) \quad R_4(R_4-R_6)}{\sin(\gamma+\beta) \sin(\theta-\beta+\varepsilon) \sin(\varepsilon-\beta)}$$

The rate of working across discontinuity FQ is given by:

$$\dot{W}_{67} = k_m . A_{FQ} . V_{67}$$

$$A_{FQ} = \pi \frac{(R_4^2 - R_2^2)}{\sin\gamma}$$

From the hodograph for matrix, $V_{67} = V_7 \frac{\sin\beta}{\sin(\beta+\gamma)}$

$$\dot{W}_{67} = \pi k_m . V_7 (R_4^2 - R_2^2) \frac{\sin\beta}{\sin\gamma \sin(\beta+\gamma)}$$

Allowance for rate of working against friction at interfaces:

The shear stress acting along the clad-die interface is given by: $\tau = m_1 . k_c$

and the rate of working along this interface is given by:

$$\dot{W}_7 = m_1 \cdot k_c \int dA_{BO} \cdot V_2 \qquad (A4.3)$$

$$\int d\,A_{BO} = \int_{R_3}^{R_o} 2\pi \frac{R.dR}{\sin\alpha}$$

The velocity V_2 changes along this interface due to circumferential straining in region (2). If $(V_2)_1$ is the velocity at point B, in Figure (2.6) the velocity at any point along the interface whose distance from the drawing axis is R may be defined as:

$$V_2 = (V_2)_1 \cdot \frac{R_o}{R} \quad \text{where R is any value between } R_o \text{ and } R_3$$

From the hodograph for clad, $(V_2)_1 = V_7 \dfrac{(R_3^2 - R_4^2)}{R_o^2 - R_7^2}$

Substituting for V_2 and $\int d\,A_{BO}$ into equation (A4.3) and integrating gives:

$$\dot{W}_7 = 2m_1 . \pi . k_c . V_7 \frac{R_o(R_o - R_3)\ (R_3^2 - R_4^2)}{(R_o^2 - R_7^2)\ \sin\alpha}$$

Similarly, the rate of working against friction across the conical portion of the plug is given by:

$$\dot{W}_9 = m_2 . k_m \cdot \int V_6 \cdot d\,A_{EQ} \qquad (A4.4)$$

It is assumed that the plug is "floating" at a position of equilibrium in the die and is stationary in relation to the flow of the matrix material.

$V_6 = (V_6)_7 \cdot \dfrac{R_2}{R}$ where R is any value between R_6 and R_2.

and from the hodograph for matrix: $(V_6)_7 = V_7 \dfrac{\sin\gamma}{\sin(\gamma+\beta)}$

$$\int d\,A_{EQ} = \int_{R_2}^{R_6} 2\pi \frac{R\,dR}{\sin\beta}$$

Substituting in equation (A4.4) and integrating, $\dot{W}_9$ is given as:

$$\dot{W}_9 = m_2 \cdot k_m \cdot 2\pi \cdot V_7 \frac{\sin\gamma \cdot R_2(R_6-R_2)}{\sin\beta(\gamma+\beta)}$$

The power dissipated at the clad/matrix interface CF due to the velocity difference can be computed as:

$$\dot{W}_8 = m_3 \cdot k_i \cdot \int V_i \cdot dA \qquad \text{(A4.5)}$$

At any radius R along this interface an element area is given by:

$$dA = 2\pi \cdot R\frac{dR}{\sin\theta}$$

V_i is the absolute velocity difference at a point along the interface CF and k_i is the shear yield stress of the clad or matrix which ever has the lower value.

Considering volume constancy, if V_3 is the velocity in region (3) at any radius R, then: $V_3 = \frac{R_4}{R}(V_3)_7$

Similarly for region (5), if V_5 is the velocity at any radius R (between R_5 and R_4), then:

$$V_5 = \frac{R_4}{R}(V_5)_7$$

From the hodographs for clad and matrix:

$$(V_3)_7 = \frac{V_7 \sin\phi}{\sin(\phi+\theta)}$$

and $$(V_5)_7 = \frac{(V_6)_7 \sin\varepsilon}{\sin(\theta-\beta+\varepsilon)}$$

$$(V_6)_7 = V_7 \frac{\sin\gamma}{\sin(\beta+\gamma)}$$

$$\therefore V_3 = V_7 \frac{R_4}{R} \frac{\sin\phi}{\sin(\phi+\theta)}$$

$$\therefore V_5 = V_7 \frac{R_4}{R} \frac{\sin\gamma \sin\varepsilon}{\sin(\beta+\gamma) \sin(\theta-\beta+\varepsilon)}$$

$$V_i = |V_3 - V_5|$$

$$= V_7 \frac{R_4}{R} \left| \frac{\sin\phi}{\sin(\phi+\theta)} - \frac{\sin\gamma \sin\varepsilon}{\sin(\beta+\gamma) \sin(\theta-\beta+\varepsilon)} \right|$$

Substituting these values into equation (A4.5) and integrating between R_4 and R_5 gives:

$$\dot{W}_8 = 2\pi . m_3 . k_i . \frac{R_4 (R_5 - R_4)}{\sin\theta} V_7 \left| \frac{\sin\phi}{\sin(\phi+\theta)} - \frac{\sin\gamma \sin\varepsilon}{\sin(\beta+\gamma) \sin(\theta-\beta+\varepsilon)} \right|$$

The rate of working against friction along the die land is given by: $\dot{W}_{D1} = 2\pi\, m_1\, k_c . R_3 . D_1 . V_7$

and the rate of working against friction along the plug land is given by:

$$\dot{W}_{pl} = m_2 . k_m . 2\pi R_2 . P_1 . V_7$$

Plastic work due to circumferential straining:

The rate of work in circumferential straining is given by:

$$\dot{W} = \dot{v} . \bar{\sigma}\, \bar{\varepsilon}$$

According to von Mises yield criterion:

$$\bar{\sigma} = \sqrt{3}\, k \quad \text{and} \quad \bar{\varepsilon} = \frac{2}{\sqrt{3}} \left[\varepsilon_R^2 + \varepsilon_R \varepsilon_\theta + \varepsilon_\theta^2 \right]^{\frac{1}{2}}$$

For the clad material:

$$\varepsilon_{\theta c} = \ln\left[\frac{R_o + R_7}{R_3 + R_4}\right]$$

$$\dot{v}_c = \pi(R_3^2 - R_4^2) . V_7$$

For the matrix material:

$$\varepsilon_{\theta m} = \ln\left[\frac{R_5 + R_1}{R_2 + R_4}\right]$$

$$\dot{v}_m = \pi\ (R_4^2 - R_2^2).\ V_7$$

To accommodate for strain hardening, a mean yield stress value is used to compute the value of shear yield stress, k.

For both the clad and matrix materials, the value of $\varepsilon_R = 0$ in this case.

$\therefore$ the rate of working due to circumferential straining for the clad and matrix respectively are:

$$\dot{W}_c = 2\pi\ k_c\ (R_3^2 - R_4^2).\ V_7.\ \ln\left[\frac{R_o + R_7}{R_3 + R_4}\right]$$

$$\dot{W}_m = 2\pi k_m\ (R_4^2 - R_2^2).\ V_7\ \ln\left[\frac{R_5 + R_1}{R_2 + R_4}\right]$$

The rate of working of the external pull is given by:

$$\dot{W}_7 = \sigma_x.\ \pi\left[R_3^2 - R_2^2\right].\ V_7$$

By equating this expression to the sum of the rate of work computed from equations for $\dot{W}$ worked out above, this is given as:

$$\dot{W}_T = \Sigma\dot{W}$$

$$\dot{W}_T = \dot{W}_{12} + \dot{W}_{23} + \dot{W}_{37} + \dot{W}_{45} + \dot{W}_{56} + \dot{W}_{67} + \dot{W}_7 + \dot{W}_8 + \dot{W}_9 + \dot{W}_{D1} + \dot{W}_{P1} + \dot{W}_c + \dot{W}_m$$

$$\sigma_x\ \pi\left[R_3^2 - R_2^2\right].\ V_7 = \Sigma\dot{W}$$

$$\sigma_x = \frac{\Sigma \dot{W}}{\pi (R_3^2 - R_2^2) . V_7}$$

$$\frac{\sigma_x}{Y_e} = \frac{\Sigma \dot{W}}{\pi (R_3^2 - R_2^2) . V_7 . Y_e}$$

where Y_e is the modified or equivalent yield stress of the bimetal tube.

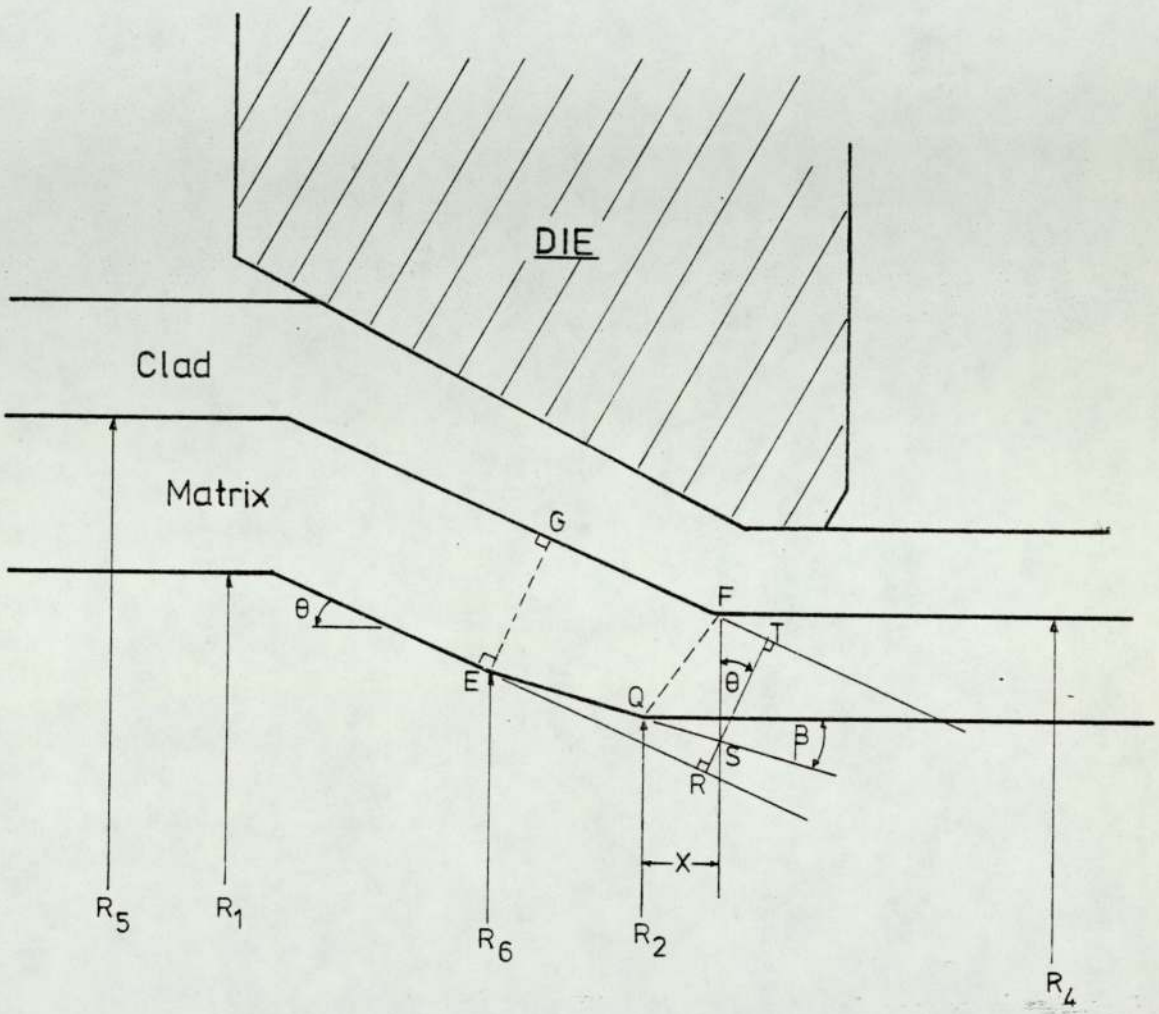

Fig. A4.1 BIMETAL TUBE DRAWING ON A FLOATING PLUG

To calculate the length of contact between the taper portion of the floating plug and the inner tube

Referring to figure A4.1, assuming that there is no variation in tube wall thickness whilst the tube is being sunk,

$$EG = RT = R_5 - R_1$$

$$FS = R_4 - R_2 + x \tan\beta$$

$$TS = FS \cos\theta$$

$$= (R_4 - R_2 + x \tan\beta)\cos\theta$$

but $$RT = TS + SR$$

$$SR = RT - TS$$

$$= R_5 - R_1 - (R_4 - R_2 + x \tan\beta)\cos\theta$$

also $$SR = ES \sin(\theta - \beta)$$

$$= (EQ + QS)\sin(\theta - \beta)$$

$$EQ = \frac{SR}{\sin(\theta - \beta)} - QS$$

therefore, $$EQ = \frac{R_5 - R_1 - (R_4 - R_2 + x \tan\beta)\cos\theta}{\sin(\theta - \beta)} - \frac{x}{\cos\beta}$$

COMPUTER PROGRAMMES

Appendix

A5 ..... Mandrel

A6 ..... UBM

A7 ..... UBFP

```
#LISTING OF :EPP7051_NLBM(3/)   PRODUCED ON  2APR79 AT 16.54.58

#G8.63A AT ASTON    IN ':EPP7051_MOPNOUSERLF' ON  5APR79 AT 13.12.21 USING  U15

DOCUMENT    NLBM


      0       MASTER MANDREL
      1 C   THIS PROGRAM CALCULATES THE DRAW FORCE AND DRAW STRESS RATIO
      2 C   FOR BIMETAL TUBE MANDREL DRAWING - AN EQUILIBRIUM APPROACH
      3 C   THE NAG SUBROUTINE D02ABF IS USED
      4       EXTERNAL DERIV
      5       REAL K,  MAN, LOAD, MFORCE, MANF
      6       INTEGER TUBENO,T
      7       DIMENSION TUPE(8), FRICT(11), FORCE(11,11),SONY(11,11), SM(3),
      8      *          G(3),ZO(3), ZA(3), ZB(3), ZC(3), ZD(3), ZE(3)
      9       COMMON/SYMBOL/SHEARC,COEFS,COEFM,HP,FHC,FHM
     10       COMMON/CONSTANT/PIE,ALPHA,THETA,YC,YM
     11 C      ALPHA IS DIE SEMI ANGLE
     12       ALPHA=9.0
     13       PIE = 3.141592654
     14       ALPHA=ALPHA*PIE/180.0
     15 C      ANGLE ALPHA CHANGED TO RADIAN MEASURE
     16 C       TUPE DEFINES BIMETAL TUBE COMBINATIONS
     17 C       TUBENO DEFINES TUBE NUMBER
     18    40 READ(1,10)TUPE
     19    10 FORMAT(8A5)
     20       READ(1,20)YC,YM
     21    20 FORMAT(2F0.0)
     22       WRITE(2, 100)TUPE, YC, YM
     23   100 FORMAT(/,5X, 8A5,10X,'YC =',F6.3,5X,'YM =',F6.3)
     24    80 READ(1,30)TUBENO,COEFS,COEFM
     25    30 FORMAT(I0,2F0.0)
     26       IF (TUBENO) 40,50,60
     27    60 READ(1,31)HC,HM,FHC,FHM
     28    31 FORMAT(4F0.0)
     29 C    FHC, FHM ARE THE FINAL CLAD AND MATRIX THICKNESSES
     30 C      MAN IS DIAMETER OF MANDREL
     31       READ(1,61)OD,DIE,BORE,MAN
     32    61 FORMAT(4F0.0)
     33       HP=MAN/2.0
     34       AC=PIE*HC*(OD-HC)
     35       AM=PIE*HM*(BORE+HM)
     36 C    YE IS EQUIVALENT MEAN YIELD STRESS
     37       YE=(AC*YC+AM*YM)/(AC+AM)
     38       WRITE(2,101)TUBENO, HC,HM,HP,YE
     39   101 FORMAT(/,5X,'TUBE NO.',I4,35X,'HC =',F7.4,
     40      *       9X,'HM=', F7.4,9X, 'HP=',F7.4, 5X, 'YE=',F6.3)
     41       R = 1.0 - (DIE**2 - MAN**2)*PIE/(4.0*(AM+AC))
     42 C      R IS CALCULATION OF REDUCTION IN AREA OF TUBE
     43       WRITE(2,63)OD,DIE,FHC,FHM,R
     44    63 FORMAT(/,5X,'OD =',F6.4,6X, 'DIE=',F6.4,20X,'FHC =',F7.4,
     45      *        8X, 'FHM=',F7.4, 9X, 'REDUCTION=',F7.3)
     46       IF ( FHM .GE. HM) GO TO 80
     47       THETA = ATAN((HM - FHM)*TAN(ALPHA)/(HC+HM-FHC-FHM))
     48       DO 99 M =1,9,2
     49       COEFS = (M-1)*0.01
```

```
      SM(1) = 0.0
      SM(2) = 0.0
      SM(3) = 0.0
      G(1) = 0.0001
      G(2) = 0.0001
      G(3) = 0.0001
      H =0.0001
      T = 1
      N = 3
      I = 0
      HOM = FHM - HM
      CALL D02ABF( H2,SM,G,T,N,I,HOM,H,DERIV,ZO,ZA,ZB,ZC,ZD,ZE)
      IF (I .NE. 0)GO TO 98
      FAC = PIE*FHC*(DIE - FHC)
      FAM = PIE*FHM*(MAN + FHM)
      CFORCE = SM(3) * FAC
      MFORCE = SM(1) * FAM
      MANF = SM(2)* PIE * HP**2
      FORCE(M,J) = CFORCE + MFORCE + MANF
      SONY(M,J) = FORCE(M,J)/(YE*(FAC+FAM))
      FRICT(M) =COEFS
   99 CONTINUE
      WRITE(2,130)(FRICT(N),N=1,9,2)
  130 FORMAT(/,5X,'COEFS& COEFM', 5F10.2,/)
      WRITE(2,132)(FRICT(M),(FORCE(M,N),N=1,9,2),M=1,9,2)
  132 FORMAT(5(6X, F4.2, 13X, F6.4, 4F10.4,/))
      WRITE(2,133)
  133 FORMAT(1X,/,'STRESS RATIO')
      WRITE(2,134)
  134 FORMAT(1X,'============')
      WRITE(2,131)(FRICT(M),(SONY(M,N),N=1,9,2),M=1,9,2)
  131 FORMAT(5(6X, F4.2, 13X, F6.4, 4F10.4,/))
      GO TO 80
   98 WRITE(2,95)
   95 FORMAT(10X, 'IFAIL IS NOT EQUAL TO ZERO')
      GO TO 80
   50 STOP
      END

      SUBROUTINE DERIV( B, SM, H2)
      REAL K
      DIMENSION B(3), SM(3)
      COMMON/SYMBOL/SHEARC,COEFS,COEFM,HP,FHC,FHM
      COMMON/CONSTANT/PIE, ALPHA,THETA,YC,YM
      AA = TAN(ALPHA)
      TE = TAN(THETA)
      H1 = FHC + (H2 - FHM)*(AA/TE - 1.0)
      AT = H1*H2 + (H1 + H2)*HP
      BT = -SM(1)*HP*TE
      CT = -YC*((H2 + HP)*AA + (H1 - H2 -HP)*TE)
      DT = -H1*AA + (H1 -H2 -HP)*TE + COEFM*HP
      ET = (DT - COEFS*(H1 + H2 + HP))*(YM - SM(1))
      B(1) = (BT + CT + ET)/(AT*TE)
      B(2) = -2.0* COEFM *(YM - SM(1))/(HP*TE)
      BB = 1.0/H1 + 1.0/H2 + 1.0/HP
      EA = (YM-YC+SM(3))*TE/H2 + YC*TE/H1
      EB = -SM(3)*AA/H1 - SM(3)*TE/(H2+HP)
      EC = -(1.0/(H2+HP) + 1.0/H1)*(AA + COEFS)
      ED = EC - COEFM/H2 + (1.0/HP + 1.0/H2)*TE
      SHEARC = (EA + EB + (YC-SM(3))*ED)/BB
      CA = YC*TE - SM(3)*AA - SM(3)*H1*TE/(H2 + HP)
      CB = -(AA + COEFS)*(YC - SM(3))*(H1/(H2 + HP) + 1.0)
```

NUMBER OF PAGES 3

```
 #     #   #   #####    # .    SSSS        MOP        SSSSSSSSSSSS    :EPP7051.MOPNOUSERLF            SSSSSSS+SSSSSSSSSSSS
 #     #   #       #    #      SSSS                   SSSSSSSSSSSS                                    SSSSSSS+SSSSSSSSSSSS
 #     #   #       #    #      SSSS                   SSSSSSSSSSSS                                    SSSSSSS+SSSSSSSSSSSS
 #   #####  #####  #####       SSSSSSSSSSSSSSSSSSSSSSSSSSSSSSSSSSSSSSSSSSSSSSSSSSSSSSSSSSSSSSSSSSSSSSSSSSSSSSSSS+SSSSSSSSSSSS

#LISTING OF :EPP7051.UBM71(17/) PRODUCED ON  2APR79 AT 16.59.46

#G8.63A AT ASTON    IN ':EPP7051.MOPNOUSERLF' ON  5APR79 AT 11.09.53 USING  U15

DOCUMENT     UBM

          MASTER UBM
 C    THIS PROGRAM CALCULATES THE DRAW STRESS/2K OF BIMETAL TUBE DRAWING
 C        WITH A MOVING MANDREL - AN UPPER BOUND SOLUTION

 C      TUPE DEFINES COMBINATION OF TUBE
        REAL K,M1,M2,KC,KM,M3,MATRIX(11,11),MANDREL
        INTEGER TUBENO
        DIMENSION TUPE(8),SRATIO(11,11),CLAD(11,11),FRICT(11)
        PIE = 3.141592654
 C       ALPHA IS DIE SEMI ANGLE
        ALPHA=9.0 * PIE/180.0
 C      ANGLE ALPHA  CHANGED TO RADIAN MEASURE
        READ(1,7)M3
      7 FORMAT(F0.0)
     40 READ(1,10)TUPE
     10 FORMAT(8A5)
        READ(1,20)YC,YM
     20 FORMAT(2F0.0)
     80 READ(1,30)TUBENO
     30 FORMAT(I0)
 C      IF TUBENO IS NEGATIVE READ NEW TUBE COMBINATION
        IF(TUBENO)40,50,60
     60 READ(1,31)HC,HM,FHC,FHM
     31 FORMAT(4F0.0)
 C     FHC, FHM ARE THE FINAL TUBE WALL THICKNESSES
 C       MANDREL IS DIAMETER OF MANDREL
        READ(1,61)OD,DIE,BORE,MANDREL
     61 FORMAT(4F0.0)
        AC = PIE * HC*(OD-HC)
        AM = PIE * HM*(BORE +HM)
 C       Y IS EQUIVALENT MEAN YIELD STRESS
        Y = (AC*YC + AM*YM)/(AC+AM)
        WRITE(2,100)TUBENO,TUPE,HC,HM,MANDREL,YC,YM,Y
    100 FORMAT(1H0,2X,9HTUBE NO.=,I4,5X,8A5,
       *       2X,9H     HC =,F6.4,5X,5H  HM=,F6.4,5X,'MANDREL=',F6.4,
       *       8X,9H     YC =,F6.3,5X,5H  YM=,F6.3    ,
       *          5X,'  YE =',F6.3)
        R = 1.0 - PIE*(DIE**2-MANDREL**2)/(4.0*(AC+AM))
 C      R IS CALCULATION OF REDUCTION IN AREA OF TUBE
        WRITE(2,120)FHC,FHM,R
    120 FORMAT(1H ,62X,9H    FHC =,F9.6,5X,5H FHM=,F9.6,7X,'R =',F5.3)
        HAPIE = PIE/2.0
        RO = OD/2.0
        R1   = BORE/2.0
        R2   = MANDREL  /2.0
        R3   = DIE/2.0
        R5 = R2 + HM
        R7 = RO - HC
        F = R3-R2
        K = Y/2.0
```

```
      OMEGA = ATAN((R3-R5)/Z3)
      DO  100  M=1,11,2
      M1 = (M-1)*.01
      DO 100  N=1,11,2
      M2 = (N-1)*0.01
      C1 = 1000.0
      C2 = 1000.0
      C3 = 1000.0
      F2 = R3-R2-HC*COS(ALPHA)-0.001
C   THE FINAL MATRIX THICKNESS IS INCREMENTED 0.001 INCH
C   EACH TIME - THIS COULD BE CHANGED DEPENDING ON ACCURACY
C   OF PREDICTED FINAL CLAD AND MATRIX THICKNESSES REQUIRED
 360  F2 = F2 + 0.001
      IF ( F2 .GE. (HM-0.0002)) GO TO 820
      IF ( F2 .LT. 0.009) GO TO 360
      F1 = R3-R2-F2
      IF ( F1 .LT. 0.008) GO TO 820
      R4= R2+F2
      Q = SQRT(Z3**2-4.0*F1*(R5-R4))
      IF ((Z3-Q) .LE. 0.0) GO TO 460
C      THETAO IS INITIAL VALUE OF ANGLE THETA
      THETAO= ATAN((Z3-Q)/(2.0*F1))
      GO TO 470
  460 THETAO=ATAN((Z3+Q)/(2.0*F1))
  470 PHI = HAPIE - THETAO + PIE/18.0
  480 PHI = PHI - PIE/18.0
      X = F1/TAN(PHI)
      IF (X .GE. (Z3-.0002)) GO TO  360
      THETA = ATAN((R5-R4)/(Z3-X))
      IF (THETA .GT. ALPHA) GO TO 360
      Z2 = Z3 - X
      BETA = ATAN(F2/Z2)
  550 BETA = BETA + PIE/18.0
      IF (BETA .GE. HAPIE) GO TO 480
      Z2 = F2/TAN(BETA)
      Z4 = Z3-X-Z2
      EPSILON = ATAN((R5-R2)/Z4)
      A7 = Z4
      V9 = ABS(SIN(PHI)/SIN(PHI+THETA) - SIN(BETA)/SIN(THETA+BETA))
      W1 = 2.0*KC*SIN(PHI)*SIN(THETA + OMEGA)*TAN(ALPHA/2.0)*HC
      W1 = W1/(SIN(PHI+THETA)*SIN(ALPHA+OMEGA))
      W2 = KC*SIN(PHI)*SIN(ALPHA-THETA)*(R3-R5)/(SIN(PHI+THETA)*
     +       SIN(ALPHA + OMEGA)*SIN(OMEGA))
      W3 = KC * F1*SIN(THETA)/(SIN(PHI)*SIN(THETA+PHI))
      W4 = KM*(R5-R2)*SIN(THETA)*SIN(BETA)/(SIN(EPSILON)**2
     +       *SIN(THETA+BETA))
      W5 = KM*F2*SIN(THETA)/(SIN(THETA+BETA)*SIN(BETA))
      W6 = M1*KC*SIN(PHI)*SIN(THETA+OMEGA)*(RO-R3)/(SIN(PHI+THETA)*
     +      SIN(ALPHA+OMEGA)*SIN(ALPHA))
      W7 = M2*KM*ABS(1.0-SIN(BETA)*SIN(EPSILON-THETA)/(SIN(EPSILON)*
     +      SIN(THETA + BETA)))*A7
      IF (KC .GT. KM) GO TO 740
      W8 = M3 * KC * V9* (R5-R4)/SIN(THETA)
      GO TO 750
  740 W8 = M3 * KM * V9 * (R5-R4)/SIN(THETA)
  750 W = W1+W2+W3+W4+W5+W6+W7+W8
      S1 = W/(F*Y)
      IF (S1 .GT. C1) GO TO 550
  780 C2 = F1
      C3 = F2
      C1 = S1
      GO TO 550
```

```
  100 CONTINUE
      WRITE(2,130)(FRICT(N),N=1,11,2)
  130 FORMAT(/,33X, 6( 'M2 =', F4.2,3X))
      WRITE(2,131)(FRICT(M),(SRATIO(M,N),N=1,11,2),M=1,11,2)
  131 FORMAT( 6(19X, 'M1 =',F4.2,3X, 6F10.4,/))
      WRITE(2,200)((CLAD(M,N), N=1,11,2),M=1,11,2)
  200 FORMAT( 19X, 'CLAD ',/, 6(30X, 6F10.4))
      WRITE(2,201) ((MATRIX(M,N),N=1,11,2), M=1,11,2)
  201 FORMAT( 19X, 'MATRIX ', /, 6(30X, 6F10.4))
      GO TO 80
   50 STOP
      END
      FINISH
```

```
+SSSSSSSSSSSSSSSSSSSSSSSSSSSSSSSSSSSSSSSSSSSSSSSSSSSSSSSSSSSSSSSSSSSSSSSSSSSSSSSSSSSSSSSSSSSSSSSSSSSSSSSSSSSSSSSSSSSSSSS+SSSSSSSSSSSS
+SSSSSSS                                SSSSSSSSSSSSSSSSSSSSSSSSSSSSSSSSSSSSSSSSSSSSSSSSSSSSSSSSSSSSSSSSSSSSSSSSSSSSSSS+SSSSSSSSSSSS
+SSSSSSS     NUMBER OF PAGES    3       SSSSSSSSSSSSSSSSSSSSSSSSSSSSSSSSSSSSSSSSSSSSSSSSSSSSSSSSSSSSSSSSSSSSSSSSSSSSSSS+SSSSSSSSSSSS
+SSSSSSS                                SSSSSSSSSSSSSSSSSSSSSSSSSSSSSSSSSSSSSSSSSSSSSSSSSSSSSSSSSSSSSSSSSSSSSSSSSSSSSSS+SSSSSSSSSSSS
+SSSSSSSSSSSSSSSSSSSSSSSSSSSSSSSSSSSSSSSSSSSSSSSSSSSSSSSSSSSSSSSSSSSSSSSSSSSSSSSSSSSSSSSSSSSSSSSSSSSSSSSSSSSSSSSSSSSSSSS+SSSSSSSSSSSS
```

```
REM  ******** UPPER BOUND SOLUTION FOR BIMETAL TUBE *******
REM  ******** DRAWING ON A FLOATING PLUG             *******
REM
DIM M$[30],Q[7]
REM  READ IN BIMETAL TUBE COMBINATION
READ M$
MAT S=ZER[7,7]
MAT C=ZER[7,7]
MAT L=ZER[7,7]
 REM O1 IS TUBE INITIAL OUTER DIAMETER
 REM I IS INITIAL BORE SIZE
 REM P6 IS PLUG DIAMETER
 REM H5 AND H6 ARE INITAL CLAD AND MATRIX THICKNESSES RESPECTIVELY
 REM Y1 AND Y2 ARE MEAN YIELD STRESSES OF CLAD AND MATRIX RESPECTIVELY
 REM D IS DIE DIAMETER
 READ O1,I,P6,H5,H6,Y1,Y2
 READ D
 P1=3.14159
 REM 'A' IS ANGLE ALPHA IN RADIANS
 REM 'B' IS ANGLE BETA IN RADIANS
 A=15*P1/180
 B=10*P1/180
 H=(O1-I)/2
 F=(D-P6)/2
 R0=O1/2
 R1=I/2
 R2=P6/2
 R3=D/2
 R5=R1+H6
 R7=R0-H5
 E1=H5*(O1-H5)
 E2=H6*(I+H6)
 LET Y=(E1*Y1+E2*Y2)/(E1+E2)
 K=Y/2
 K1=Y1/2
 K2=Y2/2
 A0=2*R3*.17
 A9=2*R2*.2
 R=1-(D^2-P6^2)/(O1^2-I^2)
 Z3=(R0+R5-R3-R7)/TAN(A)+(R0-R7)*TAN(A/2)
 REM O IS ANGLE OMEGA
 O=ATN(ABS(R5-R3)/Z3)
 FOR M=1 TO 11 STEP 2
 M1=(M-1)*.01
 FOR N=1 TO 11 STEP 2
 M2=(N-1)*.01
 C1=C2=C3=1000
 F2=R3-R2-H5*COS(A)-.001
 F2=F2+.001
 F1=F-F2
 IF F2 >= H6 THEN 1070
 R4=R2+F2
```

```
0  E4=LOG((R0-H5/2)/(R3-F1/2))
0  E6=LOG((R5-H6/2)/(R2+F2/2))
0  E7=2*K1*(R3^2-R4^2)*E4
0  E8=2*K2*(R4^2-R2^2)*E6
0  Q=SQR(Z3^2-4*F1*(R5-R4))
0  IF (Z3-Q) <= 0 THEN 620
0  REM TO IS INITIAL VALUE OF ANGLE THETA
0  T0=(Z3-Q)/(2*F1)
0  GOTO 630
0  T0=(Z3+Q)/(2*F1)
0  P=P1/2-ATN(T0)+P1/18
0  P=P-P1/18
0  X=F1/TAN(P)
0  REM T IS ANGLE THETA
0  T=ATN((R5-R4)/(Z3-X))
0  IF T>A THEN 490
0  IF T<B THEN 490
0  Z0=(H6-F2*COS(T))/SIN(T)
0  Z=Z0
0  Z=Z-.0005
0  IF Z <= F2*TAN(B) THEN 640
0  G=ATN(F2/Z)
0  T1=(H6-(F2+X*TAN(B))*COS(T))/SIN(T-B)-X/COS(B)
0  IF T1<0 THEN 720
0  R6=R2+T1*SIN(B)
0  REM E IS ANGLE EPSILON
0  E=B+ATN((R4-R6)/(T1*COS(B)+Z))
0  V9=ABS(SIN(P)/SIN(P+T)-SIN(G)*SIN(E)/(SIN(B+G)*SIN(T-B+E)))
0  W1=2*K1*(R3^2-R4^2)*TAN(A/2)
0  W2=2*K1*R3*ABS(R5-R3)*SIN(P)*SIN(A-T)
0  IF R5>R3 THEN 860
0  W2=W2/(SIN(A+0)*SIN(T+P)*SIN(0))
0  GOTO 870
0  W2=W2/(SIN(A-0)*SIN(T+P)*SIN(0))
0  W3=K1*(R3^2-R4^2)*SIN(T)/(SIN(P)*SIN(T+P))
0  W4=2*K2*(R4^2-R2^2)*TAN(T/2)
0  W5=2*K2*R4*(R4-R6)*SIN(G)*SIN(T-B)/(SIN(G+B)*SIN(E-B)*SIN(T-B+E))
0  W6=K2*(R4^2-R2^2)*SIN(B)/(SIN(G)*SIN(B+G))
0  W7=2*M1*K1*R0*(R0-R3)*(R3^2-R4^2)/((R0^2-R7^2)*SIN(A))
0  M3=.02
0  IF K2<K1 THEN 960
0  W8=2*M3*K1*V9*R4*(R5-R4)/SIN(T)
0  GOTO 970
0  W8=2*M3*K2*V9*R4*(R5-R4)/SIN(T)
0  W9=2*M2*K2*SIN(G)*R2*(R6-R2)/(SIN(G+B)*SIN(B))
0  L9=M1*K1*A0+M2*K2*A9
0  W=W1+W2+W3+W4+W5+W6+W7+W8+W9+L9+E7+E8
00  S1=W/((R3^2-R2^2)*Y)
10  IF S1<0 THEN 1480
20  IF S1>C1 THEN 720
30  C1=S1
40  C2=F1
50  C3=F2
60  GOTO 720
```

```
70  S[M,N]=C1
80  C[M,N]=C2
90  L[M,N]=C3
00  Q[N]=M2
10  PRINT C1,C2,C3
20  REM THE PREVIOUS STATEMENT IS FOR CHECKING PROGRESS IN THE CALCULATIO
30  NEXT N
40  NEXT M
50  PRINT
60  PRINT M$,"       DIE=";D;"REDUCTION=";R
70  PRINT
80  PRINT " YC =";Y1;"YM =";Y2;"    YE =";Y
90  PRINT
00  PRINT " OD=";O1;"    BORE=";I;"    HC=";H5;"    HM=";H6
10  PRINT
20  PRINT "  SIGMA/YE "
30  PRINT "  ========= "
40  PRINT " M2 =",
50  FOR M=1 TO 7 STEP 2
60  PRINT Q[M],
70  NEXT M
80  FOR M=1 TO 7 STEP 2
90  PRINT '9'9'9'9'9;
00  PRINT S[M,1],S[M,3],S[M,5],S[M,7]
10  PRINT
20  NEXT M
30  PRINT "   CLAD"
40  PRINT "   ===="
50  FOR M=1 TO 7 STEP 2
60  PRINT '9'9'9'9'9;
70  PRINT C[M,1],C[M,3],C[M,5],C[M,7]
80  PRINT
90  NEXT M
00  PRINT "  MATRIX  "
10  PRINT "  ======  "
20  FOR M=1 TO 7 STEP 2
30  PRINT '9'9'9'9'9;
40  PRINT L[M,1],L[M,3],L[M,5],L[M,7]
50  PRINT
60  NEXT M
70  GOTO 170
80  PRINT "S1 IS NEGATIVE";S1
90  REM SAMPLE DATA
00  DATA "STAINLESS STEEL ON BRASS"
10  DATA .5,.426,.341,.0132,.0238,79,44.8
20  DATA .404
30  END
```

BIMETAL TUBE MANDREL DRAWING		Table No: M1		
Tube No:		1	130	133
Materials	Clad	Stainless steel	Stainless steel	Stainless steel
	Matrix	Mild steel	Mild steel	Mild steel
Mean Yield Stress (tonf.in^{-2})	Clad	79.0	78.8	79.1
	Matrix	42.5	42.8	42.2
Initial Diameter (in)	Outer	0.4696	0.4696	0.475
	Bore	0.417	0.4167	0.412
Final Diameter (in)	Outer	0.46	0.46	0.46
	Bore	0.412	0.412	0.412
Clad Thickness (in)	Initial (H_c)	0.0131	0.0125	0.015
	Final (Exp) (h_c)	0.0125	0.0116	0.0125
	Theory (h_c)	0.0119	0.0118	0.0128
	% Error in h_c	4.8	1.7	2.4
Matrix Thickness (in)	Initial (H_m)	0.0128	0.0126	0.0161
	Final (Exp) (h_m)	0.0115	0.0121	0.0125
	Theory (h_m)	0.0121	0.0122	0.0112
	% Error in h_m	5.2	0.8	10.4
Reduction in Area (%)		8.86	3.22	24.1
Exp. Draw Load (tonf)	Static	0.36	0.22	0.753
	with Die Rotation	0.32	0.19	0.672
Axial Load "S" (tonf)		0.33	0.2	0.69
Equivalent Yield Stress		61.5	61.3	60.7
Coefficient of Friction	tube/die interface (μ_s)	0.08	0.08	0.08
	tube/mandrel interface (μ_m)	0.02	0.02	0.02

BIMETAL TUBE MANDREL DRAWING				Table No: M2
Tube No:		7	27	101
Materials	Clad	Stainless steel	Stainless steel	Stainless steel
	Matrix	Copper	Copper	Copper
Mean Yield Stress (tonf.in^{-2})	Clad	79.4	78.8	79.2
	Matrix	34.0	34.2	33.8
Initial Diameter (in)	Outer	0.486	0.486	0.4815
	Bore	0.415	0.413	0.415
Final Diameter (in)	Outer	0.46	0.4696	0.461
	Bore	0.412	0.412	0.412
Clad Thickness (in)	Initial (H_c)	0.0123	0.0118	0.0132
	Final (Exp) (h_c)	0.0091	0.0113	0.0102
	Theory (h_c)	0.0091	0.0107	0.0110
	% Error in h_c	0	5.3	7.8
Matrix Thickness (in)	Initial (H_m)	0.0208	0.0185	0.02
	Final (Exp) (h_m)	0.0142	0.0175	0.0145
	Theory (h_m)	0.0149	0.0181	0.0135
	% Error in h_m	4.9	3.4	6.9
Reduction in Area (%)		29.7	6.5	28.1
Exp. Draw Load (tonf)	Static	0.84	0.248	0.83
	with Die Rotation	0.75	0.22	0.75
Axial Load "S" (tonf)		0.7	0.2	0.68
Equivalent Yield Stress		51.8	52.6	52.7
Coefficient of Friction	tube/die interface (μ_s)	0.08	0.08	0.07
	tube/mandrel interface (μ_m)	0.04	0.04	0.04

BIMETAL TUBE MANDREL DRAWING				Table No: M3
Tube No:		102	104	105
Materials	Clad	Stainless steel	Stainless steel	Stainless steel
	Matrix	Brass	Brass	Brass
Mean Yield Stress (tonf.in^{-2})	Clad	78.0	79.0	78.4
	Matrix	43.8	44.8	44.2
Initial Diameter (in)	Outer	0.487	0.484	0.489
	Bore	0.42	0.41	0.417
Final Diameter (in)	Outer	0.467	0.46	0.46
	Bore	0.412	0.399	0.412
Clad Thickness (in)	Initial (H_c)	0.0117	0.0125	0.012
	Final (Exp) (h_c)	0.0099	0.0112	0.0089
	Theory (h_c)	0.0106	0.0113	0.0089
	% Error in h_c	7.1	0.9	0.0
Matrix Thickness (in)	Initial (H_m)	0.0215	0.023	0.0227
	Final (Exp) (h_m)	0.0175	0.0193	0.0152
	Theory (h_m)	0.0169	0.0192	0.0151
	% Error in h_m	3.4	0.5	0.6
Reduction in Area (%)		19.7	17.4	33.4
Exp. Draw Load (tonf)	Static	0.655	0.535	1.02
	with Die Rotation	0.6	0.485	0.93
Axial Load "S" (tonf)		0.59	0.488	0.93
Equivalent Yield Stress		56.7	57.5	57.0
Coefficient of Friction	tube/die interface (μ_s)	0.05	0.06	0.06
	tube/mandrel interface (μ_m)	0.02	0.02	0.02

BIMETAL TUBE MANDREL DRAWING				Table No: M4
Tube No:		106	9	10
Materials	Clad	Stainless steel	Mild steel	Mild steel
	Matrix	Brass	Copper	Copper
Mean Yield Stress (tonf.in^{-2})	Clad	78.7	42.5	42.1
	Matrix	44.0	43.0	34.4
Initial Diameter (in)	Outer	0.489	0.4815	0.4815
	Bore	0.42	0.4173	0.415
Final Diameter (in)	Outer	0.46	0.46	0.4716
	Bore	0.412	0.412	0.412
Clad Thickness (in)	Initial (H_c)	0.0121	0.012	0.0122
	Final (Exp) (h_c)	0.0088	0.0085	0.0115
	Theory (h_c)	0.009	0.0089	0.009
	% Error in h_c	2.3	4.7	21.7
Matrix Thickness (in)	Initial (H_m)	0.0224	0.0198	0.021
	Final (Exp) (h_m)	0.015	0.0153	0.0182
	Theory (h_m)	0.015	0.0151	0.0208
	% Error in h_m	0	1.3	14.3
Reduction in Area (%)		33.3	26.3	11.5
Exp. Draw Load (tonf)	Static	0.98	0.518	0.295
	with Die Rotation	0.89	0.484	0.274
Axial Load "S" (tonf)		0.879	0.46	0.264
Equivalent Yield Stress		56.8	37.4	37.4
Coefficient of Friction	tube/die interface (μ_s)	0.06	0.04	0.04
	tube/mandrel interface (μ_m)	0.02	0.02	0.02

BIMETAL TUBE MANDREL DRAWING				Table No: M5
Tube No:		13	14	127
Materials	Clad	Mild steel	Mild steel	Mild steel
	Matrix	Brass	Brass	Brass
Mean Yield Stress ($tonf.in^{-2}$)	Clad	42.5	42.5	42.8
	Matrix	43.8	44.8	44.9
Initial Diameter (in)	Outer	0.488	0.484	0.504
	Bore	0.416	0.416	0.419
Final Diameter (in)	Outer	0.469	0.46	0.461
	Bore	0.412	0.412	0.412
Clad Thickness (in)	Initial (H_c)	0.012	0.0118	0.0123
	Final (Exp) (h_c)	0.0089	0.0082	0.0088
	Theory (h_c)	0.0089	0.0087	0.0101
	% Error in h_c	0	6.1	14.8
Matrix Thickness (in)	Initial (H_m)	0.024	0.0225	0.0239
	Final (Exp) (h_m)	0.0195	0.0158	0.0155
	Theory (h_m)	0.0196	0.0153	0.0144
	% Error in h_m	0.5	3.2	7.1
Reduction in Area (%)		22.8	32.2	35.7
Exp. Draw Load (tonf)	Static	0.51	0.651	0.714
	with Die Rotation	0.488	0.63	0.685
Axial Load "S" (tonf)		0.45	0.57	0.635
Equivalent Yield Stress		43.3	44.0	44.1
Coefficient of Friction	tube/die interface (μ_s)	0.02	0.02	0.02
	tube/mandrel interface (μ_m)	0.02	0.02	0.02

BIMETAL TUBE MANDREL DRAWING				Table No: M6
Tube No:		30	123	124
Materials	Clad	Copper	Brass	Brass
	Matrix	Stainless steel	Copper	Copper
Mean Yield Stress (tonf.in^{-2})	Clad	34.2	46.0	44.8
	Matrix	78.6	34.0	34.8
Initial Diameter (in)	Outer	0.486	0.5	0.5
	Bore	0.42	0.410	0.410
Final Diameter (in)	Outer	0.4696	0.4815	0.4716
	Bore	0.412	0.400	0.399
Clad Thickness (in)	Initial (H_c)	0.0209	0.0223	0.0223
	Final (Exp) (h_c)	0.0171	0.0213	0.0196
	Theory (h_c)	0.0176	0.0220	0.0200
	% Error in h_c	2.9	3.2	2.04
Matrix Thickness (in)	Initial (H_m)	0.0121	0.020	0.0178
	Final (Exp) (h_m)	0.0117	0.0194	0.0167
	Theory (h_m)	0.0112	0.0187	0.0163
	% Error in h_m	4.3	3.6	2.4
Reduction in Area (%)		15.1	6.71	13.5
Exp. Draw Load (tonf)	Static	0.32	0.135	0.28
	with Die Rotation	0.31	0.129	0.269
Axial Load "S" (tonf)		0.26	0.124	0.25
Equivalent Yield Stress		49.7	40.6	40.6
Coefficient of Friction	tube/die interface (μ_s)	0.02	0.02	0.02
	tube/mandrel interface (μ_m)	0.03	0.01	0.02

BIMETAL TUBE MANDREL DRAWING				Table No: M7
Tube No:		114	115	117
Materials	Clad	Copper	Copper	Copper
	Matrix	Stainless steel	Stainless Steel	Stainless Steel
Mean Yield Stress (tonf.in^{-2})	Clad	34.0	33.2	34.4
	Matrix	79.0	78.4	78.6
Initial Diameter (in)	Outer	0.486	0.475	0.489
	Bore	0.418	0.407	0.422
Final Diameter (in)	Outer	0.462	0.461	0.461
	Bore	0.412	0.399	0.411
Clad Thickness (in)	Initial (H_c)	0.021	0.0208	0.0206
	Final (Exp) (h_c)	0.0146	0.018	0.0143
	Theory (h_c)	0.0127	0.0185	0.0123
	% Error in h_c	13.0	2.8	14
Matrix Thickness (in)	Initial (H_m)	0.0129	0.0132	0.0129
	Final (Exp) (h_m)	0.0103	0.0130	0.0108
	Theory (h_m)	0.0123	0.0125	0.0127
	% Error in h_m	19.4	3.8	17.6
Reduction in Area (%)		28.7	11.1	28.6
Exp. Draw Load (tonf)	Static	0.625	0.25	0.63
	with Die Rotation	0.6	0.23	0.605
Axial Load "S" (tonf)		0.528	0.215	0.55
Equivalent Yield Stress		50.3	50.0	50.7
Coefficient of Friction	tube/die interface (μ_s)	0.02	0.02	0.02
	tube/mandrel interface (μ_m)	0.03	0.03	0.03

BIMETAL TUBE MANDREL DRAWING				Table No: M8
Tube No:		18	119	121
Materials	Clad	Copper	Copper	Copper
	Matrix	Mild steel	Mild steel	Mild steel
Mean Yield Stress (tonf.in^{-2})	Clad	33.9	34.1	34.5
	Matrix	42.8	42.5	41.8
Initial Diameter (in)	Outer	0.484	0.4975	0.4975
	Bore	0.419	0.429	0.426
Final Diameter (in)	Outer	0.46	0.4778	0.461
	Bore	0.412	0.412	0.412
Clad Thickness (in)	Initial (H_c)	0.019	0.0212	0.0217
	Final (Exp) (h_c)	0.0143	0.0201	0.0147
	Theory (h_c)	0.0138	0.02	0.0144
	% Error in h_c	3.5	0.5	2.0
Matrix Thickness (in)	Initial (H_m)	0.0125	0.013	0.0129
	Final (Exp) (h_m)	0.0097	0.0128	0.0098
	Theory (h_m)	0.0102	0.0129	0.0101
	% Error in h_m	5.2	0.8	3.1
Reduction in Area (%)		26.5	7.5	33.1
Exp. Draw Load (tonf)	Static	0.453	0.15	0.57
	with Die Rotation	0.436	0.145	0.54
Axial Load "S" (tonf)		0.405	0.13	0.51
Equivalent Yield Stress		37.3	37.1	37.1
Coefficient of Friction	tube/die interface (μ_s)	0.02	0.02	0.02
	tube/mandrel interface (μ_m)	0.03	0.03	0.02

BIMETAL TUBE MANDREL DRAWING			Table No: M9	
Tube No:		109	110	118
Materials	Clad	Copper	Copper	Copper
	Matrix	Brass	Brass	Brass
Mean Yield Stress (tonf.in^{-2})	Clad	34.3	34.0	34.4
	Matrix	44.7	44.6	44.9
Initial Diameter (in)	Outer	0.475	0.4815	0.4716
	Bore	0.405	0.413	0.407
Final Diameter (in)	Outer	0.461	0.461	0.447
	Bore	0.399	0.399	0.399
Clad Thickness (in)	Initial (H_c)	0.015	0.0156	0.0145
	Final (Exp) (h_c)	0.0142	0.0148	0.0112
	Theory (h_c)	0.0148	0.0134	0.0123
	% Error in h_c	4.2	9.5	9.8
Matrix Thickness (in)	Initial (H_m)	0.0179	0.0178	0.0157
	Final (Exp) (h_m)	0.0168	0.0162	0.0127
	Theory (h_m)	0.0162	0.0176	0.0117
	% Error in h_m	3.6	8.6	7.9
Reduction in Area (%)		7.9	10.8	23.5
Exp. Draw Load (tonf)	Static	0.13	0.2	0.37
	with Die Rotation	0.125	0.19	0.357
Axial Load "S" (tonf)		0.116	0.179	0.333
Equivalent Yield Stress		40.0	39.5	40.0
Coefficient of Friction	tube/die interface (μ_s)	0.02	0.03	0.02
	tube/mandrel interface (μ_m)	0.02	0.02	0.02

BIMETAL TUBE MANDREL DRAWING				Table No: M10
Tube No:		21	29	23
Materials	Clad	Brass	Brass	Brass
	Matrix	Stainless steel	Stainless steel	Mild steel
Mean Yield Stress (tonf.in^{-2})	Clad	44.4	44.0	43.6
	Matrix	79.2	78.8	41.8
Initial Diameter (in)	Outer	0.492	0.4975	0.492
	Bore	0.422	0.42	0.416
Final Diameter (in)	Outer	0.462	0.4716	0.4716
	Bore	0.412	0.412	0.413
Clad Thickness (in)	Initial (H_c)	0.0224	0.0215	0.021
	Final (Exp) (h_c)	0.0155	0.0189	0.0188
	Theory (h_c)	0.0141	0.0192	0.0167
	% Error in h_c	9.0	1.6	11.2
Matrix Thickness (in)	Initial (H_m)	0.0126	0.0125	0.013
	Final (Exp) (h_m)	0.0095	0.0119	0.0106
	Theory (h_m)	0.0109	0.0116	0.0126
	% Error in h_m	14.7	2.5	18.9
Reduction in Area (%)		31.7	13.2	16.2
Exp. Draw Load (tonf)	Static	0.855	0.35	0.355
	with Die Rotation	0.82	0.338	0.34
Axial Load "S" (tonf)		0.705	0.295	0.28
Equivalent Yield Stress		56.3	56.0	43.0
Coefficient of Friction	tube/die interface (μ_s)	0.02	0.02	0.02
	tube/mandrel interface (μ_m)	0.03	0.03	0.04

BIMETAL TUBE MANDREL DRAWING			Table No: M11	
Tube No:		24	125	122
Materials	Clad	Brass	Brass	Brass
	Matrix	Mild steel	Mild steel	Copper
Mean Yield Stress ($tonf.in^{-2}$)	Clad	44.8	44.5	45.0
	Matrix	43.0	42.5	34.8
Initial Diameter (in)	Outer	0.489	0.489	0.4975
	Bore	0.415	0.415	0.405
Final Diameter (in)	Outer	0.46	0.4716	0.461
	Bore	0.412	0.412	0.399
Clad Thickness (in)	Initial (H_c)	0.0239	0.0223	0.0215
	Final (Exp) (h_c)	0.0145	0.0190	0.0165
	Theory (h_c)	0.0144	0.019	0.0170
	% Error in h_c	6.9	0	3.03
Matrix Thickness (in)	Initial (H_m)	0.0131	0.0133	0.02
	Final (Exp) (h_m)	0.0095	0.0108	0.0145
	Theory (h_m)	0.0096	0.0108	0.0140
	% Error in h_m	1.05	0	3.4
Reduction in Area (%)		37.43	18.25	28.85
Exp. Draw Load (tonf)	Static	0.83	0.43	0.6
	with Die Rotation	0.796	0.414	0.58
Axial Load "S" (tonf)		0.66	0.336	0.56
Equivalent Yield Stress		44.2	43.8	40.4
Coefficient of Friction	tube/die interface (μ_s)	0.02	0.02	0.02
	tube/mandrel interface (μ_m)	0.04	0.04	0.01

BIMETAL TUBE DRAWING ON A FLOATING PLUG						Table No: F1	
Tube No:		F2	F5	F43	F15	F31	F21
Materials	Clad	Stainless steel	Stainless steel	Stainless steel.	Brass	Brass	Aluminium
	Matrix	Mild steel	Mild steel	Mild steel	Stainless steel	Stainless steel	Stainless steel
Mean Yield Stress	Clad (tonf.in^{-2})	76.2	76.4	76	76.19	76.19	11.02
	Matrix (tonf.in^{-2})	46.2	46	46	42.5	42.35	72.9
Initial Diameter (in)	Outer	0.5	0.501	0.5	0.5	0.5	0.5
	Bore	0.435	0.435	0.428	0.426	0.428	0.426
Final Diameter (in)	Outer	0.4	0.392	0.396	0.406	0.400	0.406
	Bore	0.341	0.341	0.341	0.341	0.341	0.341
Clad Thickness (in)	Initial (H_c)	0.0150	0.0144	0.015	0.0215	0.205	0.218
	Final (Exp) (h_c)	0.0145	0.0130	0.0138	0.0184	0.0165	0.0183
	Theory (h_c)	0.0145	0.0139	0.0145	0.0196	0.0198	0.0200
	% Error in h_c	0	6.9	5.1	6.5	7.9	9.3
Matrix Thickness (in)	Initial (H_m)	0.016	0.0125	0.016	0.0155	0.0157	0.0152
	Final (Exp) (h_m)	0.015	0.0110	0.014	0.0141	0.0130	0.0142
	Theory (h_m)	0.014	0.0116	0.013	0.0127	0.0117	0.0124
	% Error in h_m	6.7	5.5	7.1	9.9	10	12.6
Reduction in Area (%)		24.6	39.5	29.5	29.1	34.9	29.1
Exp. Draw Load (tonf)		0.935	1.325	1.2	1.397	1.46	0.95

BIMETAL TUBE DRAWING ON A FLOATING PLUG						Table No: F2	
Tube No:		F34	F44	F45	F16	F18	F19
Materials	Clad	Aluminium	Aluminium	Aluminium	Aluminium	Aluminium	Aluminium
	Matrix	Stainless Steel	Stainless Steel	Stainless Steel	Mild steel	Mild steel	Mild steel
Mean Yield Stress	Clad (tonf.in^{-2})	11.09	11.05	11.02	11.00	11.02	11.1
	Matrix (tonf.in^{-2})	76.2	76.19	76.11	46.2	46.02	46.0
Initial Diameter (in)	Outer	0.5	0.5	0.5	0.5	0.5	0.5
	Bore	0.428	0.428	0.428	0.426	0.426	0.426
Final Diameter (in)	Outer	0.396	0.400	0.392	0.406	0.400	0.400
	Bore	0.341	0.341	0.341	0.341	0.341	0.341
Clad Thickness (in)	Initial (H_c)	0.021	0.0205	0.0203	0.0212	0.0223	0.023
	Final (Exp) (h_c)	0.0145	0.0163	0.017	0.017	0.0171	0.0182
	Theory (h_c)	0.0163	0.0178	0.0186	0.0194	0.0174	0.0192
	% Error in h_c	12.4	9.2	9.4	14.1	1.8	5.5
Matrix Thickness (in)	Initial (H_m)	0.0152	0.0152	0.0157	0.0157	0.0147	0.0140
	Final (Exp) (h_m)	0.0132	0.0131	0.0154	0.0155	0.0124	0.0113
	Theory (h_m)	0.0122	0.0117	0.0139	0.0130	0.0121	0.0103
	% Error in h_m	7.6	10.9	9.7	16.1	2.4	8.8
Reduction in Area (%)		39.7	34.0	26.3	28.9	36.2	36.2
Exp. Draw Load (tonf)		1.025	1.075	0.91	0.635	.675	.66

BIMETAL TUBE DRAWING ON A FLOATING PLUG						Table No: F3	
Tube No:		F46	F26	F40	F28	F7	F9
Materials	Clad	Aluminium	Stainless steel	Stainless steel	Stainless steel	Mild steel	Mild steel
	Matrix	Mild steel	Brass	Brass	Brass	Stainless steel	Stainless steel
Mean Yield Stress	Clad (tonf.in^{-2})	11.2	76.25	76.19	76.1	46.0	45.8
	Matrix (tonf.in^{-2})	46.1	42.4	42.35	43.09	76.19	76.17
Initial Diameter (in)	Outer	0.5	0.5	0.5	0.5	0.5	0.5
	Bore	0.427	0.426	0.426	0.426	0.435	0.435
Final Diameter (in)	Outer	0.404	0.396	0.4	0.404	0.396	0.4
	Bore	0.341	0.341	0.341	0.341	0.341	0.3416
Clad Thickness (in)	Initial (H_c)	0.0205	0.0152	0.0158	0.015	0.0151	0.0153
	Final (Exp) (h_c)	0.0180	0.0122	0.0142	0.0146	0.0135	0.0146
	Theory (h_c)	0.0188	0.0117	0.0153	0.0145	0.0146	0.0148
	% Error in h_c	4.4	4.1	7.7	0.7	8.1	1.4
Matrix Thickness (in)	Initial (H_m)	0.0158	0.0201	0.0170	0.0198	0.0152	0.0153
	Final (Exp) (h_m)	0.0135	0.0153	0.0151	0.0168	0.014	0.0149
	Theory (h_m)	0.0127	0.0158	0.0142	0.0170	0.0129	0.0147
	% Error in h_m	5.9	3.3	6.0	1.2	7.9	1.3
Reduction in Area (%)		30.3	38.0	28.0	29.1	28.5	22.6
Exp. Draw Load (tonf)		0.672	1.32	1.01	0.98	1.35	1.125

BIMETAL TUBE DRAWING ON A FLOATING PLUG						Table No: F4	
Tube No:		F10					
Materials	Clad	Mild steel					
	Matrix	Stainless steel					
Mean Yield Stress	Clad (tonf.in^{-2})	46.2					
	Matrix (tonf.in^{-2})	76.25					
Initial Diameter (in)	Outer	0.5					
	Bore	0.436					
Final Diameter (in)	Outer	0.392					
	Bore	0.341					
Clad Thickness (in)	Initial (H_c)	0.015					
	Final (Exp) (h_c)	0.0125					
	Theory (h_c)	0.0125					
	% Error in h_c	0					
Matrix Thickness (in)	Initial (H_m)	0.0153					
	Final (Exp) (h_m)	0.0130					
	Theory (h_m)	0.0130					
	% Error in h_m	0					
Reduction in Area (%)		34.1					
Exp. Draw Load (tonf)		1.43					

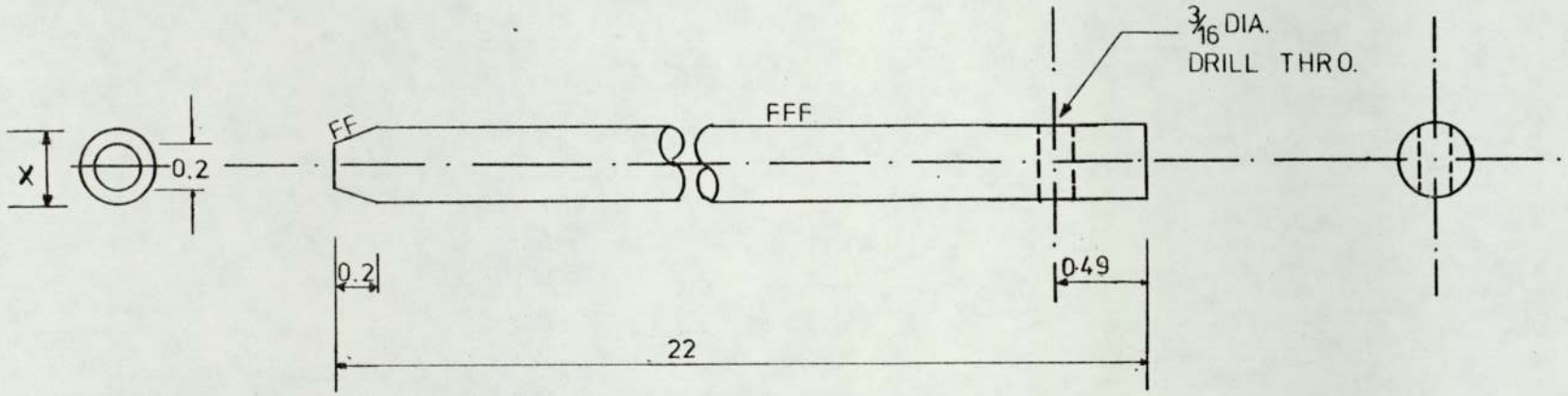

HEAT TREATMENT: HARDENING, HEAT TO 830°C AND QUENCH IN OIL.
TEMPER AT 200°C FOR HIGH YIELD STRESS
EXCEEDING 100 TONF IN^{-2}

ITEM NO.	DIMENSION X
1	0.400 $^{-0.0016}_{-0.0020}$
2	0.41 $^{-0.0016}_{-0.0020}$

TOLERANCE ON MACHINING DIMENSIONS ±0.01" UNLESS OTHERWISE STATED

LIMITS ON HOLES AND SHAFTS TO B.S. 308:1916

F =ROUGH M/C
FF =FINISH M/C
FFF =GRIND OR EQUIVALENT

THIRD ANGLE PROJECTION

UNIVERSITY OF ASTON IN BIRMINGHAM

DEPT. OF PRODUCTION ENGINEERING

DESCRIPTION

MANDREL

ALL DIMENSIONS IN INCHES EXCEPT WHERE OTHERWISE STATED

SCALE			
FULL SIZE	DESIGNED	20.10.76	S. K. LOKE
	DRAWN	20.10.76	S. K. LOKE
	APPROVED		

MATERIAL EN 26

DRG. NO: MT-001

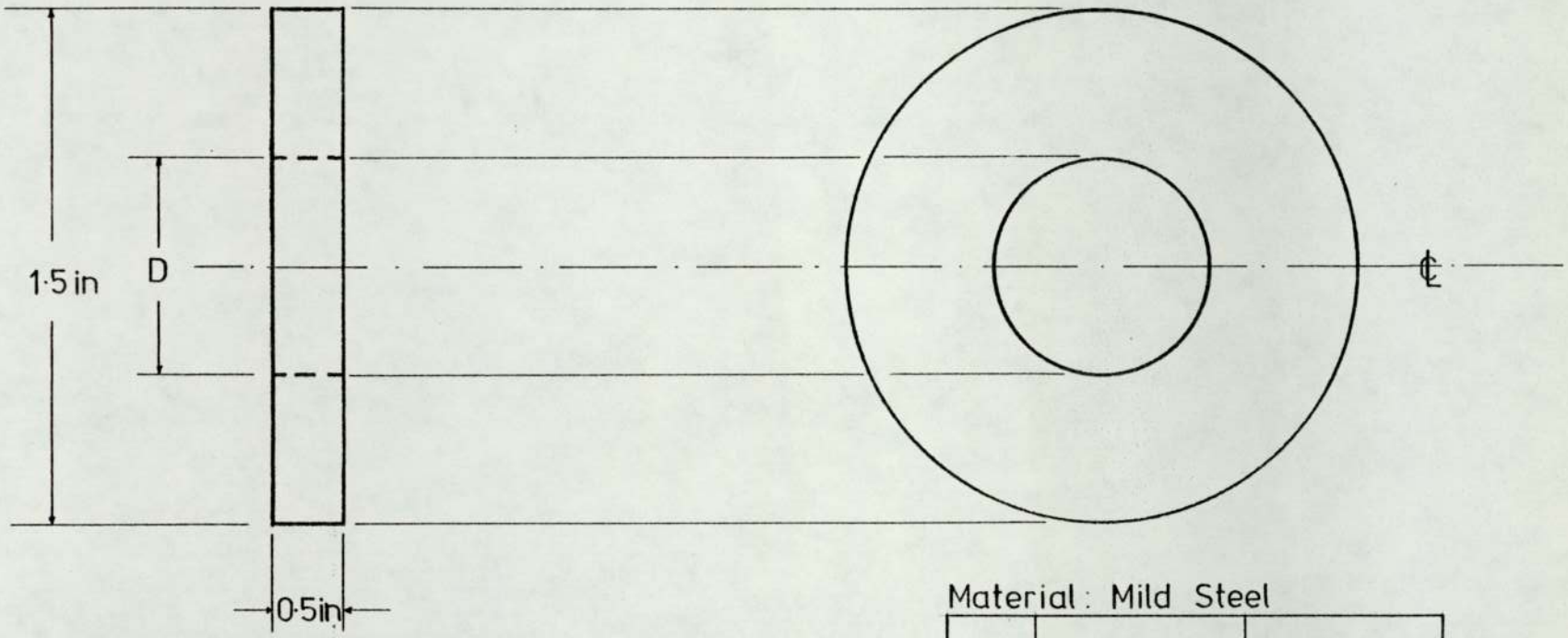

Material : Mild Steel

No.	QUANTITY	Size of 'D'
1	1	0·420 in.
2	1	0·410 in.

Drawing No: MT002 BLANK USED FOR REMOVING MANDREL FROM BIMETAL TUBE

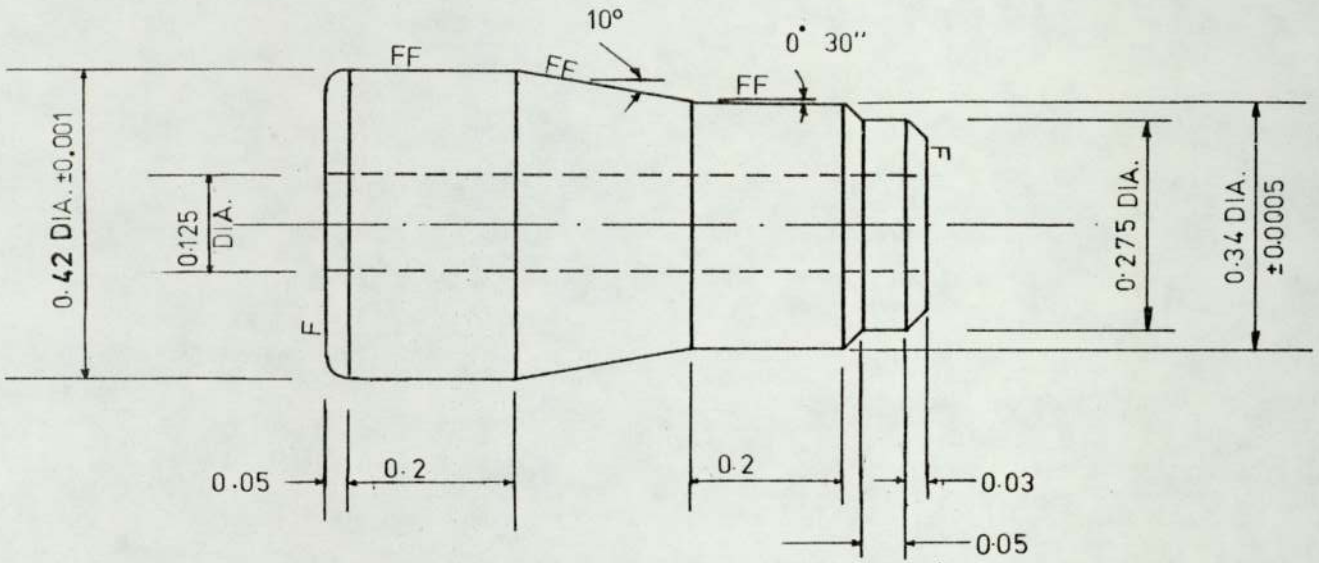

TOLERANCE ON MACHINING DIMENSIONS ±0,01 UNLESS OTHERWISE STATED

LIMITS ON HOLES TO B.S. 308:1916

F = FINISH MACHINING
FF = GROUND OR EQUIVALENT

UNIVERSITY OF ASTON IN BIRMINGHAM DEPT. OF PRODUCTION ENGINEERING	DESCRIPTION FLOATING PLUG	ALL DIMENSIONS IN INCHES EXCEPT WHERE OTHERWISE STATED			MATERIAL: TUNGSTEN CARBIDE
		SCALE: FOUR TIMES FULL SIZE	DESIGNED 9.5.77	S.K, LOKE	FT-001
			DRAWN 9.5.77	S.K. LOKE	
			APPROVED		

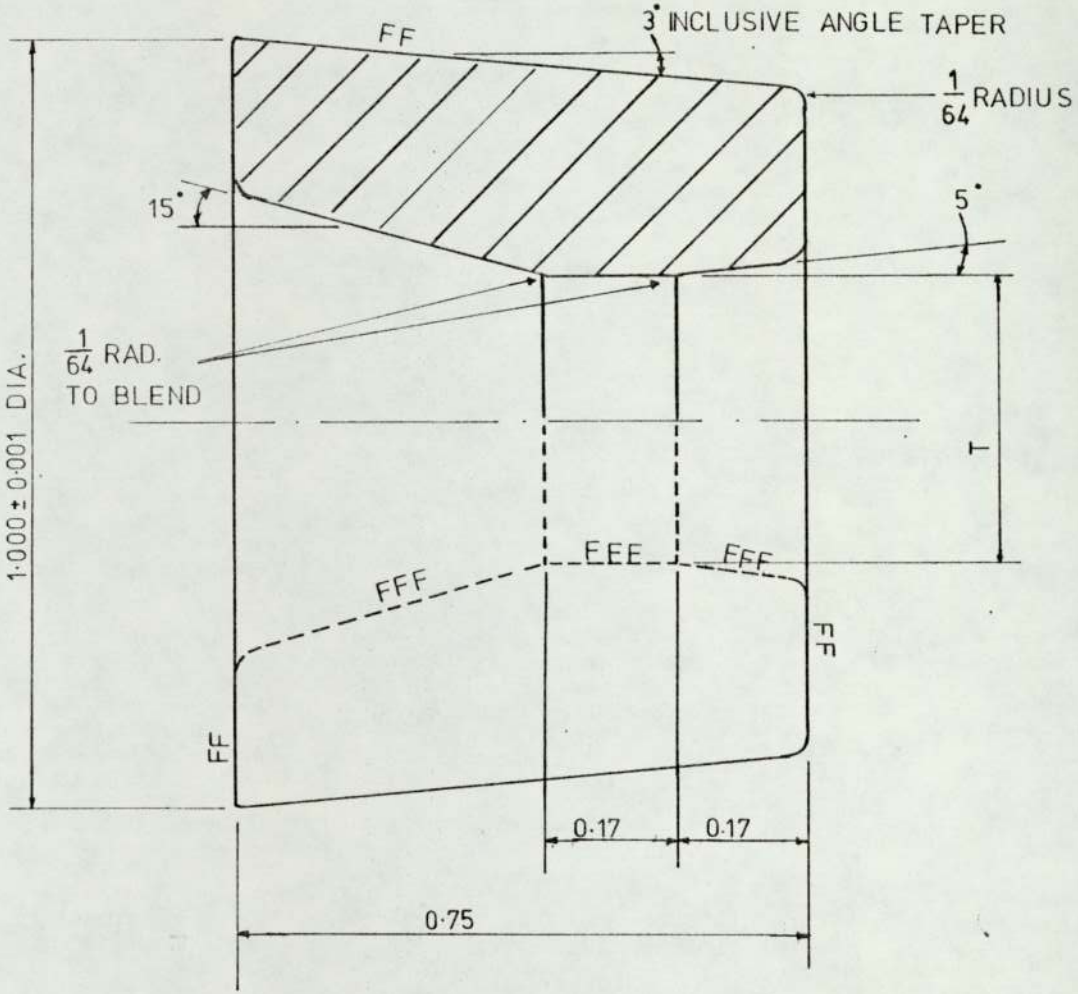

TOLERANCE ON MACHINING DIMENSIONS 0·01 IN. UNLESS OTHERWISE STATED

FF= FINISH MACHINING
FFF=GROUND OR EQUIVALENT

QUANTITY: ONE OFF OF EACH

DIE NO.	DIMENSION T ± 0·0002 DIA.
1	0·406
2	0·404
3	0·400
4	0·396
5	0·392
6	0·388

UNIVERSITY OF ASTON IN BIRMINGHAM

DEPT. OF PRODUCTION ENGINEERING

DESCRIPTION

15° DIE FOR FLOATING PLUG

ALL DIMENSIONS IN INCHES EXCEPT WHERE OTHERWISE STATED

SCALE : FOUR TIMES FULL SIZE			
	DESIGNED	9.5.77	S. K. LOKE
	DRAWN	9.5.77	S. K. LOKE
	APPROVED		

MATERIAL: TUNGSTEN CARBIDE

DRG. NO. FT-002

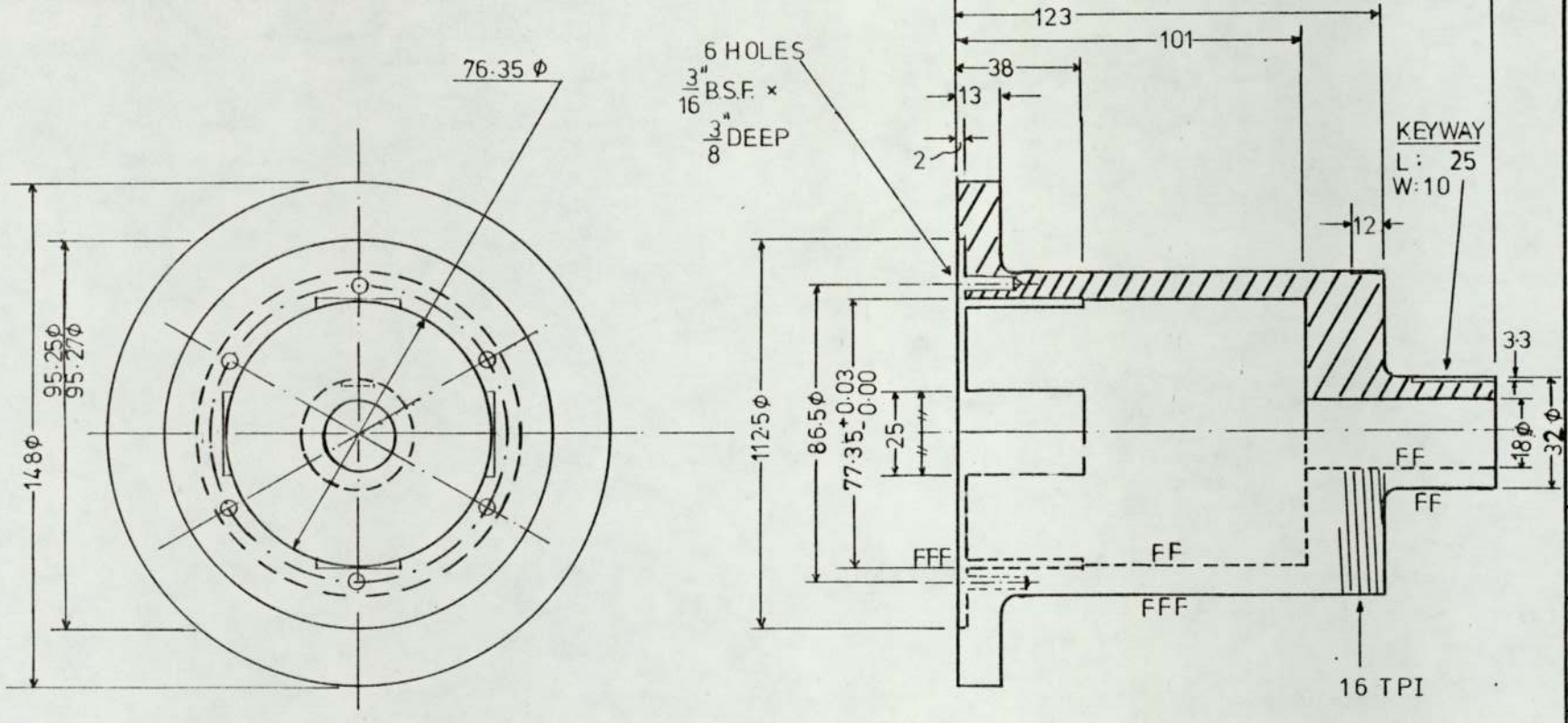

LIMITS ON HOLES AND SHAFTS TO B.S. 4500:1969

F = ROUGH MACHINING
FF=FINISH MACHINING
FFF=GROUND OR EQUIVALENT

TOLERANCE ON MACHINING DIMENSIONS ± 0·3mm UNLESS OTHERWISE STATED

THIRD ANGLE PROJECTION

UNIVERSITY OF ASTON IN BIRMINGHAM DEPT. OF PRODUCTION ENGINEERING	DESCRIPTION DIE HOUSING FOR DIE ROTATION UNIT	ALL DIMENSIONS IN mm EXCEPT WHERE OTHERWISE STATED			MATERIAL MILD STEEL
		SCALE	20.11.76	DESIGNED S.K. LOKE	
		HALF SIZE	20.11.76	DRAWN S.K. LOKE	MD-2

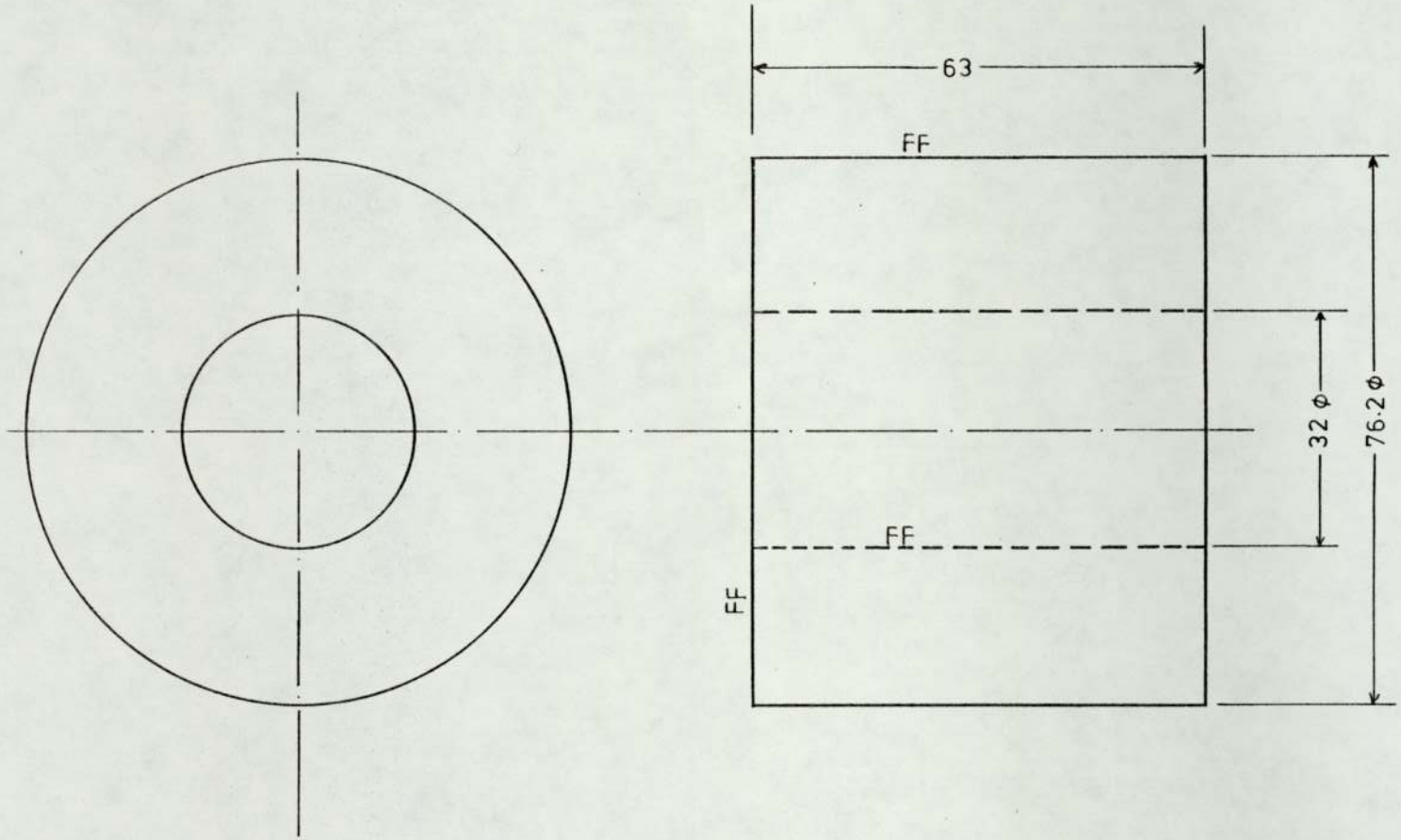

FF=FINISH MACHINING

TOLERANCE ON MACHINING DIMENSIONS ±0·3mm UNLESS OTHERWISE STATED

THIRD ANGLE PROJECTION

UNIVERSITY OF ASTON IN BIRMINGHAM DEPT. PRODUCTION ENGINEERING	DESCRIPTION: DIE SPACER	ALL DIMENSIONS IN mm EXCEPT WHERE OTHERWISE STATED SCALE: FULL SIZE	DESIGNED	20.11.76	S. K.LOKE
			DRAWN	20.11.76	S. K. LOKE
			APPROVED		
		MATERIAL: MILD STEEL DRG. NO: MD-3			

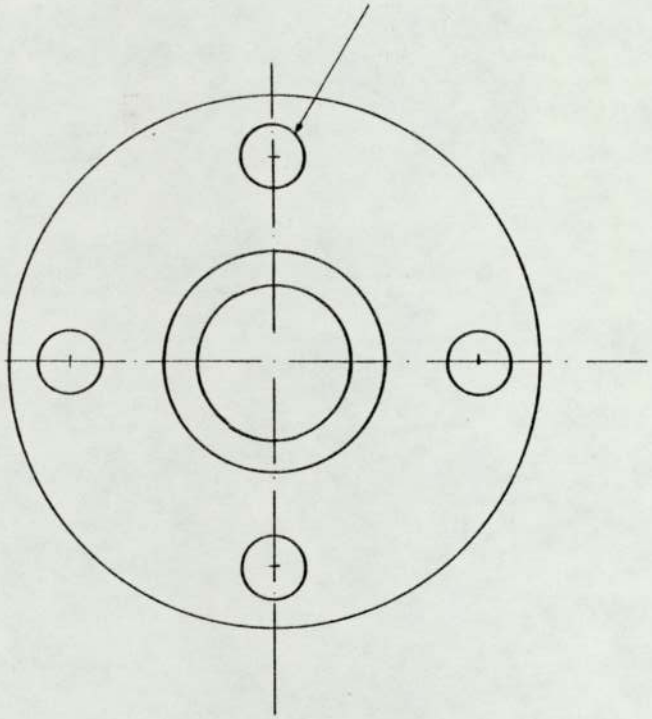

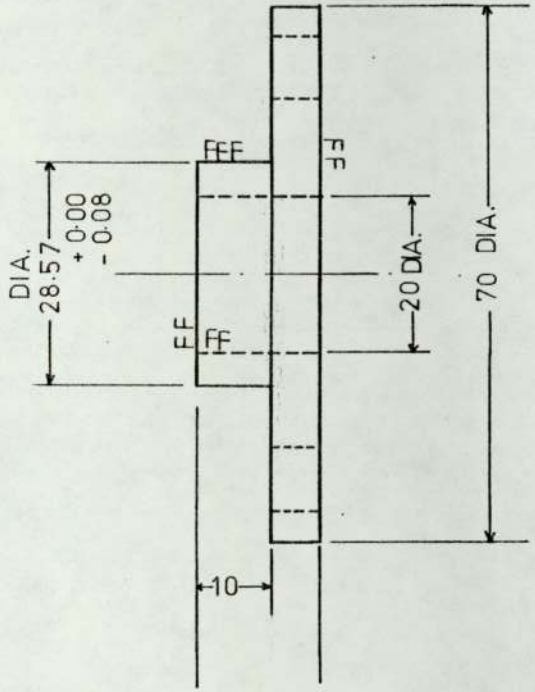

LIMITS ON HOLES AND SHAFTS TO B.S. 4500:1969

F = ROUGH MACHINING
FF = FINISH MACHINING
FFF = GROUND OR EQUIVALENT

TOLERANCE ON MACHINING DIMENSIONS ±0·3 mm UNLESS OTHERWISE STATED.

THIRD ANGLE PROJECTION

UNIVERSITY OF ASTON IN BIRMINGHAM DEPT OF PRODUCTION ENGINEERING	DESCRIPTION THRUST BEARING SUPPORT	ALL DIMENSIONS IN mm EXCEPT WHERE STATED OTHERWISE	MATERIAL MILD STEEL DRG. NO. MD-4
		DESIGNED 22.11.76 S. K. LOKE	
		DRAWN 22.11.76 S. K. LOKE	
		APPROVED	

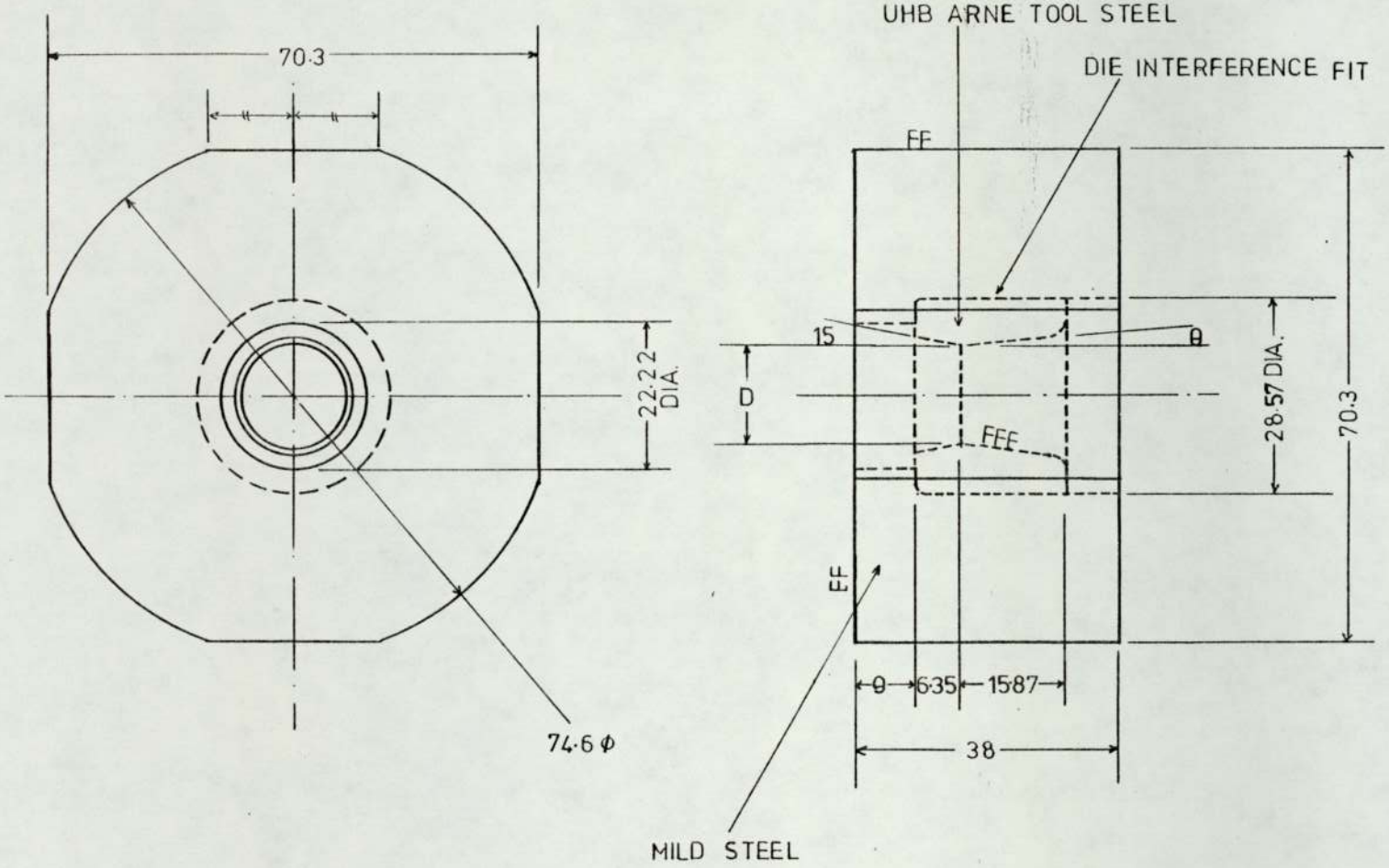

$0.467 \pm \frac{0.001}{0.000}$	9°
$0.475 \pm \frac{0.001}{0.000}$	9°
$0.486 \pm \frac{0.001}{0.000}$	9°
$0.500 \pm \frac{0.001}{0.000}$	9°

F = ROUGH MACHINING
FF = FINISH MACHINING
FFF = GROUND OR EQUIVALENT

TOLERANCE ON MACHINING DIMENSIONS ±0·3 mm UNLESS OTHERWISE STATED

THIRD ANGLE PROJECTION

UNIVERSITY OF ASTON IN BIRMINGHAM DEPT OF PRODUCTION ENGINEERING	DESCRIPTION MODIFIED DRAWING DIE	ALL DIMENSIONS IN mm EXCEPT WHERE OTHERWISE STATED			MATERIAL: AS SHOWN
		SCALE FULL SIZE	DRAWN	22.11.76	S.K. LOKE	DRG NO: MD-5
			MODIFIED	22.11.76	S.K. LOKE	
			APPROVED			

A11 SPECIFICATION FOR NAG SUBROUTINE — D02ABF

1. Purpose

D02ABF integrates a system of ordinary differential equations over a range, using Merson's method.

IMPORTANT: before using this routine, read the appropriate machine implementation document to check the interpretation of italicised terms and other implementation-dependent details.

2. Specification (FORTRAN IV)

```
      SUBROUTINE D02ABF(X,Y,G,T,N,IFAIL,H0,H,AUX,Y0,E,A,B,C,D)
C     INTEGER T,N,IFAIL
C     real X,Y,G,H0,H,Y0,E,A,B,C,D
C     DIMENSION Y(N),G(N),Y0(N),E(N),A(N),B(N),C(N),D(N)
C     EXTERNAL AUX
```

3. Description

The routine advances the solution of a system of ordinary differential equations

$$\frac{dy_i}{dx} = f_i(x, y_1, y_2, \ldots, y_N), \quad i = 1,2,\ldots,N,$$

from x to x + h0, using a number of steps of Merson's form of the Runge-Kutta method. The system is defined by a subroutine AUX supplied by the user, which evaluates the derivatives f_i in terms of x and $y_1, y_2, \ldots, y_N$ (see Section 5 for specification).

The routine D02ABF obtains an estimate of the local truncation error at each step, and varies the step-length automatically to keep this estimate below an error bound specified by the user. If the step-length becomes less than 10^{-4}×(initial step-length), the routine sets an error marker and stops the calculation.

4. References

[1] LAMBERT, J.D.
Computational Methods in Ordinary Differential Equations.
Wiley, 1973, pp. 130-135.

[2] MAYERS, D.F.
Methods of Runge-Kutta type, in:
Numerical Solution of Ordinary and Partial Differential Equations.
Fox, L. (ed.) Pergamon, 1962, pp. 16-27.

D02ABF

5. Parameters

X - *real*.
Before entry, X must be set to the initial value of the independent variable x, and on exit it will contain x + h0, unless an error has occurred, when it will contain the current value.

Y - *real* array, DIMENSION at least (N).
Before entry, Y must be set to the initial values of $y_1, y_2, \ldots, y_N$, and on exit it will contain the computed values at x + h0, unless an error has occurred, when it will contain the current values.

G - *real* array, DIMENSION at least (N).
Before entry, G must be set to error bounds specified by the user for each component of the solution. Unchanged on exit. The type of error test required (relative, absolute or mixed) is specified by the parameter T.

T - INTEGER.
On entry, T must contain either 1,2, or 3, to define the type of error test to be used. If the local error in Y(I) is estimated as E(I), then

T = 1 gives a mixed test: $|E(I)| < G(I) \times (1+|Y(I)|)$,

T = 2 gives an absolute test: $|E(I)| < G(I)$,

T = 3 gives a relative test: $|E(I)| < G(I) \times |Y(I)|$.

For most cases T = 1 is recommended. (See Section 11 for discussion.) T is unchanged on exit.

N - INTEGER.
On entry, N must contain the number of differential equations. It is unchanged on exit.

IFAIL - INTEGER.
Before entry, IFAIL must be assigned a value. For users not familiar with this parameter (described in Chapter P01) the recommended value is 0. Unless the routine detects an error (see Section 6), IFAIL contains 0 on exit.

H0 - *real*.
On entry, H0 must contain the interval h0 over which integration is required. It is unchanged on exit.

5. Parameters (contd)

H - *real*.
Before entry, H must be set to an estimate of the step-length needed for integration. (The routine will modify this if necessary to maintain local accuracy.) If H is zero on entry it will be set initially to H0. On exit H will contain the final value of the step-length.

AUX - SUBROUTINE supplied by the user, with specification

```
SUBROUTINE AUX(F,Y,X)
real F,Y,X
DIMENSION F(n),Y(n)
```

where n is the numerical value of N. AUX evaluates the derivatives of Y(1),Y(2),...,Y(N) at a general point X, and places them in F(1),F(2),...,F(N). (See Section 13 for an example.)
AUX must be declared as EXTERNAL in the (sub) program from which D02ABF is called.

YO - *real* array of DIMENSION at least (N), used as working space.

E - *real* array of DIMENSION at least (N), used as working space.

A - *real* array of DIMENSION at least (N), used as working space.

B - *real* array of DIMENSION at least (N), used as working space.

C - *real* array of DIMENSION at least (N), used as working space.

D - *real* array of DIMENSION at least (N), used as working space.

6. Error Indicators

Errors detected by the routine:

IFAIL = 1 This indicates that the step-length has been halved repeatedly until it is less than 10^{-4}×(initial step-length). The values of X and Y(I) are those at the current stage of integration. (See Section 11.)

IFAIL = 2 This indicates that the routine has been entered with T not equal to 1, 2, or 3. The values of X and Y(I) are the initial values.

IFAIL = 3 This indicates that the number of steps required exceeds the largest integer representable in the machine.

D02ABF

7. Auxiliary Routines

This routine calls the NAG Library routines D02AAF, P01AAF, X02AAF and X02BBF.

8. Timing

This depends on the complexity of the system. The routine AUX is called five times for each integration step of length H.

9. Storage

There are no internally declared arrays.

10. Accuracy

The error per step is of order H^5 for small H. The error estimates obtained from Merson's method are not strict bounds, but they are fairly reliable over one step. Note that only the local error is controlled by varying the step-length H. Over a number of steps the errors may accumulate in various ways, depending on the system, and there is no guarantee that the overall error will be less than the bound specified. The user can check the results by repeating the calculation with a different set of error bounds G(I).

11. Further Comments

The user can choose the type of error test to be applied by specifying the appropriate value of T. The mixed test (given by T = 1) is effectively an absolute test for $|Y(1)| \ll 1$, and a relative test for $|Y(1)| \gg 1$, and so it meets most cases. The absolute test (T = 2) may be more appropriate if the solution oscillates, but only a fixed number of decimal places are required. The relative test (T = 3) may be appropriate if the solution increases rapidly over the range, provided no component passes through zero.

If the routine terminates with IFAIL = 1 (step-length too small), the program can be tried again with a smaller initial value of H. However, if the failure persists, or if the computing time is getting too large, the user should consider whether there is a more fundamental difficulty. For example,

(i) In the region of a singularity (infinite value) of the solution, the routine will usually stop with H too small, unless overflow occurs first. Numerical integration cannot be continued through a singularity, and analytical treatment should be considered.

11. Further Comments (contd)

(ii) For 'stiff' equations, where the solution contains rapidly decaying components, the routine will require a very small H in order to preserve stability, and this may make the computing time excessively long. To recognise such systems, the user should print out the value of H obtained with D02ABF. If it seems very small when the solution is not varying rapidly, the equations are probably stiff. Merson's method is inefficient in such cases, and the user should try D02AJF.

12. Keywords

Differential Equations, Ordinary.
Initial-value problem.
Merson's method.
Runge-Kutta method.

13. Example

To integrate the following equations (for a projectile)

$$y' = \tan(\phi)$$

$$V' = -0.032 \times \tan(\phi)/V - 0.02 \times V \times \sec(\phi)$$

$$\phi' = -0.032/V^2$$

over four intervals of length 2, starting at $x = 0$ with $y = 0$, $V = 0.5$, $\phi = 36^\circ$ $(= \pi/5)$. We write $y = Z(1)$, $V = Z(2)$, $\phi = Z(3)$. The derivatives are calculated by the subroutine DERIV below, and the estimated step-length is 1.

Program

This single precision example program may require amendment
i) for use in a DOUBLE PRECISION implementation
ii) for use in either precision in certain implementations.
The results produced may differ slightly.

```
C     D02ABF EXAMPLE PROGRAM TEXT
C     NAG COPYRIGHT 1975
C     MARK 4.5 REVISED
      INTEGER NOUT, I, J, M
      REAL X, H, Z(3), G(3), Z0(3), E(3), P(3), Q(3), R(3), S(3)
      EXTERNAL DERIV
      DATA NOUT /6/
      WRITE (NOUT,99999)
      WRITE (NOUT,99998)
      X = 0.0
```